Thesis for the degree of Doctor of Philosophy

Estimation and Performance Analysis of Wireless Multiple Antenna Communication Channels

by

Mikael Coldrey

CHALMERS

Department of Signals and Systems
Signal Processing Group
Chalmers University of Technology

Göteborg, Sweden 2006

Estimation and Performance Analysis of Wireless Multiple Antenna Communication Channels

Mikael Coldrey

ISBN 91-7291-758-X

This thesis has been prepared using LaTeX.

Doktorsavhandlingar vid Chalmers Tekniska Högskola
Ny serie nr 2440
ISSN 0346-718X

Department of Signals and Systems
Signal Processing Group
Chalmers University of Technology
SE-412 96 Göteborg, Sweden

Phone: +46 (0)31 772 1780
Fax: +46 (0)31 772 1748
E-mail: mito@chalmers.se

Printed by Chalmers Reproservice
Göteborg, Sweden, March 2006

To my beloved family

Michelle, Viktor, and ...

Abstract

The focus of this thesis is on channel estimation in wireless communication systems that employ multiple antennas.

The thesis is divided into two parts, whereof the first part addresses the problem of parameter estimation of distributed sources. Due to, e.g., local scattering around the transmitter, the source (as seen from the receiver) appears spatially distributed. A characterization of the spatial channel, in particular mean direction of arrival and spatial spread, is of interest for optimization and performance prediction of future communication systems. Nonparametric beamforming-based estimators are derived and analyzed for the localization of distributed sources, and it is found that they provide good estimation performance. Parametric generalized beamformers are also presented and analyzed. It is found that they also yield competitive performance compared to existing algorithms.

The second part of the thesis deals with Multiple-Input Multiple-Output (MIMO) and Single-Input Single-Output (SISO) channel estimation. A simple and straightforward way of estimating the unknown channel is to transmit known training/pilot sequences. In the recent past, a number of publications have suggested Superimposed Pilots (SIP) for channel estimation in communication systems. However, the performance gain achieved by SIP compared to conventional (time-multiplexed) training is still questionable. To evaluate the performance of the various training-based schemes, a lower bound on the mutual information of a general training-based scheme applied to block-wise fading MIMO and SISO channels is derived and maximized. It is found that in certain scenarios it is beneficial to also transmit data during the training mode (i.e., use SIP). The main conclusion though, is that the general SIP-scheme quite often reduces to the conventional time-multiplexed scheme, and, hence, renders the same performance. The theory is also extended to the case when detected data symbols are used as additional training symbols, which significantly improves the channel estimation performance. An improved channel estimate leads to an improvement in the effective Signal-to-Noise Ratio (SNR), and, thus, a higher coding rate may successfully be applied. The extended scheme shows a performance close to the fundamental capacity of the noncoherent MIMO channel.

Keywords: Wireless communications, distributed sources, generalized beamforming, MIMO, channel estimation, training, capacity, performance bounds.

Contents

Acknowledgments

In sickness and in health, I have finally finished writing my Ph.D. thesis. On the one hand, it is a great feeling to have finished writing it, although, on the other hand, I feel a little bit saddened to leave the job that I have dedicated five years of my life to, and the people around it. But, I guess that everything that has a beginning also needs to have an ending. It is my supervisor Professor Mats Viberg who has provided me with this unique time frame to write this thesis. Besides his impressive technical competence, he is greatly appreciated for providing a friendly working atmosphere, where the students are encouraged to develop into independent researchers, who find their own paths, and realize their own potentials. The path can sometimes be tough, but it provides an appreciated freedom and a unique way of learning.

Being a Ph.D. student can often feel lonely, since there is no one to share your enthusiasm (or sometimes lack of) with, as you solve problems (or get stuck). The most fun and inspiring time of my studies was, therefore, when I worked together with Dr. Patrik Bohlin. He deserves my thanks for teaching me that one should not *always* let complicated theory get in the way of producing research results. His hand-waving argumentation techniques are truly fascinating and often (or was it sometimes?) even convincing. Dr. Lennart Svensson also deserves special thanks for always being available for fruitful discussions regarding pretty much anything and everything.

Throughout the years, there has been numerous people who have proof read some version of the manuscript for this thesis. You all deserve a special thank you for helping me with preparing the final version, and I am truly grateful for your insightful comments.

Finally, my deepest gratitude goes to my loving family, my wife Michelle and our son Viktor, who sometimes makes it just too easy to leave work and go home, because I love you so much!

Mikael Coldrey
Göteborg, March 2006

Abbreviations and Acronyms

1-D	One-Dimensional
2-D	Two-Dimensional
AWGN	Additive White Gaussian Noise
BPSK	Binary Phase-Shift Keying
CBF	Conventional BeamFormer
CM	Constant Modulus
CoM	Centre of Mass
CP	Conventional Pilot
CRLB	Cramér-Rao Lower Bound
DD	Decision-Directed
DD-CP	Decision-Directed Conventional Pilot
DD-SIP	Decision-Directed Super-Imposed Pilot
DISPARE	DIspersed Signal PARametric Estimation
DOA	Direction-Of-Arrival
DSPE	Distributed Signal Parameter Estimator
G-Capon	Generalized Capon beamformer
G-CBF	Generalized Conventional BeamFormer
GSM	Global System Mobile
LMMSE	Linear Minimum Mean Square Error
LOS	Line-Of-Sight
MI	Mutual Information
MIMO	Multiple-Input Multiple-Output
MMSE	Minimum Mean Square Error
MSE	Mean Square Error
MUSIC	MUltiple SIgnal Classification
MVDR	Minimum Variance Distortionless Response

NLLS	Non-Linear Least-Squares
OP	Overlay Pilot
PAS	Power Azimuth Spectrum
PCC	Personal Computing and Communication
PDF	Probability Density Function
RMSE	Root Mean Square Error
SIP	Super-Imposed Pilot
SISO	Single-Input Single-Output
SNR	Signal-to-Noise Ratio
SPDF	Spatial Power Density Function
TDMA	Time Division Multiple Access
ULA	Uniform Linear Array
WPSF	Weighted Pseudo-Subspace Fitting
WSF	Weighted Subspace Fitting

Notation

In the thesis, matrices and vectors are set in boldface, with upper-case letters used for matrices and lower-case letters for vectors. If nothing else is explicitly stated, the meaning of the following symbols are

$\mathbf{A}^T$	Transpose operator.
$\mathbf{A}^*$	Complex conjugate.
$\mathbf{A}^H$	Hermitian transpose, i.e., complex conjugate transpose.
$\mathbf{A}^{1/2}$	Hermitian (i.e., $(\mathbf{A}^{1/2})^H = \mathbf{A}^{1/2}$) square-root factor, i.e., $\mathbf{A} = \mathbf{A}^{1/2}\mathbf{A}^{1/2}$.
$\mathrm{Tr}\{\mathbf{A}\}$	Trace operator.
$\lvert\mathbf{A}\rvert$ or $\det(\mathbf{A})$	Matrix determinant.
$\mathrm{vec}(\mathbf{A})$	The column vector that is obtained by stacking the columns of $\mathbf{A}$.
$[\mathbf{A}]_{ij}$ or a_{ij}	The $(i,j)^{\text{th}}$ element of the matrix $\mathbf{A}$.
$\lVert\mathbf{A}\rVert_F$	The Frobenius matrix norm, defined as $\lVert\mathbf{A}\rVert_F^2 = \mathrm{Tr}\{\mathbf{A}\mathbf{A}^H\}$.
$\lVert\mathbf{a}\rVert$	The Euclidean norm, defined as $\lVert\mathbf{a}\rVert = \sqrt{\mathbf{a}^H\mathbf{a}}$.
$\lvert x\rvert$	The absolute value of the (complex) scalar x, defined as $\lvert x\rvert = \sqrt{x^*x}$.
j	The imaginary unit; $j^2 = -1$.
$\mathbf{A} \otimes \mathbf{B}$	The Kronecker product. For an $N \times M$ matrix $\mathbf{A}$ and

a $K \times L$ matrix $\mathbf{B}$ it is defined as the $NK \times ML$ matrix

$$\mathbf{A} \otimes \mathbf{B} \triangleq \begin{bmatrix} a_{11}\mathbf{B} & \cdots & a_{1M}\mathbf{B} \\ \vdots & \ddots & \vdots \\ a_{N1}\mathbf{B} & \cdots & a_{NM}\mathbf{B} \end{bmatrix}$$

$\mathbf{A} > \mathbf{B}$	The matrix $\mathbf{A} - \mathbf{B}$ is positive definite. Furthermore, $\mathbf{A} \geq \mathbf{B}$ means that $\mathbf{A} - \mathbf{B}$ is positive semidefinite.
$\mathrm{diag}\,(a_1, \ldots, a_K)$	The $K \times K$ diagonal matrix with diagonal elements a_1 through a_K.
$\mathbf{I}_m$	The $m \times m$ identity matrix. Frequently, the subscript m is omitted when there is no risk of confusion.
$\mathbf{0}_{m \times n}$	The $m \times n$ all zero matrix. Sometimes, a '$\mathbf{0}$' (or '0') is written when there is no risk for confusion.
$\mathbf{e}_i$	All zero vector except for a one in the i^{th} position. The length of the vector is given by the context.
$\hat{\theta}$	An estimate of the parameter θ.
$\mathrm{E}[\cdot]$	The expectation of a random variable.
$\mathrm{ETr}\,\{\mathbf{A}\}$	The expectation of the trace of a random matrix $\mathbf{A}$.
$\mathrm{mse}(\hat{\theta})$	The mean square error of an estimate.
$\mathrm{var}(\hat{\theta})$	The variance of an estimate.
$\mathrm{Re}\{\cdot\}$	The real part of a complex quantity.
$\mathrm{Im}\{\cdot\}$	The imaginary part of a complex quantity.
$I(X;Y)$	The mutual information between the two random variables X and Y.
$h(X)$	The differential entropy (self-information) of the continuous random variable X.
$\mathbf{X}_n = O_p(a_n)$	The elements of the random matrix $\mathbf{X}_n$ is at most of order in probability a_n, i.e., for every $\epsilon > 0$ there exists a positive real number M_ϵ such that $P(\lvert x_{ij,n} \rvert \geq M_\epsilon a_n) \leq \epsilon$ for all n.

$\mathbb{C}^{m\times n}$	The set of all complex-valued $m \times n$ matrices.
$\mathbf{x} \sim \mathcal{N}(\boldsymbol{\mu}, \mathbf{C})$	The random vector $\mathbf{x}$ is distributed as a normal random vector with mean $\boldsymbol{\mu}$ and covariance matrix $\mathbf{C}$.
$\mathbf{x} \sim \mathcal{CN}(\boldsymbol{\mu}, \mathbf{C})$	The random vector $\mathbf{x}$ is distributed as a complex normal random vector with mean $\boldsymbol{\mu}$ and covariance matrix $\mathbf{C}$.
$\mathbf{x} \sim \text{As}\mathcal{N}(\boldsymbol{\mu}, \mathbf{C})$	The random vector $\mathbf{x}$ is asymptotically distributed as a normal random vector with mean $\boldsymbol{\mu}$ and covariance matrix $\mathbf{C}$.
$\{X_i\}$ are i.i.d.	The sequence of random variables $\{X_i\}$ are independent and identically distributed.
$\delta(t)$	Dirac's generalized delta function; $\int_{-\infty}^{\infty} \delta(t - t_0) f(t)\, dt = f(t_0)$.
δ_{ts}	The Kronecker delta; $\delta_{ts} = \begin{cases} 1 & t = s \\ 0 & t \neq s \end{cases}$
$\arg\min_x f(x)$	The minimizing argument of the function $f(x)$.
$\arg\max_x f(x)$	The maximizing argument of the function $f(x)$.
$\log_2(x)$	The base-2 logarithm of x.
s.t.	Is read *subject to*.
w.r.t.	Is read *with respect to*.
iff	Is read *if and only if*.

Chapter 1

General Introduction

This thesis[1] addresses the field of signal processing for wireless communications and contains contributions to the topic of channel estimation in wireless communication systems that employ multiple antennas.

1.1 Wireless Communications

From the 1990's up until today, there has been a tremendous growth in the application of wireless communications. In this day and age, a mobile phone is more or less a standard accessory for most people in the developed countries, and Wireless Local Area Networks (WLAN) are becoming more and more popular also for home users. We also see that the so-called electronic calendars come with built in WLAN and Bluetooth[2] for connectivity. To attract consumers and finance the growth of wireless communications, new mobile services are developed. That is, the more users we have, together with the use of resource demanding services such as streaming music, video, etc., the loads on our communication systems become larger and larger. Modern systems need to provide fast communication to many users simultaneously, which is to say the least a challenging task. This motivates the development of new techniques for more efficient use of the available frequency spectrum. Spectrum is a scarce resource, therefore it needs to be utilized in an efficient way. One way of increasing the performance of wireless communication systems, without consuming more frequency spectrum, is to equip them with

[1]The work in this thesis has been supported in part by the Personal Computing and Communication Program (PCC/PCC++), and in part by the Swedish Research Council (VR). PCC/PCC++ is funded by the Swedish Foundation for Strategic Research.

[2]Bluetooth is a low cost short-range wireless technique for connecting mobile devices.

multiple antennas. As of late, these so-called *antenna arrays* (also called *smart antennas*) have attracted a lot of attention in the communication research community and are expected to have a commercial breakthrough. As well as exploiting the time and frequency domains, antenna arrays also enable exploitation of the spatial domain. The use of multiple antennas enables; e.g., interference cancellation, directional transmission and reception, increased range, spatial multiplexing, and diversity of the wireless channel in order to increase the performance. These are all desirable properties in the mobile up- and down-links, WLANs, high-rate point-to-point communications, etc. For a good introduction to the application of antenna arrays, the interested reader is referred to, e.g., [God97a, God97b, PP97].

1.2 The Communication System Model

The primary purpose of a digital communication system is the transmission of information that is generated by a source and is to be received by one or multiple destinations. Figure 1.1 is adopted from [Gal68] and it illustrates the functional diagram of a digital communication system.

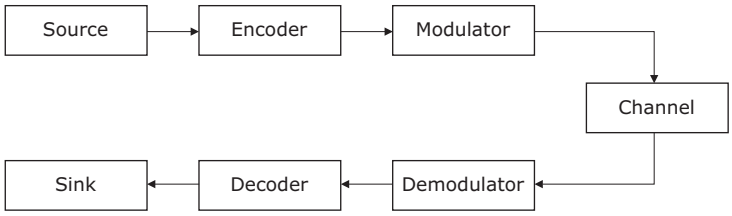

Figure 1.1: Basic block diagram of a digital communication system.

The output from the source might be either a digital or analog signal. Examples of digital signals include; sequences of data, and characters, etc., and examples of analog signals include; speech, audio, and video, etc. In general, the source output is a sequence of binary digits, and ideally it is represented by as few binary digits as possible. The process of efficiently converting the source into a stream of binary digits is called *source encoding*. Source coding is a research topic in itself, and since we do not deal with source coding in this thesis, the source encoder is assumed to be included in the source block. The output from the source encoder is called the binary *information sequence*, and it is passed to the *channel encoder*, which in essence introduces redundancy to protect the data from errors introduced by the *channel*. Channel coding is also in itself a whole research area, and

it is beyond the scope of this thesis. The *modulator* is the interface to the continuous time channel, and it transforms the encoded binary information sequence into continuous time waveforms. When we look at the discrete time representation of the communication channel, we assume that the modulator and its reverse operator, the *demodulator*, are included in the channel model. The channel is the physical medium that is used to transmit the signal from the transmitter to the receiver, and in wireless transmission the channel is typically the atmosphere. Other physical media include; wire lines, optical fiber, etc. The channel corrupts the transmitted signal in a random fashion, and it represents the hard reality that we have to adapt to when designing our communication systems. Typically, we can only describe the random mechanisms behind the channel and we use random models to represent it mathematically. The channel models used in this thesis are presented in the actual chapters where they appear. The primary task in this thesis is to estimate parameters that are used in the mathematical models of the channel. Once we have methods (algorithms) for finding the model parameters, they can be used to better understand the physical channel when studying measurement data from, e.g, channel measurement campaigns and/or to simplify the *decoding* process of the corrupted information sequence that was communicated over the imperfect channel. In general, the decoding process is complicated, but if the *decoder* has channel knowledge it can be greatly simplified. In the end, it is the *sink* that is the destination of the transmitted information sequence, and here it represents both the destination as well as any possible *source decoder*. Ideally, it is desired that the received and decoded information sequence contains no errors, but in practice we usually have to accept a certain amount of errors.

1.3 Channel Estimation

Sometimes estimation theory is used as a synonym to statistical signal processing, since signal processing is all about extracting useful information from signals, which can be done by, e.g., applying the very general concepts from estimation theory. An *estimator* can be seen as the mapping from N data samples to an *estimate*, i.e.,

$$\hat{\theta}_N = f(\mathbf{x}), \tag{1.1}$$

where $\hat{\theta}_N$ denotes the parameter estimate, $f(\cdot)$ the estimator, and $\mathbf{x} = [x(1), \ldots, x(N)]^T$ is the measurement vector from the time series $x(t)$ generated by the modeled process. The subscript N is included to denote that we usually only have access to a finite number of N data samples, i.e., $x(t)$ is

measured for $t = 1, \ldots, N$. Given a set of N data samples, the objective is, thus, to find an estimate of the unknown parameter θ. The parameter θ can either be modeled as an unknown *deterministic* parameter or as a *realization* of a *stochastic* (random) variable. In fact, the first part of this thesis deals with estimation of deterministic parameters, while the second part deals with estimation of stochastic parameters. The subject of estimation theory is vast, and a good introduction to statistical estimation theory can be found in, e.g., [Kay93].

Channel estimation is a classical problem in communications and the area is, therefore, well covered in the literature, see, e.g., [TSD04] and the extensive reference list therein. Basically, it is desired that the receiver *equalizes* the effect of the unknown channel. One straightforward way of doing that is first to estimate the unknown channel. Once the channel is known, its effect of introducing errors to the transmitted information can be removed to some extent.

When different estimators are evaluated qualitatively, one usually talks about some *figure-of-merit*. That is, a figure-of-merit is defined and the performances of the estimators are evaluated with respect to the chosen figure-of-merit. In general, it is desired that the estimated parameter $\hat{\theta}_N$, in some predefined sense, is close to the true parameter θ. For example in the case of a deterministic parameter, a figure-of-merit that is also intuitively appealing, is the *Mean Square Error (MSE)*. We will, therefore, focus some of the discussion on the MSE. The best estimator, out of a collection of estimators, is the one that yields the lowest MSE, where the MSE is defined as

$$\mathrm{mse}\left(\hat{\theta}_N\right) \triangleq \mathrm{E}\left[\left(\hat{\theta}_N - \theta\right)^2\right], \tag{1.2}$$

and where $\mathrm{E}[\cdot]$ denotes statistical expectation. The MSE measures the mean of the squared deviation of the estimate from the true value. Given an estimator, the MSE is a natural criterion to assess the estimation performance. However, if we are not given an estimator, but instead want to find the optimal estimator by employing the MSE criterion, the criterion will unfortunately lead to unrealizable estimators, since, in general, the optimal estimator depends on the unknown parameter. For example, the estimator which yields the minimum (zero) MSE is given by the clairvoyant estimator $\hat{\theta}_N = \theta$. There exist less extreme examples of unrealizable estimator, and this can be seen by recognizing that the MSE is composed of two terms [Kay93]

$$\mathrm{mse}\left(\hat{\theta}_N\right) = b^2\left(\theta\right) + \mathrm{var}\left(\hat{\theta}_N\right), \tag{1.3}$$

where $b(\theta)$ is the *bias* (yet to be defined), and $\mathrm{var}(\hat{\theta}_N)$ denotes the variance. Hence, the MSE is composed of errors due to the bias and the variance of

the estimator, where the bias depends on the unknown parameter θ. One way of trying to find other estimators is to, for example, introduce additional constraints such as forcing them to be *unbiased*, i.e., let $b(\theta) = 0$. Within the class of unbiased estimators, the one with the lowest variance (implying highest figure-of-merit) is sought. Unfortunately, the variance of the estimator also typically depends on the parameter θ, and the minimum variance unbiased estimator does neither exist in general. This can be illustrated by an example where we have two different estimators, and the first estimator might have lower variance for parameter values $\theta \leq \theta_1$, and the second estimator might have lower variance for $\theta > \theta_1$. Hence, there is no global minimum variance unbiased estimator and even further constraints need to be imposed for such cases. For example, forcing the estimator to be linear in the data typically leads to easily implementable, although suboptimal, estimators.

There exist some other concepts that are used in the thesis, and they include; *bias*, *efficiency*, and *consistency*. An estimator is said to be *unbiased iff* it does on-the-average produces the true parameter value, i.e., $\mathrm{E}[\hat{\theta}_N] = \theta$, otherwise it is said to be *biased*. Often we can only hope that the estimator is *asymptotically unbiased*. That is, the estimator is unbiased as the number of data samples goes to infinity, i.e., $\lim_{N\to\infty} \mathrm{E}[\hat{\theta}_N] = \theta$. An estimator is said to be *efficient* if the variance of the estimates coincides with the *Cramér-Rao Lower Bound (CRLB)*, which is a lower bound on the variance achieved by *any* unbiased estimator. Also here, we most often have to settle with estimators that are only *asymptotically efficient*, or sometimes not even that. Finally, we have *consistency*, and an estimator is said to be *weakly consistent* if the *probability* of the event that the estimation error $\hat{\theta}_N - \theta$ is larger than an arbitrarily small number ϵ, goes to zero as the number of data samples tends to infinity. If the event that the estimate tends to the true value has probability one as $N \to \infty$, the estimator is said to be *strongly consistent*. We have to talk about statistical expectations and probabilities, since in general, the data measurement are considered to be random, which also makes the estimates random. The estimator is often also called an *algorithm* or *method* whose primary task is to produce random estimates, given random data samples. Thus, when empirically evaluating, e.g., the MSE performance of an estimator, K sets of N data samples are used to create a sequence of K estimates $\hat{\theta}_{N,1}, \ldots, \hat{\theta}_{N,K}$. The parameter estimates can then be used to estimate the MSE as

$$\widehat{\mathrm{mse}}\left(\hat{\theta}_N\right) \triangleq \frac{1}{K}\sum_{i=1}^{K}\left(\hat{\theta}_{N,i} - \theta\right)^2, \tag{1.4}$$

where $\widehat{\text{mse}}(\hat{\theta}_N)$ is called the empirical MSE. To avoid having to rely on empirical results obtained from long simulation runs, i.e., for every parameter setting having to compute (1.4) for large K, we sometimes in this thesis perform a so-called *statistical performance analysis*. That is, we analytically calculate the asymptotic (as $N \to \infty$) distribution of the estimation error $\hat{\theta}_N - \theta$. The results from such a performance analysis can be used to quickly assess the performance of estimators for different parameter settings.

The performance evaluation w.r.t. the MSE (as described above) applies to estimation of deterministic parameters. In the case of estimating realizations of random variables that are assigned a prior knowledge in the form of a *Probability Density Function (PDF)*, the data is described by the *joint* PDF

$$p(\mathbf{x}, \theta) = p(\mathbf{x}|\theta)p(\theta), \tag{1.5}$$

where $p(\theta)$ is the *prior* PDF. The optimal *Bayesian* estimator is the one that minimizes the Bayesian MSE (the integrated risk)

$$\text{Bmse}\left(\hat{\theta}_N\right) \triangleq \text{E}\left[\left(\hat{\theta}_N - \theta\right)^2\right] = \int \left(\hat{\theta}_N - \theta\right)^2 p(\mathbf{x}, \theta) d\mathbf{x}\, d\theta, \tag{1.6}$$

where the expectation is w.r.t the joint PDF $p(\mathbf{x}, \theta)$, since θ is regarded random. The Bayesian MSE is, because of this, fundamentally different to the MSE in the classical (deterministic) case, and, typically, the optimal Bayesian estimator is uniquely defined given a prior PDF. The estimator that minimizes the Bayesian MSE is called the *Minimum Mean Square Error (MMSE)* estimator, and it is given by the mean of the *posterior* PDF $p(\theta|\mathbf{x})$ (the conditional mean)

$$\hat{\theta}_{\text{MMSE}} = \text{E}[\theta|\mathbf{x}] = \int \theta p(\theta|\mathbf{x}) d\theta, \tag{1.7}$$

where the posterior PDF is given by Baye's rule

$$p(\theta|\mathbf{x}) = \frac{p(\mathbf{x}|\theta)p(\theta)}{\int p(\mathbf{x}|\theta)p(\theta)d\theta}\,. \tag{1.8}$$

The MMSE estimator is often difficult to find in closed-form, and may be too computationally intensive to implement in practice, since, for multiple parameters, it involves multidimensional integration. A practical estimator that is easily found in closed-form given the the appropriate moments, is the *Linear Minimum Mean Square (LMMSE)* estimator. Unless the MMSE estimator happens to be linear, the LMMSE estimator is suboptimal, and

it is given by the linear estimator that yields the lowest Bayesian MSE. In fact, in the second part of the thesis we incorporate the LMMSE estimator to estimate the realizations of a random channel. As previously stated, the interested reader is referred to, e.g., [Kay93] for more information on the interesting topics of signal processing and estimation theory.

In the parts of the thesis where classical parameter estimation is addressed, the estimation performance is evaluated w.r.t. the MSE or the *Root Mean Square Error (RMSE)*, which is defined as the square root of the MSE. However in other parts, the performance is evaluated w.r.t. the *capacity* of a *training-based* communication system. The information theoretic terminology, such as capacity and its related terms, is described in Chapter 6. The same chapter also describes what a training-based system is, and how it works. In a training-based communication system, the capacity is a highly relevant figure-of-merit since it tells how the available time and power should be distributed over the training and information data, respectively, in order to maximize the reliable communication rate. Minimizing the MSE alone in such a system, would give the very unsatisfactory solution of spending all the available time and power on transmission of known training sequences, i.e., yielding zero throughput (meaning no transmission of information).

1.4 Motivation and Aim of the Thesis

The use of antenna arrays in communication systems shows a promising increase in the system performance. However, there are many things to improve in order to fully exploit the potential in using antenna arrays. In general, a great performance limiting factor of *any* system is how well the mathematical models describe the physical reality. Particularly in a communication system, we have to accurately model the channel to enable efficient communication over the channel. However, one should also keep in mind that the physical reality is rarely simple enough to be precisely described by mathematically tractable models. This implies that there is a trade-off between, on the one hand, realistic models, and, on the other hand, tractable models. Thus we need to, e.g., learn more about the nature of the communication channel, and how radio waves propagate in different environments to be able to find tractable models that at the same time are somewhat realistic.

A mathematical model is typically *parameterized* in a set of known and unknown *parameters*, where the unknown parameters are typically sought for. A channel model parameter can, for example, be the direction or angle from where a certain mobile user's signal is arriving to the base station. Knowledge of this direction enables the base station to focus its transmit energy towards

this direction and, hence, create less interference to surrounding mobile users [ZO95].

Very promising theoretical results on the performance of *Multiple-Input Multiple-Output (MIMO)* communication systems have been reported in the literature, e.g., [Fos96, FG98, Tel99]. Measurements have also indicated high performance gains in using MIMO systems [Gan02]. Most of the theoretical work and measurements are based on something called the *channel capacity*, where it is assumed that the channel is known to the receiver. One simple and straightforward way of gaining knowledge of the channel is to use pilot training [Pro01], and various training-schemes for doing so have been proposed in the literature. This motivates the investigation of how these different schemes effect the channel capacity, and to find the (in some sense) optimal training scheme.

The work covered in this thesis is split into two self-contained parts, namely:

Part I: Beamforming-Based Channel Parameter Estimation The aim of this part is to derive and evaluate new beamforming-based estimators for channel parameter estimation. Both nonparametric and parametric estimators are derived, evaluated, and analyzed for localization of distributed sources.

Part II: Training-Aided Channel Parameter Estimation This part of the thesis deals with performance evaluation of various proposed training-based schemes for MIMO and SISO channel estimation. The aim is to find out how much gain there is in using so-called superimposed pilots in favor of conventional time-multiplexed pilots. The work presented in this part is based on research done in close cooperation with Patrik Bohlin at S2, Chalmers University of Technology.

1.5 Outline and Contributions

The thesis consists of two self-contained parts and the main contributions are chapter-wise summarized in the following outline.

Chapter 1 *General introduction*
The present and introductory chapter of the thesis.

Part I: Beamforming-Based Channel Parameter Estimation

Chapter 2 *Introduction*
This is the first chapter in Part I which contains the background to the problem of localization of distributed sources. It also introduces the basic concepts of array signal processing and describes the models that are used in the following chapters.

Chapter 3 *Nonparametric Estimation: Beamforming*
This chapter contains the derivation of a nonparametric scheme for localization of distributed sources. Numerical examples that compare the performance of the derived estimators to that of some more complex high-resolution methods are provided. The chapter is concluded by applying the estimators to indoor MIMO channel measurement data, followed by a statistical performance analysis. The material comprised in this chapter has previously been published in the conference papers [Col02b, Col02a, Col03, CV03].

Chapter 4 *Parametric Estimation: Generalized Beamforming*
In this chapter, the nonparametric point source-based Conventional Beamformer (CBF) is generalized to localization of multiple Incoherently Distributed (ID) and Coherently Distributed (CD) sources that appear in sensor array processing. The generalized CBF is a parametric method that uses the principal eigenvector of the parameterized signal covariance matrix as its weight vector, which is also a matched filter. The desired parameter estimates are taken as the peaks of the generalized 2-D beamforming spectrum. Furthermore, we compare the performance of the generalized CBF numerically to that of the generalized Capon beamformer. Here, the Capon beamformer is also applied to CD sources, and has previously been proposed for ID sources in [HSG04]. Finally, an asymptotic statistical performance analysis of the generalized beamformers is provided and numerically verified. The material presented in this chapter compromises mostly unpublished work. Some material has been submitted as a conference paper in [CV06].

Chapter 5 *Conclusions*
This is the concluding chapter of Part I and it contains a discussion on the obtained results and suggestions for future work.

Part II: Training-Aided Channel Parameter Estimation

Chapter 6 *Introduction*
Chapter 6 is the introductory chapter and it describes the background to the work presented in the second part of the thesis. Further, it gives a brief introduction to information theory concepts that are used in the subsequent chapters.

Chapter 7 *Performance of Training-Aided MIMO Systems*
In this chapter, we compare the performance of two different training-based schemes for MIMO channel estimation. The compared schemes are the conventional time-multiplexed pilot scheme and the superimposed pilot scheme. Their performance is evaluated by deriving, optimizing, and comparing a lower bound on their respective capacity. The material in this chapter has been previously published in the conference papers [CB03, BC04b], and has been submitted as a journal article in [CB05a].

Chapter 8 *Performance of Decision-Directed MIMO Systems*
The work presented in this chapter is an extension to the training schemes of the previous chapter, which allows channel re-estimation when additional information in the form of detected symbols is made available. Detected data symbols are used as additional training symbols, which significantly improves the channel estimate. An improved channel estimate leads to an improvement in the receiver SNR, and, thus, a higher coding rate may successfully be applied. The material in this chapter has been published in the conference paper [BC04a], and has been submitted as a journal article in [CB05b].

Chapter 9 *Performance of Training-Aided SISO Systems*
In this chapter, we apply the same problem formulation as in the previous two chapters to a frequency-selective block-wise fading Single-Input Single-Output (SISO) channel. The work presented in this chapter has previously been published in the conference paper [CB04].

Chapter 10 *Conclusions*
The concluding chapter of Part II of the thesis contains a discussion on the obtained results and suggestions for future research.

1.5.1 List of Publications

Parts of the material that is covered in the first part of the thesis has been published or is under review in the following conference papers:

- M. (Tapio) Coldrey. "Direction and Spread Estimation of Spatially Distributed Signals via The Power Azimuth Spectrum". In *Proc. IEEE ICASSP 02*, volume 3, pages 3005–3008, Orlando, FL, May 2002.

- M. (Tapio) Coldrey. "Beamforming-based Estimators for Spatially Distributed Signals". In *Proc. PCC Workshop & Radiovetenskap och Kommunikation, RVK'02*, pages 319–323, Stockholm, Sweden, June 2002.

- M. (Tapio) Coldrey. "On the use of beamforming for estimation of spatially distributed signals". In *Proc. IEEE ICASSP 03*, volume 5, pages 369–372, Hong Kong, China, April 2003.

- M. (Tapio) Coldrey and M. Viberg. "Analysis of Spectral-based Localization of Spatially Distributed Sources". In *Proc. SYSID 2003, 13th IFAC Symposium on System Identification*, Rotterdam, Netherlands, August 2003.

- M. (Tapio) Coldrey and M. Viberg. "Generalization and Analysis of the Conventional Beamformer for Localization of Spatially Distributed Sources". In *review for the 14th European Signal Processing Conference, EUSIPCO 2006*, Florence, Italy, September 2006.

The second part of the thesis has been published or is under review in the following papers:

- M. (Tapio) Coldrey and P. Bohlin. "Performance Evaluation of MIMO Wireless Communication Systems Employing Pilot Training for Channel Estimation". In *Proc. PCC Workshop & Ericsson/TeliaSonera Research Days 2003*, pages 33–37, Stockholm, Sweden, November 2003.

- P. Bohlin and M. (Tapio) Coldrey. "Performance Evaluation of MIMO Communication Systems based on Superimposed Pilots". In *Proc. IEEE ICASSP 04*, volume 4, Montreal, Canada, May 2004.

- P. Bohlin and M. (Tapio) Coldrey. "Optimized Data Aided Training in MIMO Systems". In *Proc. IEEE VTC 2004 Spring*, volume 2, pages 679–683, Milan, Italy, May 2004.

- M. (Tapio) Coldrey and P. Bohlin. "A Capacity Comparison between Time-Multiplexed and Superimposed Pilots". In *Proc. 38th Asilomar Conference on Signals, Systems and Computers*, volume 1, pages 1049–1053, Monterey, USA, November 2004.

- M. (Tapio) Coldrey and P. Bohlin. "Training-Based MIMO Systems: Part I–Performance Comparison". *Submitted for review to IEEE Trans. on Signal Processing. Also available as technical report no. R032/2005 at http://www.chalmers.se/s2*, November 2005.

- M. (Tapio) Coldrey and P. Bohlin. "Training-Based MIMO Systems: Part II–Improvements using a Variable Coding Rate Scheme". *Submitted for review to IEEE Trans. on Signal Processing. Also available as technical report no. R033/2005 at http://www.chalmers.se/s2*, November 2005.

Part I
Beamforming-Based Channel Parameter Estimation

Chapter 2

Introduction

This chapter gives a introduction to the problem addressed in the first part of the thesis, a short motivation and outline, and introduces the models that are used.

2.1 Background and Overview

In short, direction finding or *Direction-Of-Arrival (DOA)* estimation is the problem of estimating the azimuth angle from which a propagating wavefront is impinging upon an array of sensors. One can also think of a 3-D setting, and estimating both the azimuth and elevation angles, although it is beyond the scope of this thesis. The sensor array enables the collection of *spatio-temporal* (both space and time) *samples*, which are processed to give the desired estimates. Good introductory articles on array signal processing and DOA estimation can be found in, e.g., [VB88, KV96].

Spatially distributed sources appear in many applications, e.g., sonar, radar, seismology, and wireless communications, to only mention a few. Many classical DOA estimation methods are based on a simple point source model. For example, in indoor radio communications the point source assumption is violated due to multiple reflections of the transmitted signal, and a distributed source model would instead be a better approximation [TF93]. Another example is fast fading in mobile communications, where the elevated base station antenna, due to local scattering (reflections) around the mobile, experiences the received signal as distributed in space rather than a point source [Zet97, PMF00]. Depending on the physical media causing the reflections, the signals arriving from different directions exhibit various degrees of correlation, ranging from totally uncorrelated to fully correlated. If the

signals from different directions are uncorrelated, it is called a *Incoherently Distributed (ID)* signal (or source), and if the signals are fully correlated, it is said to be a *Coherently Distributed (CD)* source. Of course, these are the two extreme cases, and one can think of a mix between the two, which leads to *Partially Coherently Distributed (PCD)* sources. A presentation of the distributed models is provided in this chapter, and the interested reader can also be referred to, e.g., [VCK95, RGM00] for a discussion on the different source models and their validity.

If the signal arrives uncorrelated (as in the ID case) from multiple directions, the signal covariance matrix is not rank-one, which in turn leads to that point source-based algorithms deteriorate in performance [Jän92, AO98]. This has resulted in numerous publications of new algorithms that can handle full-rank models, see, e.g., [VCK95, TO96, MSW96, RGM00, BS00, BO00, BO01, SVB01, HSG04, SVG04] and references therein. In [VCK95] a generalization of the popular MUSIC algorithm [Sch79] was presented, and in [TO96] a Maximum Likelihood (ML) estimator was proposed to estimate the parameters of distributed sources. In [MSW96] another generalization of the MUSIC algorithm was presented, and in [RGM00] an ML estimator was developed for a partially coherently distributed source model. In order to reduce the numerical complexity, a decoupled estimator that requires two successive 1-D searches was presented in [BS00], and in [BO00] a standard point source-based algorithm such as, e.g., root-MUSIC [Bar83] was used to fit a rank-two model to a distributed source. A generalization of the idea of weighted subspace fitting to full-rank models was presented in [BO01], and in [SVB01] the ESPRIT algorithm [RK89] was used to estimate a distributed source. Finally, in [HSG04] a generalization of the popular Capon's beamformer [Cap69] to ID sources was introduced, and in [SVG04], a covariance fitting approach was used to find the moments of the source's spatial power density function. While the ID source yields a full-rank covariance matrix, the signal covariance matrix of a CD source is rank one, which means that most standard point source algorithms can be extended to localization of CD sources by simply generating a new *array manifold* (to be defined) for CD sources. For example, a MUSIC-based algorithm is presented in [VCK95], the algorithm in [SVB01] also works for CD sources, and the ML estimator for CD sources is studied in [RGM00]. This is by no means a full overview of all the existing algorithms, but it represents some of the most cited algorithms in the literature of today.

What commonly characterizes parametric estimators is that they require knowledge of the shape of the angular distribution of the source and assume narrow angular spreads. Many of them require solving a multi-dimensional optimization problem, implying high computational loads. In this thesis, we

start by investigating the possibility of using classical low-complexity *beamforming* techniques for localization and spread estimation of an ID source. Due to unknown scattering, the signal from a mobile user arrives from several different directions and we know little or nothing about the angular distribution of the arriving signal. It would therefore be attractive to have a robust and simple *beamformer*, which can give the desired estimates (nominal DOA and spread) without making any assumptions on the shape of the angular distribution. As such, the beamformer is considered to be *nonparametric*. The beamformer would, therefore, be well suited, for example, for characterizing the communication channel's spatio-temporal behavior. Since the power radiated from a distributed source and received by an array contains information about the angular distribution, the conceptual idea is, thus, to compute the received power as a function of angle by digitally steering and scanning the source with a narrow beam. The parameters of interest, namely nominal angle and spread, are then estimated from the attained power distribution. The idea is very simple in its nature, and has been previously suggested in [Lee73] to estimate the distribution of wave arrival of a mobile signal. In [Lee73], an antenna array was pointed at a fixed angle, and then the received power was computed over a test run, followed by mechanically rotating the antenna to the next angle, and computing the power over a new test run, and so on. The effect of noise was never considered in [Lee73]. Here we compute the covariance matrix from a single batch of snapshots, and apply digital beamforming techniques to compute the power spectrum.

The desired parameters are extracted from the first and second moments of the computed spectrum attained by, e.g., CBF or Capon's beamformer. The method is, therefore, related to spectral moments estimation, e.g., [MB99,Da00], and has been used in [Mon00,MB04] to observe extended targets in radar applications.

We continue with applying the suggested beamforming-based estimators to indoor *Multiple-Input Multiple-Output (MIMO)* measurement data. Finally, a statistical performance analysis is presented together with numerical examples to validate the theoretical results.

The attention is then turned to *generalized beamforming* techniques, and we derive and analyze some *parametric* beamforming techniques that are based on generalizations of the classical beamformers to also handle multiple distributed sources. The generalized beamformers can be applied both to ID and CD sources. As opposed to nonparametric techniques, a parametric technique makes use of model-based information in the form of knowing the covariance structure of the data. The parametric approach, thus, exploits that it has full knowledge of the shape of the *spatial power distribution function* (yet to be defined). Generalized beamformers are attractive in that

they do not only yield parameter estimates with competitive performance, but also function as spatial filters. For example, the generalized conventional beamformer is also a *matched filter* in the sense that it maximizes the output *Signal-to-Noise Ratio (SNR)*.

2.2 Data Modeling

This section describes the data models and the terminology used in the first part of the thesis. We present the point source model and the distributed source models. These models frequently appear in array signal processing for, e.g., wireless communications.

2.2.1 Point Source Model and Definitions

The conventional data model assumes that the signal impinging upon an array of sensors to be *narrow-band* and emitted from a *point source* in the *far-field region*[1]. In Figure 2.1, the far-field *Electro-Magnetic (EM)* wave is incident at an DOA angle θ upon a *Uniform Linear Array (ULA)* consisting of K identical antenna elements. The EM field induces K voltages $\{x_i(t), i = 1, \ldots, K\}$, which are simultaneously measured at a time instant t and collected as spatial samples into a vector (*snapshot*) $\mathbf{x}(t) = [x_1(t), \ldots, x_K(t)]^T$.

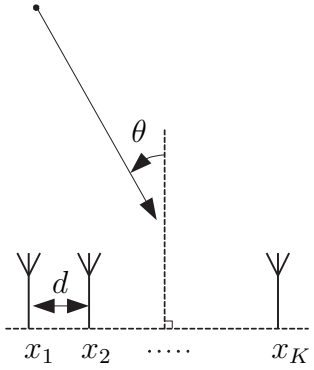

Figure 2.1: Point source signal incident upon an antenna array from the direction θ.

Using a complex signal representation, the *modulated signal* impinging

[1]The wavefront is considered to be planar at a distance greater than $2D^2/\lambda$ (where λ is the wavelength and $D > \lambda$ is the largest dimension of the antenna) away from the transmitting antenna. This region is called the far-field (Fraunhofer) region.

upon the array is modeled as

$$\bar{s}(t) = u(t)e^{j(\omega_c t+\psi(t))} , \tag{2.1}$$

where $u(t)$ and $\psi(t)$ are the modulated signal's *amplitude* and *phase*, respectively, and ω_c the *carrier frequency*. In general, the modulated signal $\bar{s}(t)$ occupies a narrow bandwidth B, compared to the carrier frequency ω_c, i.e., $B \ll \omega_c$. However, in array processing the signal is assumed to be narrow-band when the signal amplitude $u(t)$ and phase $\psi(t)$ vary slowly relative to the propagation time τ_i across the array, i.e., $|\tau_i| \ll 1/B, \forall i = 1, \ldots, K$, and, therefore,

$$\begin{aligned} u(t-\tau_i) &\approx u(t) && (2.2)\\ \psi(t-\tau_i) &\approx \psi(t) , && (2.3) \end{aligned}$$

where τ_i is the time it takes for the wave to propagate from the phase reference point, i.e., the origin (usually the first element), to the i^{th} element. This is the *first* part of what in array signal processing is called the *narrow-band assumption*, and implies that the signal only undergoes phase-shifts when propagating across the array, i.e.,

$$\begin{aligned} \bar{s}(t-\tau_i) &= u(t-\tau_i)e^{j(\omega_c(t-\tau_i)+\psi(t-\tau_i))} \\ &\approx e^{-j\omega_c\tau_i}u(t)e^{j(\omega_c t+\psi(t))} \\ &= e^{-j\omega_c\tau_i}\bar{s}(t) . \end{aligned} \tag{2.4}$$

Let $h_i(t)$ denote the impulse response of the i^{th} sensor, which is assumed to be linear. Using the above narrow-band assumption, the modulated output signal of the i^{th} element is, in the absence of noise, given by

$$\bar{x}_i(t) = h_i(t) * \bar{s}(t-\tau_i) \approx h_i(t) * e^{-j\omega_c\tau_i}\bar{s}(t) , \tag{2.5}$$

where $*$ denotes convolution. The Fourier-transform $H_i(\omega)$ of $h_i(t)$ is assumed to be constant over the signal bandwidth B. This is the *second* and last part of the narrow-band assumption in array signal processing. Under these assumptions we can write the i^{th} element's output signal as

$$\bar{x}_i(t) = H_i(\omega_c)e^{-j\omega_c\tau_i}\bar{s}(t) , \tag{2.6}$$

where approximation has been omitted in favor of equality.

The propagation time τ_i is a function of the DOA parameter θ, i.e., $\tau_i = \tau_i(\theta)$. For a ULA the time delay of the signal at the i^{th} element is

$$\tau_i(\theta) = \frac{(i-1)d\sin\theta}{c} , \tag{2.7}$$

where d is the element spacing, and c the wave propagation speed. If we also assume that the identical array elements are isotropic and that their frequency responses are identically equal to unity, the i^{th} output can be written as

$$\bar{x}_i(t) = e^{-j(i-1)kd\sin\theta}\bar{s}(t) \ , \tag{2.8}$$

where $k = 2\pi/\lambda$ (λ is the wavelength) denotes the *circular wave number*[2]. We reserve the term *standard ULA* for a ULA with isotropic, identical, and unit frequency response elements with an element separation of half-a-wavelength. The separation $d = \lambda/2$ is the maximum allowable separation to avoid steering vector ambiguities, and it is the spatial equivalent to the Nyquist sampling rate of continuous time signals.

The *demodulated signal* is acquired by simply removing the complex carrier, $e^{j\omega_c t}$, as $s(t) = u(t)e^{j\psi(t)}$, and is referred to as the *baseband signal*. Hence, we can express the i^{th} baseband output as

$$x_i(t) = e^{-j(i-1)kd\sin\theta}s(t) \triangleq a_i(\theta)s(t) \ , \tag{2.9}$$

and by using vector notation we acquire the whole baseband array output (snapshot) as

$$\begin{aligned} \mathbf{x}(t) &= [x_1(t), \ldots, x_K(t)]^T \\ &= [a_1(\theta), \ldots, a_K(\theta)]^T s(t) \\ &= \mathbf{a}(\theta)s(t) \ , \end{aligned} \tag{2.10}$$

where $\mathbf{a}(\theta)$ is the complex length-K *steering vector* or *array response vector*. The set of steering vectors over some *parameter space* Θ of interest, e.g., $\Theta = (-\pi/2, \pi/2)$, is called the *array manifold*, and is denoted by

$$\mathcal{A} = \{\mathbf{a}(\theta) \mid \theta \in \Theta\} \ . \tag{2.11}$$

Assuming that we have L narrowband signals arriving from directions $\{\theta_1, \ldots, \theta_L\}$, we simply use superposition to get the received signal

$$\mathbf{x}(t) = \sum_{\ell=1}^{L} \mathbf{a}(\theta_\ell)s_\ell(t) \ , \tag{2.12}$$

which in matrix form becomes

$$\mathbf{x}(t) = [\mathbf{a}(\theta_1), \ldots, \mathbf{a}(\theta_L)] \begin{bmatrix} s_1(t) \\ \vdots \\ s_L(t) \end{bmatrix} = \mathbf{A}(\boldsymbol{\theta})\mathbf{s}(t) \ , \tag{2.13}$$

[2]The circular wave number is commonly used in wave propagation theory.

where $\boldsymbol{\theta} = [\theta_1, \ldots, \theta_L]^T$ is the $L \times 1$ DOA parameter vector, and $\mathbf{A}(\boldsymbol{\theta})$ is referred to as the $K \times L$ *steering matrix*.

Because of the effects of modeling errors, random noise, etc., the model can not explain the observed data perfectly. These effects are simply accounted for by including an additive random noise term in the model

$$\mathbf{x}(t) = \mathbf{A}(\boldsymbol{\theta})\mathbf{s}(t) + \mathbf{n}(t) \; . \tag{2.14}$$

Throughout the thesis, the noise is commonly modeled as a zero-mean complex circularly symmetric and spatio-temporally white Gaussian process,

$$\mathrm{E}\left[\mathbf{n}(t)\right] = 0 \; , \;\; \mathrm{E}\left[\mathbf{n}(t)\mathbf{n}^H(s)\right] = \sigma_n^2 \mathbf{I}\delta_{ts} \; , \;\; \mathrm{E}\left[\mathbf{n}(t)\mathbf{n}^T(s)\right] = \mathbf{0} \;\; \forall \, t, s \; , \tag{2.15}$$

where σ_n^2 is the variance of the noise.

Using the above definitions, the covariance matrix of the output signal vector can be written as

$$\begin{aligned} \mathbf{R}_x &= \mathrm{E}\left[\mathbf{x}(t)\mathbf{x}^H(t)\right] \\ &= \mathrm{E}\left[\big(\mathbf{A}(\boldsymbol{\theta})\mathbf{s}(t) + \mathbf{n}(t)\big)\big(\mathbf{A}(\boldsymbol{\theta})\mathbf{s}(t) + \mathbf{n}(t)\big)^H\right] \\ &= \mathbf{A}(\boldsymbol{\theta})\mathbf{P}\mathbf{A}^H(\boldsymbol{\theta}) + \sigma_n^2\mathbf{I} \; , \end{aligned} \tag{2.16}$$

where the matrix $\mathbf{P} = \mathrm{E}\left[\mathbf{s}(t)\mathbf{s}^H(t)\right]$ for random signals, and $\mathbf{P} = \mathbf{s}(t)\mathbf{s}^H(t)$ for deterministic signals.

2.2.2 Distributed Source Models

In many environments for modern radio communications, the transmitted signal is often obstructed by buildings, vehicles, trees, etc., and/or reflected by rough surfaces. Hence, the absence of a single *Line-Of-Sight (LOS)* ray will violate the classical point source assumption. The receiver is likely to experience a spatially dispersed signal consisting of several arriving rays *spread* around some *nominal direction* (or *nominal angle*). In general, the performance of *any* system depends on how well the mathematical model describes the physical reality, and in the case of a mobile system the distributed source model narrows the gap between the model and reality. Typically, the statistics of a distributed source are parameterized by the nominal direction and spread of the source, and the two parameters compose a compact statistical representation of the slow variations of a distributed source. The aim here is to estimate these two slowly varying channel statistics rather than the actual channel realization (full channel estimation is addressed in the second part of the thesis). The two parameters can, e.g., be used for channel characterization and "off-line" performance evaluation. For example, in [ZO95],

knowledge of the nominal direction and spread parameters are used to design and evaluate a transmit beamforming scheme at the base station of a mobile cellular network. In [JF04], the effect of angular spreading on the detection performance of distributed sources is investigated.

Figure 2.2 displays a source with a spatial extension around a nominal DOA. One way to model distributed signals is to model them as if they were emitted from a cluster of closely spaced point sources with random complex gains, e.g., [Zet97, Ben99, God02]. The time delay differences within each cluster of point sources is small relative to the inverse source signal bandwidth, i.e., every individual point source will, due to the complex gain, introduce a attenuation and phase-shift of the transmitted source signal. For an overview of spatial channel models, the interested reader is referred to, e.g., [Ert98].

Incoherently Distributed Sources

If we have a tight cluster consisting of L point sources with complex gains, and sum over all the contributing sources, the array output for a single distributed signal becomes

$$\mathbf{x}(t) = \sum_{\ell=1}^{L} \gamma_\ell(t)\mathbf{a}(\theta_\ell(t))s(t) + \mathbf{n}(t) \ , \tag{2.17}$$

where $\gamma_\ell(t)$ is the random complex gain of the ℓ^{th} point source, $\theta_\ell(t)$ is the corresponding DOA, and $s(t)$ is the transmitted narrow-band and *Constant-Modulus (CM)* source signal (CM is required for stationarity). The individual time delays of each path are approximated by a random phase shift, which without loss of generality, are included in the complex path gains $\gamma_\ell(t)$.

Since the point sources are distributed around the nominal DOA θ_0, the ℓ^{th} DOA can be modeled as $\theta_0 + \tilde{\theta}_\ell(t)$, where $\tilde{\theta}_\ell(t)$ is a zero-mean random angular deviation from the nominal DOA and with *Probability Density Function (PDF)* $p(\tilde{\theta}; \sigma_\theta)$. The PDF is parameterized by a *spread* (or *standard deviation*) parameter σ_θ. The array output is then written as

$$\begin{aligned} \mathbf{x}(t) &= \sum_{\ell=1}^{L} \gamma_\ell(t)\mathbf{a}(\theta_0 + \tilde{\theta}_\ell(t))s(t) + \mathbf{n}(t) \\ &= \mathbf{h}(t; \boldsymbol{\eta}_0)s(t) + \mathbf{n}(t) \ , \end{aligned} \tag{2.18}$$

where $\boldsymbol{\eta}_0 = [\theta_0, \sigma_\theta]^T$ is the unknown parameter vector, and $\mathbf{h}(t; \boldsymbol{\eta}_0)$ is the random *channel vector*. As in, e.g., [TO96, Ben99], it is assumed that the scattering environment changes rapidly compared to the mean DOA and

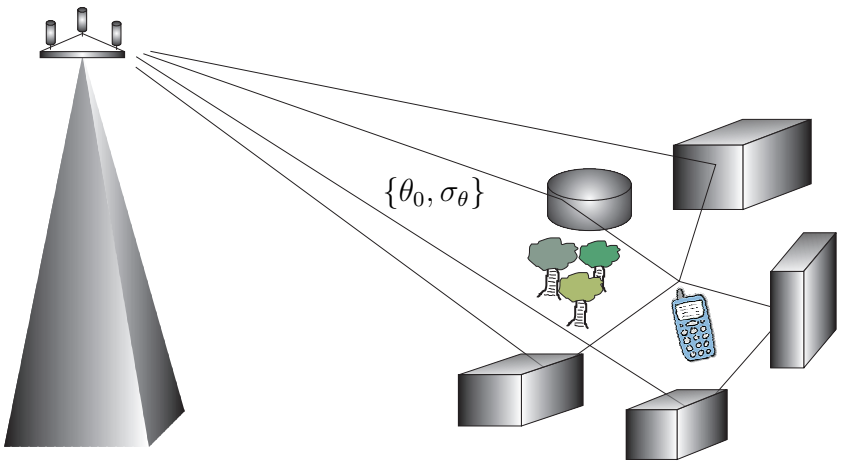

Figure 2.2: Multipath propagation leads to a signal with a spatial distribution. The distribution is commonly described by its nominal direction and spread $\{\theta_0, \sigma_\theta\}$.

spread parameters as well as to the sampling time. Thus, the random complex gains $\gamma_\ell(t)$ are assumed to be temporally white from snapshot to snapshot. For an *Incoherently Distributed (ID)* source, they are also assumed to be uncorrelated from ray to ray, zero mean, and circularly symmetric, i.e.,

$$\begin{aligned} \mathrm{E}\left[\gamma_\ell(t)\right] = 0 \;, \quad \mathrm{E}\left[\gamma_\ell(t)\gamma_k(t)\right] = 0 \;, \\ \mathrm{E}\left[\gamma_\ell(t)\gamma_\ell(s)\right] = 0 \;, \quad \mathrm{E}\left[\gamma_\ell(t)\gamma_k^*(s)\right] = \frac{1}{L}\sigma_\gamma^2 \delta_{\ell k}\delta_{ts} \quad \forall\; \ell, k, t, s \;. \end{aligned} \tag{2.19}$$

By assuming large L and using a central limit theorem type of argument, $\mathbf{h}(t;\boldsymbol{\eta}_0)$ is approximately a zero-mean complex Gaussian vector, which makes the model (2.18) a generalization of the scalar frequency-flat Rayleigh fading multipath channel, e.g., [Pro01], to the vector case. Hence, if the transmitted signal is modeled as deterministic, and since the noise is zero-mean and complex Gaussian, the received signal vector $\mathbf{x}(t)$ will also be zero-mean and complex Gaussian.

Alternatively, if we assume a continuum of scatterers within a cluster, the output signal can be modeled as [VCK95]

$$\begin{aligned} \mathbf{x}(t) &= \int_{\tilde{\theta}\in\Theta} \gamma(\tilde{\theta}, t)\mathbf{a}(\theta_0 + \tilde{\theta}) d\tilde{\theta}\, s(t) + \mathbf{n}(t) \\ &= \mathbf{h}(t;\boldsymbol{\eta}_0)s(t) + \mathbf{n}(t) \;, \end{aligned} \tag{2.20}$$

where Θ denotes the angular support of the distributed source. The spatio-temporal complex gain $\gamma(\tilde{\theta}, t)$ is described by a temporal stochastic process

which is assumed to have a continuous spatial distribution with spatial covariance kernel $\mathrm{E}\big[\gamma(\tilde{\theta},t)\gamma^*(\tilde{\theta}',t)\big] = \sigma_\gamma^2 p(\tilde{\theta};\sigma_\theta)\delta(\tilde{\theta}-\tilde{\theta}')$, where $\delta(\cdot)$ is the Dirac delta function. In this context, $p(\tilde{\theta};\sigma_\theta)$ is often referred to as being the *Spatial Power Density Function (SPDF)* of the distributed source. For large L and tight clusters, there is little difference between the discrete (2.18) and continuous (2.20) models. They both model what is called an ID source, i.e., uncorrelated signals arrive from distinct directions. The relevance of the ID source model has been both theoretically and experimentally justified for wireless communications with elevated base stations in, e.g., [Zet97,PMF00]. In the measurement campaign conducted in [PMF00], spreads in the order of 10° and more were reported.

Under the previous assumptions, the covariance matrix of the received signal is given by

$$\begin{aligned}\mathbf{R}_x(\boldsymbol{\eta}_0) &= \mathrm{E}\left[\mathbf{x}(t)\mathbf{x}^H(t)\right] \\ &= |s(t)|^2\sigma_\gamma^2 \int_{\tilde{\theta}\in\Theta} p(\tilde{\theta};\sigma_\theta)\mathbf{a}(\theta_0+\tilde{\theta})\mathbf{a}^H(\theta_0+\tilde{\theta})d\tilde{\theta} + \sigma_n^2\mathbf{I} \\ &= \sigma_s^2\mathbf{R}_h(\boldsymbol{\eta}_0) + \sigma_n^2\mathbf{I}\,, \end{aligned} \tag{2.21}$$

where $\sigma_s^2 = \sigma_\gamma^2|s(t)|^2$ is the source signal power including the path gain factor, and $\mathbf{R}_h(\boldsymbol{\eta}_0)$ is the covariance matrix (excluding the path gain since it is included in σ_s^2) of the zero-mean complex Gaussian channel vectors.

By introducing the following change of variables

$$\omega = kd\sin\theta \tag{2.22}$$

$$\sigma_\omega = kd\sigma_\theta\cos\theta\,, \tag{2.23}$$

where ω denotes the *spatial frequency* or *electric angle* and σ_ω denotes the corresponding standard deviation, an approximate closed-form expression for the integral in (2.21) has been derived for uniform and Gaussian angular distributions in, e.g., [ZO95,MSW96,TO96,Ben99]. For a K-sensor standard ULA and a small angular spread, the covariance matrix can be rewritten as

$$\mathbf{R}_h(\boldsymbol{\psi}) = \mathbf{D}(\omega)\mathbf{B}(\sigma_\omega)\mathbf{D}^H(\omega)\,, \tag{2.24}$$

where $\boldsymbol{\psi} = [\omega,\sigma_\omega]^T$ is the transformed parameter vector, and $\mathbf{D}(\omega)$ only involves the nominal spatial frequency of the source such that

$$\mathbf{D}(\omega) = \mathrm{diag}\left(1, e^{-j\omega}, \ldots, e^{-j(K-1)\omega}\right)\,, \tag{2.25}$$

and $\mathbf{B}(\sigma_\omega)$ depends on the shape of the angular distribution. In general, $\mathbf{B}(\sigma_\omega)$ is a full-rank matrix. If the random angular deviation is *uniform* over

$[-\delta_\omega, \delta_\omega]$, then

$$[\mathbf{B}(\sigma_\omega)]_{ij} = \frac{\sin((i-j)\delta_\omega)}{(i-j)\delta_\omega} , \quad \delta_\omega = \sqrt{3}\sigma_\omega \tag{2.26}$$

or if the deviation is *Gaussian* with zero mean and standard deviation σ_ω

$$[\mathbf{B}(\sigma_\omega)]_{ij} = e^{-((i-j)\sigma_\omega)^2/2} . \tag{2.27}$$

It should be noted that these expressions for the covariance matrix are approximations that have been derived for PDFs that are symmetric in ω, which does not necessarily imply symmetry in θ. Therefore, they are valid for small angular deviations $\tilde{\theta}$, thus, we can write

$$\begin{aligned} kd\sin(\theta_0 + \tilde{\theta}) &= kd\left(\sin\theta_0\cos\tilde{\theta} + \sin\tilde{\theta}\cos\theta_0\right) \\ &\approx kd\left(\sin\theta_0 + \tilde{\theta}\cos\theta_0\right) \\ &\triangleq \omega_0 + \tilde{\omega}. \end{aligned}$$

Hence, a spread in physical angle σ_θ corresponds approximately to a spread in electric angle given by $\sigma_\omega = kd\sigma_\theta\cos\theta_0$. Thanks to the convenient decomposition in (2.24) and their closed-form expressions, they become very useful when analyzing the algorithms described in the thesis.

We can easily extend the model to handle multiple, say q, diffuse signals with nominal DOAs $\boldsymbol{\theta}_0 = [\theta_1, \ldots, \theta_q]^T$ and corresponding spreads $\boldsymbol{\sigma}_\theta = [\sigma_{\theta_1}, \ldots, \sigma_{\theta_q}]^T$, by summing over the q distributed signals

$$\mathbf{x}(t) = \sum_{k=1}^{q} \mathbf{h}(t; \theta_k, \sigma_{\theta_k}) s_k(t) + \mathbf{n}(t) = \mathbf{H}(t; \boldsymbol{\theta}_0, \boldsymbol{\sigma}_\theta)\mathbf{s}(t) + \mathbf{n}(t) , \tag{2.28}$$

where the channel matrix is $\mathbf{H}(t; \boldsymbol{\theta}_0, \boldsymbol{\sigma}_\theta) = \big[\mathbf{h}(t; \theta_1, \sigma_{\theta_1}), \ldots, \mathbf{h}(t; \theta_q, \sigma_{\theta_q})\big]$, and the signal vector is $\mathbf{s}(t) = [s_1(t), \ldots, s_q(t)]^T$. Finally, if we assume uncorrelated signals, the array output covariance matrix is given by

$$\mathbf{R}_x(\boldsymbol{\theta}_0, \boldsymbol{\sigma}_\theta) = \sum_{k=1}^{q} \sigma_{s_k}^2 \mathbf{R}_h(\theta_k, \sigma_{\theta_k}) + \sigma_n^2\mathbf{I} , \tag{2.29}$$

where $\sigma_{s_k}^2$ and $\mathbf{R}_h(\theta_k, \sigma_{\theta_k})$ are the signal power and the channel covariance matrix of the k^{th} diffuse source, respectively.

The parametrization of $\mathbf{R}_h(\boldsymbol{\eta})$ becomes important when we have multiple and closely spaced distributed sources. Parametric methods that exploit the model can resolve closely spaced sources. By using a nonparametric method, which does not exploit the model, it still is possible to resolve multiple distributed sources, but it requires the sources to be well separated, and, thereby, to have non-overlapping spectra. Figure 2.3 shows two Gaussian-like distributed sources that have overlapping spectra.

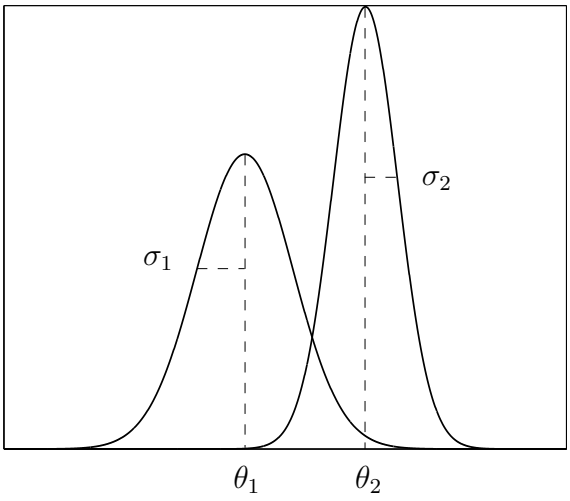

Figure 2.3: Two Gaussian-like distributed sources with overlapping spectra and parameter vectors $[\theta_1, \sigma_1]^T$ resp. $[\theta_2, \sigma_2]^T$.

Cramér-Rao Lower Bound for ID Sources

Given the approximate closed-form expression for the covariance matrix $\mathbf{R}_x(\boldsymbol{\phi})$, the *Cramér-Rao Lower Bound (CRLB)* is computed for the incoherent source model. The CRLB serves as a lower bound on the estimation performance of any unbiased estimator. Assuming some regularity conditions (see, e.g., [Kay93]), the CRLB for the extended parameter vector $\boldsymbol{\phi} = [\theta, \sigma_\theta, \sigma_s^2, \sigma_n^2]^T$ is given by [Kay93]

$$\mathrm{E}\left[(\hat{\boldsymbol{\phi}} - \boldsymbol{\phi})(\hat{\boldsymbol{\phi}} - \boldsymbol{\phi})^T\right] \geq \mathbf{J}^{-1}(\boldsymbol{\phi}), \tag{2.30}$$

where $\mathbf{J}(\boldsymbol{\phi})$ is the 4×4 *Fisher Information Matrix (FIM)*, and $\mathbf{A} \geq \mathbf{B}$ means that $\mathbf{A} - \mathbf{B}$ is positive semidefinite. The FIM is defined by

$$[\mathbf{J}(\boldsymbol{\phi})]_{ij} = -\mathrm{E}\left[\frac{\partial^2 \ln p(\mathbf{X}_N; \boldsymbol{\phi})}{\partial \phi_i \partial \phi_j}\right], \quad i, j = 1, \ldots, 4 \tag{2.31}$$

where $p(\mathbf{X}_N; \boldsymbol{\phi})$ is the multivariate Gaussian PDF of the $K \times N$ data matrix $\mathbf{X}_N = [\mathbf{x}(1), \ldots, \mathbf{x}(N)]$, where $\mathbf{x}(t)$ is given by (2.20). Since the snapshots are zero-mean, circularly symmetric, i.i.d., and complex Gaussian vectors, the FIM is, thus, given by [Kay93]

$$[\mathbf{J}(\boldsymbol{\phi})]_{ij} = N\mathrm{Tr}\left\{\mathbf{R}_x^{-1}\frac{\partial \mathbf{R}_x}{\partial \phi_i}\mathbf{R}_x^{-1}\frac{\partial \mathbf{R}_x}{\partial \phi_j}\right\}, \tag{2.32}$$

where

$$\frac{\partial \mathbf{R}_x}{\partial \phi_1} = \frac{\partial \mathbf{R}_x}{\partial \theta} = \sigma_s^2 \frac{\partial \mathbf{R}_h}{\partial \theta} \tag{2.33}$$

$$\frac{\partial \mathbf{R}_x}{\partial \phi_2} = \frac{\partial \mathbf{R}_x}{\partial \sigma_\theta} = \sigma_s^2 \frac{\partial \mathbf{R}_h}{\partial \sigma_\theta} \tag{2.34}$$

$$\frac{\partial \mathbf{R}_x}{\partial \phi_3} = \frac{\partial \mathbf{R}_x}{\partial \sigma_s^2} = \mathbf{R}_h \tag{2.35}$$

$$\frac{\partial \mathbf{R}_x}{\partial \phi_4} = \frac{\partial \mathbf{R}_x}{\partial \sigma_n^2} = \mathbf{I}_K. \tag{2.36}$$

The derivatives (2.33) and (2.34) can be found in, e.g., [TO96, Ben99]. In most of the figures in the thesis, we plot the square-root of the CRLB, since in most performance evaluations the *Root-Mean Square Error (RMSE)* is used.

Coherently Distributed Sources

In contrast to the ID source we have the CD source, where signals arriving from distinct directions are fully correlated. That is, the received signal consists of signal components from different angles that are delayed and scaled replicas of the same signal. The CD source model is valid, for example, when a narrowband signal is reflected by an object, and the signal components that are reflected from different parts of the object differ by a deterministic phase component. This in turn depends on the reflection coefficients of the reflecting media, incident angles, difference in propagation time, and the frequency of the plane wave [VCK95]. In this thesis we consider both the case of incoherently distributed sources, which lead to a high-rank signal contribution, and coherently distributed sources, which yield a rank-one signal contribution. The case of a mix between these two models is left as a topic for future research.

The received signal emitted from a CD source can be written as

$$\mathbf{x}(t) = \gamma(t)\mathbf{b}(\boldsymbol{\eta}_0)s(t) + \mathbf{n}(t), \tag{2.37}$$

where $\gamma(t)$ is a random process that represents the temporal behavior of the CD source, $\mathbf{b}(\boldsymbol{\eta})$ is the generalized array response vector, $s(t)$ the transmitted CM signal, and $\mathbf{n}(t)$ the random noise process. The generalized array response vector is given by

$$\mathbf{b}(\boldsymbol{\eta}_0) = \int_{\theta \in \Theta} g(\theta; \boldsymbol{\eta}_0)\mathbf{a}(\theta) d\theta, \tag{2.38}$$

where $g(\theta;\boldsymbol{\eta})$ denotes the deterministic *spatial density function* of the CD source with support set Θ. The generalized steering vector in (2.38) is, thus, the integral of the conventional steering vector weighted by the deterministic angular density function. The integral in (2.38) is in Appendix 4.B evaluated for Gaussian and uniform density functions $g(\omega;\boldsymbol{\psi}_0)$, $\boldsymbol{\psi}_0 = [\omega_0, \sigma_\omega]^T$, that are symmetric in electric angle ω, and for the *Gaussian* density function we have

$$[\mathbf{b}(\boldsymbol{\psi}_0)]_k = \exp(-(k\sigma_\omega)^2/2)[\mathbf{a}(\omega_0)]_k, \quad k = 0, \ldots, K-1. \tag{2.39}$$

Similarly, a density function that is *uniform* over $|\omega - \omega_0| < \delta_\omega$, yields

$$[\mathbf{b}(\boldsymbol{\psi}_0)]_k = \frac{\sin(k\delta_\omega)}{k\delta_\omega}[\mathbf{a}(\omega_0)]_k, \quad \delta_\omega = \sqrt{3}\sigma_\omega, \quad k = 0, \ldots, K-1. \tag{2.40}$$

It is further assumed that $\gamma(t)$ is an i.i.d., circularly symmetric, complex normal process, which makes the received snapshot sequence realizations of an i.i.d., circularly symmetric, complex normal vector process. Thus, $\mathbf{x}(t) \sim \mathcal{CN}(0, \sigma_s^2\mathbf{b}\mathbf{b}^H + \sigma_n^2\mathbf{I})$ and i.i.d., where we have included $\sigma_\gamma^2 = \mathrm{E}[|\gamma(t)|^2]$ in the power of the deterministic CM signal $s(t)$, i.e., $\sigma_s^2 = \sigma_\gamma^2|s(t)|^2$. One can also let the signal $s(t)$ be random by letting it absorb the temporal process $\gamma(t)$. Anyway, it yields the same snapshot process, and it is simply a matter of definition in doing so. The extension to multiple CD sources is straightforward once they are assumed to be uncorrelated.

Cramér-Rao Lower Bound for CD Sources

The CRLB for a coherently distributed source has been calculated in [GM98], and is given by

$$\mathrm{E}\left[(\hat{\boldsymbol{\eta}} - \boldsymbol{\eta})(\hat{\boldsymbol{\eta}} - \boldsymbol{\eta})^T\right] \geq \frac{1+\beta\rho}{2N\beta\rho^2}\left[\mathrm{Re}\left\{\mathbf{B}_{\boldsymbol{\eta}}^H\mathbf{P}_{\mathbf{b}}^{\perp}\mathbf{B}_{\boldsymbol{\eta}}\right\}\right]^{-1}, \tag{2.41}$$

where $\boldsymbol{\eta} = [\theta, \sigma_\theta]^T$, and

$$\mathbf{P}_{\mathbf{b}}^{\perp} = \mathbf{I}_K - \frac{\mathbf{b}\mathbf{b}^H}{\beta}, \quad \beta = \mathbf{b}^H\mathbf{b}, \quad \rho = \frac{\sigma_s^2}{\sigma_n^2}, \quad \mathbf{B}_{\boldsymbol{\eta}} = \left[\frac{\partial\mathbf{b}}{\partial\theta}, \frac{\partial\mathbf{b}}{\partial\sigma_\theta}\right]. \tag{2.42}$$

2.3 Beamforming

A digital beamformer can be seen as a spatial filter that can enhance a signal coming from a certain direction (the signal of interest) while, for example, attenuating noise and interfering signals. The desired application of the

beamformer yields different design criteria, and a more detailed treatment of the various beamformers and their respective design criteria can be found in [VB88].

In order to attenuate certain spatial directions in favor of others, a linear combination of the array outputs is formed

$$y(t) = \sum_{i=1}^{K} w_i^* x_i(t) = \mathbf{w}^H \mathbf{x}(t) \ , \tag{2.43}$$

where $y(t)$ is the output of the spatial filter (beamformer), and $\mathbf{w}$ the weight vector. Two popular ways of choosing the weight vector is the *conventional beamforming* approach and *Capon's beamformer*.

Conventional Beamformer

Given the output signal $y(t)$, the expected beamformer output power is given by

$$P(\mathbf{w}) = \mathrm{E}[|y(t)|^2] = \mathbf{w}^H \mathrm{E}[\mathbf{x}(t)\mathbf{x}^H(t)]\mathbf{w} = \mathbf{w}^H \mathbf{R}_x \mathbf{w} \ , \tag{2.44}$$

where $\mathbf{R}_x$ is the data covariance matrix.

The *Conventional Beamformer (CBF)* (or *Bartlett* beamformer) attempts to maximize the expected output power, which in white noise is equivalent of maximizing the expected output SNR. Therefore, it is sometimes also called the maximum SNR beamformer. Suppose there is only one point source signal present, i.e.,

$$\mathbf{x}(t) = \mathbf{a}(\theta)s(t) + \mathbf{n}(t) \ , \tag{2.45}$$

then, the problem is formulated as

$$\begin{aligned} &\max_{\mathbf{w}} \mathrm{E}\left[\mathbf{w}^H \mathbf{x}(t)\mathbf{x}^H(t)\mathbf{w}\right] \quad \text{s.t.} \quad \|\mathbf{w}\| = 1 \quad \Longleftrightarrow \\ &\max_{\mathbf{w}} \left\{ \mathrm{E}\left[|s(t)|^2\right] \left|\mathbf{w}^H \mathbf{a}(\theta)\right|^2 + \sigma_n^2 \right\} \quad \text{s.t.} \quad \|\mathbf{w}\| = 1. \end{aligned} \tag{2.46}$$

The maximum obviously is found when $\mathbf{w}$ is chosen parallel to $\mathbf{a}(\theta)$, i.e.,

$$\mathbf{w}_{\mathrm{CBF}} = \frac{\mathbf{a}(\theta)}{\|\mathbf{a}(\theta)\|}. \tag{2.47}$$

Intuitively, this weight vector can be seen as if it equalizes the delays experienced by the signals on the different sensors to maximally combine their respective contribution to the beamformer output, i.e., it is a *matched filter*.

By inserting the obtained weighting vector into (2.44), the conventional beamforming spectrum is obtained as

$$P_{\mathrm{CBF}}(\theta) = \frac{\mathbf{a}^H(\theta)\mathbf{R}_x\mathbf{a}(\theta)}{\|\mathbf{a}(\theta)\|^2}, \tag{2.48}$$

which is the criterion function in (2.44). In the case of a ULA, the conventional beamforming spectrum is the spatial equivalent to the nonparametric Fourier-based *periodogram* which can be used for estimating the spectrum of a time series [Hay96]. It also inherits the limited resolution of the periodogram, which means that the resolution can not be better than the array beamwidth, no matter how many snapshots are collected or high the SNR is.

The DOA estimate is identified from the largest peak of the 1-D beamforming spectrum (2.48), and the DOAs of multiple, say q, point sources are identified from the q largest peaks of the beamforming spectrum. Under the assumption of a single point source and a Gaussian data model, the DOA estimate attained by the conventional beamformer coincides with the *Maximum Likelihood (ML)* estimate [KV96].

The standard beamwidth (also called Rayleigh beamwidth) for a ULA is $\omega_B = 2\pi/K$ rad. in electric angle, which approximately implies for a standard ULA, $\theta_B = 360^\circ/(\pi K)$ in physical angle. This means that point sources that are less than θ_B degrees apart will not be resolved by the conventional beamformer.

In practice, the data covariance matrix is replaced by the sample covariance matrix $\hat{\mathbf{R}}_x$, which is defined as

$$\hat{\mathbf{R}}_x = \frac{1}{N}\sum_{t=1}^{N}\mathbf{x}(t)\mathbf{x}^H(t)\ , \tag{2.49}$$

where N is the number of snapshots. The sample covariance matrix is a consistent estimate of the covariance matrix $\mathbf{R}_x$ under fairly general conditions [WF91].

Capon's Beamformer

While the conventional beamformer attempts to maximize the output power in a certain direction, *Capon's* or the *Minimum Variance Distortionless Response (MVDR)* beamformer [Cap69, Lac71] attempts to minimize the output power in every other direction, while keeping a fixed gain in the "looking" direction. In short, it works like a narrow spatial bandpass filter. The problem is formulated as follows

$$\min_{\mathbf{w}} \mathbf{w}^H\mathbf{R}_x\mathbf{w} \quad \text{s.t.} \quad \mathbf{w}^H\mathbf{a}(\theta) = 1\ , \tag{2.50}$$

and with the following change of variables

$$\tilde{\mathbf{w}} = \mathbf{R}_x^{1/2}\mathbf{w} \ , \quad \tilde{\mathbf{a}}(\theta) = \mathbf{R}_x^{-1/2}\mathbf{a}(\theta) \ ,$$

and by using the fact that $\mathbf{R}_x^{1/2}$ is the Hermitian square root, the problem becomes

$$\min_{\tilde{\mathbf{w}}} \tilde{\mathbf{w}}^H\tilde{\mathbf{w}} \quad \text{s.t.} \quad \tilde{\mathbf{w}}^H\tilde{\mathbf{a}}(\theta) = 1, \tag{2.51}$$

where $\tilde{\mathbf{w}}^H\tilde{\mathbf{w}} = \|\tilde{\mathbf{w}}\|^2$. The solution is now the least-norm vector $\tilde{\mathbf{w}}$ which satisfies the inner-product $\tilde{\mathbf{w}}^H\tilde{\mathbf{a}}(\theta) = 1$, i.e., $\tilde{\mathbf{w}}$ is parallel to $\tilde{\mathbf{a}}(\theta)$, and to be more exact $\tilde{\mathbf{w}} = \tilde{\mathbf{a}}(\theta)/\left\|\tilde{\mathbf{a}}(\theta)\right\|^2$. Finally back-substituting gives us

$$\mathbf{w}_{\text{Cap}} = \frac{\mathbf{R}_x^{-1}\mathbf{a}(\theta)}{\mathbf{a}^H(\theta)\mathbf{R}_x^{-1}\mathbf{a}(\theta)} \ , \tag{2.52}$$

which results in the following spectrum for Capon's beamformer

$$P_{\text{Cap}}(\theta) = \frac{1}{\mathbf{a}^H(\theta)\mathbf{R}_x^{-1}\mathbf{a}(\theta)} \tag{2.53}$$

Compared to the conventional beamformer, Capon's beamformer has the advantage that it reduces the spectral interference from other closely spaced sources by placing "spatial nulls" in the directions of these "interfering" sources. Capon's beamformer is therefore suited for scenarios with closely spaced point sources where it can more successfully resolve the sources. Capon's beamformer is also called an *adaptive beamformer* since its weight vector depends on the data, while the conventional beamformer is data independent. In practice, since Capon's beamformer uses the inverse of the sample covariance matrix, it requires that the number of snapshots is much larger than the number of sensors, i.e., $N \gg K$.

Modified Capon's Spectrum

Pisarenko introduced in [Pis72] extensions to Capon's beamformer that are based on non-linear functions of the covariance matrix. In Pisarenko's extended version of Capon's method, the DOA estimates are taken from the modified spectrum

$$P_{\text{mCap}}(\theta) = \frac{1}{\left[\mathbf{a}^H(\theta)\mathbf{R}_x^{-m}\mathbf{a}(\theta)\right]^{1/m}} \ , \tag{2.54}$$

where $m \geq 1$ (the special case $m = 1$ renders Capon's method). By taking the m^{th} root of the spectrum its unit is still power. It is shown in [VB96]

that Pisarenko's modification gives higher resolution compared to the original Capon's method, and if the background noise is spatially white, it tends to the *Multiple Signal Classification (MUSIC)* algorithm [Sch79] as $m \to \infty$.

If we eigen-decompose the covariance matrix into

$$\mathbf{R}_x = \sum_{i=1}^{K} \lambda_i \mathbf{e}_i \mathbf{e}_i^H = \mathbf{E}\mathbf{\Lambda}\mathbf{E}^H,$$

then, the inverse raised to the power of m can be written as

$$\mathbf{R}_x^{-m} = \sum_{i=1}^{K} \lambda_i^{-m} \mathbf{e}_i \mathbf{e}_i^H = \mathbf{E}\mathbf{\Lambda}^{-m}\mathbf{E}^H.$$

We can now see that Pisarenko's method, using the inverse of the eigenvalues raised to the power of m, performs a weighting of the eigenvectors. This way, the contribution to the *inverse* spectrum made by the eigenvectors that correspond to small eigenvalues (typically noise or weak signal vectors) is enhanced, and the contribution by the eigenvectors corresponding to large eigenvalues (typically strong signal vectors) is suppressed, i.e., the main contribution comes from the noise eigenvectors. With this observation in mind, we see how Pisarenko's modified spectrum presented in 1972 is similar to a weighted version of the original MUSIC spectrum presented by Schmidt in 1979 [Sch79]. The difference is that all eigenvectors are used instead of, as in MUSIC, only the noise eigenvectors.

Chapter 3

Nonparametric Estimation: Beamforming

This chapter introduces low-complexity spectral-based estimators for nonparametric estimation of a Incoherently Distributed (ID) source. The estimates are simply acquired from the moments of the beamforming spectrum which serves as an estimate of true power spectrum. The performance is evaluated by numerical examples and the estimators are also applied to indoor measurement data. Finally a statistical performance analysis is conducted and verified numerically. The material comprised in this chapter has previously been published in the conference papers [Col02b, Col02a, Col03, CV03].

3.1 Spectral-Based ID Source Parameter Estimation

The DOA of a single deterministic point source is usually identified from the peak of the beamforming spectrum

$$\hat{\theta} = \arg\max_{\theta} \hat{P}(\theta) \ , \tag{3.1}$$

where $\hat{P}(\theta)$ denotes the estimated spectrum, from the sample covariance matrix. The performance of CBF for distributed sources was analyzed in [RGM98], where the nominal DOA estimate was taken from (3.1). In general, the performance of the peak-finding algorithm is poor for ID sources, and it is found in the simulations (Section 3.3.1) that the *Center of Mass (CoM)* of the estimated spectrum is a better estimate of the nominal angle of a single ID source. Next, we will derive a spectral-based algorithm for ID source parameter estimation.

When deriving our spectral-based estimates we use the assumption of orthogonal steering vectors. It is shown in Appendix 3.A that the steering vectors of a ULA that correspond to distinct directions are orthogonal as $K \to \infty$, i.e.,

$$\lim_{K\to\infty} \frac{1}{K}\mathbf{a}^H(\theta)\mathbf{a}(\eta) = \begin{cases} 1\,, & \theta = \eta \\ 0\,, & \theta \neq \eta. \end{cases} \tag{3.2}$$

Hence, for large K we have $\frac{1}{K}\mathbf{A}^H(\boldsymbol{\theta})\mathbf{A}(\boldsymbol{\theta}) \approx \mathbf{I}_L$, where $\mathbf{A}(\boldsymbol{\theta})$ denotes the $K \times L$ steering matrix of the vector $\boldsymbol{\theta} = [\theta_1, \ldots, \theta_L]^T$. Note that letting the numbers of sensors tend to infinity has impact on the validity of the model, since the narrowband assumption does not hold for infinitely large arrays, and the array gain would be infinite. The assumption of orthogonal steering vectors is a mathematical result which is purely used to simplify the derivations. For example in the simulations section, we use K-values ranging from four to twenty, which clearly does not satisfy the orthogonality property.

The discrete version of the channel covariance matrix in (2.21) can be written as

$$\mathbf{R}_h = \sum_{\ell=1}^{L} p(\theta_\ell; \theta_0, \sigma_\theta)\mathbf{a}(\theta_\ell)\mathbf{a}^H(\theta_\ell) = \mathbf{A}(\boldsymbol{\theta})\mathbf{P}(\boldsymbol{\theta})\mathbf{A}^H(\boldsymbol{\theta})\,, \tag{3.3}$$

where $\mathbf{P}(\boldsymbol{\theta})$ denotes a diagonal matrix with the power mass entries $[\mathbf{P}(\boldsymbol{\theta})]_{\ell\ell} = p(\theta_\ell; \theta_0, \sigma_\theta)$. Since it is only non-zero values of $p(\theta_\ell; \theta_0, \sigma_\theta)$ that contribute to the channel covariance matrix, we assume $p(\theta_\ell; \theta_0, \sigma_\theta) > 0$ to make $\mathbf{P}(\boldsymbol{\theta})$ full rank. Note that in this context, θ_ℓ is equal to the nominal DOA θ_0 plus the previously introduced random deviation $\tilde{\theta}_\ell$ of ray ℓ.

To find the inverse of the covariance matrix, we use the matrix inversion lemma, which is stated as [HJ85]

Lemma 1 (MATRIX INVERSION LEMMA) *If A is $(n \times n)$, B is $(n \times m)$, C is $(m \times m)$, and D is $(m \times n)$. Then, if all the involved inverses exist, the following equality holds*

$$(A + BCD)^{-1} = A^{-1} - A^{-1}B(DA^{-1}B + C^{-1})^{-1}DA^{-1}. \tag{3.4}$$

Proof: The details of the proof are omitted, although it follows by attaining the identity matrix when multiplying the matrix $(A + BCD)$ with its inverse given by the right-handside of (3.4). □

For notational simplicity, we will use the following short-hand notation: $\mathbf{a}_\ell = \mathbf{a}(\theta_\ell)$, $p_\ell = p(\theta_\ell; \theta_0, \sigma_\theta)$, $\mathbf{A} = \mathbf{A}(\boldsymbol{\theta})$, and $\mathbf{P} = \mathbf{P}(\boldsymbol{\theta})$, where the vector $\boldsymbol{\theta} = [\theta_1, \ldots, \theta_L]^T$.

Using the assumption of orthogonal steering vectors (i.e., $\mathbf{A}^H\mathbf{A} = K\mathbf{I}_L$) together with the matrix inversion lemma, the inverse covariance matrix becomes

$$\begin{aligned}\mathbf{R}_x^{-1} &= (\sigma_s^2\mathbf{R}_h + \sigma_n^2\mathbf{I})^{-1} = (\sigma_s^2\mathbf{A}\mathbf{P}\mathbf{A}^H + \sigma_n^2\mathbf{I})^{-1} \\ &= \sigma_n^{-2}\mathbf{I} - \sigma_n^{-4}\sigma_s^2\mathbf{A}(\mathbf{P}^{-1} + \sigma_n^{-2}\sigma_s^2K\mathbf{I})^{-1}\mathbf{A}^H \\ &= \sigma_n^{-2}\mathbf{I} - \sigma_n^{-4}\sigma_s^2\mathbf{A}\,\mathrm{diag}\left(\frac{p_1}{1+\sigma_n^{-2}\sigma_s^2Kp_1},\ldots,\frac{p_L}{1+\sigma_n^{-2}\sigma_s^2Kp_L}\right)\mathbf{A}^H \\ &= \sigma_n^{-2}\mathbf{I} + \sigma_s^2\mathbf{A}\check{\mathbf{P}}\mathbf{A}^H, \end{aligned} \tag{3.5}$$

where $\mathbf{P}$ and $\check{\mathbf{P}}$ are diagonal matrices with entries $[\mathbf{P}]_{\ell\ell} = p_\ell \neq 0$ and $[\check{\mathbf{P}}]_{\ell\ell} = -\frac{p_\ell}{\sigma_n^4+\sigma_n^2\sigma_s^2Kp_\ell}$, respectively.

Since the steering vectors are assumed to be orthogonal, we have $\mathbf{a}_\ell^H\mathbf{A} = K\mathbf{e}_\ell^T$ and $\mathbf{A}^H\mathbf{a}_\ell = K\mathbf{e}_\ell$, where $\mathbf{e}_\ell$ is the $(K\times 1)$ all zero vector except for a one in the ℓ^{th} position. Inserting the true covariance matrix into the formula for the CBF spectrum (2.48), we obtain the following relationship

$$\begin{aligned}P_{\text{CBF}}(\theta_\ell) &= \frac{\mathbf{a}_\ell^H\mathbf{R}_x\mathbf{a}_\ell}{\|\mathbf{a}_\ell\|^2} = \frac{\mathbf{a}_\ell^H[\sigma_s^2\mathbf{A}\mathbf{P}\mathbf{A}^H + \sigma_n^2\mathbf{I}]\mathbf{a}_\ell}{K} \\ &= \frac{\sigma_s^2\mathbf{a}_\ell^H\mathbf{A}\mathbf{P}\mathbf{A}^H\mathbf{a}_\ell + \sigma_n^2K}{K} \\ &= \frac{\sigma_s^2K^2\mathbf{e}_\ell^T\mathbf{P}\mathbf{e}_\ell + \sigma_n^2K}{K} = \sigma_s^2Kp_\ell + \sigma_n^2, \quad \theta_\ell \in \Theta, \end{aligned} \tag{3.6}$$

where $\Theta = \{\theta_1,\ldots,\theta_L\}$, and if $\theta_\ell \notin \Theta$ then $P_{\text{CBF}}(\theta_\ell) = \sigma_n^2$.

Finally, we insert the inverse covariance matrix (3.5) into Capon's spectrum (2.53) to obtain the following relationship

$$\begin{aligned}P_{\text{Cap}}(\theta_\ell) &= \frac{1}{\mathbf{a}_\ell^H\mathbf{R}_x^{-1}\mathbf{a}_\ell} = \frac{1}{\mathbf{a}_\ell^H[\sigma_s^2\mathbf{A}\check{\mathbf{P}}\mathbf{A}^H + \sigma_n^{-2}\mathbf{I}]\mathbf{a}_\ell} \\ &= \frac{1}{\sigma_s^2K^2\mathbf{e}_\ell^T\check{\mathbf{P}}\mathbf{e}_\ell + \sigma_n^{-2}K} \\ &= \frac{1}{-\sigma_s^2K^2\frac{p_\ell}{\sigma_n^4+\sigma_n^2\sigma_s^2Kp_\ell} + \sigma_n^{-2}K} = \sigma_s^2p_\ell + \frac{\sigma_n^2}{K}, \quad \theta_\ell \in \Theta. \end{aligned} \tag{3.7}$$

Also here, if $\theta_\ell \notin \Theta$ then $P_{\text{Cap}}(\theta_\ell) = \frac{\sigma_n^2}{K}$.

To summarize, (3.6) and (3.7) describe relationships between the spectrum and the underlying Spatial Power Density Function (SPDF) of the ID source. These relationships are the main findings and lead to the spectral-based estimates of the nominal DOA and spread parameters. The relationship is summarized in the following equation

$$P(\theta_\ell) = \beta p(\theta_\ell;\theta_0,\sigma_\theta) + \varepsilon\ , \quad \beta \geq 0,\ \varepsilon \geq 0 \tag{3.8}$$

where $\beta = \sigma_s^2 K$, $\varepsilon = \sigma_n^2$ for the CBF spectrum, and $\beta = \sigma_s^2$, $\varepsilon = \frac{\sigma_n^2}{K}$ for Capon's spectrum. Equation (3.8) shows that the spectrum has, approximately, an affine relation to the underlying SPDF. In the noise-free case, the relation is linear.

Now, to find our parameters $\{\theta_0, \sigma_\theta\}$ we have to decide the support Θ of the underlying SPDF. Although the underlying SPDF does not necessarily have a finite support (e.g., Gaussian PDF), we have to restrict the support to be finite. For example, the support of a Gaussian PDF with mean θ_0 and standard deviation σ_θ can with negligible error be restricted to $[\theta_0 - 3\sigma_\theta, \theta_0 + 3\sigma_\theta] \subset (-90°, 90°)$. The obvious problem that arises here is how to choose the support. One criterion for choosing it is to find the region where the signal part of the spectrum is distinct from the noise power level. For a single ID source, for example, taking the median value of the spectrum or performing some averaging in the tails of the spectrum may give a good enough estimate of the noise level. Since it is reasonable to assume that the noise power is independent of the transmitted signal, another simple solution is, thus, to compute the received power while the transmitter is shut down.

When we have decided the support Θ, the unknown scaling factor β is easily found. We simply subtract the minimum value of $P(\theta)$ on Θ, which corresponds to ε, from $P(\theta)$. Then we use the fact that $p(\theta_\ell; \theta_0, \sigma_\theta)$ is a PDF (or rather a probability mass function) and should therefore sum to unity, i.e., β can be found as $\beta = \sum_{\theta_\ell \in \Theta} P_o(\theta_\ell)$, where $P_o(\theta) = P(\theta) - \min_{\theta \in \Theta} P(\theta)$ and is non-negative, and θ_ℓ is a fine grid of DOA values in Θ.

Putting it all together and using the definitions of expected value and standard deviation, the nominal DOA actually becomes the *Center of Mass (CoM)* of $P_o(\theta)$ on Θ

$$\theta_0 = \frac{\sum_{\theta_\ell \in \Theta} \theta_\ell P_o(\theta_\ell)}{\sum_{\theta_\ell \in \Theta} P_o(\theta_\ell)} \tag{3.9}$$

and the spatial spread parameter (standard deviation) is given by

$$\sigma_\theta = \left(\frac{\sum_{\theta_\ell \in \Theta} (\theta_\ell - \theta_0)^2 P_o(\theta_\ell)}{\sum_{\theta_\ell \in \Theta} P_o(\theta_\ell)} \right)^{1/2} \tag{3.10}$$

As mentioned earlier, when $L \to \infty$, the distributed source can be described by a continuous SPDF. Consequently, if we compute the spectrum densely enough, the SPDF can be acquired from the spectrum. It should also be mentioned that there is no requirement for the SPDF to be symmetric around its mean value.

Finally, since the true covariance matrix $\mathbf{R}_x$ is unknown, we have to use the sample covariance matrix which is defined as $\hat{\mathbf{R}}_x = \frac{1}{N} \sum_{t=1}^{N} \mathbf{x}(t)\mathbf{x}^H(t)$ to

estimate the spectrum. It is well known that $\hat{\mathbf{R}}_x$ converges (with probability one) to $\mathbf{R}_x$ as $N \to \infty$ [WF91]. Hence, the estimated spectrum is a consistent estimate of the true spectrum, and our estimate of $p(\theta; \theta_0, \sigma_\theta)$ becomes consistent, thus leading to consistent estimates of the nominal DOA and spread parameters. Note that we have used the assumption of orthogonal steering vectors and finite support. If the number of sensors is too small and/or the underlying SPDF is heavy-tailed, the estimate of σ_θ will deteriorate. The accuracy depends on the beamwidth, and a narrow beamwidth yields a higher accuracy. The estimate of θ_0 (being the CoM) is less sensitive to the number of sensors and the restriction to a finite support. The statistical properties of the estimates are, in more detail, analyzed in Section 3.4.

The proposed algorithm is summarized below

1. Form $\hat{\mathbf{R}}_x = \frac{1}{N}\sum_{t=1}^{N} \mathbf{x}(t)\mathbf{x}^H(t)$
2. Compute the spectrum $\hat{P}(\theta)$ either using (2.48) or (2.53), and choose the support Θ
3. Form $\hat{P}_o(\theta) = \hat{P}(\theta) - \min_{\theta\in\Theta}\hat{P}(\theta)$
4. $\hat{\theta}_0 = \dfrac{\sum_{\theta_\ell\in\Theta} \theta_\ell \hat{P}_o(\theta_\ell)}{\sum_{\theta_\ell\in\Theta} \hat{P}_o(\theta_\ell)}$
5. $\hat{\sigma}_\theta = \left(\dfrac{\sum_{\theta_\ell\in\Theta} (\theta_\ell - \hat{\theta}_0)^2 \hat{P}_o(\theta_\ell)}{\sum_{\theta_\ell\in\Theta} \hat{P}_o(\theta_\ell)}\right)^{1/2}$

Figure 3.1 illustrates $P_o(\theta)/\beta$ for the CBF and Capon spectra when the theoretical angular distribution is Gaussian. Also included are *Non-Linear Least Squares (NLLS)* curve fits of $\beta p(\theta; \theta_0, \sigma_\theta) + \varepsilon$ (where $p(\theta; \theta_0, \sigma_\theta)$ is the Gaussian PDF $\mathcal{N}(\theta_0, \sigma_\theta^2)$) to the spectrum. The NLLS problem is optimized over all four parameters, but since it is linear in β and ε it can be separated and therefore a two-dimensional search is needed to find θ_0 and σ_θ. Both spectral-based PDF estimates $P_o(\theta)/\beta$ show good fit to the underlying Gaussian PDF and motivate the relationship given by (3.8). Note that the NLLS fits are slightly worse than their corresponding PDF estimates. The support for the CBF and Capon estimates is restricted to $\Theta = [\theta_0 - 3\sigma_\theta, \theta_0 + 3\sigma_\theta]$, which causes a better fit than their corresponding NLLS fits.

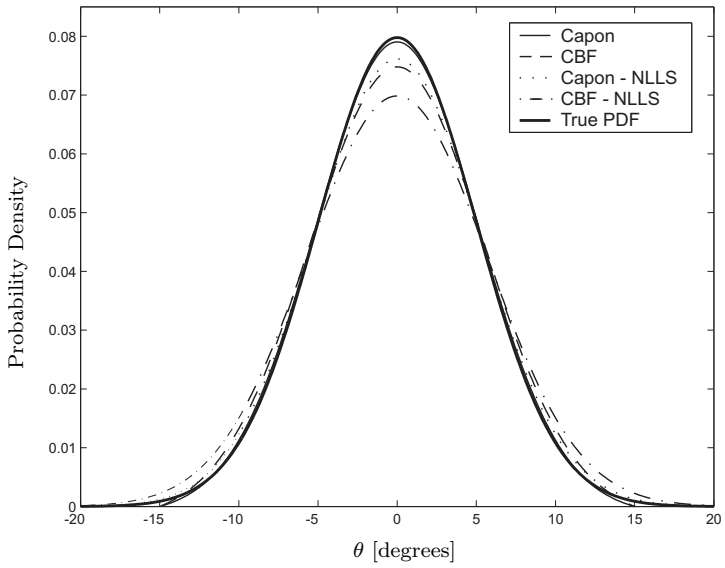

Figure 3.1: Estimated PDFs. Gaussian ID source, $\theta_0 = 0°$, $\sigma_\theta = 5°$, 18 sensors, theoretical covariance matrix with $\sigma_s^2/\sigma_n^2 = 10$ dB.

3.2 High-Resolution Methods

In this section we briefly describe three high-resolution subspace-based DOA estimation methods. Two of these are specially designed for ID sources and are included in the numerical examples for comparison.

Many point source DOA estimation techniques rely on an eigendecomposition of the Hermitian covariance matrix $\mathbf{R}_x$ in (2.16), i.e.,

$$\begin{aligned} \mathbf{R}_x &= \mathbf{A}\mathbf{P}\mathbf{A}^H + \sigma_n^2\mathbf{I} \\ &= \sum_{i=1}^{K} \lambda_i \mathbf{e}_i \mathbf{e}_i^H \\ &= \mathbf{E}_s \mathbf{\Lambda}_s \mathbf{E}_s^H + \sigma_n^2 \mathbf{E}_n \mathbf{E}_n^H \ , \end{aligned} \tag{3.11}$$

where $\mathbf{E}_s = [\mathbf{e}_1, \ldots, \mathbf{e}_L]$ contains the normalized signal eigenvectors, $\mathbf{E}_n = [\mathbf{e}_{L+1}, \ldots, \mathbf{e}_K]$ the normalized noise eigenvectors, and $\mathbf{\Lambda}_s = \mathrm{diag}\,(\lambda_1, \ldots, \lambda_L)$ the signal eigenvalues. All eigenvalues are ordered as $\lambda_1 \geq \ldots \geq \lambda_L > \lambda_{L+1} = \ldots = \lambda_K = \sigma_n^2 > 0$. It is also assumed that $L < K$, where L is the number of point sources and K the number of array elements, and that $\mathbf{A} = \mathbf{A}(\boldsymbol{\theta})$ and $\mathbf{P} = \mathrm{E}[\mathbf{s}(t)\mathbf{s}^H(t)]$ are full-rank matrices. Since $\mathbf{R}_x$ is Hermitian, all eigenvalues are real and their corresponding eigenvectors are

orthogonal (provided that the eigenvalues are distinct). Observe that any vector orthogonal to $\mathbf{A}$ is an eigenvector of $\mathbf{R}_x$ with eigenvalue σ_n^2, and that there are $K - L$ such linearly independent vectors.

MUSIC

The *Multiple Signal Classification (MUSIC)* method [Sch79] utilizes the observation that a vector which is orthogonal to the steering matrix or signal subspace belongs to the noise subspace. Eigen-decompositioning the sample covariance matrix in (2.49) into signal and noise subspace generates an estimate of the noise subspace $\hat{\mathbf{E}}_n$. Assuming one point source with corresponding steering vector $\mathbf{a}(\theta)$, and using this orthogonality observation gives $\hat{\mathbf{E}}_n^H \mathbf{a}(\theta) \approx \mathbf{0}$. The problem of finding the true steering vectors with corresponding DOAs is usually formulated as finding the L largest peaks in the MUSIC pseudo-spectrum

$$P_{\mathrm{MU}}(\theta) = \frac{1}{\mathbf{a}^H(\theta)\hat{\mathbf{E}}_n\hat{\mathbf{E}}_n^H\mathbf{a}(\theta)} \,, \tag{3.12}$$

which is simply the inverse of the squared norm $\|\hat{\mathbf{E}}_n^H \mathbf{a}(\theta)\|^2$.

Since the MUSIC criterion is based on a point source assumption, it will show great deterioration in performance since the noise-free covariance matrix of a ID source is *full-rank* (the rank is equal to the number of sensors) [AO99]. That is, MUSIC will not be able to make the usual eigen-decomposition into true signal and noise subspace.

DISPARE

The *Dispersed Signal Parametric Estimation (DISPARE)* method presented in [MSW96] is especially developed for ID sources. Since the covariance matrix for a ID source is full-rank, it can not be separated into a true signal and noise subspace. It is noticed that the signal energy is mainly concentrated within the first few eigenvalues, see Tables 3.1 and 3.2. Therefore, the dimensionality of the signal subspace is approximated by a number, D, that is smaller than the number of sensors, but usually larger than the number of signals.

From the sample covariance matrix, a pseudo-noise subspace is identified, and by exploiting the orthogonality between the pseudo-signal subspace due to the k^{th} distributed source and the estimated pseudo-noise subspace, the

σ_θ	3°	5°	7°
λ_1	7.00	5.72	4.54
λ_2	9.79×10^{-1}	2.10	2.85
λ_3	2.43×10^{-2}	1.76×10^{-1}	5.80×10^{-1}
λ_4	2.03×10^{-4}	4.37×10^{-3}	3.25×10^{-2}
λ_5	8.02×10^{-7}	4.88×10^{-5}	7.40×10^{-4}
λ_6	1.63×10^{-9}	2.77×10^{-7}	8.38×10^{-6}
λ_7	1.63×10^{-12}	7.80×10^{-10}	4.67×10^{-8}
λ_8	5.22×10^{-16}	8.58×10^{-13}	1.02×10^{-10}

Table 3.1: Eigenvalues of the true and noise-free covariance matrix of a uniform ID source for different spreads and an eight-element std. ULA.

σ_θ	3°	5°	7°
λ_1	7.05	5.95	4.98
λ_2	8.98×10^{-1}	1.75	2.25
λ_3	5.00×10^{-2}	2.69×10^{-1}	6.31×10^{-1}
λ_4	1.64×10^{-3}	2.52×10^{-2}	1.16×10^{-1}
λ_5	3.47×10^{-5}	1.55×10^{-3}	1.46×10^{-2}
λ_6	4.79×10^{-7}	6.30×10^{-5}	1.25×10^{-3}
λ_7	3.96×10^{-9}	1.56×10^{-6}	6.74×10^{-5}
λ_8	1.52×10^{-11}	1.81×10^{-8}	1.76×10^{-6}

Table 3.2: Eigenvalues of the true and noise-free covariance matrix of a Gaussian ID source for different spreads and an eight-element std. ULA.

following DISPARE criterion is formulated

$$\begin{aligned}\{\hat{\theta}_k, \hat{\sigma}_{\theta_k}\} &= \arg\min_{\theta_k,\sigma_{\theta_k}} \left\| \hat{\mathbf{E}}_{pn}^H \mathbf{R}_h(\theta_k, \sigma_{\theta_k}) \right\|_F^2 \\ &= \arg\min_{\theta_k,\sigma_{\theta_k}} \mathrm{Tr}\Big\{ \hat{\mathbf{E}}_{pn}^H \mathbf{R}_h^2(\theta_k, \sigma_{\theta_k}) \hat{\mathbf{E}}_{pn} \Big\} \ , \end{aligned} \tag{3.13}$$

where $\hat{\mathbf{E}}_{pn}$ denotes the estimated pseudo-noise subspace, and $\mathbf{R}_h(\theta_k, \sigma_{\theta_k})$ is the theoretical covariance matrix due to the k^{th} ID source (whose rank is approximately equal to the rank of the corresponding pseudo-signal subspace). By performing a two-dimensional search, the estimates of the nominal DOAs and spread parameters of multiple ID sources are found by locating the q minima of (3.13). Figure 3.2 illustrates an example of the inverse of the DISPARE criterion function.

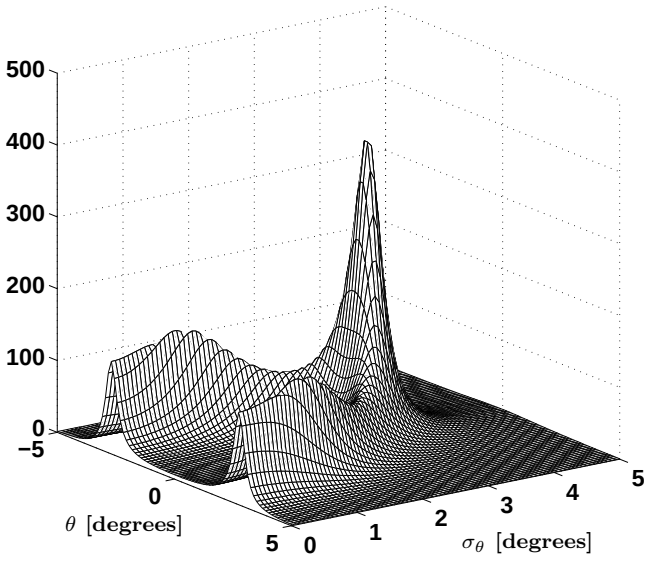

Figure 3.2: Inverse of the DISPARE criterion function. Gaussian ID source, $\theta_0 = 0°$, $\sigma_\theta = 3°$, eight sensors, $D = 2$, true covariance matrix and no noise. Estimated values: $\hat{\theta}_0 = 0.00°$, $\hat{\sigma}_\theta = 2.94°$.

A very similar algorithm is the *Distributed Signal Parameter Estimator (DSPE)* algorithm presented in [VCK95].

WPSF

While DISPARE and DSPE fail to give consistent estimates, a class of *Weighted Subspace Fitting (WSF)* algorithms for consistent estimation has been generalized to handle full-rank data models by approximating the dimensionality of the signal subspace as in DISPARE. The generalized algorithms are called *Weighted Pseudo-Subspace Fitting (WPSF)* and are presented in more detail in [BO01]. Here we describe one version which, according to some weighted norm $\|\cdot\|_{\mathbf{W}}$, attempts to make the parameterized pseudo-noise subspace as orthogonal as possible to the estimated pseudo-signal subspace, thus

$$\{\hat{\theta}_0, \hat{\sigma}_\theta\} = \arg\min_{\theta_0,\sigma_\theta} \left\| \mathbf{E}_{pn}^H(\theta_0, \sigma_\theta)\hat{\mathbf{E}}_{ps} \right\|_{\mathbf{W}} , \tag{3.14}$$

where $\mathbf{E}_{pn}$ and $\hat{\mathbf{E}}_{ps}$ denotes the theoretical pseudo-noise subspace and estimated pseudo-signal subspace respectively. Using this norm, and a consistent estimate of the optimal weighting matrix $\hat{\mathbf{W}}$, gives the following formulation of the WPSF criterion [BO01]

$$\begin{aligned}
\{\hat{\theta}_0, \hat{\sigma}_\theta\} &= \arg\min_{\theta_0,\sigma_\theta} \left\| \hat{\mathbf{\Lambda}}_{pn}^{-1/2} \left(\hat{\mathbf{\Lambda}}_{pn}\mathbf{E}_{pn}^H\hat{\mathbf{E}}_{ps} - \mathbf{E}_{pn}^H\hat{\mathbf{E}}_{ps}\hat{\mathbf{\Lambda}}_{ps} \right) \hat{\mathbf{\Lambda}}_{ps}^{-1/2} \right\|_F^2 \\
&= \arg\min_{\theta_0,\sigma_\theta} \operatorname{Tr}\Big(\hat{\mathbf{E}}_{ps}\hat{\mathbf{\Lambda}}_{ps}^{-1}\hat{\mathbf{E}}_{ps}^H\mathbf{E}_{pn}\hat{\mathbf{\Lambda}}_{pn}\mathbf{E}_{pn}^H \\
&\qquad + \hat{\mathbf{E}}_{ps}\hat{\mathbf{\Lambda}}_{ps}\hat{\mathbf{E}}_{ps}^H\mathbf{E}_{pn}\hat{\mathbf{\Lambda}}_{pn}^{-1}\mathbf{E}_{pn}^H \\
&\qquad - 2\hat{\mathbf{E}}_{ps}\hat{\mathbf{E}}_{ps}^H\mathbf{E}_{pn}\mathbf{E}_{pn}^H \Big) ,
\end{aligned} \tag{3.15}$$

where $\hat{\mathbf{\Lambda}}_{pn}$ and $\hat{\mathbf{\Lambda}}_{ps}$ are the diagonal eigenvalue matrices for the estimated pseudo-noise and pseudo-signal subspaces respectively. Figure 3.3 illustrates an example of the inverse of the WPSF criterion function.

Due to its high computational complexity, WPSF is not a very practical algorithm, but it serves as a bound on how well any low-rank approximation-based algorithm can perform. Therefore, it is included for reference in the numerical examples.

3.3 Data Examples

To illustrate the performance of the beamforming-based techniques, the estimators are, in this section, applied to synthetic data. Finally, the estimators also are applied to measurement data from an indoor channel.

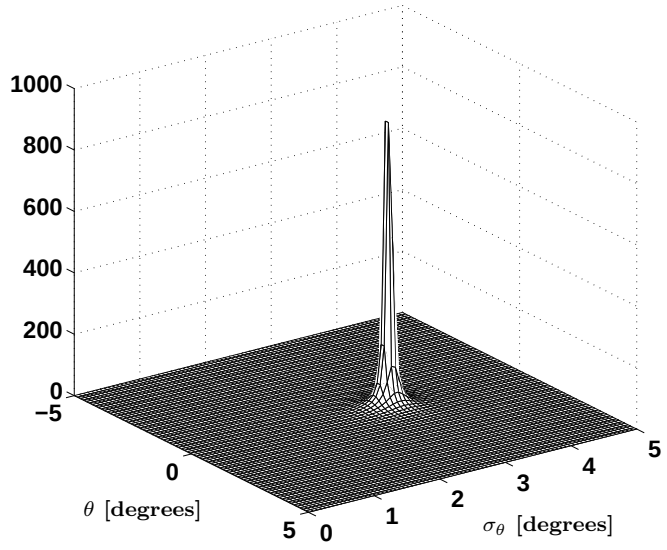

Figure 3.3: Inverse of the WPSF criterion function. Gaussian ID source, $\theta_0 = 0°$, $\sigma_\theta = 3°$, eight sensors, $D = 2$, true covariance matrix and no noise. Estimated values: $\hat{\theta}_0 = 0.00°$, $\hat{\sigma}_\theta = 3.00°$.

3.3.1 Synthetic Data Examples

Here we evaluate the spectral-based estimators' performance when applied to a single Gaussian ID source ($\theta_0 = 0°$, $\sigma_\theta = 5°$) versus the more complex subspace-based DISPARE [MSW96] and WPSF [Ben99, BO01] algorithms. The *Cramér-Rao Lower Bound (CRLB)* (which is based on the continuous model in (2.20) and is found in, e.g., [TO96, Ben99]) and NLLS curve fits based on the Capon spectrum are also included in the figures for reference. Unless otherwise stated, an eight-element standard ULA is used. The received signal is generated from the discrete model in (2.18), with $L = 100$ random DOAs and complex Gaussian gains $\gamma_\ell(t)$, and with a new independent realization for each snapshot. The source signal is an equiprobable BPSK sequence, and the sample covariance matrix is computed over 100 independent channel realizations (snapshots). The DISPARE and WPSF estimates are acquired by letting the dimension, D, (design parameter) of the pseudo-signal subspace be such that it contains at least 95% of the signal energy. To locate the solutions, a two-dimensional search, initialized at the true parameter values, is used. We also let DISPARE and WPSF use the correct

assumption that the deviation is Gaussian distributed. Again, the support of the Capon and CBF estimates is restricted to $\Theta = [\theta_0 - 3\sigma_\theta, \theta_0 + 3\sigma_\theta]$. Since the estimate of θ_0 is taken as the CoM of the spectrum, it is not that sensitive to the choice of Θ. Clearly the spread estimate becomes more sensitive to the width of the interval Θ. The beamforming spectrum is computed with a resolution of 0.1°.

Figures 3.4 and 3.5 show the *Root Mean Square Error (RMSE)* of the estimated parameters $\hat{\theta}_0$ and $\hat{\sigma}_\theta$ versus SNR, respectively. Figures 3.6 and 3.7 show the RMSE of the estimated DOA and spread versus true spread σ_θ for 10 dB SNR. Finally, Figures 3.8 and 3.9 show the RMSE of estimated DOA and spread versus number of sensors for 10 dB SNR. The RMSE is computed over 1000 independent trials for each parameter.

We see that it is better to choose the CoM instead of the peak when estimating the nominal DOA. Capon's spectrum shows very good performance when estimating both the nominal DOA and spread, while CBF suffers from resolution problems for small angular spreads. It is worth noting that the RMSE of the spread estimate is below the CRLB for low SNRs (15 dB and less). This is possible because information about the *restricted* support Θ is incorporated into the estimators but is not captured by the CRLB, which typically shows at low SNR. The CRLB is only valid for unbiased estimators, and the spread estimate is biased via the choice of support (and the array beamwidth).

For increasing spread, DISPARE shows deterioration which is probably caused by a bad choice of pseudo-signal subspace dimension, while WPSF and beamforming are less sensitive to an increasing spread. Also note that the resolution problem of the CBF is overcome for an increasing angular spread. For the same reason as briefly discussed above, the RMSE of Capon's spread estimates are again below the CRLB (SNR is 10 dB).

Finally, as one might expect, when taking the CoM, the performance increases as the number of sensors increases. This is not the case when we take the peak value. Note that the CBF spread estimates become significantly better for increasing number of sensors, which is due to higher resolution capability. The RMSE of Capon's spread estimates are again below CRLB for small numbers of sensors and low SNR (10 dB).

3.3.2 Measurement Data Example

Indoor *Multiple-Input Multiple-Output (MIMO)* channel measurements have been conducted and reported in [SW02]. Figure 3.10 shows the conventional beamforming spectrum evaluated for three different receiver (RX) positions. These spectra have been acquired using circular antenna arrays, each with

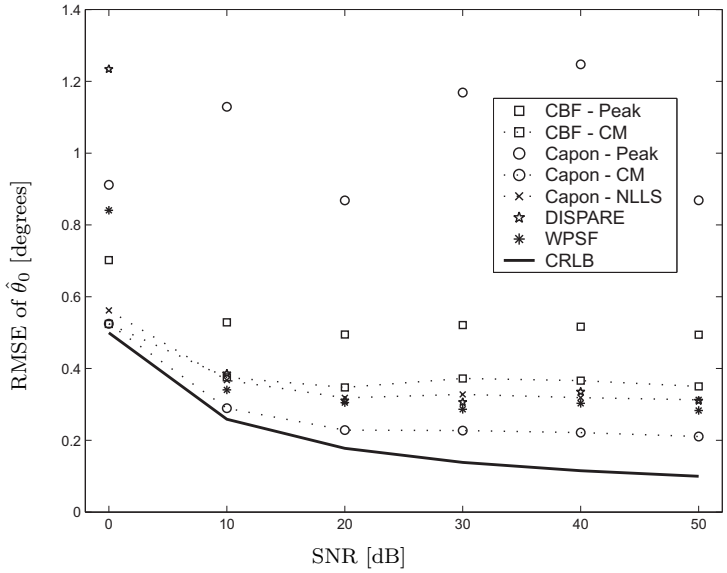

Figure 3.4: RMSE of $\hat{\theta}_0$ for different SNRs. Gaussian ID source, $\theta_0 = 0°$, $\sigma_\theta = 5°$, eight sensors, 100 scatterers.

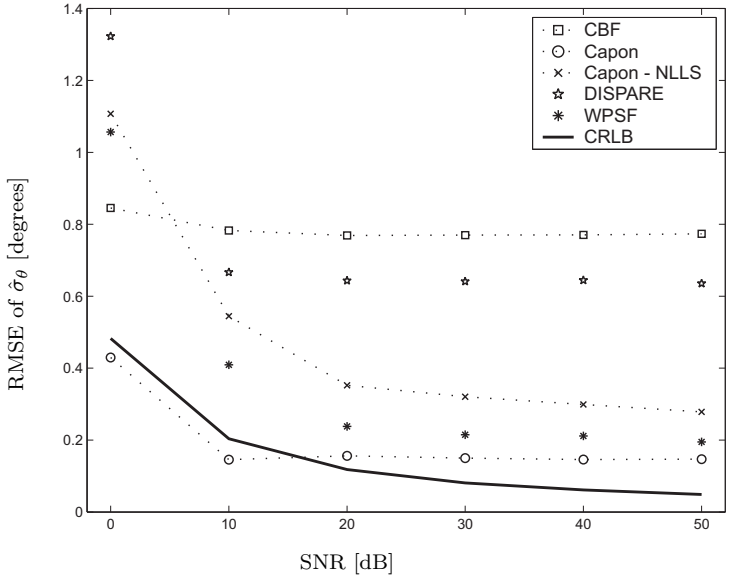

Figure 3.5: RMSE of $\hat{\sigma}_\theta$ for different SNRs. Gaussian ID source, $\theta_0 = 0°$, $\sigma_\theta = 5°$, eight sensors, 100 scatterers.

ten half-wavelength separated monopoles. The transmitter (TX) is focussing

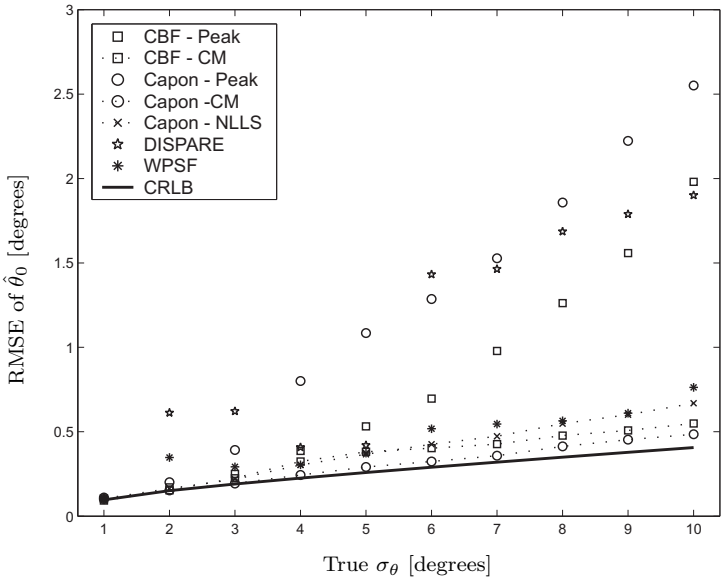

Figure 3.6: RMSE of $\hat{\theta}_0$ for different spreads σ_θ. Gaussian ID source, $\theta_0 = 0°$, eight sensors, 100 scatterers, 10 dB SNR.

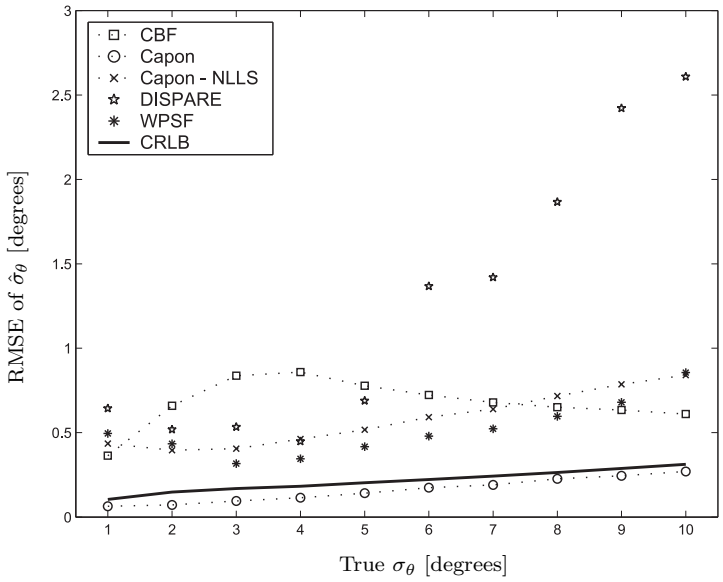

Figure 3.7: RMSE of $\hat{\sigma}_\theta$ for different spreads σ_θ. Gaussian ID source, $\theta_0 = 0°$, eight sensors, 100 scatterers, 10 dB SNR.

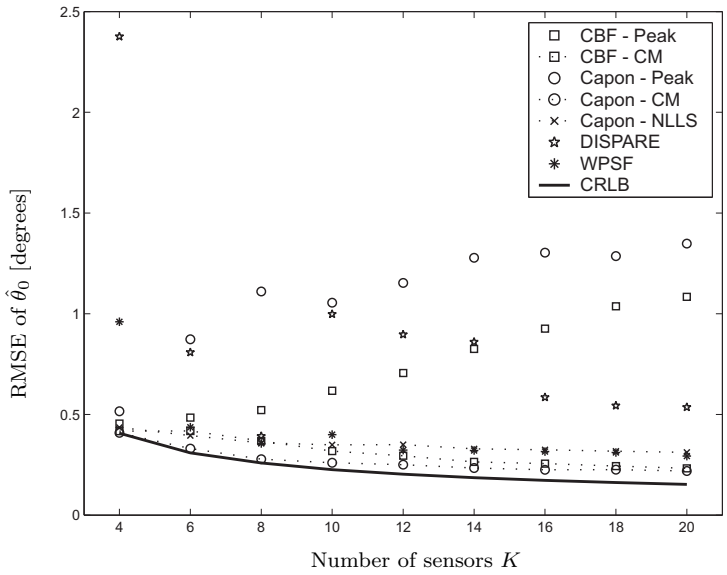

Figure 3.8: RMSE of $\hat{\theta}_0$ for different numbers of sensors K. Gaussian ID source, $\theta_0 = 0°$, $\sigma_\theta = 5°$, 100 scatterers, 10 dB SNR.

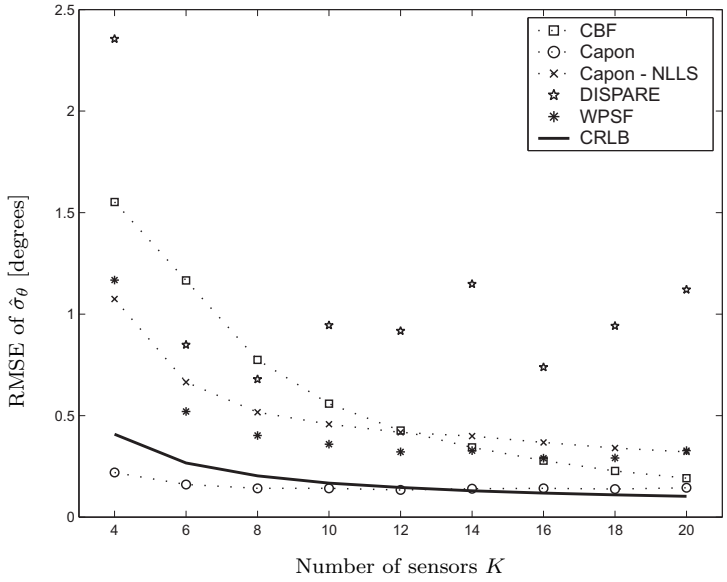

Figure 3.9: RMSE of $\hat{\sigma}_\theta$ for different numbers of sensors K. Gaussian ID source, $\theta_0 = 0°$, $\sigma_\theta = 5°$, 100 scatterers, 10 dB SNR.

its energy in an angular band in the horizontal corridor. First we identify the distributed sources and then we choose their corresponding supports in an *ad-hoc* manual fashion. The results acquired from applying our estimators to the three spectra are summarized in Table 3.3, where the DOA is measured counter-clockwise relative the left-right horizontal axis. For detailed information on the measurement setup and channel estimation procedure, we refer the reader to [SW02].

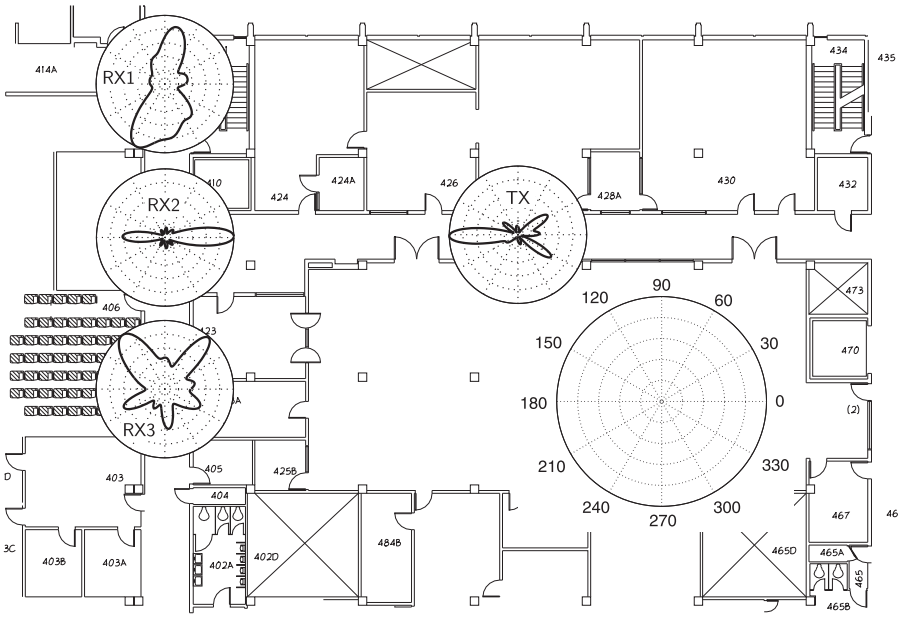

Figure 3.10: Conventional beamforming spectra acquired from a circular array in three different receiver positions.

Of course, when using real data there are no true values available. However, the obtained values agree reasonably well with the appearance of the "local power maxima" that are visible in the spectra. It is also clear that the local spatial distributions are not Gaussian.

3.4 Statistical Performance Analysis of the Nonparametric Estimation Scheme

In this section we derive closed-form analytical expressions for the MSE performances of the spectral-based estimators that were derived earlier in this chapter. Numerical examples are used to validate the theoretical results.

RX position	$\hat{\theta}_0$	$\hat{\sigma}_\theta$
1	80.3°	14.2°
1	265.1°	25.0°
2	1.3°	8.9°
2	178.3°	7.1°
3	49.5°	7.4°
3	129.0°	14.6°
3	203.5°	6.6°
3	275.9°	6.1°
3	333.8°	7.6°

Table 3.3: Estimated nominal DOAs and angular spreads from the conventional beamforming spectra in Figure 3.10.

The MSE performances of the estimators are analytically calculated and approximated by using the first terms of a geometric series expansion and known expectations of *complex Wishart* forms [TC94]. All results are approximations, and are only valid for large numbers of snapshots, i.e., we assume that $N \gg 1$ and for the Capon beamformer we also assume that $N \gg K$, where K is the number of sensors. Further, it is assumed that the noise variance σ_n^2 is known. That is, the parameter ε is known and is given by

$$\varepsilon = \begin{cases} \sigma_n^2 \,, & \text{CBF Spectrum} \\ \frac{\sigma_n^2}{K} \,, & \text{Capon Spectrum.} \end{cases} \tag{3.16}$$

We recall that the nominal DOA estimate is given by

$$\hat{\theta}_0 = \frac{\sum_{\theta_\ell \in \Theta} \theta_\ell \hat{P}_o(\theta_\ell)}{\sum_{\theta_\ell \in \Theta} \hat{P}_o(\theta_\ell)} \,, \tag{3.17}$$

and that the squared spatial spread parameter is given by

$$\hat{\sigma}_\theta^2 = \frac{\sum_{\theta_\ell \in \Theta} (\theta_\ell - \hat{\theta}_0)^2 \hat{P}_o(\theta_\ell)}{\sum_{\theta_\ell \in \Theta} \hat{P}_o(\theta_\ell)} \,, \tag{3.18}$$

where $\hat{P}_o(\theta) = \hat{P}(\theta) - \varepsilon$. Finally, $\hat{P}(\theta)$ is the estimated spectrum and is given by

$$\hat{P}(\theta) = \begin{cases} \frac{\mathbf{a}^H(\theta) \hat{\mathbf{R}}_x \mathbf{a}(\theta)}{K} \,, & \text{CBF Spectrum} \\ \frac{1}{\mathbf{a}^H(\theta) \hat{\mathbf{R}}_x^{-1} \mathbf{a}(\theta)} \,, & \text{Capon Spectrum.} \end{cases} \tag{3.19}$$

We model the transmitted signal $s(t)$ in (2.18) and (2.20) as deterministic and unknown. Hence, in the presence of many independently fading signal rays (large L), the received signal vectors $\{\mathbf{x}(t)\}_{t=1}^{N}$ are i.i.d., and according to the central limit theorem, the signal vectors are approximately $\mathbf{x}(t) \sim \mathcal{CN}(\mathbf{0}, \mathbf{R}_x)$, where $\mathbf{R}_x$ is given by (2.21). It is well known that the sample covariance matrix $\hat{\mathbf{R}}_x = \frac{1}{N}\sum_{t=1}^{N} \mathbf{x}(t)\mathbf{x}^H(t)$ is a consistent estimate of the true covariance matrix $\mathbf{R}_x = \mathrm{E}[\mathbf{x}(t)\mathbf{x}^H(t)]$, i.e., $\hat{\mathbf{R}}_x$ converges (with probability one) to $\mathbf{R}_x$ as $N \to \infty$ [WF91]. The convergence rate is proportional to $1/\sqrt{N}$, and we may write $\hat{\mathbf{R}}_x = \mathbf{R}_x + \tilde{\mathbf{R}}$, where $\tilde{\mathbf{R}} = O_p(1/\sqrt{N})$ is the zero-mean *perturbation* matrix. Further, the inverse of the sample covariance matrix will also contain a perturbation error, and the inverse can be written as

$$\begin{aligned}\hat{\mathbf{R}}_x^{-1} &= (\mathbf{R}_x + \tilde{\mathbf{R}})^{-1} = \Big(\mathbf{R}_x(\mathbf{I} + \mathbf{R}_x^{-1}\tilde{\mathbf{R}})\Big)^{-1} \\ &= \sum_{i=0}^{\infty}(-\mathbf{R}_x^{-1}\tilde{\mathbf{R}})^i\mathbf{R}_x^{-1} = \mathbf{R}_x^{-1}\underbrace{-\mathbf{R}_x^{-1}\tilde{\mathbf{R}}\mathbf{R}_x^{-1} + \cdots}_{\triangleq\tilde{\mathbf{R}}'}, \end{aligned} \tag{3.20}$$

where $\tilde{\mathbf{R}}' = O_p(1/\sqrt{N})$. Since the vectors $\{\mathbf{x}(t)\}_{t=1}^{N}$ are i.i.d. and have a zero-mean complex normal distribution, the sample covariance matrix and its inverse is said to have a *complex Wishart distribution* and a *inverse complex Wishart distribution* [TC94], respectively. Known expectations of complex Wishart forms become very useful when deriving the statistical properties of our estimates.

3.4.1 MSE of $\hat{\theta}_0$

In this section we find analytical closed-form expressions for the MSE performance of the nominal DOA estimates based on the CBF and Capon's spectra. In the derivations it is assumed that given the true covariance matrix, the estimators will render the true value of the nominal DOA. The assumption that $\hat{\theta}_0$ is unbiased is supported by the good agreement between the theoretical and simulated results that are shown in the numerical examples.

Conventional Beamforming

Using (3.17) and (3.19), the nominal DOA estimate using CBF may be written as

$$\begin{aligned}\hat{\theta}_0 &= \frac{\sum_\ell \theta_\ell [\mathbf{a}_\ell^H (\mathbf{R}_x + \tilde{\mathbf{R}}) \mathbf{a}_\ell - K\varepsilon]}{\sum_\ell [\mathbf{a}_\ell^H \hat{\mathbf{R}}_x \mathbf{a}_\ell - K\varepsilon]} \\ &= \frac{\sum_\ell \theta_\ell [\mathbf{a}_\ell^H \mathbf{R}_x \mathbf{a}_\ell - K\varepsilon]}{\sum_\ell [\mathbf{a}_\ell^H \hat{\mathbf{R}}_x \mathbf{a}_\ell - K\varepsilon]} + \frac{\sum_\ell \theta_\ell \mathbf{a}_\ell^H \tilde{\mathbf{R}} \mathbf{a}_\ell}{\sum_\ell [\mathbf{a}_\ell^H \hat{\mathbf{R}}_x \mathbf{a}_\ell - K\varepsilon]} \end{aligned} \tag{3.21}$$

where $\mathbf{a}_\ell = \mathbf{a}(\theta_\ell)$ and the summations are over $\{\ell : \theta_\ell \in \Theta\}$. The first term in (3.21) can be re-written and expanded in a geometric series according to

$$\begin{aligned}&\frac{\sum_\ell \theta_\ell [\mathbf{a}_\ell^H \mathbf{R}_x \mathbf{a}_\ell - K\varepsilon]}{\sum_\ell [\mathbf{a}_\ell^H (\mathbf{R}_x + \tilde{\mathbf{R}}) \mathbf{a}_\ell - K\varepsilon]} \\ &\qquad = \underbrace{\frac{\sum_\ell \theta_\ell [\mathbf{a}_\ell^H \mathbf{R}_x \mathbf{a}_\ell - K\varepsilon]}{\sum_\ell [\mathbf{a}_\ell^H \mathbf{R}_x \mathbf{a}_\ell - K\varepsilon]}}_{=\theta_0} \frac{1}{1 + \frac{\sum_\ell \mathbf{a}_\ell^H \tilde{\mathbf{R}} \mathbf{a}_\ell}{\sum_\ell [\mathbf{a}_\ell^H \mathbf{R}_x \mathbf{a}_\ell - K\varepsilon]}} \\ &\qquad = \theta_0 \left(1 - \frac{\sum_\ell \mathbf{a}_\ell^H \tilde{\mathbf{R}} \mathbf{a}_\ell}{\sum_\ell [\mathbf{a}_\ell^H \mathbf{R}_x \mathbf{a}_\ell - K\varepsilon]} + O_p(1/N) \right), \end{aligned} \tag{3.22}$$

where we in the second equality, since the true covariance matrix is used, have replaced the nominal DOA estimate with its true value. In a similar way, the second term becomes

$$\begin{aligned}&\frac{\sum_\ell \theta_\ell \mathbf{a}_\ell^H \tilde{\mathbf{R}} \mathbf{a}_\ell}{\sum_\ell [\mathbf{a}_\ell^H (\mathbf{R}_x + \tilde{\mathbf{R}}) \mathbf{a}_\ell - K\varepsilon]} \\ &\qquad = \frac{\sum_\ell \theta_\ell \mathbf{a}_\ell^H \tilde{\mathbf{R}} \mathbf{a}_\ell}{\sum_\ell [\mathbf{a}_\ell^H \mathbf{R}_x \mathbf{a}_\ell - K\varepsilon]} \frac{1}{1 + \frac{\sum_\ell \mathbf{a}_\ell^H \tilde{\mathbf{R}} \mathbf{a}_\ell}{\sum_\ell [\mathbf{a}_\ell^H \mathbf{R}_x \mathbf{a}_\ell - K\varepsilon]}} \\ &\qquad = \frac{\sum_\ell \theta_\ell \mathbf{a}_\ell^H \tilde{\mathbf{R}} \mathbf{a}_\ell}{\sum_\ell [\mathbf{a}_\ell^H \mathbf{R}_x \mathbf{a}_\ell - K\varepsilon]} \left(1 + O_p(1/\sqrt{N}) \right) \\ &\qquad = \frac{\sum_\ell \theta_\ell \mathbf{a}_\ell^H \tilde{\mathbf{R}} \mathbf{a}_\ell}{\sum_\ell [\mathbf{a}_\ell^H \mathbf{R}_x \mathbf{a}_\ell - K\varepsilon]} + O_p(1/N). \end{aligned} \tag{3.23}$$

Adding (3.22) and (3.23), yields

$$\hat{\theta}_0 = \theta_0 + \frac{\sum_\ell (\theta_\ell - \theta_0) \mathbf{a}_\ell^H \tilde{\mathbf{R}} \mathbf{a}_\ell}{\sum_\ell [\mathbf{a}_\ell^H \mathbf{R}_x \mathbf{a}_\ell - K\varepsilon]} + O_p(1/N). \tag{3.24}$$

Now, the MSE of $\hat{\theta}_0$ is approximated by

$$\begin{aligned} \mathrm{mse}\Big(\hat{\theta}_0\Big) &= \mathrm{E}[(\hat{\theta}_0 - \theta_0)^2] \approx \mathrm{E}\left[\left(\frac{\sum_\ell (\theta_\ell - \theta_0)\mathbf{a}_\ell^H \tilde{\mathbf{R}} \mathbf{a}_\ell}{\sum_\ell [\mathbf{a}_\ell^H \mathbf{R}_x \mathbf{a}_\ell - K\varepsilon]}\right)^2\right] \\ &= \frac{\sum_k \sum_\ell (\theta_k - \theta_0)(\theta_\ell - \theta_0)\mathbf{a}_k^H \mathrm{E}[\tilde{\mathbf{R}}\mathbf{a}_k \mathbf{a}_\ell^H \tilde{\mathbf{R}}]\mathbf{a}_\ell}{\left(\sum_\ell [\mathbf{a}_\ell^H \mathbf{R}_x \mathbf{a}_\ell - K\varepsilon]\right)^2}, \end{aligned} \tag{3.25}$$

where we have omitted all terms of higher order than $O_p(1/N)$. Since $\tilde{\mathbf{R}} = \hat{\mathbf{R}}_x - \mathbf{R}_x$, where $\hat{\mathbf{R}}_x$ has a complex Wishart distribution, and $\mathrm{E}[\hat{\mathbf{R}}_x] = \mathbf{R}_x$, we may write

$$\begin{aligned} \mathrm{E}[\tilde{\mathbf{R}}\mathbf{a}_k \mathbf{a}_\ell^H \tilde{\mathbf{R}}] &= \mathrm{E}[(\hat{\mathbf{R}}_x - \mathbf{R}_x)\mathbf{a}_k \mathbf{a}_\ell^H (\hat{\mathbf{R}}_x - \mathbf{R}_x)] \\ &= \mathrm{E}[\hat{\mathbf{R}}_x \mathbf{a}_k \mathbf{a}_\ell^H \hat{\mathbf{R}}_x] - \mathbf{R}_x \mathbf{a}_k \mathbf{a}_\ell^H \mathbf{R}_x. \end{aligned} \tag{3.26}$$

The first term in (3.26) is the expected value of a function of a matrix $\hat{\mathbf{R}}_x$ that has a complex Wishart distribution, and the expected value is given by [TC94]

$$\mathrm{E}[\hat{\mathbf{R}}_x \mathbf{a}_k \mathbf{a}_\ell^H \hat{\mathbf{R}}_x] = \mathbf{R}_x \mathbf{a}_k \mathbf{a}_\ell^H \mathbf{R}_x + \frac{1}{N} \underbrace{\mathrm{Tr}\{\mathbf{a}_k \mathbf{a}_\ell^H \mathbf{R}_x\}}_{=\mathbf{a}_\ell^H \mathbf{R}_x \mathbf{a}_k} \mathbf{R}_x. \tag{3.27}$$

Hence, (3.26) evaluates to

$$\mathrm{E}[\tilde{\mathbf{R}}\mathbf{a}_k \mathbf{a}_\ell^H \tilde{\mathbf{R}}] = \frac{1}{N} \mathbf{a}_\ell^H \mathbf{R}_x \mathbf{a}_k \mathbf{R}_x. \tag{3.28}$$

Finally, inserting (3.28) into (3.25) renders the MSE of $\hat{\theta}_0$ for the CBF spectrum

$$\mathrm{mse}\Big(\hat{\theta}_0\Big) \approx \frac{\sum_{k,\ell} (\theta_k - \theta_0)(\theta_\ell - \theta_0) |\mathbf{a}_k^H \mathbf{R}_x \mathbf{a}_\ell|^2}{N[\sum_k (\mathbf{a}_k^H \mathbf{R}_x \mathbf{a}_k - K\varepsilon)]^2} \tag{3.29}$$

where the summation is over $\{k, \ell : \theta_k, \theta_\ell \in \Theta\}$.

Capon's Beamforming

By using $\hat{\mathbf{R}}_x^{-1} = \mathbf{R}_x^{-1} + \tilde{\mathbf{R}}'$, where $\tilde{\mathbf{R}}' = O_p(1/\sqrt{N})$ is the zero-mean (for $N \gg K$) perturbation matrix given by (3.20), Capon's spectrum can be

re-written as

$$\begin{aligned}
\hat{P}(\theta_\ell) &= \frac{1}{\mathbf{a}_\ell^H \hat{\mathbf{R}}_x^{-1} \mathbf{a}_\ell} = \frac{1}{\mathbf{a}_\ell^H (\mathbf{R}_x^{-1} + \tilde{\mathbf{R}}') \mathbf{a}_\ell} = \frac{1}{\mathbf{a}_\ell^H \mathbf{R}_x^{-1} \mathbf{a}_\ell} \frac{1}{1 + \frac{\mathbf{a}_\ell^H \tilde{\mathbf{R}}' \mathbf{a}_\ell}{\mathbf{a}_\ell^H \mathbf{R}_x^{-1} \mathbf{a}_\ell}} \\
&= \frac{1}{\mathbf{a}_\ell^H \mathbf{R}_x^{-1} \mathbf{a}_\ell} \sum_{i=0}^{\infty} \left(- \frac{\mathbf{a}_\ell^H \tilde{\mathbf{R}}' \mathbf{a}_\ell}{\mathbf{a}_\ell^H \mathbf{R}_x^{-1} \mathbf{a}_\ell} \right)^i \\
&= \underbrace{\frac{1}{\mathbf{a}_\ell^H \mathbf{R}_x^{-1} \mathbf{a}_\ell}}_{= P(\theta_\ell)} \underbrace{- \frac{\mathbf{a}_\ell^H \tilde{\mathbf{R}}' \mathbf{a}_\ell}{(\mathbf{a}_\ell^H \mathbf{R}_x^{-1} \mathbf{a}_\ell)^2} + O_p(1/N)}_{\triangleq \tilde{P}(\theta_\ell)} \\
&= P(\theta_\ell) + \tilde{P}(\theta_\ell), \qquad (3.30)
\end{aligned}$$

where $\mathbf{a}_\ell = \mathbf{a}(\theta_\ell)$.

Inserting (3.30) into (3.17), the nominal DOA estimate using Capon's spectrum is given by

$$\begin{aligned}
\hat{\theta}_0 &= \frac{\sum_\ell \theta_\ell \left[P_o(\theta_\ell) + \tilde{P}(\theta_\ell) \right]}{\sum_\ell \hat{P}_o(\theta_\ell)} \\
&= \frac{\sum_\ell \theta_\ell P_o(\theta_\ell)}{\sum_\ell \hat{P}_o(\theta_\ell)} + \frac{\sum_\ell \theta_\ell \tilde{P}(\theta_\ell)}{\sum_\ell \hat{P}_o(\theta_\ell)} \qquad (3.31)
\end{aligned}$$

where the summations are over $\{\ell : \theta_\ell \in \Theta\}$.

The first term in (3.31) can also be re-written and expanded in a geometric series according to

$$\begin{aligned}
\frac{\sum_\ell \theta_\ell P_o(\theta_\ell)}{\sum_\ell [P_o(\theta_\ell) + \tilde{P}(\theta_\ell)]} &= \underbrace{\frac{\sum_\ell \theta_\ell P_o(\theta_\ell)}{\sum_\ell P_o(\theta_\ell)}}_{= \theta_0} \frac{1}{1 + \frac{\sum_\ell \tilde{P}(\theta_\ell)}{\sum_\ell P_o(\theta_\ell)}} \\
&= \theta_0 \left(1 - \frac{\sum_\ell \tilde{P}(\theta_\ell)}{\sum_\ell P_o(\theta_\ell)} + O_p(1/N) \right), \qquad (3.32)
\end{aligned}$$

where we in the second equality, since the true covariance matrix is used, have replaced the DOA estimate with its true value. In a similar fashion, the second term becomes

$$\begin{aligned}
\frac{\sum_\ell \theta_\ell \tilde{P}(\theta_\ell)}{\sum_\ell [P_o(\theta_\ell) + \tilde{P}(\theta_\ell)]} &= \frac{\sum_\ell \theta_\ell \tilde{P}(\theta_\ell)}{\sum_\ell P_o(\theta_\ell)} \frac{1}{1 + \frac{\sum_\ell \tilde{P}(\theta_\ell)}{\sum_\ell P_o(\theta_\ell)}} \\
&= \frac{\sum_\ell \theta_\ell \tilde{P}(\theta_\ell)}{\sum_\ell P_o(\theta_\ell)} \left(1 + O_p(1/\sqrt{N}) \right) \\
&= \frac{\sum_\ell \theta_\ell \tilde{P}(\theta_\ell)}{\sum_\ell P_o(\theta_\ell)} + O_p(1/N). \qquad (3.33)
\end{aligned}$$

Adding (3.32) and (3.33), yields

$$\hat{\theta}_0 = \theta_0 + \frac{\sum_\ell (\theta_\ell - \theta_0)\tilde{P}(\theta_\ell)}{\sum_\ell P_o(\theta_\ell)} + O_p(1/N), \tag{3.34}$$

and the MSE of $\hat{\theta}_0$ is now approximated by

$$\begin{aligned} \mathrm{mse}\Big(\hat{\theta}_0\Big) &= \mathrm{E}[(\hat{\theta}_0 - \theta_0)^2] \approx \mathrm{E}\left[\left(\frac{\sum_\ell (\theta_\ell - \theta_0)\tilde{P}(\theta_\ell)}{\sum_\ell P_o(\theta_\ell)}\right)^2\right] \\ &= \frac{\sum_k \sum_\ell (\theta_k - \theta_0)(\theta_\ell - \theta_0)\mathrm{E}[\tilde{P}(\theta_k)\tilde{P}(\theta_\ell)]}{\left(\sum_\ell P_o(\theta_\ell)\right)^2} \\ &= \frac{\sum_k \sum_\ell (\theta_k - \theta_0)(\theta_\ell - \theta_0)\bar{\mathbf{a}}_k^H \mathrm{E}[\tilde{\mathbf{R}}'\bar{\mathbf{a}}_k\bar{\mathbf{a}}_\ell^H\tilde{\mathbf{R}}']\bar{\mathbf{a}}_\ell}{\left(\sum_\ell P_o(\theta_\ell)\right)^2}, \end{aligned} \tag{3.35}$$

where $\bar{\mathbf{a}}_\ell \triangleq \mathbf{a}_\ell/(\mathbf{a}_\ell^H\mathbf{R}_x^{-1}\mathbf{a}_\ell)$, and we have omitted terms of higher order than $O_p(1/N)$.

Since $\tilde{\mathbf{R}}' = \hat{\mathbf{R}}_x^{-1} - \mathbf{R}_x^{-1}$ and $\mathrm{E}[\hat{\mathbf{R}}_x^{-1}] = \mathbf{R}_x^{-1}$ (valid for $N \gg K$), we may write

$$\begin{aligned} \mathrm{E}[\tilde{\mathbf{R}}'\bar{\mathbf{a}}_k\bar{\mathbf{a}}_\ell^H\tilde{\mathbf{R}}'] &= \mathrm{E}[(\hat{\mathbf{R}}_x^{-1} - \mathbf{R}_x^{-1})\bar{\mathbf{a}}_k\bar{\mathbf{a}}_\ell^H(\hat{\mathbf{R}}_x^{-1} - \mathbf{R}_x^{-1})] \\ &= \mathrm{E}[\hat{\mathbf{R}}_x^{-1}\bar{\mathbf{a}}_k\bar{\mathbf{a}}_\ell^H\hat{\mathbf{R}}_x^{-1}] - \mathbf{R}_x^{-1}\bar{\mathbf{a}}_k\bar{\mathbf{a}}_\ell^H\mathbf{R}_x^{-1}. \end{aligned} \tag{3.36}$$

For $N \gg K$, the first term in (3.36) has the expected value [TC94]

$$\mathrm{E}[\hat{\mathbf{R}}_x^{-1}\bar{\mathbf{a}}_k\bar{\mathbf{a}}_\ell^H\hat{\mathbf{R}}_x^{-1}] = \mathbf{R}_x^{-1}\bar{\mathbf{a}}_k\bar{\mathbf{a}}_\ell^H\mathbf{R}_x^{-1} + \frac{1}{N}\underbrace{\mathrm{Tr}\{\bar{\mathbf{a}}_k\bar{\mathbf{a}}_\ell^H\mathbf{R}_x^{-1}\}}_{=\bar{\mathbf{a}}_\ell^H\mathbf{R}_x^{-1}\bar{\mathbf{a}}_k}\mathbf{R}_x^{-1}. \tag{3.37}$$

Hence, (3.36) evaluates to

$$\mathrm{E}[\tilde{\mathbf{R}}'\bar{\mathbf{a}}_k\bar{\mathbf{a}}_\ell^H\tilde{\mathbf{R}}'] = \frac{1}{N}\bar{\mathbf{a}}_\ell^H\mathbf{R}_x^{-1}\bar{\mathbf{a}}_k\mathbf{R}_x^{-1}. \tag{3.38}$$

Finally, inserting (3.38) into (3.35) renders the MSE of $\hat{\theta}_0$ for Capon's spectrum

$$\mathrm{mse}\Big(\hat{\theta}_0\Big) \approx \frac{\sum_{k,\ell}(\theta_k - \theta_0)(\theta_\ell - \theta_0)|\bar{\mathbf{a}}_k^H\mathbf{R}_x^{-1}\bar{\mathbf{a}}_\ell|^2}{N[\sum_k((\mathbf{a}_k^H\mathbf{R}_x^{-1}\mathbf{a}_k)^{-1} - \varepsilon)]^2} \tag{3.39}$$

where the summation is over $\{k, \ell : \theta_k, \theta_\ell \in \Theta\}$.

3.4.2 MSE of $\hat{\sigma}_\theta^2$

To make the derivations tractable, the true nominal DOA value is used instead of its estimate in the calculations of the squared angular spread MSE. The good agreement between the analytical and simulated results, which is later shown in the numerical examples, indicate that this simplification has little effect on the MSE. That is, we replace $\hat{\theta}_0$ in (3.18) with the true value θ_0. This way, the derivations almost become identical to the ones made for the nominal DOA MSE. The only difference is that the spread estimate is biased due to the choice of support and the spectral leakage introduced by the limited number of antennas. Even if the true covariance matrix is used, the estimator (3.18) will not render the true squared spread. Hence, we can not simply replace the estimators value with the true value, as was done for the nominal DOA in (3.22) and (3.32) for CBF and Capon's spectra, respectively.

Conventional Beamforming

Let $\bar{\sigma}_\theta^2$ denote the squared value given by (3.18) when using the true covariance matrix and by replacing $\hat{\theta}_0$ with the true value θ_0. Since the derivations of the squared spread MSE almost become identical to the ones presented in Section 3.4.1, they are omitted here. The only difference between the estimators is that the numerator in (3.17) contains the parameter θ_ℓ, whilst, the numerator in (3.18) contains the expression $(\theta_\ell - \theta_0)^2$.

The details were carried out in Section 3.4.1 and, thus, the expression for the MSE of the squared angular spread follows directly as

$$\begin{aligned}\mathrm{mse}(\hat{\sigma}_\theta^2) \approx\ & (\bar{\sigma}_\theta^2 - \sigma_\theta^2)^2 \\ & + \frac{\sum_{k,\ell}[(\theta_k - \theta_0)^2 - \bar{\sigma}_\theta^2][(\theta_\ell - \theta_0)^2 - \bar{\sigma}_\theta^2]|\mathbf{a}_k^H \mathbf{R}_x \mathbf{a}_\ell|^2}{N[\sum_k (\mathbf{a}_k^H \mathbf{R}_x \mathbf{a}_k - K\varepsilon)]^2}\end{aligned} \tag{3.40}$$

Capon's Beamforming

The MSE of $\hat{\sigma}_\theta^2$ using Capon's spectrum is given by

$$\begin{aligned}\mathrm{mse}(\hat{\sigma}_\theta^2) \approx\ & (\bar{\sigma}_\theta^2 - \sigma_\theta^2)^2 \\ & + \frac{\sum_{k,\ell}[(\theta_k - \theta_0)^2 - \bar{\sigma}_\theta^2][(\theta_\ell - \theta_0)^2 - \bar{\sigma}_\theta^2]|\bar{\mathbf{a}}_k^H \mathbf{R}_x^{-1} \bar{\mathbf{a}}_\ell|^2}{N[\sum_k ((\mathbf{a}_k^H \mathbf{R}_x^{-1} \mathbf{a}_k)^{-1} - \varepsilon)]^2}\end{aligned} \tag{3.41}$$

The first term in each of the expressions (3.40) and (3.41) corresponds to the asymptotic squared bias (i.e., $\bar{\sigma}_\theta^2 \approx \mathrm{E}\{\hat{\sigma}_\theta^2\}$), whereas the second term corresponds to the variance of the squared angular spread estimate. Moreover,

the squared asymptotic biases in (3.40) and (3.41) are acquired by evaluating the squared difference between (3.18) using the true covariance matrix, and the true angular spread value. The bias is very sensitive to the choice of support – a too small support typically leads to under-estimating the spread and a too large support leads to over-estimating the spread. With knowledge of the true support together with antenna beamwidth (resolution), the support can be chosen in such a way that the bias almost vanishes.

3.5 Validation with Synthetic Data

To evaluate the analytical expressions, a number of numerical examples are studied. In all the simulations, a ULA consisting of twenty elements with half-wavelength separation is used to compute the beamforming spectrum. The angular distribution is Gaussian with a nominal DOA of $\theta_0 = 0^\circ$ and an angular spread of $\sigma_\theta = 5^\circ$. The noise-corrupted sample covariance matrices are generated as complex Wishart matrices. The SNR is 10 dB and the estimates are found by averaging over 5000 independent runs. To choose the support, a constant c times the median value of the spectrum is used (denote the resulting product as α). The signal part of the spectrum which is above this value α is used to define the support. The constant c is adjusted so that the support "on average" becomes $\Theta = [\theta_0 - 3\sigma_\theta, \theta_0 + 3\sigma_\theta]$.

Figure 3.11 shows the theoretical and simulated MSE for the nominal DOA estimate versus different numbers of snapshots. The simulated values show good fit to the theoretical curves and are close to the *Cramér-Rao Lower Bound (CRLB)*.

The bias of the squared spread estimate is large compared to its variance. Therefore, since it will dominate the MSE, the variance is plotted separately. Figure 3.12 shows the simulated and theoretical variances of the squared spread. Finally, the squared difference between the asymptotic expected value, $\bar{\sigma}_\theta^2$, and the simulated mean value, $\bar{m}(\hat{\sigma}_\theta^2)$, of the squared angular spread (*not the squared bias*) is shown in Figure 3.13. In this numerical example, the theoretical bias is $|\bar{\sigma}_\theta^2 - \sigma_\theta^2| = 1.12^\circ$ for the CBF-based estimate and $|\bar{\sigma}_\theta^2 - \sigma_\theta^2| = 0.87^\circ$ for the Capon-based estimate. The true value is $\sigma_\theta^2 = 25^\circ$. As seen in Figure 3.13, the simulated mean of the CBF-based estimate of the squared angular spread converges faster to its asymptotical expected value than does the simulated mean of the Capon-based estimate. Possible reasons for this might be that the covariance matrix is ill-conditioned and/or that the Capon spectrum has sharp peaks.

All simulated results show a good match to their analytical counterparts.

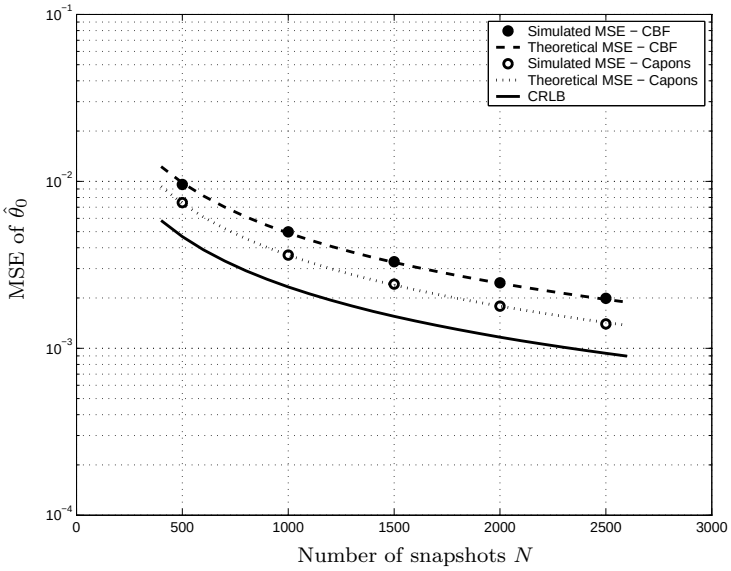

Figure 3.11: MSE of $\hat{\theta}_0$ for different numbers of snapshots N. Gaussian ID source, $\theta_0 = 0°$, $\sigma_\theta = 5°$, twenty sensors, 10 dB SNR.

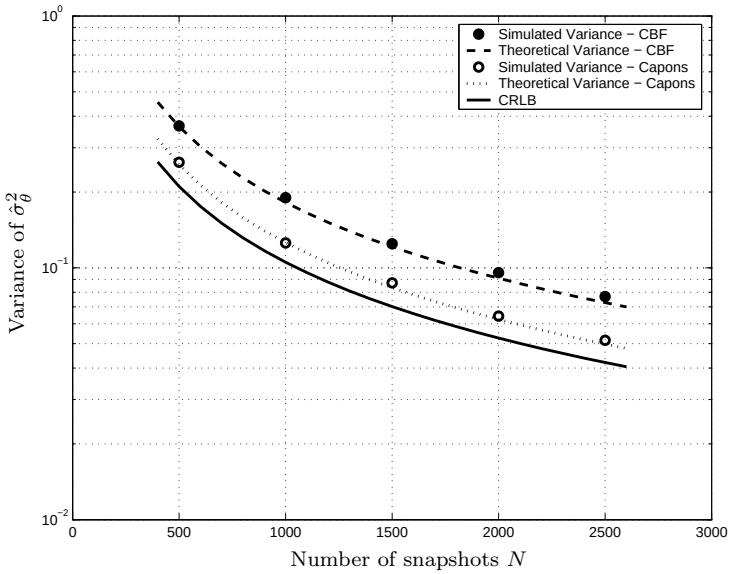

Figure 3.12: Variance of $\hat{\sigma}_\theta^2$ for different numbers of snapshots N. Gaussian ID source, $\theta_0 = 0°$, $\sigma_\theta = 5°$, twenty sensors, 10 dB SNR.

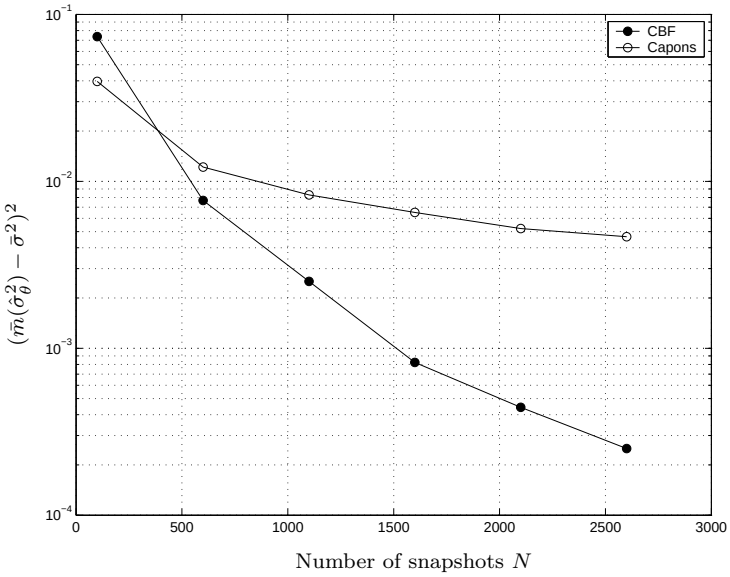

Figure 3.13: Squared difference between the theoretical asymptotic expected value, $\bar{\sigma}_\theta^2$, and the simulated mean value, $\bar{m}(\hat{\sigma}_\theta^2)$, of the squared spread estimate vs. snapshots N. Gaussian ID source, $\theta_0 = 0°$, $\sigma_\theta = 5°$, twenty sensors, 10 dB SNR.

3.A Orthogonal Steering Vectors

In the derivations of Section 3.1, we say that the steering vectors of a ULA that correspond to distinct DOAs are orthogonal as the numbers of sensors tend to infinity. The result is formulated in the following lemma.

Lemma 2 *Let* $\mathbf{a}(\omega) = [1 \quad e^{-j\omega} \quad \cdots \quad e^{-j(K-1)\omega}]^T$ *be a vector where* $\omega \in \mathbb{R}$, $K \in \mathbb{N}$ *and* $j^2 = -1$. *Then, the following result holds*

$$\lim_{K\to\infty} \frac{1}{K}\mathbf{a}^H(\omega_1)\mathbf{a}(\omega_2) = \begin{cases} 1, & \omega_1 = \omega_2 \\ 0, & \omega_1 \neq \omega_2 \end{cases} \tag{3.A.1}$$

Proof: Let $\Delta = \omega_1 - \omega_2$. *For any* $\Delta \neq 2\pi m$ *(where* m *is an integer), the magnitude of the inner-product is bounded as*

$$|\mathbf{a}^H(\omega_1)\mathbf{a}(\omega_2)| = \left|\sum_{k=0}^{K-1} e^{j\Delta k}\right| = \left|\frac{1-e^{j\Delta K}}{1-e^{j\Delta}}\right| < \frac{1}{|\sin(\Delta/2)|} = M_\Delta < \infty. \tag{3.A.2}$$

Further, if $\Delta = 2\pi m$, *the inner-product becomes* $\mathbf{a}^H(\omega_1)\mathbf{a}(\omega_2) = K$. *Hence, the proof follows as* $K \to \infty$. □

Chapter 4

Parametric Estimation: Generalized Beamforming

In this chapter, we generalize the nonparametric point source-based Conventional Beamformer (CBF) to localization of multiple Incoherently Distributed (ID) and Coherently Distributed (CD) sources that appear in sensor array processing. The generalized CBF is a parametric method that uses the principal eigenvector of the parameterized signal covariance matrix as its weight vector, which is also a matched filter. The desired parameter estimates are identified from the peaks of the generalized 2-D beamforming spectrum. Furthermore, we compare the performance of the generalized CBF numerically to the generalized Capon beamformer. The Capon beamformer is applied here to CD sources and has previously been proposed for ID sources in [HSG04]. Finally, an asymptotic statistical performance analysis of the generalized beamformers is provided and numerically verified. The material presented in this chapter is mostly composed of unpublished work. Some material has been submitted as a conference paper in [CV06].

4.1 Preliminaries

The generalized beamforming methods studied in this chapter can be used for localization of both coherently distributed and incoherently distributed sources. Therefore, we will study their performances for both of these cases.

In the ID case, signals arriving from distinct directions are assumed to be uncorrelated, and the collected snapshot sequence $\{\mathbf{x}(t)\}_{t=1}^{N}$ is modeled as an i.i.d. sequence with $\mathbf{x}(t) \sim \mathcal{CN}(0, \mathbf{R}_x(\boldsymbol{\eta}_i))$, where $\mathbf{R}_x(\boldsymbol{\eta}_i) = \sigma_s^2 \mathbf{R}_h(\boldsymbol{\eta}_i) + \sigma_n^2 \mathbf{I}_K$ is the spatial covariance matrix with the parameterized channel vector

covariance matrix $\mathbf{R}_h(\boldsymbol{\eta}_i)$ given by (2.21). The ID source represents a highly random scattering environment where the channel vectors are uncorrelated from snapshot to snapshot. Since the received signal is uncorrelated for distinct angles, it yields a high-rank signal contribution to the data covariance matrix.

In contrast to the ID source we have the CD source, where signals arriving from distinct directions are fully correlated. That is, the received signal consists of signal components from different angles that are delayed and scaled replicas of the same signal. The snapshot sequence $\{\mathbf{x}(t)\}_{t=1}^{N}$ is modeled as an i.i.d. sequence with $\mathbf{x}(t) \sim \mathcal{CN}(0, \mathbf{R}_x(\boldsymbol{\eta}_i))$, where $\mathbf{R}_x(\boldsymbol{\eta}_i) = \sigma_s^2 \mathbf{b}(\boldsymbol{\eta}_i)\mathbf{b}^H(\boldsymbol{\eta}_i) + \sigma_n^2 \mathbf{I}_K$ is the spatial covariance matrix with the generalized steering vector $\mathbf{b}(\boldsymbol{\eta}_i)$ given by

$$\mathbf{b}(\boldsymbol{\eta}_i) = \int_{\theta \in \Theta} g(\theta; \boldsymbol{\eta}_i)\mathbf{a}(\theta)\, d\theta. \tag{4.1}$$

The coherent source represents a deterministic scattering scenario where the generalized steering vector $\mathbf{b}(\boldsymbol{\eta}_i)$ remains fixed over the whole observation period, while the received signal is uncorrelated from snapshot to snapshot. The CD source gives a rank-one signal contribution to the data covariance matrix.

Throughout this chapter, the density function of a source is assumed to have a known shape and it is parameterized in the unknown parameter vector $\boldsymbol{\eta}_i = [\theta_i, \sigma_i]^T$. In the case of multiple sources, the shape is the same for the different sources, but the sources have different parameter values. See Figure 2.3 for an example with two Gaussian-like distributed sources. We also include the channel gain σ_{γ_i} in the source power, i.e., $\sigma_{s_i}^2 \triangleq \sigma_{\gamma_i}^2 |s_i(t)|^2$, where $s_i(t)$ is considered being a deterministic *Constant Modulus (CM)* signal.

4.2 Generalized Conventional Beamforming

Here, we reformulate the conventional beamforming problem by taking into account that the signal has a spatial distribution. Hence, we turn the point source based and nonparametric CBF into a parametric beamforming method, which enables us to find all our parameter estimates. The derivation is done with respect to ID sources, but the extension to CD sources is straightforward.

Given the beamformer output signal $y(t) = \mathbf{w}^H \mathbf{x}(t)$, the expected beamformer output power is given by

$$P(\mathbf{w}) = \mathrm{E}[|y(t)|^2] = \mathbf{w}^H \mathbf{R}_x \mathbf{w} = \sigma_s^2 \mathbf{w}^H \mathbf{R}_h \mathbf{w} + \sigma_n^2 \mathbf{w}^H \mathbf{w}, \tag{4.2}$$

and it is maximized w.r.t. $\mathbf{w}$ s.t. $\mathbf{w}^H\mathbf{w} = 1$. The maximizing weight vector $\mathbf{w}_{\text{opt}}$ is then given by the principal eigenvector of the, generally full-rank, channel vector covariance matrix $\mathbf{R}_h = \text{E}[\mathbf{h}\mathbf{h}^H]$, [SM97]. The principal eigenvector is defined as the unit norm eigenvector corresponding to the largest eigenvalue $\lambda_{\max}$ of $\mathbf{R}_h$. The resulting beamformer is also optimal in the sense that it maximizes the output SNR, i.e., it is a *matched filter*.

Remark: In the case of spatially colored noise with known covariance matrix $\mathbf{R}_n$, the maximum SNR beamformer is the principal eigenvector to the generalized eigenproblem $\mathbf{R}_h\mathbf{w} = \beta\mathbf{R}_n\mathbf{w}$. This is readily verified since given that $\beta = \frac{\mathbf{w}^H\mathbf{R}_h\mathbf{w}}{\mathbf{w}^H\mathbf{R}_n\mathbf{w}}$ is the expected output SNR, we have for the optimal weight vector

$$\nabla_{\mathbf{w}^*}\beta = \frac{\mathbf{R}_h\mathbf{w}(\mathbf{w}^H\mathbf{R}_n\mathbf{w}) - (\mathbf{w}^H\mathbf{R}_h\mathbf{w})\mathbf{R}_n\mathbf{w}}{(\mathbf{w}^H\mathbf{R}_n\mathbf{w})^2} = \frac{\mathbf{R}_h\mathbf{w} - \beta\mathbf{R}_n\mathbf{w}}{\mathbf{w}^H\mathbf{R}_n\mathbf{w}} = 0,$$

where $\nabla_{\mathbf{w}^*}$ denotes the vectorized differentiation (nabla) operator w.r.t. the weight vector complex conjugate. The output SNR is, thus, maximized by the generalized principal eigenvector.

We can now formulate the algorithm as finding the largest peak of the generalized 2-D power spectrum $f(\boldsymbol{\eta}, \mathbf{R}_x)$

$$\hat{\boldsymbol{\eta}} = \arg\max_{\boldsymbol{\eta}} f(\boldsymbol{\eta}, \mathbf{R}_x), \quad \boldsymbol{\eta} = [\theta, \sigma_\theta]^T \tag{4.3}$$

where $f(\boldsymbol{\eta}, \mathbf{R}_x) \triangleq \mathbf{w}^H\mathbf{R}_x\mathbf{w}$. Here, $\mathbf{R}_x$ contains the true parameters $\boldsymbol{\eta}_0$, and $\mathbf{w} = \mathbf{w}(\boldsymbol{\eta})$ is the principal eigenvector of the matrix $\mathbf{R}_h(\boldsymbol{\eta})$ which is parameterized in the unknown parameters $\boldsymbol{\eta}$. Since $\lambda_{\min} \leq \mathbf{x}^H\mathbf{R}_h\mathbf{x} \leq \lambda_{\max}$ [SM97], for any unit norm vector $\mathbf{x} \in \mathbb{C}^{K\times 1}$, the maximum value of $f(\boldsymbol{\eta}, \mathbf{R}_x)$ equals $\sigma_s^2\lambda_{\max} + \sigma_n^2$, and is attained by the principal eigenvector $\mathbf{x} = \mathbf{w}$. In general $\lambda_{\max}$ is unique, and the maximum is readily attained by $\hat{\boldsymbol{\eta}} = \boldsymbol{\eta}_0$ when the true covariance matrix is used in (4.3), which makes the estimator consistent in the sense given below.

In practice we do not have access to the true covariance matrix $\mathbf{R}_x$, so we resort to replacing it by the sample covariance matrix, which is a *sufficient statistic* under the Gaussian data model [Kay93], and is defined as

$$\hat{\mathbf{R}}_x = \frac{1}{N}\sum_{t=1}^{N}\mathbf{x}(t)\mathbf{x}^H(t). \tag{4.4}$$

It is easily verified that the criterion function $f(\boldsymbol{\eta}, \hat{\mathbf{R}}_x)$ converges uniformly

(with increasing numbers of snapshots) to its limit function $f(\boldsymbol{\eta}, \mathbf{R}_x)$, since

$$\sup_{\boldsymbol{\eta}} \left| f(\boldsymbol{\eta}, \hat{\mathbf{R}}_x) - f(\boldsymbol{\eta}, \mathbf{R}_x) \right| = \sup_{\boldsymbol{\eta}} \left| \mathbf{w}^H (\hat{\mathbf{R}}_x - \mathbf{R}_x) \mathbf{w} \right|$$
$$\leq \left\| \hat{\mathbf{R}}_x - \mathbf{R}_x \right\| \rightarrow 0, \text{ w.p.1 as } N \rightarrow \infty.$$

Hence, the maximum of $f(\boldsymbol{\eta}, \hat{\mathbf{R}}_x)$ tends to that of $f(\boldsymbol{\eta}, \mathbf{R}_x)$, and algorithm yields consistent estimates.

As in the point source case, we can identify q distributed sources from the q largest peaks of the generalized 2-D spectrum. In the case of multiple sources, i.e., $q > 1$, the estimates will be asymptotically biased due to spectral leakage from closely spaced sources.

We note that in the coherently distributed source case, the channel vector covariance matrix is given by $\mathbf{R}_h(\boldsymbol{\eta}) = \mathbf{b}(\boldsymbol{\eta})\mathbf{b}^H(\boldsymbol{\eta})$, which has the principal normalized eigenvector $\mathbf{w}(\boldsymbol{\eta}) = \mathbf{b}(\boldsymbol{\eta})/\|\mathbf{b}(\boldsymbol{\eta})\|$. Thus, for a CD source, the generalized spectrum is given by

$$f(\boldsymbol{\eta}, \mathbf{R}_x) = \frac{\mathbf{b}^H(\boldsymbol{\eta}) \mathbf{R}_x \mathbf{b}(\boldsymbol{\eta})}{\mathbf{b}^H(\boldsymbol{\eta}) \mathbf{b}(\boldsymbol{\eta})}, \tag{4.5}$$

and the q largest peaks of (4.5) correspond to the parameters of q CD sources. The same consistency arguments that we used above for ID sources also extends to CD sources. It is found in the numerical examples in Section 4.5, that the G-CBF estimates for a single CD source coincide with the corresponding Maximum-Likelihood (ML) estimates. Finally, since a point source is a special case of a coherently distributed source with the channel vector $\mathbf{a}(\theta) = \lim_{\sigma_\theta \rightarrow 0} \mathbf{b}(\boldsymbol{\eta})$, the generalized 2-D spectrum for CD sources will for point sources degenerate to the conventional 1-D spectrum given by (2.48).

4.3 Generalized Capon's Beamforming

A generalization of Capon's beamformer [Cap69] to incoherently distributed sources was introduced in [HSG04]. The algorithm is called *Generalized Capon (G-Capon)* and the weight vector is derived from the following constrained optimization problem

$$\min_{\mathbf{w}} \mathbf{w}^H \mathbf{R}_x \mathbf{w} \text{ s.t. } \mathbf{w}^H \mathbf{R}_h(\boldsymbol{\eta}) \mathbf{w} = 1. \tag{4.6}$$

The resulting spatial filter will, thus, minimize the power from interfering sources while keeping a distortionless response to a source with the parameterized covariance matrix $\mathbf{R}_h(\boldsymbol{\eta})$. If the parameterized covariance matrix is

the covariance matrix of a distributed source, the algorithm can be used to estimate the parameter vector $\boldsymbol{\eta}$.

The solution to (4.6) is given by solving the generalized eigenvalue problem

$$\mathbf{R}_x\mathbf{w} = \lambda\mathbf{R}_h(\boldsymbol{\eta})\mathbf{w}, \tag{4.7}$$

and the optimal weight vector is given by the eigenvector that corresponds to the smallest generalized eigenvalue of the matrix pencil $\{\mathbf{R}_x, \mathbf{R}_h(\boldsymbol{\eta})\}$, [HSG04]. It is easily verified that all the eigenvalues are real and non-negative.

The generalized Capon's 2-D pseudo spectrum is then defined as the beamformer's output power when the beamformer is directed to a distributed source with parameter vector $\boldsymbol{\eta}$. The algorithm for estimating $\boldsymbol{\eta}$ can then be formulated as finding the largest peak of the generalized Capon spectrum, i.e.,

$$\hat{\boldsymbol{\eta}} = \arg\max_{\boldsymbol{\eta}} f(\boldsymbol{\eta}, \mathbf{R}_x), \tag{4.8}$$

where $f(\boldsymbol{\eta}, \mathbf{R}_x)$ is given by

$$f(\boldsymbol{\eta}, \mathbf{R}_x) = \lambda_{\min}\{\mathbf{R}_x, \mathbf{R}_h(\boldsymbol{\eta})\} = \lambda_{\min}\{\mathbf{R}_h^{-1}(\boldsymbol{\eta})\mathbf{R}_x\}, \tag{4.9}$$

and $\lambda_{\min}\{\mathbf{R}_x, \mathbf{R}_h(\boldsymbol{\eta})\}$ denotes the minimum generalized eigenvalue of the matrix pencil $\{\mathbf{R}_x, \mathbf{R}_h(\boldsymbol{\eta})\}$ or, equivalently, the minimum eigenvalue of the matrix $\mathbf{R}_h^{-1}(\boldsymbol{\eta})\mathbf{R}_x$. As in the point source case, if there are q distributed sources present they can be identified as the q largest peaks of the generalized Capon spectrum.

As it was pointed out in [HSG04], for the point source case, the generalized Capon spectrum for ID sources degenerates to the conventional Capon spectrum given by (2.53). Even though it was never discussed in [HSG04], one can also formulate the generalized Capon beamformer for coherently distributed sources. The generalized Capon pseudo spectrum for CD sources is then given by

$$f(\boldsymbol{\eta}, \mathbf{R}_x) = \frac{1}{\mathbf{b}^H(\boldsymbol{\eta})\mathbf{R}_x^{-1}\mathbf{b}(\boldsymbol{\eta})}, \tag{4.10}$$

and the q largest peaks of (4.10) corresponds to the parameters of q CD sources. Here, it is clearly seen that if $\lim_{\sigma_\theta\to 0}\mathbf{b}(\boldsymbol{\eta}) = \mathbf{a}(\theta)$, the Capon's 2-D spectrum for CD sources will for point sources degenerate to the conventional 1-D Capon spectrum given by (2.53).

The normalized generalized spectra for the generalized CBF (G-CBF) and the generalized Capon's beamformer (G-Capon) are shown in Figure 4.1 for one and two equi-powered Gaussian ID sources with parameters $\boldsymbol{\eta}_0 = [0°, 3°]$ and $\boldsymbol{\eta}_1 = [30°, 3°]$, respectively. A 20-element standard ULA, and the true noise-free covariance matrix are used to compute the respective spectrum. We note that the G-CBF spectrum suffer from the same resolution problem as for 1-D DOA estimation of closely-spaced point sources. We also see that the resolution of G-CBF in the spread direction is poor, and there are no distinct peaks in that direction (there is a slight curvature). The G-Capon spectrum shows much better resolution in both dimensions.

The same parameter setting is also applied to CD sources, and the normalized spectra are shown in Figure 4.2. The G-CBF spectrum shows well-defined peaks at the corresponding true parameter values, and so does the G-Capon spectrum. The generalized beamformers manage well to capture the transmitted power of the rank-one CD sources.

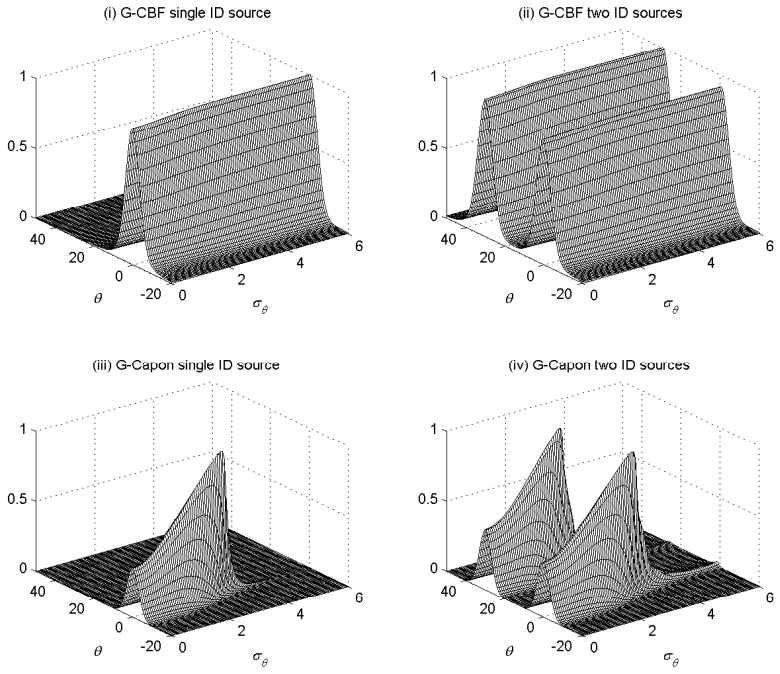

Figure 4.1: Normalized generalized beamforming spectra for one resp. two Gaussian ID sources. The noise-free true covariance matrix is used together with a std. $K = 20$ ULA.

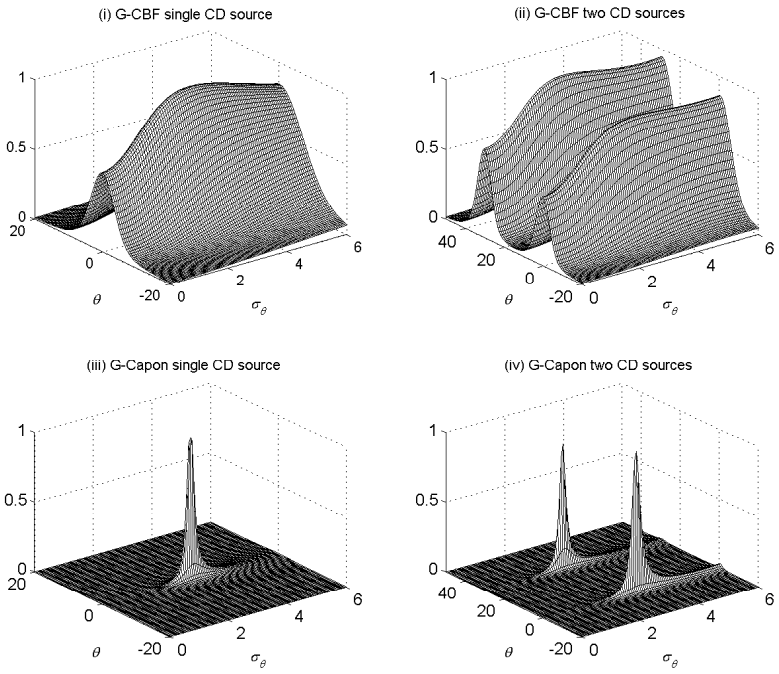

Figure 4.2: Normalized generalized beamforming spectra for one resp. two Gaussian CD sources. The noise-free true covariance matrix is used together with a std. $K = 20$ ULA.

4.4 Numerical Examples for ID Sources

In this section we study ID sources and compare the numerical performance of the generalized conventional beamformer (G-CBF) to that of the generalized Capon (G-Capon) beamformer. In [HSG04], the generalized Capon method was found to outperform the well known DISPARE [MSW96] and root-MUSIC-based [BO00] algorithms when locating two ID sources. The Cramér-Rao Lower Bound (CRLB) is also included in the figures.

All estimates are averaged over 2000 independent runs, and the noise is spatio-temporally white with a circular symmetric complex Gaussian distribution, and the SNR is defined as σ_s^2/σ_n^2.

Example 4.1: In the first example we locate a single Gaussian ID source with parameter values $\theta_0 = 0^\circ$ and $\sigma_\theta = 3^\circ$ impinging on a standard ULA with $K = 10$ sensors. The sample covariance matrix is estimated using

$N = 500$ snapshots. To reconnect the nonparametric methods in the previous chapter, in this example we have included the Capon-based angle and spread estimates. Also included for reference are the DISPARE [MSW96] and WPSF [BO01] estimates. In this scenario, G-CBF shows better performance than G-Capon.

Figure 4.3 displays the RMSE of the parameter estimates versus SNR. We observe that the RMSE of the nominal angle estimates attained by the G-CBF is insensitive to the SNR, which is an observation that is consistent with point source estimation using the data-independent CBF. For low SNR values, the spread estimate of G-CBF improves with increased SNR. For high SNR values, all estimates appear to have a remaining bias (the algorithms are only consistent as $N \to \infty$). The G-Capon spread estimate shows a performance loss for increased SNR, which is likely due to a ill-conditioned sample covariance matrix. The nonparametric Capon-based method performs the best, and the DISPARE and WPSF angle estimates are better than the angle estimated attained by the generalized beamformers, although, the generalized beamformers perform better than DISPARE when estimating the spread.

Figure 4.4 shows the RMSE versus number of sensors. Even though the results are disappointing, it is still interesting to see that the RMSE of the G-CBF spread estimate deteriorates as the number of sensors grows large. There appears to be an optimal choice (around $K = 10$ sensors) w.r.t. the number of sensors. We will return to this observation in Section 4.6. The number of sensors has little effect on the G-CBF nominal angle RMSE, and it is only slightly better than the RMSE of the conventional peak-finding algorithm [RGM98], which is included in this figure. There will always be little difference in the nominal angle estimates between the conventional beamformer and its generalized version when the the distributed source can be "seen" as a point source by the array. This is the case when the array beamwidth is large (few sensors) compared to the spread parameter. Hence, it is the relation between the array resolution and the spread parameter that controls how well a distributed source is described by a point source. In this example, the estimates based on G-Capon improves with increasing number of sensors, since we have also increased the number of snapshots according to $N = 20K$. The SNR in this example was 20 dB.

Example 4.2: The second example involves locating two Gaussian ID sources; one with parameter values $\theta_0 = 0°$, $\sigma_{\theta_0} = 3°$ and a second with values θ_1 that are varied from 10° to 40°, $\sigma_{\theta_1} = 2°$. A standard ULA with $K = 20$ sensors is used and the SNR is 20 dB per source. We see from Figure 4.5 that G-CBF

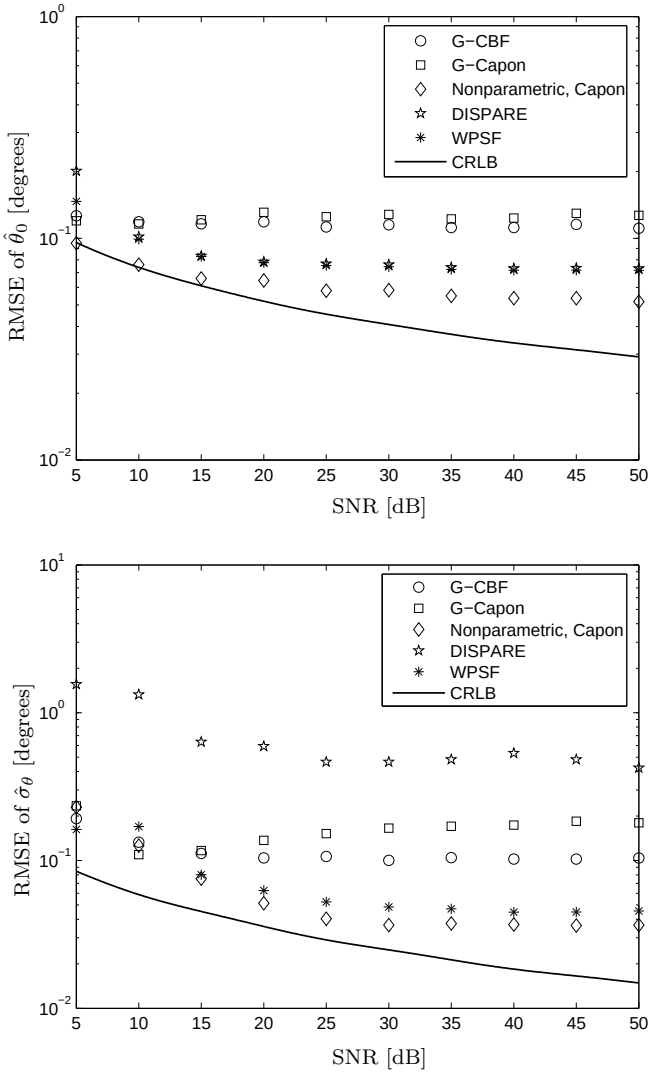

Figure 4.3: RMSE of $\hat{\theta}_0$ (top) and $\hat{\sigma}_\theta$ (bottom) for different SNRs. Gaussian ID source with $\theta_0 = 0°$, $\sigma_\theta = 3°$, $K = 10$, and $N = 500$.

captures the nominal angles quite well, while it suffers from spectral leakage when it comes to estimating the spreads of two closely spaced sources.

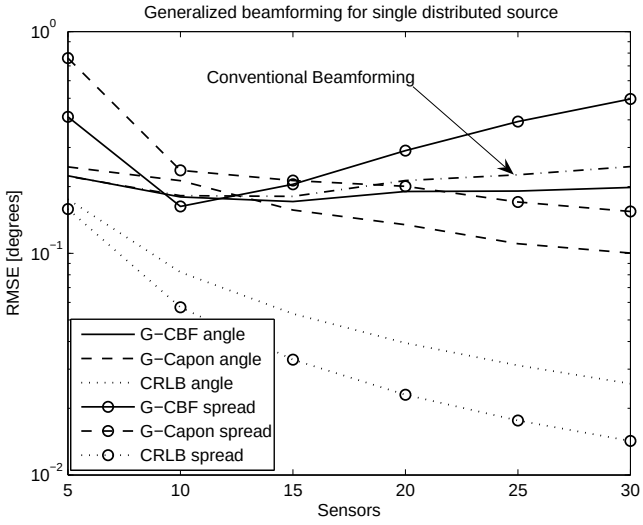

Figure 4.4: RMSE of $\hat{\theta}_0$ and $\hat{\sigma}_\theta$ versus number of sensors. The figure also includes the angle estimate based on the conventional beamformer [RGM98]. Gaussian ID source with $\theta_0 = 0°$, $\sigma_\theta = 3°$, $N = 20K$, and $\mathrm{SNR} = 20$ dB.

4.5 Numerical Examples for CD Sources

In this section we study CD sources and compare the numerical performance of the generalized conventional beamformer (G-CBF) to that of the generalized Capon (G-Capon) beamformer. The analytical error curves that are given for CD sources in Theorems 2 and 4, and the Cramér-Rao Lower Bound (CRLB) are also included in the figures.

All estimates are averaged over 2000 independent runs, and the noise is spatio-temporally white with a circular symmetric complex Gaussian distribution. The estimates are given in electric angle and spread, which are defined in (2.22) and (2.23), respectively.

Example 4.3: In this example we locate a single Gaussian CD source with parameters $\boldsymbol{\eta}_0 = [2°, 3°]^T$. A 10-element standard ULA is used and the SNR is 10 dB. Figure 4.6 shows the RMSE performance for the nominal angle estimate versus snapshots, and Figure 4.7 shows the standard deviation of the corresponding spread estimates. The standard deviation of the spread estimates are plotted since the RMSE of G-Capon is dominated by a small bias, which is asymptotically given by $\Delta\sigma_\omega = 0.0043$ rad. (corresponds to

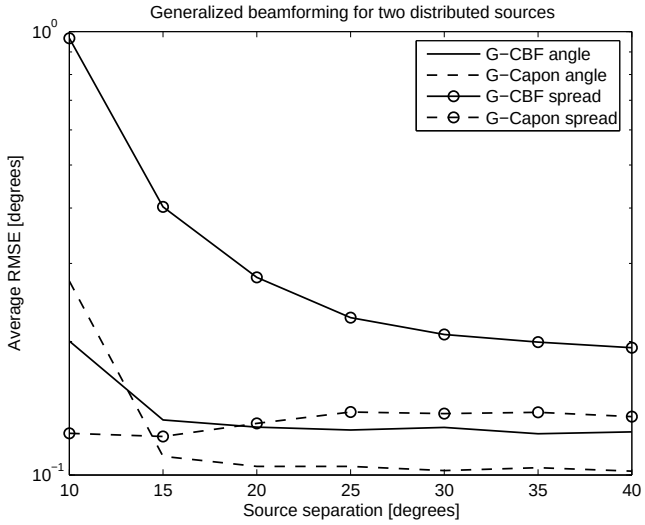

Figure 4.5: Average RMSE of $\{\hat{\theta}_0, \hat{\theta}_1\}$ and $\{\hat{\sigma}_{\theta_0}, \hat{\sigma}_{\theta_1}\}$ versus source separation. Two Gaussian ID sources with $\{\theta_0 = 0°, \sigma_{\theta_0} = 3°\}$, $\{\theta_1 = 10° \ldots 40°, \sigma_{\theta_1} = 2°\}$, $K = 20$, SNR $= 20$ dB per source, and $N = 500$.

2.6% of the true value). We see that the G-CBF angle and spread estimates are asymptotically efficient since they both reach the CRLB. In fact, one might think that, under the Gaussian data model assumption, the G-CBF estimates for a single CD source coincide with the Maximum Likelihood (ML) estimates, which is the case when locating a single point source [KV96]. We will return to this discussion in Example 4.4, where we have also simulated the ML performance.

Figures 4.8 and 4.9 show the estimation performance versus SNR. The parameter setting is the same as above, but with varying SNR and the number of snapshots fixed to $N = 500$. Both estimates attained by G-CBF are efficient, and the asymptotic bias of G-Capon is varying with the SNR and can be found in Figure 4.19.

In all figures, the theoretical asymptotic RMSE curves for G-CBF coincide with their respective CRLB curve, and the empirical estimation performance show good agreement with their analytical counterparts.

Example 4.4: Here we apply the same setting as in Example 4.3, but look more closely at the small sample size and low SNR regions. Thus, we study the region where the G-CBF RMSE converges to the CRLB, and include

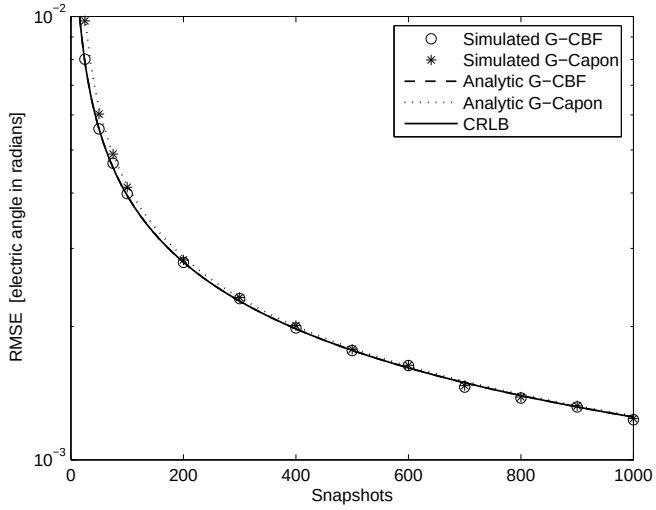

Figure 4.6: RMSE of $\hat{\omega}_0$ versus snapshots. Gaussian CD source with $\omega_0 = 0.1096$ rad., $\sigma_\omega = 0.1644$ rad., $K = 10$, SNR $= 10$ dB. The analytic G-CBF curve coincides with the CRLB curve.

the RMSE performance of the ML estimator to see if it coincides with the performance of G-CBF. Under the Gaussian data model, the concentrated form of the ML estimator is given by minimizing the negative *log-likelihood function* [Kay93]

$$\hat{\boldsymbol{\phi}}_0 = \arg\min_{\boldsymbol{\phi}} \left\{ \log|\mathbf{R}_x(\boldsymbol{\phi})| + \mathrm{Tr}\left\{ \mathbf{R}_x^{-1}(\boldsymbol{\phi})\hat{\mathbf{R}}_x \right\} \right\},$$
$$\mathbf{R}_x(\boldsymbol{\phi}) = \rho\mathbf{b}(\boldsymbol{\phi})\mathbf{b}^H(\boldsymbol{\phi}) + \mathbf{I}_K, \quad \boldsymbol{\phi} = [\omega, \sigma_\omega, \rho]^T, \quad \rho = \sigma_s^2/\sigma_n^2. \tag{4.11}$$

The G-Capon estimator is not included here, since it does not perform well for small sample sizes and/or low SNR. The estimators use the same realization of the sample covariance matrix, which is changed independently from run to run. Figures 4.10 and 4.11 show the RMSE performance versus snapshots respective SNR. We see that the performance of the G-CBF estimates coincide with the corresponding performance of ML. We have in numerical examples, although not included here, seen that the G-CBF and ML estimator produces identical estimates. This is interesting since the ML estimator requires a 3-D search over the two parameters of interest plus the SNR ρ, while the G-CBF only requires a 2-D search to find the two parameters. In both figures, the analytic G-CBF RMSE curves coincide with their respective CRLB curve. Hence, they both are asymptotically efficient.

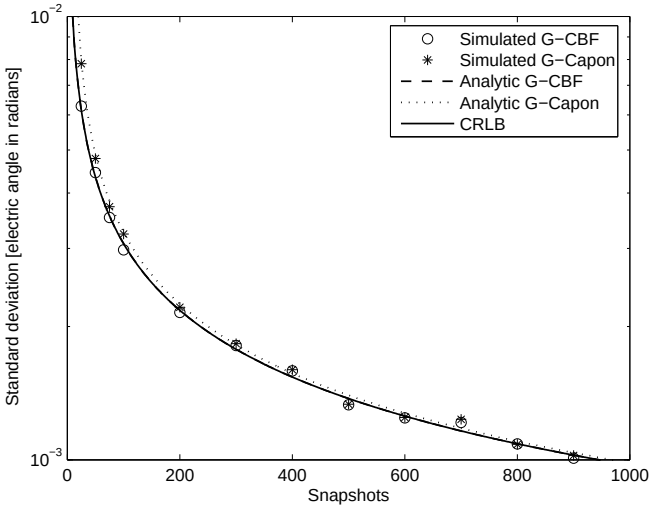

Figure 4.7: Standard deviation of $\hat{\sigma}_\omega$ versus snapshots. Gaussian CD source with $\omega_0 = 0.1096$ rad., $\sigma_\omega = 0.1644$ rad., $K = 10$, $\mathrm{SNR} = 10$ dB. The analytic G-CBF curve coincides with the CRLB curve.

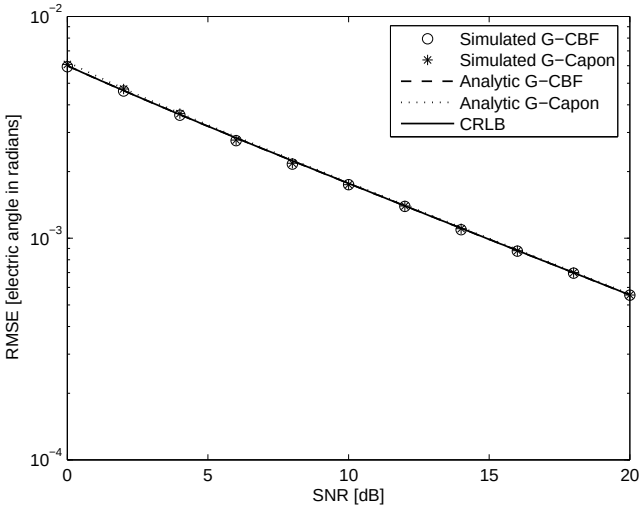

Figure 4.8: RMSE of $\hat{\omega}_0$ versus SNR. Gaussian CD source with $\omega_0 = 0.1096$ rad., $\sigma_\omega = 0.1644$ rad., $K = 10$, $N = 500$. The analytic G-CBF curve coincides with the CRLB curve.

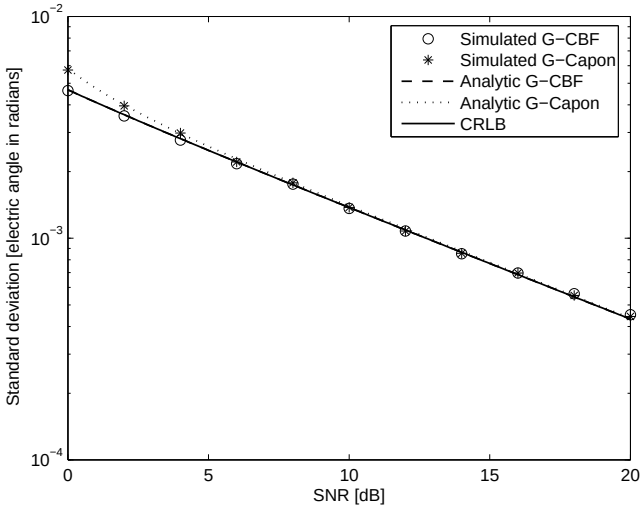

Figure 4.9: Standard deviation of $\hat{\sigma}_\omega$ versus SNR. Gaussian CD source with $\omega_0 = 0.1096$ rad., $\sigma_\omega = 0.1644$ rad., $K = 10$, $N = 500$. The analytic G-CBF curve coincides with the CRLB curve.

Example 4.5: This example displays the limited resolution of the G-CBF compared to G-Capon when they are used to locate two Gaussian CD sources. We see in Figure 4.12 how G-CBF suffers from its poor resolution, while G-Capon manage well to separate the two sources. The parameter setting is given in the figure text.

4.6 Statistical Performance Analysis of Generalized Conventional Beamforming

Here we provide a statistical performance analysis of the G-CBF algorithm. The analysis yields theoretical results that can be used to quickly assess the performance for different parameter settings instead of having to rely on empirical results attained from long simulation runs. To simplify the statistical analysis we apply a change of variables and use the concept of spatial frequency and corresponding spread, which are defined in (2.22) and (2.23), respectively. Thus, our transformed parameter vector is $\boldsymbol{\psi} = [\omega, \sigma_\omega]^T$. The asymptotic error distribution is derived by using the standard Taylor expansion method described in, e.g., [Lju87]. The results are formulated as

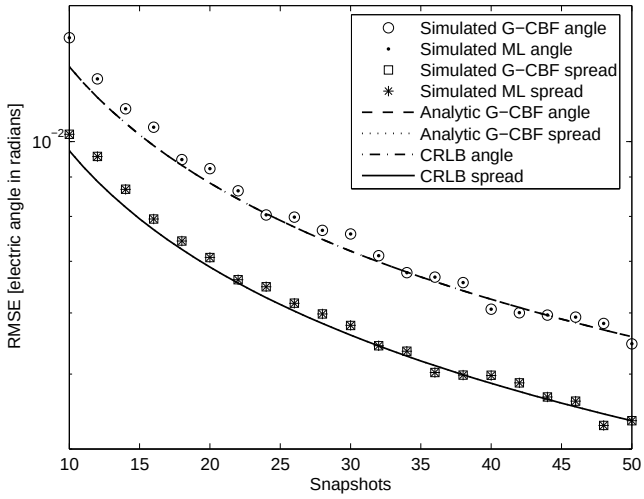

Figure 4.10: RMSE of $\hat{\omega}_0$ and $\hat{\sigma}_\omega$ versus snapshots. Gaussian CD source with $\omega_0 = 0.1096$ rad., $\sigma_\omega = 0.1644$ rad., $K = 10$, $\mathrm{SNR} = 10$ dB. The analytic curves coincide with their respective CRLB curve.

two theorems; one for localization of ID sources, and one for CD sources.

4.6.1 G-CBF for Localization of ID Sources

Theorem 1 (ASYMPTOTIC ERROR DISTRIBUTION FOR G-CBF APPLIED TO ID SOURCES) *Assume* $\mathbf{x}(t) \sim \mathcal{N}(0, \mathbf{R}_x(\boldsymbol{\psi}_0))$ *is temporally white and* $\mathbf{R}_x(\boldsymbol{\psi}_0)$ *has simple eigenvalues. Then, the asymptotic distribution of the parameters obtained by inserting the sample covariance matrix into the G-CBF algorithm (4.3) for incoherently distributed sources is given by*

$$\sqrt{N}\left(\hat{\boldsymbol{\psi}} - \boldsymbol{\psi}_0\right) \sim \mathrm{As}\mathcal{N}\left(0, \mathbf{R}_{\tilde{\psi}}\right), \tag{4.12}$$

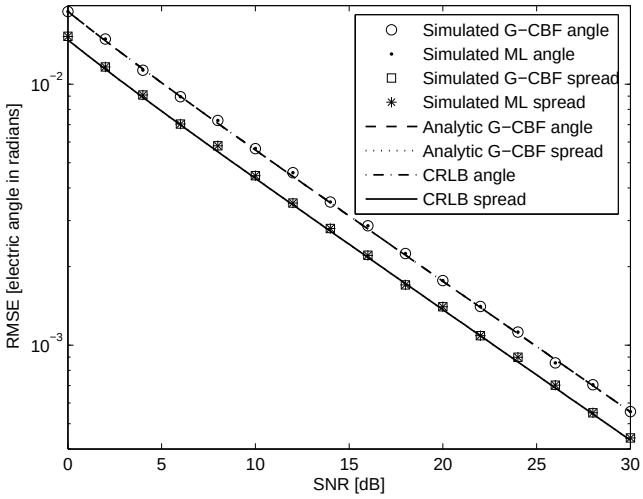

Figure 4.11: RMSE of $\hat{\omega}_0$ and $\hat{\sigma}_\omega$ versus snapshots SNR. Gaussian CD source with $\omega_0 = 0.1096$ rad., $\sigma_\omega = 0.1644$ rad., $K = 10$, $N = 50$. The analytic curves coincide with their respective CRLB curve.

where

$$\mathbf{R}_{\tilde{\psi}} = \mathbf{H}^{-1}\mathbf{\Phi}\mathbf{H}^{-1}, \tag{4.13}$$

$$[\mathbf{\Phi}]_{ij} = 2\mathrm{Re}\Big\{\Big(\mathbf{w}_1^H\mathbf{R}_x\frac{\partial\mathbf{w}_1}{\partial\psi_j}\Big)\Big(\mathbf{w}_1^H\mathbf{R}_x\frac{\partial\mathbf{w}_1}{\partial\psi_i}\Big) + \Big(\mathbf{w}_1^H\mathbf{R}_x\mathbf{w}_1\Big)\Big(\frac{\partial\mathbf{w}_1^H}{\partial\psi_j}\mathbf{R}_x\frac{\partial\mathbf{w}_1}{\partial\psi_i}\Big)\Big\}, \tag{4.14}$$

$$[\mathbf{H}]_{ij} = 2\mathrm{Re}\Big\{\mathbf{w}_1^H\mathbf{R}_x\frac{\partial^2\mathbf{w}_1}{\partial\psi_i\psi_j} + \frac{\partial\mathbf{w}_1^H}{\partial\psi_i}\mathbf{R}_x\frac{\partial\mathbf{w}_1}{\partial\psi_j}\Big\}. \tag{4.15}$$

The eigenvector derivatives are given in Appendix 4.A.

Proof: See Appendix 4.A. □

We do not provide analytic expressions in physical parameters, since the derived expressions depend on the eigenvalues and eigenvectors which, in general, are not available in closed-form. The eigenvalues and eigenvectors are attained from a numerical algorithm such as, e.g., the "svd" routine in MATLAB®. Furthermore, the asymptotic result in the above theorem has been derived for the case of a single distributed source, and with the correct

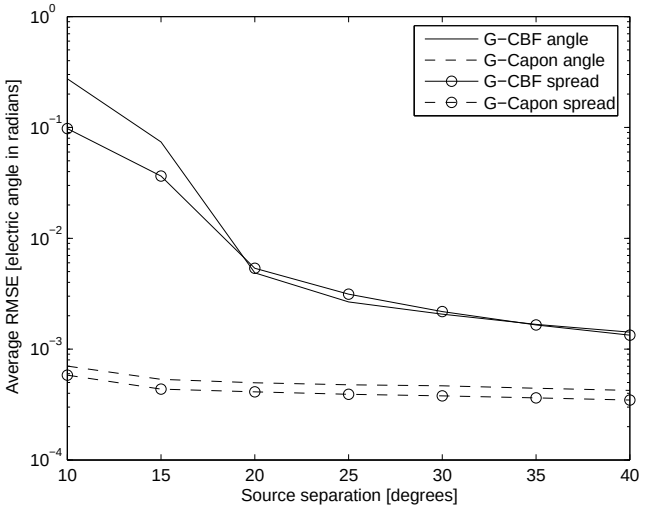

Figure 4.12: Average RMSE of $\{\hat{\omega}_0, \hat{\omega}_1\}$ and $\{\hat{\sigma}_{\omega_0}, \hat{\sigma}_{\omega_1}\}$ versus source separation in degrees. Two Gaussian CD sources with $\{\theta_0 = 0^\circ, \sigma_{\theta_0} = 3^\circ\}$, $\{\theta_1 = 10^\circ \ldots 40^\circ, \sigma_{\theta_1} = 2^\circ\}$, $K = 20$, SNR $= 20$ dB per source, and $N = 500$.

model assumption. The theorem is easily extended to the case of multiple distributed sources, and to take modeling errors, such as making an erroneous assumption on the true angular distribution, into account. This is easily seen, since the case of multiple sources only enter the true covariance matrix $\mathbf{R}_x(\boldsymbol{\psi}_0)$, and the derived asymptotic distribution is a function of this covariance matrix. The case of a model mismatch in the angular distribution is handled by choosing the appropriate $\mathbf{B}(\sigma_\omega)$ matrix. In the mentioned extensions, there will, although, be a asymptotic bias present, and the equations in the theorem should be evaluated at the point $\boldsymbol{\psi}_* \neq \boldsymbol{\psi}_0$, given by

$$\boldsymbol{\psi}_* = \arg\max_{\boldsymbol{\psi}} \mathbf{w}_1^H(\boldsymbol{\psi}) \mathbf{R}_x(\boldsymbol{\psi}_0) \mathbf{w}_1(\boldsymbol{\psi}),$$

where $\mathbf{R}_x(\boldsymbol{\psi}_0)$ is the true covariance matrix, $\mathbf{w}_1(\boldsymbol{\psi})$ is the principal eigenvector of the model covariance matrix $\mathbf{R}_h(\boldsymbol{\psi})$, and $\boldsymbol{\psi}_* - \boldsymbol{\psi}_0$ represents the asymptotic bias term. Finally, the asymptotic results were derived with the assumption of distinct eigenvalues. Therefore, as the eigenvalues become very close, e.g., when the numbers of antennas grow very large, there will be a discrepancy between the analytic and simulated results.

4.6.2 G-CBF for Localization of CD Sources

Theorem 2 (ASYMPTOTIC ERROR DISTRIBUTION FOR G-CBF APPLIED TO CD SOURCES) *Assume* $\mathbf{x}(t) \sim \mathcal{N}(0, \mathbf{R}_x(\boldsymbol{\psi}_0))$ *is temporally white, and* $\mathbf{R}_x(\boldsymbol{\psi}_0) = \sigma_s^2 \mathbf{b}(\boldsymbol{\psi}_0)\mathbf{b}^H(\boldsymbol{\psi}_0) + \sigma_n^2 \mathbf{I}_K$. *Then, the asymptotic distribution of the parameters obtained by inserting the sample covariance matrix into the G-CBF algorithm for coherent sources (4.5) is given by*

$$\sqrt{N}\left(\hat{\boldsymbol{\psi}} - \boldsymbol{\psi}_0\right) \sim \text{As}\mathcal{N}\left(0, \mathbf{R}_{\tilde{\psi}}\right), \tag{4.16}$$

where

$$\mathbf{R}_{\tilde{\psi}} = \mathbf{H}^{-1}\boldsymbol{\Phi}\mathbf{H}^{-1}, \tag{4.17}$$

$$[\boldsymbol{\Phi}]_{ij} = 2\text{Re}\Big\{\Big(\mathbf{w}^H\mathbf{R}_x\frac{\partial \mathbf{w}}{\partial \psi_j}\Big)\Big(\mathbf{w}^H\mathbf{R}_x\frac{\partial \mathbf{w}}{\partial \psi_i}\Big) + \Big(\mathbf{w}^H\mathbf{R}_x\mathbf{w}\Big)\Big(\frac{\partial \mathbf{w}^H}{\partial \psi_j}\mathbf{R}_x\frac{\partial \mathbf{w}}{\partial \psi_i}\Big)\Big\}, \tag{4.18}$$

$$[\mathbf{H}]_{ij} = 2\text{Re}\Big\{\mathbf{w}^H\mathbf{R}_x\frac{\partial^2 \mathbf{w}}{\partial \psi_i \psi_j} + \frac{\partial \mathbf{w}^H}{\partial \psi_i}\mathbf{R}_x\frac{\partial \mathbf{w}}{\partial \psi_j}\Big\}, \tag{4.19}$$

$$\mathbf{w} = \frac{\mathbf{b}}{\|\mathbf{b}\|}. \tag{4.20}$$

The weight vector derivatives are given in Appendix 4.B.

Proof: See Appendix 4.B. □

The asymptotic error variance is validated numerically in Section 4.5, and all the simulated data examples show good agreement with the theoretical results.

4.6.3 Validation with Synthetic Data for ID Sources

In this section we give a number of numerical examples, and the purpose of these examples is to validate the theoretical expressions for the variance of the asymptotic error distribution. In examples where the estimates are evaluated asymptotically in snapshots N, we plot the RMSE performance. For small N, we choose to plot the standard deviations, since in these examples the remaining bias dominates over the error variance. In all examples, the estimates are averaged over 2000 independent runs, and the noise is spatio-temporally white with a circular symmetric complex Gaussian distribution.

Example 4.6: In this example, the source has a Gaussian distribution with parameters $\omega_0 = 0$ rad and $\sigma_\omega = 0.1645$ rad. The array is a 10-sensor standard ULA and the SNR is 20dB. The sample covariance matrix is estimated from 500 snapshots and the estimates are averaged over 2000 independent runs. Figures 4.13 and 4.14 show good match between the analytical expressions and the simulated RMSE. There is a remaining bias in Figure 4.14, since the algorithm is only consistent as $N \to \infty$.

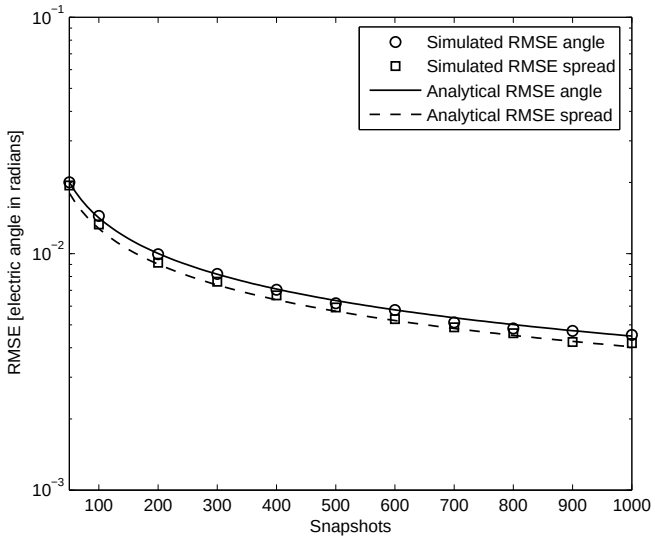

Figure 4.13: Simulated and analytical RMSE of $\hat{\omega}_0$ and $\hat{\sigma}_\omega$ versus snapshots. Gaussian ID source with $\omega_0 = 0$ rad, $\sigma_\omega = 0.1645$ rad, $K = 10$, SNR $= 20$ dB.

Example 4.7: We now return to the earlier and interesting observation that there is an optimal choice of the number of sensors that minimize the MSE of the spread estimate. Table 4.1 contains the number of antennas that minimize both the analytical and simulated MSE of the spread estimate. Also here the analytical results agree well with simulated results. The optimal choice of number of antennas has a strong dependence on the spatial spread, and both numerical and analytical results suggest that the optimal array should have a *Rayleigh beamwidth (BW)*[1] very roughly equal to the one-sided total spatial extension of the source (in this example $\mathrm{BW}_{\mathrm{opt}} \approx 4\sigma_\theta$).

[1]The Rayleigh beamwidth is defined as the angle between the main lobe peak and the first null, i.e., BW $= 2\pi/K$ rad. in electric angle.

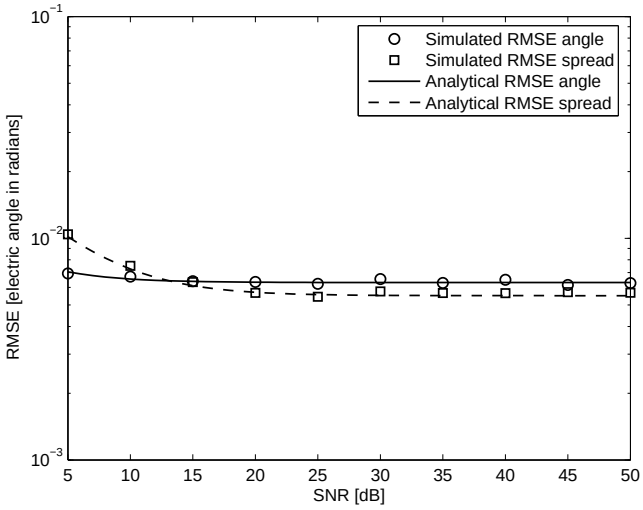

Figure 4.14: Simulated and analytical RMSE of $\hat{\omega}_0$ and $\hat{\sigma}_\omega$ versus SNR. Gaussian ID source with $\omega_0 = 0$ rad, $\sigma_\omega = 0.1645$ rad, $K = 10$, $N = 500$.

There is an intuitive explanation to this, which is that the G-CBF makes the best, in terms of maximizing the beamformer's output SNR, rank-one approximation of the distributed source by choosing the principal eigenvector as its optimal weight vector. As long as the Rayleigh beamwidth is roughly equal to or larger than the source's total spatial extension, a rank-one approximation serves as a good approximation, and an increase in the number of antennas will only give better performance. When the number of antennas is increased beyond this limit, the array will experience a source with a larger spatial spread, and the rank-one approximation is no longer a good approximation. This is the region where the distributed source really is starting to be experienced as distributed by the array, and the beamformer (matched filter) will only capture a fraction of the energy. As a consequence, there will be a degradation in the estimation performance.

Example 4.8: In this example, the true angular distribution is uniform with zero mean and standard deviation $\sigma_\omega = 0.1645$ rad, which correspond to a uniform distribution over $[-\delta_\omega, \delta_\omega]$, with $\delta_\omega = 0.2849$ rad. The model makes the erroneous assumption of a Gaussian distribution. Figure 4.15 shows good agreement between the simulated and analytical standard deviations. There is a asymptotic bias in this example and it is due to the model mismatch.

σ_θ [deg.]	1	2	3	4	5	6	7	8	9	10
K_{opt} analytical	19	11	8	6	5	4	4	4	3	3
K_{opt} simulated	20	10	7	7	5	4	4	4	3	3
BW simulated [deg.]	6	11	16	16	23	29	29	29	38	38

Table 4.1: Analytical and simulated optimal number of antennas for different angular spreads. BW is the Rayleigh beamwidth of the array. Gaussian ID source with $\theta_0 = 0°$, SNR $= 20$ dB, and $N = 500$.

The asymptotic bias in the nominal angle estimate is negligible, but in the spread estimate it is $\Delta\sigma_\omega = 0.02$ rad. If Figure 4.13 is compared to Figure 4.15, it is found that the erroneous model assumption has little impact on the nominal angle estimates.

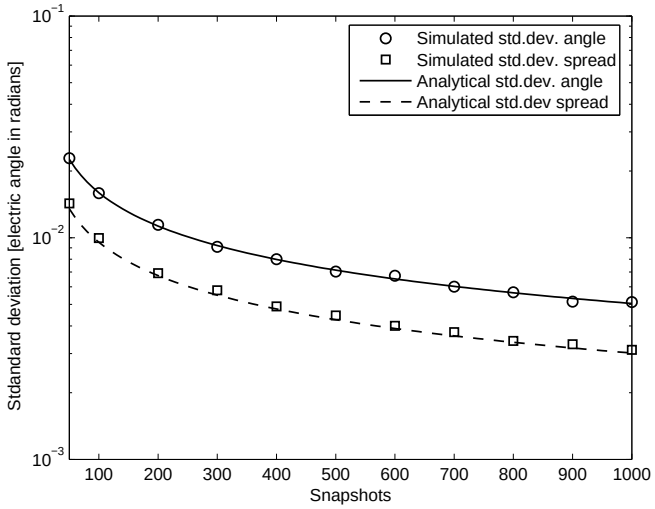

Figure 4.15: Simulated and analytical standard deviation of $\hat{\omega}_0$ and $\hat{\sigma}_\omega$ versus snapshots. Uniform ID source with $\omega_0 = 0$ rad, $\sigma_\omega = 0.1645$ rad, $K = 10$, SNR $= 20$ dB. The model assumes Gaussian ID source.

Example 4.9: Here, G-CBF is used to estimate a Gaussian distributed source with parameters $\omega_0 = 0$ rad, and $\sigma_\omega = 0.1645$ rad, respectively, when there is an interfering Gaussian source present at $\omega_1 = 1.074$ rad, which

corresponds to $\theta_1 = 20°$. The interfering source has the same spread as the source of interest. The SNR is 10 dB for the source of interest and the interfering source is 3 dB weaker. Finally, the array is a standard ULA with ten sensors. Figure 4.16 shows after convergence good agreement between the simulated and analytical standard deviations. The asymptotic bias, which is due to the spectral leakage, in this example is $\Delta\omega_0 = 0.003$ rad and $\Delta\sigma_\omega = 0.036$ rad.

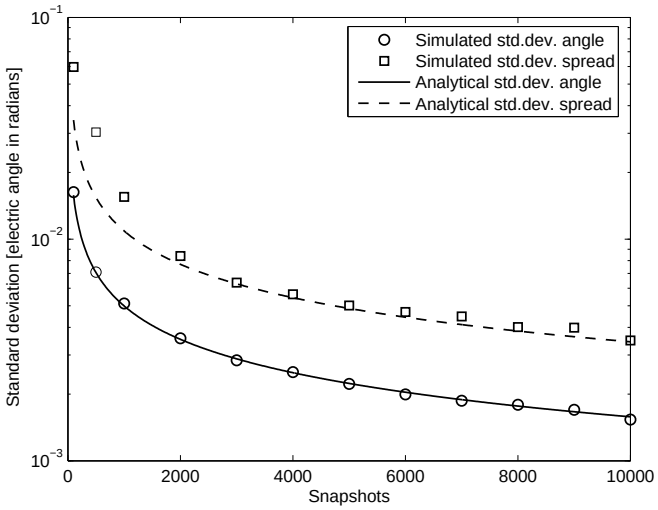

Figure 4.16: Simulated and analytical standard deviation of $\hat{\omega}_0$ and $\hat{\sigma}_{\omega_0}$ versus snapshots. Two Gaussian ID sources with $\{\omega_0 = 0, \sigma_{\omega_0} = 0.1645\}$ rad, resp. $\{\omega_1 = 1.074, \sigma_{\omega_1} = 0.1645\}$ rad. The SNR is 10 dB resp. 7 dB per source, $K = 10$.

4.7 Statistical Performance Analysis of Generalized Capon's Beamforming

As in Section 4.6 we resort to the concept of electric angle and corresponding spread. The results are formulated as two theorems; one for localization of ID sources, and one for CD sources.

4.7.1 G-Capon for Localization of ID sources

Instead of analyzing (4.8) we chose to analyze the equivalent problem

$$\min_{\boldsymbol{\psi}} \lambda_{\max}\{\mathbf{R}_x^{-1}\mathbf{R}_h(\boldsymbol{\psi})\}. \tag{4.21}$$

Typically, the minimization of the largest eigenvalue of a matrix (or equivalently maximization of the smallest eigenvalue) will lead to an optimal solution where the largest and second largest eigenvalues meet (or equivalently the smallest and second smallest). In other words, if $\hat{\theta}$ is given by

$$\hat{\theta} = \arg\min_{\theta} \lambda_{\max}\{\mathbf{A}(\theta)\},$$

for some matrix $\mathbf{A}(\theta) = \mathbf{A}^H(\theta)$, $\theta \in \mathbb{R}$, which is a matrix with eigenvalues $\lambda_1 \geq \lambda_2 \geq \cdots \geq 0$, the largest and second largest eigenvalues evaluated at $\theta = \hat{\theta}$ will be equal, i.e., $\lambda_1(\hat{\theta}) = \lambda_2(\hat{\theta})$. One can identify four cases that can occur; (i) the eigenvalues are simple, (ii) the eigenvalues are repeated with distinct first derivatives, (iii) the eigenvalues are repeated with repeated first derivatives, and (iv) the eigenvalues and their derivatives are infinitely repeated. Figure 4.17 illustrates the four cases. The case of simple eigenvalues (i) does not create any problems with carrying out the analysis, since the eigenvalues with corresponding eigenvectors are uniquely differentiable, while the other cases become hard problems to analyze. For example, case (ii) leads to a criterion function that is non-differentiable in $\theta = \hat{\theta}$, and several orders of continuous differentiability of the asymptotic (in snapshots) criterion function is a requirement to be able to carry out the asymptotic analysis described in, e.g., [Lju87]. The first derivative of an eigenvalue is a function of its corresponding eigenvector, and if the eigenvalue is repeated, say p times, there will be a p-dimensional subspace of eigenvectors that all correspond to this eigenvalue. The first derivative of a repeated eigenvalue is therefore not unique. Because of this non-uniqueness, the computation of eigenvector derivatives that correspond to repeated eigenvalues also becomes difficult. Nonetheless, there exists algorithms for finding eigenvalue derivatives of repeated eigenvalues and they rely on that the eigenvalue derivatives of some higher order are distinct. For example, case (iii) in Figure 4.17 has repeated first order derivatives but the second order derivatives are distinct. The reason for this is that the corresponding eigenvectors are non-unique only in the point $\theta = \hat{\theta}$ where the eigenvalues are repeated, but in some neighborhood around this point the eigenvectors are uniquely defined (up to complex constant), since the eigenvalues are simple for $\theta \neq \hat{\theta}$. Hence, a continuity requirement can be applied to acquire a unique basis for the

eigenspace that corresponds to the repeated eigenvalue, and a part of the problem is to find this unique basis. See, e.g., [AT98] and references therein, for numerical algorithms that can compute eigen-value/vector derivatives for repeated eigenvalues in the one-variable case.

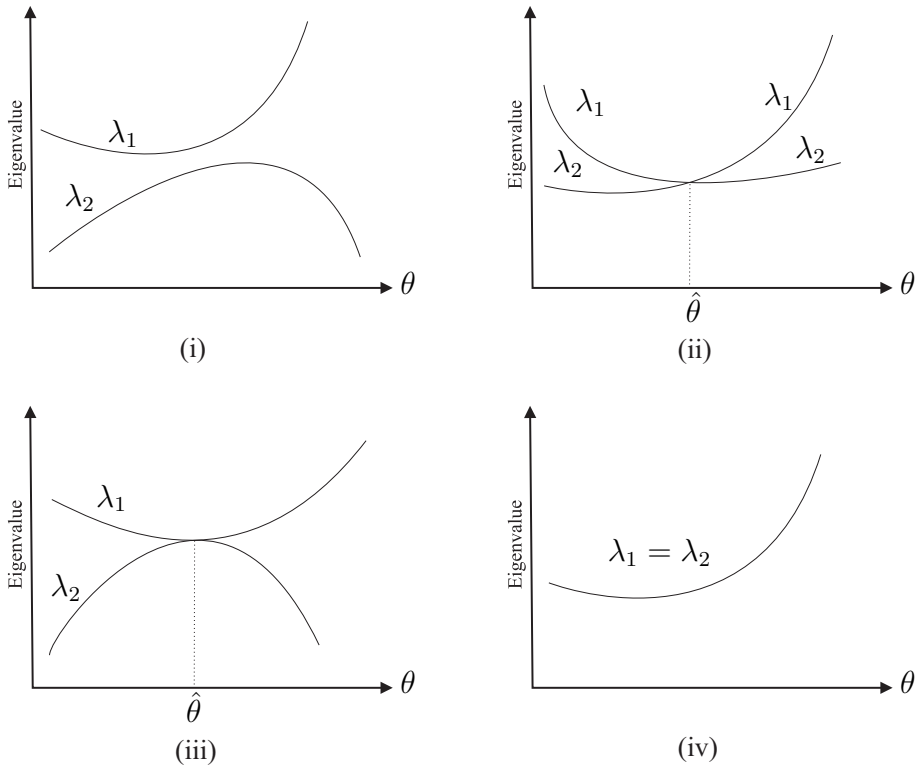

Figure 4.17: Four cases of eigenvalues as functions of a design parameter θ ($\lambda_1 \geq \lambda_2$ by definition); (i) simple eigenvalues, (ii) repeated eigenvalues with distinct first derivatives, (iii) repeated eigenvalues with repeated first derivatives, (iv) infinitely repeated eigenvalues and derivatives.

Extensive numerical evaluations, in many scenarios, of the asymptotic criterion function in (4.21) have shown that we typically have case (i) or (ii) (extended to two dimensions). Thus it is often the case that the asymptotic criterion function is non-differentiable in its optimum, but there also exists scenarios where it is differentiable, i.e., the eigenvalues are distinct. With the requirement of continuous differentiability in mind, we will restrict the analysis to scenarios with distinct eigenvalues, i.e., the eigenvalues can be close but not equal. This restriction leads to that the asymptotic results only are valid for this case. The case of repeated eigenvalues is left as future work,

since it requires the development of a new theory for asymptotic analysis of non-differentiable limit functions, which to the author's knowledge does not exist today. Nonetheless, it turns out that in most cases, the eigenvalues are repeated in the optimum, but for the case of a single source with a model mismatch (in the form of making the wrong assumption on the angular distribution), the eigenvalues are simple.

For low SNR, the G-Capon algorithm is always inconsistent (no matter the eigenvalues are distinct or not) in the sense that the minimizer, denoted by $\boldsymbol{\psi}_*$, of the criterion function $f(\boldsymbol{\psi}, \mathbf{R}_x)$ is not equal to the true parameter vector, i.e., $\boldsymbol{\psi}_* \neq \boldsymbol{\psi}_0$, where

$$\boldsymbol{\psi}_* = \arg\min_{\boldsymbol{\psi}} f(\boldsymbol{\psi}, \mathbf{R}_x), \quad f(\boldsymbol{\psi}, \mathbf{R}_x) = \lambda_{\max}\{\mathbf{R}_x^{-1}(\boldsymbol{\psi}_0)\mathbf{R}_h(\boldsymbol{\psi})\} \tag{4.22}$$

which implies

$$\nabla f(\boldsymbol{\psi}_*, \mathbf{R}_x) = 0. \tag{4.23}$$

Figure 4.18 displays the ratio $(\sigma_{\omega *} - \sigma_\omega)/\sigma_\omega$ versus SNR for a single Gaussian ID source with the true parameters $\omega_0 = 0$ rad, $\sigma_\omega = 0.1645$ rad.

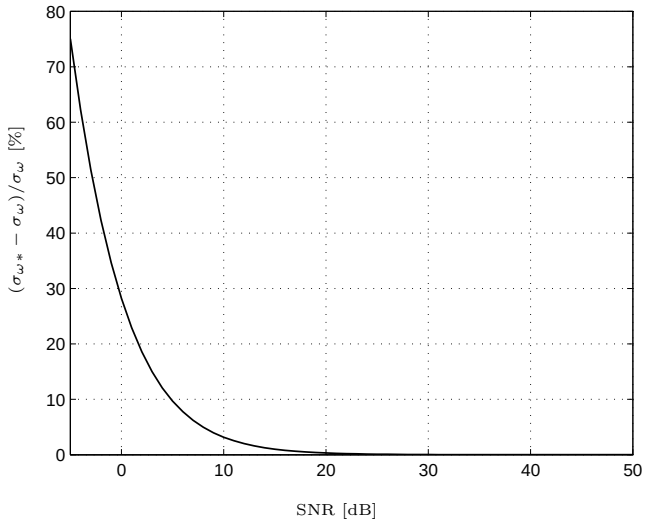

Figure 4.18: Asymptotic bias in percent of the true value vs. SNR. The minimizer $\sigma_{\omega *}$ is attained from (4.22), where $\mathbf{R}_x = \mathbf{R}_h(\boldsymbol{\psi}_0) + \sigma_n^2\mathbf{I}$. Gaussian ID source with $\boldsymbol{\psi} = [0, 0.1645]^T$ rad., $K = 10$ std. ULA.

We will therefore consider the total error $\tilde{\boldsymbol{\psi}}$ to be composed of two terms. The first term is the asymptotic bias term which is given by

$$\Delta\boldsymbol{\psi} = \boldsymbol{\psi}_* - \boldsymbol{\psi}_0, \tag{4.24}$$

and the second term is the random estimation error

$$\tilde{\boldsymbol{\psi}}_* = \hat{\boldsymbol{\psi}}_* - \boldsymbol{\psi}_*, \tag{4.25}$$

where $\hat{\boldsymbol{\psi}}_*$ is defined as

$$\hat{\boldsymbol{\psi}}_* = \arg\min_{\boldsymbol{\psi}} f(\boldsymbol{\psi}, \hat{\mathbf{R}}_x), \qquad f(\boldsymbol{\psi}, \hat{\mathbf{R}}_x) = \lambda_{\max}\{\hat{\mathbf{R}}_x^{-1}\mathbf{R}_h(\boldsymbol{\psi})\} \tag{4.26}$$

which implies that

$$\nabla f(\hat{\boldsymbol{\psi}}_*, \hat{\mathbf{R}}_x) = 0. \tag{4.27}$$

Hence, $\hat{\boldsymbol{\psi}}_*$ is a consistent (as $N \to \infty$) estimate of $\boldsymbol{\psi}_*$. The total error is then given by

$$\tilde{\boldsymbol{\psi}} = \Delta\boldsymbol{\psi} + \tilde{\boldsymbol{\psi}}_* = \hat{\boldsymbol{\psi}}_* - \boldsymbol{\psi}_0, \tag{4.28}$$

The asymptotic error distribution is, thus, derived by using the standard Taylor expansion method (see, e.g., [Lju87]) around the convergence point $\boldsymbol{\psi} = \boldsymbol{\psi}_*$. The results are given in the following theorem.

Theorem 3 (ASYMPTOTIC ERROR DISTRIBUTION FOR G-CAPON APPLIED TO ID SOURCES) *Assume $\mathbf{x}(t) \sim \mathcal{N}(0, \mathbf{R}_x(\boldsymbol{\psi}_0))$ is temporally white, the criterion function is continuously differentiable at the minimizing point, and that $\mathbf{R}_x^{-1}\mathbf{R}_h(\boldsymbol{\psi}_*)$ and $\hat{\mathbf{R}}_x^{-1}\mathbf{R}_h(\boldsymbol{\psi}_*)$ have simple eigenvalues. Then, the asymptotic error of the parameters obtained by inserting the sample covariance matrix into the G-Capon algorithm is for incoherently distributed sources given by*

$$\tilde{\boldsymbol{\psi}} = \hat{\boldsymbol{\psi}} - \boldsymbol{\psi}_0 = \Delta\boldsymbol{\psi} + \tilde{\boldsymbol{\psi}}_*, \tag{4.29}$$

where $\Delta\boldsymbol{\psi}$ and $\tilde{\boldsymbol{\psi}}_*$ are defined in (4.24) and (4.25), respectively. The random error distribution is given by

$$\sqrt{N-K}\tilde{\boldsymbol{\psi}}_* \sim \text{As}\mathcal{N}\left(0, \mathbf{R}_{\tilde{\psi}_*}\right), \tag{4.30}$$

where

$$\mathbf{R}_{\tilde{\psi}_*} = \mathbf{H}^{-1}\boldsymbol{\Phi}\mathbf{H}^{-1}, \tag{4.31}$$

$$[\mathbf{H}]_{ij} = 2\text{Re}\Big\{\mathbf{w}_1^H \frac{\partial \mathbf{R}_1}{\partial \psi_i}\frac{\partial \mathbf{w}_1}{\partial \psi_j}\Big\} + \mathbf{w}_1^H \frac{\partial^2 \mathbf{R}_1}{\partial \psi_i \partial \psi_j}\mathbf{w}_1, \tag{4.32}$$

$$\mathbf{R}_1 = \mathbf{R}_x^{-1/2}\mathbf{R}_h\mathbf{R}_x^{-1/2}. \tag{4.33}$$

The matrix $\boldsymbol{\Phi}$ is, together with the matrix and eigenvector derivatives, given in Appendix 4.C.

Proof: See Appendix 4.C. □

4.7.2 G-Capon for Localization of CD sources

We know from the previous section that G-Capon yields inconsistent estimates when applied to ID sources. This is also the case when G-Capon is applied to CD sources. Thus, the minimizer, denoted by $\boldsymbol{\psi}_*$, of the criterion function $f(\boldsymbol{\psi}, \mathbf{R}_x)$ is not equal to the true parameter vector, i.e., $\boldsymbol{\psi}_* \neq \boldsymbol{\psi}_0$, where

$$\boldsymbol{\psi}_* = \arg\min_{\boldsymbol{\psi}} f(\boldsymbol{\psi}, \mathbf{R}_x), \quad f(\boldsymbol{\psi}, \mathbf{R}_x) = \frac{1}{\mathbf{b}(\boldsymbol{\psi})\mathbf{R}_x^{-1}\mathbf{b}(\boldsymbol{\psi})}. \tag{4.34}$$

Figure 4.19 displays the ratio $(\sigma_{\omega *} - \sigma_\omega)/\sigma_\omega$ for a single Gaussian CD source with the true parameters $\omega_0 = 0.1096$ rad, $\sigma_\omega = 0.1645$ rad. The asymptotic bias is, although, smaller than it was for the ID source in Figure 4.18.

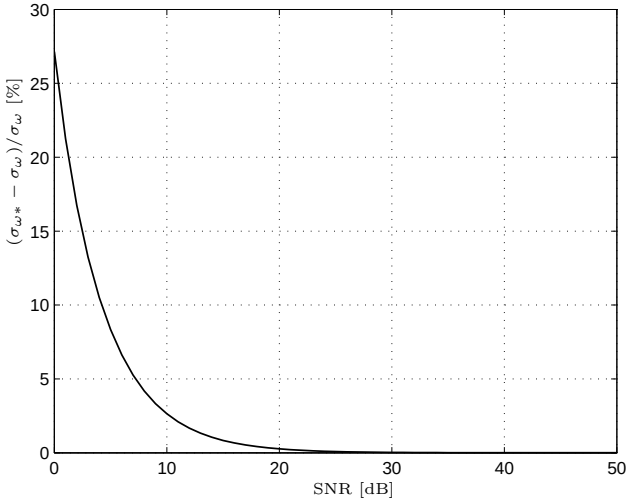

Figure 4.19: Asymptotic bias in percent of the true value vs. SNR. The minimizer $\sigma_{\omega *}$ is attained from (4.34), where $\mathbf{R}_x = \mathbf{R}_h(\boldsymbol{\psi}_0) + \sigma_n^2\mathbf{I}$. Gaussian CD source with $\boldsymbol{\psi} = [0.1096, 0.1645]^T$ rad., $K = 10$ std. ULA.

Theorem 4 (ASYMPTOTIC ERROR DISTRIBUTION FOR G-CAPON APPLIED TO CD SOURCES) *Assume* $\mathbf{x}(t) \sim \mathcal{N}(0, \mathbf{R}_x(\boldsymbol{\psi}_0))$ *is temporally white, and* $\mathbf{R}_x(\boldsymbol{\psi}_0) = \sigma_s^2\mathbf{b}(\boldsymbol{\psi}_0)\mathbf{b}^H(\boldsymbol{\psi}_0) + \sigma_n^2\mathbf{I}_K$. *Then, the asymptotic error of the parameters obtained by inserting the sample covariance matrix into the G-Capon*

algorithm is for coherently distributed sources given by

$$\tilde{\boldsymbol{\psi}} = \hat{\boldsymbol{\psi}} - \boldsymbol{\psi}_0 = \Delta\boldsymbol{\psi} + \tilde{\boldsymbol{\psi}}_*, \tag{4.35}$$

where $\Delta\boldsymbol{\psi}$ and $\tilde{\boldsymbol{\psi}}_*$ are defined in (4.24) and (4.25), respectively. The random error distribution is given by

$$\sqrt{N-K}\tilde{\boldsymbol{\psi}}_* \sim \text{As}\mathcal{N}\left(0, \mathbf{R}_{\tilde{\psi}_*}\right), \tag{4.36}$$

where

$$\mathbf{R}_{\tilde{\psi}_*} = \mathbf{H}^{-1}\boldsymbol{\Phi}\mathbf{H}^{-1}, \tag{4.37}$$

$$[\boldsymbol{\Phi}]_{ij} = 2\text{Re}\Big\{\Big(\mathbf{b}^H\mathbf{R}_x^{-1}\frac{\partial\mathbf{b}}{\partial\psi_j}\Big)\Big(\mathbf{b}^H\mathbf{R}_x^{-1}\frac{\partial\mathbf{b}}{\partial\psi_i}\Big) + \Big(\mathbf{b}^H\mathbf{R}_x^{-1}\mathbf{b}\Big)\Big(\frac{\partial\mathbf{b}^H}{\partial\psi_j}\mathbf{R}_x^{-1}\frac{\partial\mathbf{b}}{\partial\psi_i}\Big)\Big\}, \tag{4.38}$$

$$[\mathbf{H}]_{ij} = 2\text{Re}\Big\{\mathbf{b}^H\mathbf{R}_x^{-1}\frac{\partial^2\mathbf{b}}{\partial\psi_i\partial\psi_j} + \frac{\partial\mathbf{b}^H}{\partial\psi_i}\mathbf{R}_x^{-1}\frac{\partial\mathbf{b}}{\partial\psi_j}\Big\}. \tag{4.39}$$

The vector derivatives are given in Appendix 4.D.

Proof: See Appendix 4.D. □

The asymptotic error variance is validated numerically in Section 4.5, and all the simulated data examples show good agreement with the theoretical results.

4.7.3 Validation with Synthetic Data for ID Sources

In this section, all estimates are averaged over 2000 independent runs, and the noise is spatio-temporally white with a circular symmetric complex Gaussian distribution.

Example 4.10: In this example, G-Capon is used to estimate the parameters of a uniformly distributed source when the model erroneously assumes a Gaussian distribution. The angular distribution is uniform with zero mean and standard deviation $\sigma_\omega = 0.1645$ rad, which correspond to a uniform distribution over $[-\delta_\omega, \delta_\omega]$, with $\delta_\omega = 0.2849$ rad. The array is a standard ULA with 10 sensors, and the SNR is 20 dB. This particular parameter setting yields the asymptotic bias in the spread estimate $\Delta\sigma_\omega = 0.025$ rad. Figure 4.20 shows after 1000 snapshots good agreement between the analytical and simulated standard deviations.

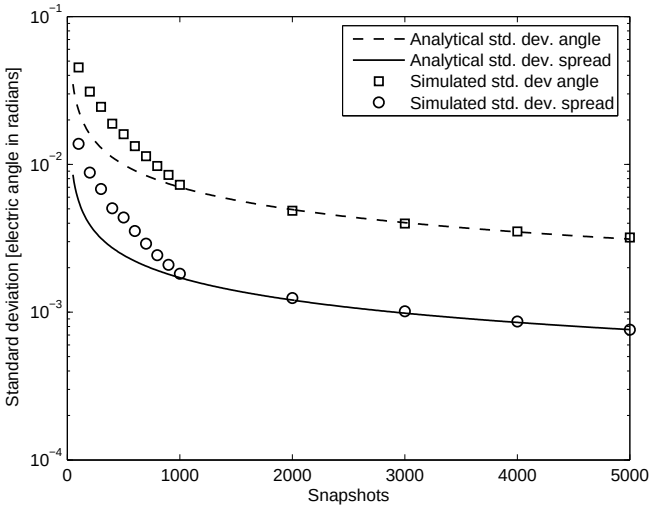

Figure 4.20: Simulated and analytical standard deviation of $\hat{\omega}_0$ and $\hat{\sigma}_\omega$ versus snapshots. Uniform ID source with $\omega_0 = 0$ rad, $\sigma_\omega = 0.1645$ rad, $K = 10$, SNR $= 20$ dB. The model assumes Gaussian ID source.

4.A Proof of Theorem 1: Asymptotic Error Distribution for G-CBF Applied to ID Sources

It is well known that the channel covariance matrix $\mathbf{R}_h(\boldsymbol{\psi})$ can be diagonalized as [MSW96]

$$\mathbf{R}_h(\boldsymbol{\psi}) = \mathbf{D}(\omega)\mathbf{B}(\sigma_\omega)\mathbf{D}^H(\omega), \tag{4.A.1}$$

where $\mathbf{D}(\omega) = \text{diag}\left(1, e^{-j\omega}, \ldots, e^{-j(K-1)\omega}\right)$ and $\mathbf{B}(\sigma_\omega)$ is a $K \times K$ Hermitian matrix that depends only on the shape of the angular distribution $p(\omega; \boldsymbol{\psi}_0)$, and is generally of full rank. Closed-form expressions these matrices have for uniform and Gaussian shapes been derived in, e.g., [Ben99]. For a Gaussian distribution that is symmetric around ω_0, we have

$$[\mathbf{B}(\sigma_\omega)]_{k\ell} = e^{-((k-\ell)\sigma_\omega)^2/2}, \tag{4.A.2}$$

and for a source with uniform distribution over $[-\delta_\omega, \delta_\omega]$, we have

$$[\mathbf{B}(\sigma_\omega)]_{k\ell} = \frac{\sin((k-\ell)\delta_\omega)}{(k-\ell)\delta_\omega}, \quad \delta_\omega = \sqrt{3}\sigma_\omega. \tag{4.A.3}$$

It can be shown that $\mathbf{R}_h(\boldsymbol{\psi})$ and $\mathbf{B}(\sigma_\omega)$ share eigenvalues and that their respective eigenvectors are related according to [MSW96]

$$\mathbf{w}_k(\boldsymbol{\psi}) = \mathbf{D}(\omega)\mathbf{v}_k(\sigma_\omega), \quad k = 1, \ldots, K, \tag{4.A.4}$$

where $\mathbf{w}_k$ and $\mathbf{v}_k$ denote the k^{th} eigenvector of $\mathbf{R}_h(\boldsymbol{\psi})$ and $\mathbf{B}(\sigma_\omega)$, respectively. Since the matrix $\mathbf{B}(\sigma_\omega)$ is Hermitian and positive definite, the eigenvalues become real-valued and positive. We also assume that the eigenvalues, in the point $\boldsymbol{\psi} = \boldsymbol{\psi}_0$, are simple and sorted in a decreasing order $\lambda_1 > \cdots > \lambda_K > 0$, which provides us with a *unique* (up to a complex scalar) set of orthogonal eigenvectors that are sorted as column vectors into the eigenmatrix $\mathbf{V} = [\mathbf{v}_1, \ldots, \mathbf{v}_K]$.

Let $f(\boldsymbol{\psi}, \hat{\mathbf{R}}_x) = \mathbf{w}^H(\boldsymbol{\psi})\hat{\mathbf{R}}_x\mathbf{w}(\boldsymbol{\psi})$ denote the criterion function using the sample covariance matrix, and $f(\boldsymbol{\psi}, \mathbf{R}_x) = \mathbf{w}^H(\boldsymbol{\psi})\mathbf{R}_x\mathbf{w}(\boldsymbol{\psi})$ its limit function (as $N \to \infty$). Applying a standard first order Taylor expansion (neglecting the second and higher order terms) of the gradient $\nabla f(\hat{\boldsymbol{\psi}}, \hat{\mathbf{R}}_x)$ around $\boldsymbol{\psi} = \boldsymbol{\psi}_0$ and equating it to zero yields [Lju87]

$$\tilde{\boldsymbol{\psi}} \triangleq \hat{\boldsymbol{\psi}} - \boldsymbol{\psi}_0 \approx -\mathbf{H}^{-1}\nabla f(\boldsymbol{\psi}_0, \hat{\mathbf{R}}_x), \tag{4.A.5}$$

where $\mathbf{H}^{-1} \triangleq \left(\nabla^2 f(\boldsymbol{\psi}_0, \mathbf{R}_x)\right)^{-1}$ is the inverse asymptotic Hessian matrix and $\nabla f(\boldsymbol{\psi}_0, \hat{\mathbf{R}}_x)$ is the random gradient, both evaluated at $\boldsymbol{\psi} = \boldsymbol{\psi}_0$. The point $\boldsymbol{\psi}_0$ is the true parameter vector, and it yields $\nabla f(\boldsymbol{\psi}_0, \mathbf{R}_x) = 0$. Hence, the covariance matrix of the asymptotic distribution of $\hat{\boldsymbol{\psi}}$ can be expressed as

$$\mathrm{E}\left[\tilde{\boldsymbol{\psi}}\tilde{\boldsymbol{\psi}}^T\right] \approx \mathbf{H}^{-1}\mathrm{E}\left[\nabla f(\boldsymbol{\psi}_0, \hat{\mathbf{R}}_x)\nabla^T f(\boldsymbol{\psi}_0, \hat{\mathbf{R}}_x)\right]\mathbf{H}^{-1}, \tag{4.A.6}$$

and it remains to find the asymptotic Hessian matrix together with the covariance matrix of the asymptotically Gaussian gradient vector. The gradient vector is a linear combination of the sample covariance matrix, thus, the asymptotic normality of the gradient vector follows from the asymptotic normality of the sample covariance matrix.

Finding the Asymptotic Hessian Matrix

To calculate the symmetric matrix $\mathbf{H}$, we need the second order partial derivatives of $f(\boldsymbol{\psi}, \mathbf{R}_x)$ w.r.t. ω and σ_ω, which involves finding the first and second order partial derivatives of the principal eigenvector $\mathbf{w}_1(\boldsymbol{\psi})$, since

$$\begin{aligned}[\mathbf{H}]_{ij} &= \frac{\partial^2 f(\boldsymbol{\psi}, \mathbf{R}_x)}{\partial\psi_i\partial\psi_j} \\ &= 2\mathrm{Re}\left\{\mathbf{w}_1^H\mathbf{R}_x\frac{\partial^2\mathbf{w}_1}{\partial\psi_i\partial\psi_j} + \frac{\partial\mathbf{w}_1^H}{\partial\psi_i}\mathbf{R}_x\frac{\partial\mathbf{w}_1}{\partial\psi_j}\right\},\end{aligned} \tag{4.A.7}$$

where $i, j = 1, 2$, $\psi_1 = \omega$, and $\psi_2 = \sigma_\omega$. From (4.A.4) it follows that the partial derivatives of $\mathbf{w}_1$ simply can be expressed in the derivatives of $\mathbf{D}(\omega)$ and $\mathbf{v}_1(\sigma_\omega)$, according to

$$\frac{\partial \mathbf{w}_1(\boldsymbol{\psi})}{\partial \omega} = \frac{\partial \mathbf{D}(\omega)}{\partial \omega}\mathbf{v}_1(\sigma_\omega) \tag{4.A.8}$$

$$\frac{\partial \mathbf{w}_1(\boldsymbol{\psi})}{\partial \sigma_\omega} = \mathbf{D}(\omega)\frac{\partial \mathbf{v}_1(\sigma_\omega)}{\partial \sigma_\omega} \tag{4.A.9}$$

$$\frac{\partial^2 \mathbf{w}_1(\boldsymbol{\psi})}{\partial \omega^2} = \frac{\partial^2 \mathbf{D}(\omega)}{\partial \omega^2}\mathbf{v}_1(\sigma_\omega) \tag{4.A.10}$$

$$\frac{\partial^2 \mathbf{w}_1(\boldsymbol{\psi})}{\partial \sigma_\omega^2} = \mathbf{D}(\omega)\frac{\partial^2 \mathbf{v}_1(\sigma_\omega)}{\partial \sigma_\omega^2} \tag{4.A.11}$$

$$\frac{\partial^2 \mathbf{w}_1(\boldsymbol{\psi})}{\partial \omega \partial \sigma_\omega} = \frac{\partial \mathbf{D}(\omega)}{\partial \omega}\frac{\partial \mathbf{v}_1(\sigma_\omega)}{\partial \sigma_\omega}, \tag{4.A.12}$$

where

$$\frac{\partial \mathbf{D}(\omega)}{\partial \omega} = \operatorname{diag}\left(0, -je^{-j\omega}, \ldots, -j(K-1)e^{-j(K-1)\omega}\right) \tag{4.A.13}$$

$$\frac{\partial^2 \mathbf{D}(\omega)}{\partial \omega^2} = \operatorname{diag}\left(0, -e^{-j\omega}, \ldots, -(K-1)^2 e^{-j(K-1)\omega}\right). \tag{4.A.14}$$

It remains to find the first and second order derivatives of the eigenvector $\mathbf{v}_1(\sigma_\omega)$, which has similarities to perturbation analysis of eigenvectors. The method we use is, thus, inspired by the first order eigenvector perturbation analysis described in [FW98], and is modified to suit our purpose.

Equipped with the previous assumption of simple eigenvalues, the eigenvectors form a unique orthonormal basis of the whole space $\mathbb{C}^K$. Therefore, we can express the first derivative of the k^{th} eigenvector as a linear combination of all the eigenvectors

$$\frac{\partial \mathbf{v}_k(\sigma_\omega)}{\partial \sigma_\omega} = \sum_{\ell=1}^{K} \alpha_\ell(\sigma_\omega)\mathbf{v}_\ell(\sigma_\omega). \tag{4.A.15}$$

The eigenvector derivative is then found by differentiating the eigen-equation

$$\mathbf{B}(\sigma_\omega)\mathbf{v}_k(\sigma_\omega) = \lambda_k(\sigma_\omega)\mathbf{v}_k(\sigma_\omega)$$

w.r.t. σ_ω, which after some re-arranging results in

$$(\mathbf{B} - \lambda_k \mathbf{I})\frac{\partial \mathbf{v}_k}{\partial \sigma_\omega} = -\frac{\partial \mathbf{B}}{\partial \sigma_\omega}\mathbf{v}_k + \frac{\partial \lambda_k}{\partial \sigma_\omega}\mathbf{v}_k. \tag{4.A.16}$$

Since the matrix $\mathbf{B}-\lambda_k\mathbf{I}$ has rank $K-1$, we can not simply solve for $\partial\mathbf{v}_k/\partial\sigma_\omega$ by using matrix inversion. Instead we note that

$$(\mathbf{B}-\lambda_k\mathbf{I}) = \mathbf{V}_k\mathbf{\Lambda}_k\mathbf{V}_k^H = \sum_{\substack{\ell=1\\ \ell\neq k}}^{K}(\lambda_\ell-\lambda_k)\mathbf{v}_\ell\mathbf{v}_\ell^H, \tag{4.A.17}$$

where

$$\mathbf{V}_k = [\mathbf{v}_1,\ldots,\mathbf{v}_{k-1},\mathbf{v}_{k+1},\ldots,\mathbf{v}_K] \tag{4.A.18}$$

$$\mathbf{\Lambda}_k = \operatorname{diag}(\lambda_1-\lambda_k,\ldots,\lambda_{k-1}-\lambda_k,\lambda_{k+1}-\lambda_k,\ldots,\lambda_K-\lambda_k). \tag{4.A.19}$$

By multiplying (4.A.16) by $\mathbf{V}_k\mathbf{\Lambda}_k^{-1}\mathbf{V}_k^H$ from the left we arrive at

$$\begin{aligned}\mathbf{V}_k\mathbf{V}_k^H\frac{\partial\mathbf{v}_k}{\partial\sigma_\omega} &= -\mathbf{V}_k\mathbf{\Lambda}_k^{-1}\mathbf{V}_k^H\frac{\partial\mathbf{B}}{\partial\sigma_\omega}\mathbf{v}_k + \frac{\partial\lambda_k}{\partial\sigma_\omega}\mathbf{V}_k\mathbf{\Lambda}_k^{-1}\underbrace{\mathbf{V}_k^H\mathbf{v}_k}_{=0}\\ &= \mathbf{p}_k,\end{aligned} \tag{4.A.20}$$

where $\mathbf{p}_k$ is the projection of $\partial\mathbf{v}_k/\partial\sigma_\omega$ into the column space of $\mathbf{V}_k$, and the derivative of $\mathbf{B}(\sigma_\omega)$ is readily found from differentiating the applicable matrix (4.A.2) or (4.A.3). We can, therefore, write

$$\frac{\partial\mathbf{v}_k(\sigma_\omega)}{\partial\sigma_\omega} = \mathbf{p}_k(\sigma_\omega)+\alpha_k(\sigma_\omega)\mathbf{v}_k(\sigma_\omega). \tag{4.A.21}$$

The weight α_k represents the component of each eigenvector derivative along the eigenvector itself, and it can be chosen by introducing some additional normalization. The eigenvectors have unit norm, therefore, by differentiating the inner product $\mathbf{v}_k^H\mathbf{v}_k = 1$, it is readily found (see below) that $\operatorname{Re}\{\alpha_k\} = 0$, $k = 1,\ldots,K$. The imaginary part can be found by introducing an additional constraint, such as, e.g., the one that MATLAB® uses in its "svd" (singular value decomposition) routine where it forces all singular vectors (which can be used in lieu of eigenvectors of positive definite Hermitian matrices) to have a real-valued first element. Instead, to use a less pragmatic approach, we use the fact that a normalized complex-valued eigenvector multiplied by a arbitrary complex phase rotation $e^{j\phi}$, $\phi\in\mathbb{R}$, also is an eigenvector that corresponds to the same eigenvalue. Thus without any loss of generality, we can always choose a new phase rotated orthonormal basis of eigenvectors whose derivative of each eigenvector has no component along the eigenvector itself, i.e., $\alpha_k = 0$, $k = 1,\ldots,K$. This approach is valid as long as the eigenvectors, as here, are functions of one variable, and we show the existence of such a phase rotated basis next.

It is readily verified that if $\mathbf{v}_k(\sigma_\omega)$, $\sigma_\omega \in \mathbb{R}$, is a complex-valued eigenvector with corresponding eigenvalue $\lambda_k(\sigma_\omega)$, then the vector $e^{j\phi_k(\sigma_\omega)}\mathbf{v}_k(\sigma_\omega)$ is also an eigenvector that corresponds to the same eigenvalue $\lambda_k(\sigma_\omega)$. We want to find a phase rotation $e^{j\phi_k(\sigma_\omega)}$ such that

$$\frac{\partial}{\partial\sigma_\omega}\left(e^{j\phi_k(\sigma_\omega)}\mathbf{v}_k(\sigma_\omega)\right) \perp e^{j\phi_k(\sigma_\omega)}\mathbf{v}_k(\sigma_\omega).$$

Since the eigenvectors uniquely span the whole space $\mathbb{C}^K$, we can assume that the eigenvector derivative is given by (4.A.15). To find the phase rotation, we form the following inner product and equate it to zero

$$\begin{aligned}\left(e^{j\phi_k}\mathbf{v}_k\right)^H \frac{\partial}{\partial\sigma_\omega}\left(e^{j\phi_k}\mathbf{v}_k\right) &= e^{-j\phi_k}\mathbf{v}_k^H\left(j\frac{\partial\phi_k}{\partial\sigma_\omega}e^{j\phi_k}\mathbf{v}_k + e^{j\phi_k}\frac{\partial\mathbf{v}_k}{\partial\sigma_\omega}\right)\\ &= j\frac{\partial\phi_k}{\partial\sigma_\omega}\underbrace{\mathbf{v}_k^H\mathbf{v}_k}_{=1} + \underbrace{\mathbf{v}_k^H\frac{\partial\mathbf{v}_k}{\partial\sigma_\omega}}_{=\alpha_k}\\ &= 0, \end{aligned} \tag{4.A.22}$$

where α_k is imaginary, since differentiating the inner product $\mathbf{v}_k^H\mathbf{v}_k = 1$ yields

$$\frac{\partial\mathbf{v}_k^H}{\partial\sigma_\omega}\mathbf{v}_k + \mathbf{v}_k^H\frac{\partial\mathbf{v}_k}{\partial\sigma_\omega} = 2\mathrm{Re}\left\{\mathbf{v}_k^H\frac{\partial\mathbf{v}_k}{\partial\sigma_\omega}\right\} = 2\mathrm{Re}\left\{\alpha_k\right\} = 0. \tag{4.A.23}$$

The solution to (4.A.22) is then given by

$$\phi_k(\sigma_\omega) = -\int \mathrm{Im}\{\alpha_k(\sigma_\omega)\}\, d\sigma_\omega,$$

and we can conclude that there is no loss in generality by setting the derivative of a complex-valued normalized eigenvector to be orthogonal to the eigenvector itself. This can be done since we can always choose to work with the eigenvectors that yield $\alpha_k = 0$, and we now know how to find them. In the case of real-valued eigenvectors, equation (4.A.23) alone yields the orthogonality property.

Once the first derivatives $\{\mathbf{v}_k'(\sigma_\omega)\}_{k=1}^K$ are found, it is straightforward to find the second derivative of the principal eigenvector $\mathbf{v}_1''(\sigma_\omega)$ by setting α_1 to zero and differentiating $\mathbf{p}_1$ in (4.A.20) w.r.t. σ_ω

$$\begin{aligned}\frac{\partial^2\mathbf{v}_1(\sigma_\omega)}{\partial\sigma_\omega^2} = \frac{\partial\mathbf{p}_1(\sigma_\omega)}{\partial\sigma_\omega} &= -\frac{\partial\mathbf{V}_1}{\partial\sigma_\omega}\mathbf{\Lambda}_1^{-1}\mathbf{V}_1^H\frac{\partial\mathbf{B}}{\partial\sigma_\omega}\mathbf{v}_1 - \mathbf{V}_1\frac{\partial\mathbf{\Lambda}_1^{-1}}{\partial\sigma_\omega}\mathbf{V}_1^H\frac{\partial\mathbf{B}}{\partial\sigma_\omega}\mathbf{v}_1\\ &\quad - \mathbf{V}_1\mathbf{\Lambda}_1^{-1}\frac{\partial\mathbf{V}_1^H}{\partial\sigma_\omega}\frac{\partial\mathbf{B}}{\partial\sigma_\omega}\mathbf{v}_1 - \mathbf{V}_1\mathbf{\Lambda}_1^{-1}\mathbf{V}_1^H\frac{\partial^2\mathbf{B}}{\partial\sigma_\omega^2}\mathbf{v}_1\\ &\quad - \mathbf{V}_1\mathbf{\Lambda}_1^{-1}\mathbf{V}_1^H\frac{\partial\mathbf{B}}{\partial\sigma_\omega}\frac{\partial\mathbf{v}_1}{\partial\sigma_\omega}, \end{aligned} \tag{4.A.24}$$

where the elements of the derivative of the inverted eigenvalue matrix are given by

$$\left[\frac{\partial \mathbf{\Lambda}_1^{-1}}{\partial \sigma_\omega}\right]_{kk} = \frac{1}{(\lambda_k - \lambda_1)^2}\left(\frac{\partial \lambda_1}{\partial \sigma_\omega} - \frac{\partial \lambda_k}{\partial \sigma_\omega}\right). \tag{4.A.25}$$

The eigenvalue derivatives are easily attained by multiplying (4.A.16) from the left by $\mathbf{v}_k^H$, and after re-arranging it yields

$$\frac{\partial \lambda_k(\sigma_\omega)}{\partial \sigma_\omega} = \mathbf{v}_k^H \frac{\partial \mathbf{B}}{\partial \sigma_\omega}\mathbf{v}_k. \tag{4.A.26}$$

Thus, we have all we need to evaluate the elements of the asymptotic Hessian matrix (4.A.7).

Finding the Gradient Covariance Matrix

Since the sample covariance matrix is asymptotically Gaussian distributed, the random gradient also becomes asymptotically Gaussian. The covariance matrix of the random gradient vector in (4.A.6) is found by differentiating $f(\boldsymbol{\psi}, \hat{\mathbf{R}}_x)$ w.r.t. ω and σ_ω in the same fashion as described above. Once the gradient vector is found, a first order perturbation of the gradient vector is performed. By removing terms that are zero and omitting second and higher order terms, the $(i,j)^{\text{th}}$ entry of the gradient covariance matrix becomes

$$\begin{aligned}[\mathbf{\Phi}]_{ij} \triangleq \mathrm{E}\left[\nabla f(\boldsymbol{\psi}_0, \hat{\mathbf{R}}_x)\nabla^T f(\boldsymbol{\psi}_0, \hat{\mathbf{R}}_x)\right]_{ij} = 2\mathrm{E}\Bigg[\mathrm{Re}\Bigg\{ \mathbf{w}_1^H \tilde{\mathbf{R}}_x \frac{\partial \mathbf{w}_1}{\partial \psi_i} \mathbf{w}_1^H \tilde{\mathbf{R}}_x \frac{\partial \mathbf{w}_1}{\partial \psi_j} \\ + \mathbf{w}_1^H \tilde{\mathbf{R}}_x \frac{\partial \mathbf{w}_1}{\partial \psi_i} \frac{\partial \mathbf{w}_1^H}{\partial \psi_j} \tilde{\mathbf{R}}_x \mathbf{w}_1 \Bigg\}\Bigg],\end{aligned} \tag{4.A.27}$$

where $\tilde{\mathbf{R}}_x$ is the zero mean perturbation matrix, i.e., $\tilde{\mathbf{R}}_x = \hat{\mathbf{R}}_x - \mathbf{R}_x$, and is of order in probability $1/\sqrt{N}$.

Since $N\hat{\mathbf{R}}_x \sim \mathcal{CW}_K(\mathbf{R}_x, N)$, where $\mathcal{CW}_K(\mathbf{R}_x, N)$ denotes a complex central Wishart distribution with N degrees of freedom, we can invoke known expectations of complex Wishart forms. From, e.g., [TC94] we have

$$\mathrm{E}\left[\mathbf{y}_1^H \tilde{\mathbf{R}}_x \mathbf{y}_2 \mathbf{y}_3^H \tilde{\mathbf{R}}_x \mathbf{y}_4\right] = \frac{1}{N}\left(\mathbf{y}_1^H \mathbf{R}_x \mathbf{y}_4\right)\left(\mathbf{y}_3^H \mathbf{R}_x \mathbf{y}_2\right),$$

where the $\mathbf{y}_i$'s are deterministic vectors. This will yield a closed-form expression for the covariance of the asymptotic distribution, and it is given

by

$$[\mathbf{\Phi}]_{ij} = \frac{2}{N}\mathrm{Re}\Bigg\{ \left(\mathbf{w}_1^H \mathbf{R}_x \frac{\partial \mathbf{w}_1}{\partial \psi_j}\right)\left(\mathbf{w}_1^H \mathbf{R}_x \frac{\partial \mathbf{w}_1}{\partial \psi_i}\right) + \left(\mathbf{w}_1^H \mathbf{R}_x \mathbf{w}_1\right)\left(\frac{\partial \mathbf{w}_1^H}{\partial \psi_j}\mathbf{R}_x \frac{\partial \mathbf{w}_1}{\partial \psi_i}\right)\Bigg\}, \tag{4.A.28}$$

where the weight vector derivatives are respectively given by (4.A.8), and by inserting (4.A.21) with $\alpha_k = 0$ into (4.A.9), this concludes the proof. □

4.B Proof of Theorem 2: Asymptotic Error Distribution for G-CBF Applied to CD Sources

That the G-CBF algorithm for CD sources provides consistent estimates is readily verified by using the same arguments that were used for showing the consistency of G-CBF for ID sources.

Direct application of the Taylor expansion method in, e.g., [Lju87] yields the asymptotic error covariance matrix. Therefore, we only calculate the asymptotic Hessian matrix and the covariance matrix of the random gradient.

Finding the Asymptotic Hessian Matrix

Let $\boldsymbol{\psi} = [\omega, \sigma_\omega]^T$. The first partial derivatives of the criterion function

$$f(\boldsymbol{\psi}, \mathbf{R}_x) = \frac{\mathbf{w}^H(\boldsymbol{\psi})\mathbf{R}_x\mathbf{w}(\boldsymbol{\psi})}{\mathbf{w}^H(\boldsymbol{\psi})\mathbf{w}(\boldsymbol{\psi})}, \quad \mathbf{w}(\boldsymbol{\psi}) = \frac{\mathbf{b}(\boldsymbol{\psi})}{\|\mathbf{b}(\boldsymbol{\psi})\|}$$

are given by

$$\frac{\partial f(\boldsymbol{\psi}, \mathbf{R}_x)}{\partial \psi_i} = 2\mathrm{Re}\left\{\mathbf{w}^H \mathbf{R}_x \frac{\partial \mathbf{w}}{\partial \psi_i}\right\}. \tag{4.B.1}$$

The $(i,j)^{\text{th}}$ element of the asymptotic Hessian matrix $\mathbf{H}$ is given by

$$[\mathbf{H}]_{ij} = \frac{\partial^2 f(\boldsymbol{\psi}_0, \mathbf{R}_x)}{\partial \psi_i \partial \psi_j} = 2\mathrm{Re}\left\{\mathbf{w}^H \mathbf{R}_x \frac{\partial^2 \mathbf{w}}{\partial \psi_i \partial \psi_j} + \frac{\partial \mathbf{w}^H}{\partial \psi_i}\mathbf{R}_x \frac{\partial \mathbf{w}}{\partial \psi_j}\right\}, \tag{4.B.2}$$

where

$$\frac{\partial \mathbf{w}}{\partial \psi_i} = \frac{\frac{\partial \mathbf{b}}{\partial \psi_i}\|\mathbf{b}\| - \mathbf{b}\frac{\partial \|\mathbf{b}\|}{\partial \psi_i}}{\|\mathbf{b}\|^2}, \tag{4.B.3}$$

and

$$\frac{\partial^2 \mathbf{w}}{\partial\psi_i\partial\psi_j} = \left(\left(\frac{\partial^2 \mathbf{b}}{\partial\psi_i\partial\psi_j}\|\mathbf{b}\| + \frac{\partial \mathbf{b}}{\partial\psi_i}\frac{\partial\|\mathbf{b}\|}{\partial\psi_j} - \frac{\partial \mathbf{b}}{\partial\psi_j}\frac{\partial\|\mathbf{b}\|}{\partial\psi_i} - \mathbf{b}\frac{\partial^2\|\mathbf{b}\|}{\partial\psi_i\partial\psi_j} \right) \|\mathbf{b}\|^2 - \left(\frac{\partial \mathbf{b}}{\partial\psi_i}\|\mathbf{b}\| - \mathbf{b}\frac{\partial\|\mathbf{b}\|}{\partial\psi_i} \right) \frac{\partial\|\mathbf{b}\|^2}{\partial\psi_j} \right) \Big/ \|\mathbf{b}\|^4. \tag{4.B.4}$$

The partial derivative of $\|\mathbf{b}\|^2$ is given by

$$\frac{\partial\|\mathbf{b}\|^2}{\partial\psi_i} = \frac{\partial}{\partial\psi_i}(\mathbf{b}^H\mathbf{b}) = 2\mathrm{Re}\left\{ \mathbf{b}^H\frac{\partial \mathbf{b}}{\partial\psi_i} \right\},$$

and the partial derivative of $\|\mathbf{b}\|$ is, thus, given by

$$\frac{\partial\|\mathbf{b}\|}{\partial\psi_i} = \frac{\partial}{\partial\psi_i}(\mathbf{b}^H\mathbf{b})^{1/2} = \frac{1}{\|\mathbf{b}\|}\mathrm{Re}\left\{ \mathbf{b}^H\frac{\partial \mathbf{b}}{\partial\psi_i} \right\}.$$

Finally, the second order partial derivative of $\|\mathbf{b}\|$ becomes

$$\frac{\partial^2\|\mathbf{b}\|}{\partial\psi_i\partial\psi_j} = \frac{\partial}{\partial\psi_j}\left(\frac{1}{\|\mathbf{b}\|}\mathrm{Re}\left\{ \mathbf{b}^H\frac{\partial \mathbf{b}}{\partial\psi_i} \right\} \right) = \left(\mathrm{Re}\left\{ \frac{\partial \mathbf{b}^H}{\partial\psi_j}\frac{\partial \mathbf{b}}{\partial\psi_i} + \mathbf{b}^H\frac{\partial^2 \mathbf{b}}{\partial\psi_i\partial\psi_j} \right\} \|\mathbf{b}\| - \mathrm{Re}\left\{ \mathbf{b}^H\frac{\partial \mathbf{b}}{\partial\psi_i} \right\} \frac{\partial\|\mathbf{b}\|}{\partial\psi_j} \right) \Big/ \|\mathbf{b}\|^2. \tag{4.B.5}$$

The derivatives we derived for the weight vector correspond to a general steering vector $\mathbf{b}(\boldsymbol{\psi})$. The expressions can be simplified if we assume that $\mathbf{b}(\boldsymbol{\psi})$ is the generalized steering vector of a ULA, and the angular density function $g(\omega;\boldsymbol{\psi})$ is, e.g., Gaussian or uniform. The generalized steering vector is, thus, given by

$$\mathbf{b}(\boldsymbol{\psi}) = \int_{\omega\in\Omega} g(\omega;\boldsymbol{\psi})\mathbf{a}(\omega)d\omega. \tag{4.B.6}$$

Now, if $g(\omega;\boldsymbol{\psi})$ is a *Gaussian* density function that is symmetric around ω_0, and has a small standard deviation σ_ω, we can calculate the elements of $\mathbf{b}(\boldsymbol{\psi})$ by solving the following integral

$$\begin{aligned}
[\mathbf{b}(\boldsymbol{\psi})]_k &= \frac{1}{\sqrt{2\pi\sigma_\omega^2}}\int_{-\infty}^{\infty} \exp(-(\omega-\omega_0)^2/(2\sigma_w^2))\exp(-jk\omega)d\omega \\
&= \frac{1}{\sqrt{2\pi\sigma_\omega^2}}\int_{-\infty}^{\infty} \exp(-\omega^2/(2\sigma_\omega^2))\exp(-jk(\omega+\omega_0))d\omega \\
&= \frac{\exp(-jk\omega_0)}{\sqrt{2\pi\sigma_\omega^2}}\int_{-\infty}^{\infty} \exp(-\omega^2/(2\sigma_\omega^2))\exp(-jk\omega)d\omega \\
&= \exp(-(k\sigma_\omega)^2/2)\exp(-jk\omega_0) \\
&= \exp(-(k\sigma_\omega)^2/2)[\mathbf{a}(\omega_0)]_k, \quad k=0,\ldots,K-1.
\end{aligned} \tag{4.B.7}$$

Similarly, a density function that is *uniform* over $|\omega - \omega_0| < \delta_\omega$, yields

$$\begin{aligned}[\mathbf{b}(\boldsymbol{\psi})]_k &= \frac{1}{2\delta_\omega}\int_{\omega_0-\delta_\omega}^{\omega_0+\delta_\omega}[\mathbf{a}(\omega)]d\omega = \frac{\exp(-jk\omega_0)}{2\delta_\omega}\int_{-\delta_\omega}^{\delta_\omega}\exp(-jk\omega)d\omega \\ &= \operatorname{sinc}(k\delta_\omega/\pi)[\mathbf{a}(\omega_0)]_k, \quad k = 0,\ldots,K-1. \end{aligned} \tag{4.B.8}$$

Thus, the norm $\|\mathbf{b}(\boldsymbol{\psi})\|$ becomes independent of ω, which implies that any order partial derivative of $\|\mathbf{b}(\boldsymbol{\psi})\|$ w.r.t. $\psi_1 = \omega$ is zero. The partial derivatives of the vector $\mathbf{b}(\boldsymbol{\psi})$ are easily obtained from, e.g., (4.B.7) or (4.B.8).

Finding the Gradient Covariance Matrix

The elements of the random gradient are found by inserting the sample covariance matrix into (4.B.1), and the gradient covariance matrix is then found by recognizing the covariance matrix as the expected value of a complex Wishart form [TC94]. Hence, we get

$$\begin{aligned}[\boldsymbol{\Phi}]_{ij} &\triangleq \mathrm{E}\left[\nabla f(\boldsymbol{\psi}_0,\hat{\mathbf{R}}_x)\nabla^T f(\boldsymbol{\psi}_0,\hat{\mathbf{R}}_x)\right]_{ij} \\ &= \frac{2}{N}\mathrm{Re}\left\{\left(\mathbf{w}^H\mathbf{R}_x\frac{\partial\mathbf{w}}{\partial\psi_j}\right)\left(\mathbf{w}^H\mathbf{R}_x\frac{\partial\mathbf{w}}{\partial\psi_i}\right) + \left(\mathbf{w}^H\mathbf{R}_x\mathbf{w}\right)\left(\frac{\partial\mathbf{w}^H}{\partial\psi_j}\mathbf{R}_x\frac{\partial\mathbf{w}}{\partial\psi_i}\right)\right\}, \end{aligned} \tag{4.B.9}$$

where the weight vector derivatives are given by (4.B.3). □

4.C Proof of Theorem 3: Asymptotic Error Distribution for G-Capon Applied to ID Sources

We let $f(\boldsymbol{\psi},\hat{\mathbf{R}}_x) = \lambda_{\max}\{\hat{\mathbf{R}}_x^{-1}\mathbf{R}_h(\boldsymbol{\psi})\}$ denote the criterion function when the sample covariance matrix is used, and $f(\boldsymbol{\psi},\mathbf{R}_x) = \lambda_{\max}\{\mathbf{R}_x^{-1}\mathbf{R}_h(\boldsymbol{\psi})\}$ be its limit function as the numbers of snapshots tend to infinity. The convergence is uniform and w.p.1. as long as the largest eigenvalue is a continuous function of the matrix elements. To ensure that both the criterion function and its limit function are continuously differentiable at their respective minimizing points, and to provide a unique eigenvector basis, we assume that the first two eigenvalues of the matrix $\hat{\mathbf{R}}_x^{-1}\mathbf{R}_h(\boldsymbol{\psi})$, at the minimizing point $\boldsymbol{\psi} = \hat{\boldsymbol{\psi}}_*$, are distinct, i.e., $\lambda_1(\hat{\boldsymbol{\psi}}_*,\hat{\mathbf{R}}_x) > \lambda_2(\hat{\boldsymbol{\psi}}_*,\hat{\mathbf{R}}_x)$. This ensures differentiability of the random criterion function. Similarly, we assume that *all* the eigenvalues of the matrices $\hat{\mathbf{R}}_x^{-1}\mathbf{R}_h(\boldsymbol{\psi})$ and $\mathbf{R}_x^{-1}\mathbf{R}_h(\boldsymbol{\psi})$, at the minimizing point $\boldsymbol{\psi} = \boldsymbol{\psi}_*$, are distinct and sorted in a decreasing fashion, i.e., $\lambda_1(\boldsymbol{\psi}_*,\hat{\mathbf{R}}_x) > \lambda_2(\boldsymbol{\psi}_*,\hat{\mathbf{R}}_x) > \cdots > \lambda_K(\boldsymbol{\psi}_*,\hat{\mathbf{R}}_x) > 0$, and

$\lambda_1(\boldsymbol{\psi}_*, \mathbf{R}_x) > \lambda_2(\boldsymbol{\psi}_*, \mathbf{R}_x) > \cdots > \lambda_K(\boldsymbol{\psi}_*, \mathbf{R}_x) > 0$, respectively. This ensures both differentiability and unique eigenvector bases. For notational simplicity, we will often write the eigenvalue's (eigenvector's) dependence on $\mathbf{R}_x$ and $\hat{\mathbf{R}}_x$ as λ_k ($\mathbf{w}_k$), respective $\hat{\lambda}_k$ ($\hat{\mathbf{w}}_k$). Their dependence on the variable $\boldsymbol{\psi}$ is implicitly assumed, but not always explicitly written out.

The asymptotic error distribution is derived in the same way as was done for the generalized conventional beamformer. Thus, the asymptotic error is given by [Lju87]

$$\tilde{\boldsymbol{\psi}}_* = \hat{\boldsymbol{\psi}}_* - \boldsymbol{\psi}_* \approx -\mathbf{H}^{-1} \nabla f(\boldsymbol{\psi}_*, \hat{\mathbf{R}}_x), \tag{4.C.1}$$

where $\mathbf{H}^{-1} \triangleq (\nabla^2 f(\boldsymbol{\psi}_*, \mathbf{R}_x))^{-1}$ is the inverse asymptotic Hessian matrix and $\nabla f(\boldsymbol{\psi}_*, \hat{\mathbf{R}}_x)$ is the random gradient, both evaluated at $\boldsymbol{\psi} = \boldsymbol{\psi}_*$. Hence, the covariance matrix of the asymptotic distribution of $\tilde{\boldsymbol{\psi}}_*$ can be expressed as

$$\mathrm{E}\left[\tilde{\boldsymbol{\psi}}_* \tilde{\boldsymbol{\psi}}_*^T\right] \approx \mathbf{H}^{-1} \mathrm{E}\left[\nabla f(\boldsymbol{\psi}_*, \hat{\mathbf{R}}_x) \nabla^T f(\boldsymbol{\psi}_*, \hat{\mathbf{R}}_x)\right] \mathbf{H}^{-1}. \tag{4.C.2}$$

Since the following relation between the eigenvalues holds [Lüt96]

$$\lambda\{\mathbf{R}_x^{-1}\mathbf{R}_h\} = \lambda\{\mathbf{R}_1(\boldsymbol{\psi})\} = \lambda\{\mathbf{R}_2(\boldsymbol{\psi})\},$$

where $\mathbf{R}_1(\boldsymbol{\psi}) \triangleq \mathbf{R}_x^{-1/2}\mathbf{R}_h\mathbf{R}_x^{-1/2}$, and $\mathbf{R}_2(\boldsymbol{\psi}) \triangleq \mathbf{R}_h^{1/2}\mathbf{R}_x^{-1}\mathbf{R}_h^{1/2}$ (all matrix square roots are Hermitian square roots), we can and will interchange between between the last two forms when we calculate the asymptotic Hessian matrix and the random gradient vector, respectively. The eigenvalues of the last two equalities are eigenvalues of Hermitian matrices and, therefore, correspond to orthogonal eigenvectors.

Finding the Asymptotic Hessian Matrix

When we calculate the asymptotic Hessian matrix, we use the criterion function $f(\boldsymbol{\psi}, \mathbf{R}_x) = \lambda_1\{\mathbf{R}_1(\boldsymbol{\psi})\}$ (read $\lambda_1 = \lambda_{\max}$). The first order partial derivative of the largest eigenvalue $\lambda_1(\boldsymbol{\psi})$ of the matrix $\mathbf{R}_1(\boldsymbol{\psi})$ with the corresponding eigenvector $\mathbf{w}_1(\boldsymbol{\psi})$ is given by

$$\frac{\partial \lambda_1(\boldsymbol{\psi})}{\partial \psi_i} = \mathbf{w}_1^H(\boldsymbol{\psi}) \frac{\partial \mathbf{R}_1(\boldsymbol{\psi})}{\partial \psi_i} \mathbf{w}_1(\boldsymbol{\psi}), \tag{4.C.3}$$

and the second order partial derivative is given by

$$\frac{\partial^2 \lambda_1(\boldsymbol{\psi})}{\partial \psi_i \partial \psi_j} = \frac{\partial \mathbf{w}_1^H}{\psi_j} \frac{\partial \mathbf{R}_1}{\partial \psi_i} \mathbf{w}_1 + \mathbf{w}_1^H \frac{\partial^2 \mathbf{R}_1}{\partial \psi_i \partial \psi_j} \mathbf{w}_1 + \mathbf{w}_1^H \frac{\partial \mathbf{R}_1}{\partial \psi_i} \frac{\partial \mathbf{w}_1}{\psi_j}, \tag{4.C.4}$$

where

$$\frac{\partial \mathbf{R}_1(\boldsymbol{\psi})}{\partial \psi_i} = \mathbf{R}_x^{-1/2} \frac{\partial \mathbf{R}_h(\boldsymbol{\psi})}{\partial \psi_i} \mathbf{R}_x^{-1/2} \tag{4.C.5}$$

$$\frac{\partial^2 \mathbf{R}_1(\boldsymbol{\psi})}{\partial \psi_i \partial \psi_j} = \mathbf{R}_x^{-1/2} \frac{\partial^2 \mathbf{R}_h(\boldsymbol{\psi})}{\partial \psi_i \partial \psi_j} \mathbf{R}_x^{-1/2}, \tag{4.C.6}$$

and where the derivatives of $\mathbf{R}_h(\boldsymbol{\psi})$ are readily found by differentiating the diagonalized matrix (4.A.1) for the applicable angular shape. The eigenvector derivatives are found by differentiating the eigen-equation $\mathbf{R}_1(\boldsymbol{\psi})\mathbf{w}_1(\boldsymbol{\psi}) = \lambda_1 \mathbf{w}_1(\boldsymbol{\psi})$ w.r.t. ψ_i, which after some re-arranging results in

$$(\mathbf{R}_1 - \lambda_1 \mathbf{I}) \frac{\partial \mathbf{w}_1}{\partial \psi_i} = -\frac{\partial \mathbf{R}_1}{\partial \psi_i} \mathbf{w}_1 + \frac{\partial \lambda_1}{\partial \psi_i} \mathbf{w}_1. \tag{4.C.7}$$

Since the matrix $\mathbf{R}_1 - \lambda_1 \mathbf{I}$ has rank $K-1$, we can not simply solve for $\partial \mathbf{w}_1 / \partial \psi_i$ by using matrix inversion. Instead we use that

$$(\mathbf{R}_1 - \lambda_1 \mathbf{I}) = \mathbf{W}_1 \boldsymbol{\Lambda}_1 \mathbf{W}_1^H = \sum_{k=2}^{K} (\lambda_k - \lambda_1) \mathbf{w}_k \mathbf{w}_k^H, \tag{4.C.8}$$

where $\mathbf{W}_1 = [\mathbf{w}_2, \ldots, \mathbf{w}_K]$ and $\boldsymbol{\Lambda}_1 = \operatorname{diag}(\lambda_2 - \lambda_1, \ldots, \lambda_K - \lambda_1)$. By multiplying (4.C.7) by $\mathbf{W}_1 \boldsymbol{\Lambda}_1^{-1} \mathbf{W}_1^H$ from the left we arrive at

$$\mathbf{W}_1 \mathbf{W}_1^H \frac{\partial \mathbf{w}_1}{\partial \psi_i} = -\mathbf{W}_1 \boldsymbol{\Lambda}_1^{-1} \mathbf{W}_1^H \frac{\partial \mathbf{R}_1}{\partial \psi_i} \mathbf{w}_1 + \frac{\partial \lambda_1}{\partial \psi_i} \mathbf{W}_1 \boldsymbol{\Lambda}_1^{-1} \underbrace{\mathbf{W}_1^H \mathbf{w}_1}_{=0} \tag{4.C.9}$$

$$= \mathbf{p}_i, \tag{4.C.10}$$

where $\mathbf{p}_i$ is the projection of $\partial \mathbf{w}_1 / \partial \psi_i$ into the column space of $\mathbf{W}_1$. Since the eigenvectors span the whole space $\mathbb{C}^K$, we have for both derivatives

$$\frac{\partial \mathbf{w}_1}{\partial \psi_i} = \mathbf{p}_i + \alpha_i \mathbf{w}_1, \quad i = 1, 2. \tag{4.C.11}$$

In Appendix 4.A, we chose the eigenvectors such that $\alpha = 0$, but since there are now two partial derivatives, we do not have enough degrees of freedom to simply set both constants α_i, $i = 1, 2$, to zero. To determine the constants, we instead take a different approach and differentiate the normalization constraint

$$\mathbf{w}_1^H \mathbf{w}_1 = 1,$$

w.r.t. ψ_1 and ψ_2, which yields

$$2\mathrm{Re}\left\{ \mathbf{w}_1^H \tfrac{\partial \mathbf{w}_1}{\partial \psi_i} \right\} = \mathrm{Re}\{\alpha_i\} = 0 \quad \Leftrightarrow \quad \alpha_i = -\alpha_i^*. \tag{4.C.12}$$

The same normalization as the "svd" routine in MATLAB® is applied. That is, we force all singular vectors (which can be used in lieu of eigenvectors of positive definite Hermitian matrices) to have a real-valued (one can also impose the additional constraint of being non-negative to remove the sign ambiguity) first element, i.e., $\mathrm{Im}\{\mathbf{w}_k(1)\} = 0 \Leftrightarrow \mathbf{w}(1) = \mathbf{w}_1^*(1)$. The eigenvector derivatives will, therefore, also have real-valued first elements, i.e., $\mathrm{Im}\{\partial\mathbf{w}_1(1)/\partial\psi_i\} = 0 \Leftrightarrow \partial\mathbf{w}_1(1)/\partial\psi_i = \partial\mathbf{w}_1^*(1)/\partial\psi_i$. Written out, this yields

$$\begin{aligned}\frac{\partial\mathbf{w}_1(1)}{\partial\psi_i} - \frac{\partial\mathbf{w}_1^*(1)}{\partial\psi_i} &= \mathbf{p}_i(1) + \alpha_i\mathbf{w}_1(1) - (\mathbf{p}_i(1) + \alpha_i\mathbf{w}_1(1))^* \\ &= \mathbf{p}_i(1) - \mathbf{p}_i^*(1) + 2\alpha_i\mathbf{w}_1(1) \\ &= 0. \end{aligned} \tag{4.C.13}$$

The component of $\partial\mathbf{w}_1/\partial\psi_i$ along $\mathbf{w}_1$ is, thus, given by

$$\alpha_i = \frac{\mathbf{p}_i^*(1) - \mathbf{p}_i(1)}{2\mathbf{w}_1(1)} = -j\frac{\mathrm{Im}\{\mathbf{p}_i(1)\}}{\mathbf{w}_1(1)}, \quad i = 1, 2, \tag{4.C.14}$$

which together with (4.C.5), (4.C.6), and (4.C.11) inserted into (4.C.4) gives the elements of the asymptotic Hessian matrix. The asymptotic Hessian is to be evaluated at the point $\boldsymbol{\psi} = \boldsymbol{\psi}_*$, where $\boldsymbol{\psi}_*$ is given by (4.22).

Finding the Gradient Covariance Matrix

When we calculate the random gradient, we use the criterion function given by $f(\boldsymbol{\psi}, \hat{\mathbf{R}}_x) = \lambda_1\{\hat{\mathbf{R}}_2(\boldsymbol{\psi})\}$ where $\hat{\mathbf{R}}_2(\boldsymbol{\psi}) \triangleq \mathbf{R}_h^{1/2}(\boldsymbol{\psi})\hat{\mathbf{R}}_x^{-1}\mathbf{R}_h^{1/2}(\boldsymbol{\psi})$, which enables the usage of known results for expected values of forms of inverted complex Wishart matrices [TC94].

As previously stated, the derivative of the largest eigenvalue is given by

$$\frac{\partial\hat{\lambda}_1(\boldsymbol{\psi})}{\partial\psi_i} = \hat{\mathbf{w}}_1^H(\boldsymbol{\psi})\frac{\partial\hat{\mathbf{R}}_2(\boldsymbol{\psi})}{\partial\psi_i}\hat{\mathbf{w}}_1(\boldsymbol{\psi}), \tag{4.C.15}$$

where $\hat{\mathbf{w}}_1(\boldsymbol{\psi})$ denotes the eigenvector that corresponds to the estimated eigenvalue $\hat{\lambda}_1(\boldsymbol{\psi}) = \lambda_1\{\hat{\mathbf{R}}_2(\boldsymbol{\psi})\}$, and the matrix derivative is given by

$$\frac{\partial\hat{\mathbf{R}}_2(\boldsymbol{\psi})}{\partial\psi_i} = 2\mathrm{Re}\left\{\mathbf{R}_h^{1/2}\hat{\mathbf{R}}_x^{-1}\frac{\partial\mathbf{R}_h^{1/2}}{\partial\psi_i}\right\}. \tag{4.C.16}$$

The derivative of $\mathbf{R}_h^{1/2}(\boldsymbol{\psi})$ w.r.t. $\psi_1 = \omega$ is easily found since

$$\mathbf{R}_h^{1/2}(\boldsymbol{\psi}) = \mathbf{D}(\omega)\mathbf{B}^{1/2}(\sigma_\omega)\mathbf{D}^H(\omega),$$

where $\mathbf{B}^{1/2}(\sigma_\omega)$ is a Hermitian square root, which yields

$$\frac{\partial \mathbf{R}_h^{1/2}(\boldsymbol{\psi})}{\partial \omega} = 2\mathrm{Re}\left\{ \frac{\partial \mathbf{D}(\omega)}{\partial \omega} \mathbf{B}^{1/2}(\sigma_\omega) \mathbf{D}^H(\omega) \right\}, \tag{4.C.17}$$

where $\frac{\partial \mathbf{D}(\omega)}{\partial \omega}$ is given by (4.A.13). The derivative of $\mathbf{R}_h^{1/2}(\boldsymbol{\psi})$ w.r.t. $\psi_2 = \sigma_\omega$ is found as

$$\frac{\partial \mathbf{R}_h^{1/2}(\boldsymbol{\psi})}{\partial \sigma_\omega} = \mathbf{D}(\omega) \frac{\partial \mathbf{B}^{1/2}(\sigma_\omega)}{\partial \sigma_\omega} \mathbf{D}^H(\omega), \tag{4.C.18}$$

where $\partial \mathbf{B}^{1/2}(\sigma_\omega)/\partial \sigma_\omega$ is attained by performing the following differentiation

$$\frac{\partial \mathbf{B}(\sigma_\omega)}{\partial \sigma_\omega} = \frac{\partial}{\partial \sigma_\omega} \left(\mathbf{B}^{1/2} \mathbf{B}^{1/2} \right) = \frac{\partial \mathbf{B}^{1/2}}{\partial \sigma_\omega} \mathbf{B}^{1/2} + \mathbf{B}^{1/2} \frac{\partial \mathbf{B}^{1/2}}{\partial \sigma_\omega}, \tag{4.C.19}$$

and by applying the following identity, $\mathbf{X}$ $(m \times n)$, $\mathbf{Y}$ $(n \times p)$, [Lüt96]

$$\mathrm{vec}(\mathbf{XY}) = (\mathbf{I}_p \otimes \mathbf{X})\,\mathrm{vec}(\mathbf{Y}) = (\mathbf{Y}^T \otimes \mathbf{I}_m)\,\mathrm{vec}(\mathbf{X}).$$

Thus, we have

$$\mathrm{vec}\left(\frac{\partial \mathbf{B}(\sigma_\omega)}{\partial \sigma_\omega} \right) = \left[\left(\left(\mathbf{B}^{1/2} \right)^T \otimes \mathbf{I}_K \right) + \left(\mathbf{I}_K \otimes \mathbf{B}^{1/2} \right) \right] \mathrm{vec}\left(\frac{\partial \mathbf{B}^{1/2}}{\partial \sigma_\omega} \right), \tag{4.C.20}$$

and $\partial \mathbf{B}^{1/2}(\sigma_\omega)/\partial \sigma_\omega$ is finally given by

$$\frac{\partial \mathbf{B}^{1/2}(\sigma_\omega)}{\partial \sigma_\omega} = \mathrm{unvec}_K \left(\left[\left(\left(\mathbf{B}^{1/2} \right)^T \otimes \mathbf{I}_K \right) + \left(\mathbf{I}_K \otimes \mathbf{B}^{1/2} \right) \right]^{-1} \mathrm{vec}\left(\frac{\partial \mathbf{B}}{\partial \sigma_\omega} \right) \right), \tag{4.C.21}$$

where $\mathbf{X} = \mathrm{unvec}_K(\mathbf{x})$ is the reverse vectorization operator, which takes the first set of K elements of $\mathbf{x}$ as the first column vector into $\mathbf{X}$, and the second set of K elements as the second column vector, and so on. The derivative of $\mathbf{B}(\sigma_\omega)$ is easily found from differentiating the applicable matrix (4.A.2) or (4.A.3).

Next, we study the perturbed eigenproblem. The perturbation analysis follows the ideas presented in [FW98]. If $\hat{\mathbf{R}}_x^{-1}$ is perturbed we have

$$\hat{\mathbf{R}}_2 \hat{\mathbf{w}}_1 = \hat{\lambda}_1 \hat{\mathbf{w}}_1 \tag{4.C.22}$$

$$(\mathbf{R}_2 + \tilde{\mathbf{R}}_2)(\mathbf{w}_1 + \tilde{\mathbf{w}}_1) = (\lambda_1 + \tilde{\lambda}_1)(\mathbf{w}_1 + \tilde{\mathbf{w}}_1), \tag{4.C.23}$$

where $\tilde{\mathbf{R}}_2 = \mathbf{R}_h^{1/2}\tilde{\mathbf{R}}_x^{-1}\mathbf{R}_h^{1/2}$, $\tilde{\mathbf{R}}_x^{-1} = \hat{\mathbf{R}}_x^{-1} - \mathbf{R}_x^{-1}$ is the perturbation of the inverse sample covariance matrix, $\tilde{\mathbf{w}}_1 = \hat{\mathbf{w}}_1 - \mathbf{w}_1$ is the eigenvector perturbation, and $\tilde{\lambda}_1 = \hat{\lambda}_1 - \lambda_1$ is the eigenvalue perturbation. In general, algorithms that compute eigenvectors (e.g., MATLAB's "eig" and "svd" routines), return eigenvectors that are normalized to unit norm. We will, therefore, assume that $\|\mathbf{w}_1\| = \|\hat{\mathbf{w}}_1\| = 1$, which means that the perturbation $\tilde{\mathbf{w}}_1$ moves $\mathbf{w}_1$ from one point on the shell of a K-dimensional sphere of radius one to another point $\hat{\mathbf{w}}_1$ on the shell. Using the following first order approximation

$$\hat{\mathbf{w}}_1^H\hat{\mathbf{w}}_1 = (\mathbf{w}_1 + \tilde{\mathbf{w}}_1)^H(\mathbf{w}_1 + \tilde{\mathbf{w}}_1) \cong \mathbf{w}_1^H\mathbf{w}_1 + \tilde{\mathbf{w}}_1^H\mathbf{w}_1 + \mathbf{w}_1^H\tilde{\mathbf{w}}_1, \tag{4.C.24}$$

together with the normalization, leads to the approximate result

$$\tilde{\mathbf{w}}_1^H\mathbf{w}_1 + \mathbf{w}_1^H\tilde{\mathbf{w}}_1 = 2\mathrm{Re}\{\mathbf{w}_1^H\tilde{\mathbf{w}}_1\} \cong 0. \tag{4.C.25}$$

By only keeping the first order terms of (4.C.23), we have

$$(\mathbf{R}_2 - \lambda_1\mathbf{I})\tilde{\mathbf{w}}_1 = -\tilde{\mathbf{R}}_2\mathbf{w}_1 + \tilde{\lambda}_1\mathbf{w}_1, \tag{4.C.26}$$

where we have recognized the fact that $\mathbf{R}_2\mathbf{w}_1 = \lambda_1\mathbf{w}_1$. We again note that the matrix $\mathbf{R}_2 - \lambda_1\mathbf{I}$ has rank $K-1$. Therefore we can use exactly the same calculations as was done in (4.C.8) and (4.C.9) to find the projection of the eigenvector derivative. Thus, we can define the projection of $\tilde{\mathbf{w}}_1$ into the column space of $\mathbf{W}_1 = [\mathbf{w}_2, \ldots, \mathbf{w}_K]$ as

$$\mathbf{W}_1\mathbf{W}_1^H\tilde{\mathbf{w}}_1 = -\mathbf{W}_1\mathbf{\Lambda}_1^{-1}\mathbf{W}_1^H\tilde{\mathbf{R}}_2\mathbf{w}_1 = \mathbf{q}_1, \tag{4.C.27}$$

where $\mathbf{\Lambda}_1 = \mathrm{diag}\,(\lambda_2 - \lambda_1, \ldots, \lambda_K - \lambda_1)$. Finally, since the eigenvectors span the whole space, the eigenvector perturbation can be written as

$$\tilde{\mathbf{w}}_1 = \mathbf{q}_1 + \beta\mathbf{w}_1. \tag{4.C.28}$$

By inserting (4.C.28) into (4.C.25), we find that

$$\mathrm{Re}\{\mathbf{w}_1^H\tilde{\mathbf{w}}_1\} = \mathrm{Re}\{\beta\} = 0. \tag{4.C.29}$$

Here we can choose to apply the additional MATLAB® "svd" constraint to find β or we can select the eigenvectors such that $\beta = 0$, since there exists a phase rotation of the perturbed eigenvector $\hat{\mathbf{w}}_{1,\mathrm{new}} = e^{j\phi}\hat{\mathbf{w}}_1$ such that the perturbation $\tilde{\mathbf{w}}_{1,\mathrm{new}} = e^{j\phi}\hat{\mathbf{w}}_1 - \mathbf{w}_1$ becomes orthogonal to $\mathbf{w}_1$. The phase rotation is found by performing the following inner product and equating it to zero

$$\tilde{\mathbf{w}}_{1,\mathrm{new}}^H\mathbf{w}_1 = \left(e^{j\phi}\hat{\mathbf{w}}_1 - \mathbf{w}_1\right)^H\mathbf{w}_1 = e^{-j\phi}\hat{\mathbf{w}}_1^H\mathbf{w}_1 - 1 \tag{4.C.30}$$

$$= 0, \tag{4.C.31}$$

and from (4.C.29), we already have that the real part of (4.C.30) is zero. Hence, the solution is given by the rotation that makes the imaginary part of (4.C.30) equal to zero, i.e.,

$$\mathrm{Im}\{\tilde{\mathbf{w}}_{1,\mathrm{new}}^H \mathbf{w}_1\} = \mathrm{Im}\{e^{-j\phi}\hat{\mathbf{w}}_1^H \mathbf{w}_1\} = 0,$$

which yields the solution

$$e^{j\phi} = \frac{\hat{\mathbf{w}}_1^H \mathbf{w}_1}{|\hat{\mathbf{w}}_1^H \mathbf{w}_1|},$$

where the denominator ensures unit modulus. Finally, since normalized eigenvectors are invariant to phase rotations, it means that to a first order approximation, we have $\tilde{\mathbf{w}}_1 \cong \mathbf{q}_1$, where $\mathbf{q}_1$ is given by (4.C.27).

The two entries of the perturbed gradient vector $\nabla f(\boldsymbol{\psi}, \hat{\mathbf{R}}_x)$ are given by

$$\frac{\partial \hat{\lambda}_1(\boldsymbol{\psi})}{\partial \psi_i} = (\mathbf{w}_1 + \tilde{\mathbf{w}}_1)^H \left(\frac{\partial \mathbf{R}_h^{1/2}}{\partial \psi_i} (\mathbf{R}_x^{-1} + \tilde{\mathbf{R}}_x^{-1}) \mathbf{R}_h^{1/2} + \mathbf{R}_h^{1/2} (\mathbf{R}_x^{-1} + \tilde{\mathbf{R}}_x^{-1}) \frac{\partial \mathbf{R}_h^{1/2}}{\partial \psi_i} \right) (\mathbf{w}_1 + \tilde{\mathbf{w}}_1), \quad i = 1, 2, \tag{4.C.32}$$

where $\tilde{\mathbf{w}}_1 = \hat{\mathbf{w}}_1 - \mathbf{w}_1$ is the eigenvector perturbation, and $\tilde{\mathbf{R}}_x^{-1} = \hat{\mathbf{R}}_x^{-1} - \mathbf{R}_x^{-1}$ is the perturbation of the inverse sample covariance matrix. The inverse sample covariance matrix is defined as

$$\hat{\mathbf{R}}_x^{-1} = \left(\frac{1}{N} \sum_{t=1}^{N} \mathbf{x}(t) \mathbf{x}^H(t) \right)^{-1}. \tag{4.C.33}$$

Also here we make a first order approximation of the perturbed gradient vector. This, leads to

$$\begin{aligned} \frac{\partial \hat{\lambda}_1(\boldsymbol{\psi})}{\partial \psi_i} \cong\ & 2\mathrm{Re}\left\{ \mathbf{w}_1^H \frac{\partial \mathbf{R}_h^{1/2}}{\partial \psi_i} \mathbf{R}_x^{-1} \mathbf{R}_h^{1/2} \mathbf{w}_1 \right\} \\ & + 2\mathrm{Re}\left\{ \mathbf{w}_1^H \left(\frac{\partial \mathbf{R}_h^{1/2}}{\partial \psi_i} \mathbf{R}_x^{-1} \mathbf{R}_h^{1/2} + \mathbf{R}_h^{1/2} \mathbf{R}_x^{-1} \frac{\partial \mathbf{R}_h^{1/2}}{\partial \psi_i} \right) \tilde{\mathbf{w}}_1 \right\} \\ & + 2\mathrm{Re}\left\{ \mathbf{w}_1^H \frac{\partial \mathbf{R}_h^{1/2}}{\partial \psi_i} \tilde{\mathbf{R}}_x^{-1} \mathbf{R}_h^{1/2} \mathbf{w}_1 \right\}, \quad i = 1, 2, \end{aligned} \tag{4.C.34}$$

where the first term corresponds to $\nabla f(\boldsymbol{\psi}, \mathbf{R}_x)$ and equals to zero when evaluated at $\boldsymbol{\psi} = \boldsymbol{\psi}_*$. The result in (4.C.34) is then used to calculate the

$(i,j)^{\text{th}}$ entry of the gradient covariance matrix, which is given by

$$[\mathbf{\Phi}]_{ij} \triangleq \mathrm{E}\left[\nabla f(\boldsymbol{\psi}_*, \hat{\mathbf{R}}_x)\nabla^T f(\boldsymbol{\psi}_*, \hat{\mathbf{R}}_x)\right]_{ij} = \mathrm{E}\left[\frac{\partial\hat{\lambda}_1(\boldsymbol{\psi}_*)}{\partial\psi_i}\frac{\partial\hat{\lambda}_1(\boldsymbol{\psi}_*)}{\partial\psi_j}\right]. \quad (4.C.35)$$

At first glance, it seems rather tedious to calculate the expected value in (4.C.35), but after omitting first order terms that are equal to zero, and all of the second and higher order terms, we are left with the following terms

$$\begin{aligned}[\mathbf{\Phi}]_{ij} = \mathrm{E}\left[\frac{\partial\hat{\lambda}_1(\boldsymbol{\psi}_*)}{\partial\psi_i}\frac{\partial\hat{\lambda}_1(\boldsymbol{\psi}_*)}{\partial\psi_j}\right] \cong \mathrm{E}\Big[&2\mathrm{Re}\left\{\mathbf{w}_1^H\mathbf{A}_i\tilde{\mathbf{w}}_1\mathbf{w}_1^H\mathbf{A}_j\tilde{\mathbf{w}}_1\right\} \\ &+2\mathrm{Re}\left\{\mathbf{w}_1^H\mathbf{A}_i\tilde{\mathbf{w}}_1\mathbf{w}_1^H\tilde{\mathbf{A}}_j\mathbf{w}_1\right\} + 2\mathrm{Re}\left\{\mathbf{w}_1^H\mathbf{A}_i\tilde{\mathbf{w}}_1\tilde{\mathbf{w}}_1^H\mathbf{A}_j\mathbf{w}_1\right\} \\ +2\mathrm{Re}\left\{\mathbf{w}_1^H\tilde{\mathbf{A}}_i\mathbf{w}_1\mathbf{w}_1^H\mathbf{A}_j\tilde{\mathbf{w}}_1\right\} &+ \mathbf{w}_1^H\tilde{\mathbf{A}}_i\mathbf{w}_1\mathbf{w}_1^H\tilde{\mathbf{A}}_j\mathbf{w}_1\Big], \quad i,j=1,2,\end{aligned} \quad (4.C.36)$$

where $\mathbf{A}_i$ and $\tilde{\mathbf{A}}_i$ are defined as

$$\mathbf{A}_i = \frac{\partial\mathbf{R}_h^{1/2}}{\partial\psi_i}\mathbf{R}_x^{-1}\mathbf{R}_h^{1/2} + \mathbf{R}_h^{1/2}\mathbf{R}_x^{-1}\frac{\partial\mathbf{R}_h^{1/2}}{\partial\psi_i} = 2\mathrm{Re}\left\{\mathbf{R}_h^{1/2}\mathbf{R}_x^{-1}\frac{\partial\mathbf{R}_h^{1/2}}{\partial\psi_i}\right\} \quad (4.C.37)$$

$$\tilde{\mathbf{A}}_i = \frac{\partial\mathbf{R}_h^{1/2}}{\partial\psi_i}\tilde{\mathbf{R}}_x^{-1}\mathbf{R}_h^{1/2} + \mathbf{R}_h^{1/2}\tilde{\mathbf{R}}_x^{-1}\frac{\partial\mathbf{R}_h^{1/2}}{\partial\psi_i} = 2\mathrm{Re}\left\{\mathbf{R}_h^{1/2}\tilde{\mathbf{R}}_x^{-1}\frac{\partial\mathbf{R}_h^{1/2}}{\partial\psi_i}\right\} \quad (4.C.38)$$

and $\tilde{\mathbf{w}}_1$ is given by $\mathbf{q}_1$ in (4.C.27).

We can now invoke known expectations of forms of inverted complex Wishart matrices. From [TC94] we have

$$\mathrm{E}\left[\mathbf{y}_1^H\tilde{\mathbf{R}}_x^{-1}\mathbf{y}_2\mathbf{y}_3^H\tilde{\mathbf{R}}_x^{-1}\mathbf{y}_4\right] = \frac{1}{N-K}\left(\mathbf{y}_1^H\mathbf{R}_x^{-1}\mathbf{y}_4\right)\left(\mathbf{y}_3^H\mathbf{R}_x^{-1}\mathbf{y}_2\right),$$

where the $\mathbf{y}_i$'s are deterministic vectors. The gradient covariance matrix is, therefore, found by inserting (4.C.27), (4.C.37), and (4.C.38) into (4.C.36), followed by applying the above expectation. Finally, the asymptotic error covariance matrix is, hence, given by (4.C.2). □

4.D Proof of Theorem 4: Asymptotic Error Distribution for G-Capon Applied to CD Sources

Direct application of the Taylor expansion method in, e.g., [Lju87] yields the asymptotic error covariance matrix. Thus, we only calculate the asymptotic Hessian matrix and the covariance matrix of the random gradient.

Finding the Asymptotic Hessian Matrix

Let $\boldsymbol{\psi} = [\omega, \sigma_\omega]^T$. The first partial derivatives of the criterion function (we study the equivalent problem of minimizing the Capon pseudo spectrum for CD sources)

$$f(\boldsymbol{\psi}, \mathbf{R}_x) = \mathbf{b}^H(\boldsymbol{\psi})\mathbf{R}_x^{-1}\mathbf{b}(\boldsymbol{\psi})$$

are given by

$$\frac{\partial f(\boldsymbol{\psi}, \mathbf{R}_x)}{\partial \psi_i} = 2\mathrm{Re}\left\{\mathbf{b}^H\mathbf{R}_x^{-1}\frac{\partial \mathbf{b}}{\partial \psi_i}\right\}. \tag{4.D.1}$$

The $(i,j)^{\text{th}}$ element of the asymptotic Hessian matrix $\mathbf{H}$ is given by

$$[\mathbf{H}]_{ij} = \frac{\partial^2 f(\boldsymbol{\psi}_*, \mathbf{R}_x)}{\partial \psi_i \partial \psi_j} = 2\mathrm{Re}\left\{\mathbf{b}^H\mathbf{R}_x^{-1}\frac{\partial^2 \mathbf{b}}{\partial \psi_i \partial \psi_j} + \frac{\partial \mathbf{b}^H}{\partial \psi_i}\mathbf{R}_x^{-1}\frac{\partial \mathbf{b}}{\partial \psi_j}\right\}, \tag{4.D.2}$$

where the derivatives of $\mathbf{b}(\boldsymbol{\psi})$ for a ULA and Gaussian or uniform density functions, are easily obtained by differentiating (4.B.7) or (4.B.8), respectively.

Finding the Gradient Covariance Matrix

The elements of the random gradient are found by inserting the sample covariance matrix into (4.D.1), and the gradient covariance matrix is then found by recognizing the covariance matrix as the expected value of an inverted complex Wishart form [TC94]. Therefore, we have

$$\begin{aligned}
[\boldsymbol{\Phi}]_{ij} &\triangleq \mathrm{E}\left[\nabla f(\boldsymbol{\psi}_*, \hat{\mathbf{R}}_x)\nabla^T f(\boldsymbol{\psi}_*, \hat{\mathbf{R}}_x)\right]_{ij} \\
&= \frac{2}{N-K}\mathrm{Re}\Bigg\{\left(\mathbf{b}^H\mathbf{R}_x^{-1}\frac{\partial \mathbf{b}}{\partial \psi_j}\right)\left(\mathbf{b}^H\mathbf{R}_x^{-1}\frac{\partial \mathbf{b}}{\partial \psi_i}\right) \\
&\quad + \left(\mathbf{b}^H\mathbf{R}_x^{-1}\mathbf{b}\right)\left(\frac{\partial \mathbf{b}^H}{\partial \psi_j}\mathbf{R}_x^{-1}\frac{\partial \mathbf{b}}{\partial \psi_i}\right)\Bigg\},
\end{aligned} \tag{4.D.3}$$

which concludes the proof. □

Chapter 5

Conclusions

This chapter concludes the first part of the thesis, and provides a discussion of the findings and limitations, followed by suggestions for future work.

5.1 Nonparametric Estimation: Beamforming

In Chapter 3, we investigated the use of simple beamforming-based techniques to estimate the nominal *Direction-Of-Arrival (DOA)* and spatial spread of a *Incoherently Distributed (ID)* source. A relationship between the beamforming spectrum and the underlying *Spatial Power Density Function (SPDF)* was derived, and from that result we found our estimators. Without making any assumption on the unknown angular distribution (implying robustness) or numerical searches to find the optimal parameters, the estimators based on Capon's spectrum outperformed the two subspace-based estimators that were used in the numerical examples. The two subspace-based estimators assumed the angular distribution to be known and required a two-dimensional search to find the optimal parameters. It was also found that it is much better to take the spectrum's *Center of Mass (CoM)* than its peak, when estimating the nominal DOA.

Despite the spectral-based estimator's nice performance, one open problem remains and that is how to choose the support or decide on the interval of the signal part of the spectrum. The choice of support has a strong influence on the spread estimate, while the nominal DOA estimate is less sensitive to the choice of support. In the numerical examples, the support for the Gaussian PDF was restricted to $\theta_0 \pm 3\sigma_\theta$ which also was a reason for the bias that was shown by the spread estimates. Further, unless the multiple

sources are well separated, any nonparametric estimator will only work well for a single ID source. To be able to locate sources with overlapping spectra, a parametric approach that exploits the data covariance structure needs to be employed.

The nonparametric approach was also used to determine nominal DOA and spatial spread for real indoor data. Although no quantitative evaluation is available for the real data, the obtained results agree well with a visual inspection of the spatial spectra.

We also presented a statistical analysis of the proposed nonparametric method, and closed-form expressions of the asymptotic *Mean Square Error (MSE)* of the parameter estimates were provided. The theoretical expressions were found to agree well with results from simulated data. Additionally the MSE of the nominal DOA and the variance of the squared spread parameter estimates are close to the *Cramér-Rao Lower Bound (CRLB)* for a Gaussian ID source.

5.1.1 Future Work

A less *ad-hoc* way of choosing the support for the nonparametric beamforming scheme needs to be found, and it needs to be data-dependent. One criterion for choosing the support is to find the region where the signal part of the spectrum is distinct from the noise power level. This has clear similarities to the problem of choosing the threshold when making the partitioning into signal and noise eigenvalues in a subspace-based algorithm for distributed source localization, where the pseudo-subspace dimensionality is a so-called design parameter. For a single distributed source, for example, taking the median value of the spectrum or performing some averaging in the tails of the spectrum may give a good enough estimate of the noise level. Since it is reasonable to assume that the noise power is independent of the transmitted signal, another simple solution is, thus, to compute the received power while the transmitter is shut down.

One approach to overcome the sensitivity to the limited antenna size which results in a not infinitely narrow beamwidth, is to use windowing in the spectral domain, i.e., let

$$\hat{\theta}_0 = \frac{\sum_\theta \theta \hat{P}_o(\theta) w(\theta)}{\sum_\theta \hat{P}_o(\theta) w(\theta)} \tag{5.1}$$

$$\hat{\sigma}_\theta^2 = \frac{\sum_\theta (\theta - \hat{\theta}_0)^2 \hat{P}_o(\theta) w(\theta)}{\sum_\theta \hat{P}_o(\theta) w(\theta)}, \tag{5.2}$$

where $w(\theta)$ is a window function. In this thesis, we simply have used the rectangular window

$$w(\theta) = \begin{cases} 1\,, & \theta \in \Theta \\ 0\,, & \theta \notin \Theta\,. \end{cases} \tag{5.3}$$

Other choices of window functions could be considered as possible future work, and the window should depend on the array beampattern. An interesting observation related to this, is that the periodogram (equivalent to the conventional beamforming spectrum) of a distributed source can be seen as the convolution between the ID source's spatial power density function $p(\omega)$ and the power radiation pattern of the antenna array $|G(\omega)|^2$. This can be seen by computing the periodogram as

$$\begin{aligned} P(\omega) &= \frac{\mathbf{a}^H(\omega)\mathbf{R}_x\mathbf{a}(\omega)}{K} = \frac{\sigma_s^2\mathbf{a}^H(\omega)\mathbf{R}_h\mathbf{a}(\omega)}{K} + \sigma_n^2 \\ &= \frac{\sigma_s^2}{K}\mathbf{a}^H(\omega)\left(\int p(\nu)\mathbf{a}(\nu)\mathbf{a}^H(\nu)d\nu\right)\mathbf{a}(\omega) + \sigma_n^2 \\ &= \frac{\sigma_s^2}{K}\int p(\nu)\mathbf{a}^H(\omega)\mathbf{a}(\nu)\mathbf{a}^H(\nu)\mathbf{a}(\omega)d\nu + \sigma_n^2 \\ &= \frac{\sigma_s^2}{K}\int p(\nu)|G(\omega-\nu)|^2 d\nu + \sigma_n^2 \\ &= \frac{\sigma_s^2}{K}p(\omega) * |G(\omega)|^2 + \sigma_n^2, \end{aligned} \tag{5.4}$$

where $*$ denotes convolution, and $|G(\omega)|^2$ is the power radiation pattern (also called *radiation intensity* in the antenna literature [Bal97]) of the standard uniform linear antenna array with steering vector

$$\mathbf{a}(\omega) = [1, e^{j\omega}, \ldots, e^{j(K-1)\omega}]^T,$$

and is given by

$$\begin{aligned} |G(\omega-\nu)|^2 &= \mathbf{a}^H(\omega)\mathbf{a}(\nu)\mathbf{a}^H(\nu)\mathbf{a}(\omega) \\ &= \sum_{k=0}^{K-1} e^{-jk(\omega-\nu)} \sum_{k=0}^{K-1} e^{jk(\omega-\nu)} \\ &= G^*(\omega-\nu)G(\omega-\nu) \end{aligned} \tag{5.5}$$

where $G(\omega)$ is the so-called *array factor* [Bal97]. The array factor can be re-written as

$$\begin{aligned} G(\omega) &= \sum_{k=0}^{K-1} e^{jk\omega} = \frac{1-e^{jK\omega}}{1-e^{j\omega}} = e^{j(K-1)\omega/2}\frac{e^{-jK\omega/2} - e^{jK\omega/2}}{e^{-j\omega/2} - e^{j\omega/2}} \\ &= e^{j(K-1)\omega/2}\frac{\sin(K\omega/2)}{\sin(\omega/2)} \approx e^{j(K-1)\omega/2}K\frac{\sin(K\omega/2)}{K\omega/2}, \end{aligned} \tag{5.6}$$

where the approximation is valid for small ω. The amplitude radiation pattern (or beampattern) $|G(\omega)|$ is, thus, nothing else but K times the well known sinc-function, which appears when applying a spatial rectangular window in the form of an finite-length array to "truncate" an electromagnetic wave. This is the spatial equivalent to the periodogram of a windowed continuous time signal. As the array grows larger, the radiation pattern approaches the Dirac delta function, which inserted into (5.4) yields

$$P(\omega) = \beta \int p(\nu)\delta(\omega - \nu)d\nu + \varepsilon = \beta p(\omega) + \varepsilon, \tag{5.7}$$

which indeed was the derived approximation given by (3.8). Since the spatial power density function is smoothed by the array power radiation pattern, the approximation will be poor for small arrays. The approximation is valid as long as the beamwidth of the radiation pattern is at least a few times smaller than the total spatial extension of the source. Figure 5.1 shows the convolution between a normalized bell-shaped spatial power spectrum and the power radiation pattern of a 20 element standard ULA. We see that the result of the convolution is equal to the conventional beamforming spectrum, and that it overestimates the spread of the true power spectrum, which can be compensated for by, e.g., applying a window function in the spectral domain. Also included is the Capon beamforming spectrum, which thanks to its higher resolution better captures the width of the true power spectrum. Related to these observations, in the very recent publication [LLZZ06] the power spectrum is estimated by measuring the received power with a highly directional single antenna element. The spatial power density function is then found by performing *deconvolution* of the power spectrum and the antenna power radiation pattern.

5.2 Parametric Estimation: Generalized Beamforming

In Chapter 4, a generalization of the conventional point source-based beamforming techniques was introduced. The generalized conventional beamformer (G-CBF) works as a *matched filter*, and is able to estimate the parameters of multiple ID and *Coherently Distributed (CD)* sources by locating the largest peaks of the generalized 2-D spectrum. Its performance is compared numerically to a generalized Capon (G-Capon) estimator (developed for ID sources in [HSG04], and in this thesis also suggested for CD sources), and it shows competitive performance for localization of a single ID source,

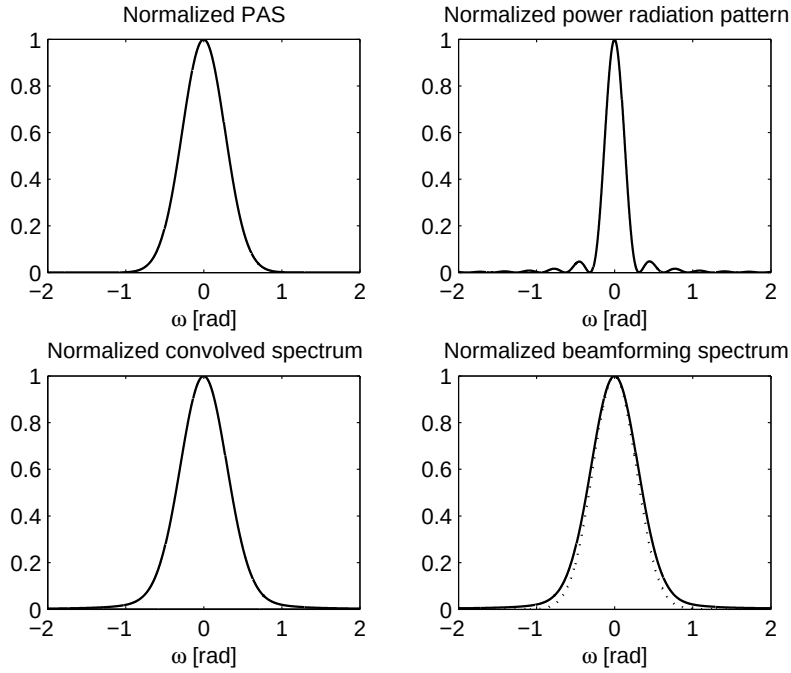

Figure 5.1: Convolution between the true Power Azimuth Spectrum (PAS) (top left) and the 20 element std. ULA radiation pattern (top right). The result from the convolution is shown in the bottom left figure and the bottom right figure shows the beamforming spectra attained by conventional (solid) and Capon's beamforming (dotted).

but suffers from its limited resolution when applied to multiple ID sources. Under the Gaussian data model assumption, the numerical performance of G-CBF when applied to a single CD source coincides with the numerical performance of the concentrated Maximum-Likelihood (ML) estimator, which is asymptotically efficient. It is an interesting observation since the concentrated ML estimator requires a 3-D search over the parameter space (the two parameters of interest plus the SNR), while the G-CBF estimator only requires a 2-D search. In general, the G-CBF suffers from limited resolution, and the G-Capon beamformer shows better numerical performance for multiple ID and CD sources. It is also found that the G-Capon estimator is asymptotically biased for both ID and CD sources.

A performance analysis for ID sources is provided and the G-CBF algorithm's interesting "feature" of having an optimal choice w.r.t. the number of

antennas is investigated. It turns out that the optimal array that minimizes the MSE is the one that yields a Rayleigh beamwidth approximately equal to the total spatial extension of the source. The intuitive explanation for this, is that the G-CBF serves as the best, in terms of maximizing the output SNR, rank-one approximation of the source, and when the number of sensors is increased until the Rayleigh beamwidth becomes less than the source's angular extension, the rank-one approximation becomes a poor approximation. For large spreads, the beamformer (matched filter) will, therefore, only capture a fraction of the total radiated energy. As a consequence, there will be a degradation in the parameter estimation performance.

The performance of G-CBF is also analyzed for CD sources, and the asymptotic curves coincide with the CRLB for single CD sources. Hence, under the Gaussian data model, it is asymptotically efficient for localization of single CD sources. This is in agreement with applying the conventional beamformer to locate a single point source [KV96].

Finally, a performance analysis of the generalized Capon estimator in [HSG04] is presented. The estimator is inconsistent and it also turns out that the asymptotic criterion function most often is non-differentiable in the optimum. Since the analysis relies on differentiability, the derived asymptotic results are only valid for scenarios where differentiability is ensured. These scenarios typically occur when modeling errors, in the form of wrong assumption on the angular distribution, are present. The performance of G-Capon is also analyzed for CD sources, and the algorithm is also here inconsistent, although, there is no problem with differentiability of the G-Capon criterion function for CD sources.

As a general comment, conducting a statistical performance analysis yields analytical results that can be used to quickly assess the performance of estimators for different parameter settings, instead of having to rely on empirical results obtained from long simulation runs. As an added value, it also brings deeper understanding to the underlying mechanisms of the algorithms that are analyzed.

5.2.1 Future Work

That the performance of G-CBF for single CD sources coincides with the performance of ML, needs to be verified analytically. Further, it should also be verified analytically that it is asymptotically efficient. The estimators performance could also be studied for *Partially Coherently Distributed (PCD)* sources [RGM00]. One might expect that the performance for PCD sources would lie somewhere in between that of the CD and ID source cases.

As a final remark, the analysis of the generalized beamformers is lim-

ited to the case of distinct eigenvalues. The analysis should be made more general so it also becomes valid for repeated eigenvalues. Once we know that the eigenvalues are repeated, the corresponding eigenvector derivatives can be obtained by exploiting the fact that the eigenvalues are repeated. In order to analyze the generalized Capon algorithm with repeated and non-differentiable eigenvalues, a new theory needs to be developed which can handle the non-differentiable asymptotic criterion function. For example in the area of robust estimation, the absolute error criterion function is non-differentiable. The development of such a general theory would, therefore, be a good contribution in itself to the research community.

Part II
Training-Aided Channel Parameter Estimation

Chapter 6

Introduction

This chapter provides an introduction to the problem addressed in the second part of the thesis, namely; performance evaluation of pilot-assisted channel estimation schemes.

6.1 Background and Overview

While the first part of the thesis only involved estimation of two statistics of a random channel, the second part involves estimation of the actual channel realization. This is what usually is meant when one talks about channel estimation in a communications context.

Channel estimation is a classical problem in communication, and the use of pilot symbols is the most commonly employed technique today. Thus, the area is well covered in the literature, see, e.g., [TSD04] and references therein. The problem of channel estimation by using transmission of known pilot sequences has been addressed using various performance criteria. These criteria can basically be divided into: 1) information theoretic (mutual information and channel capacity bounds, cutoff rate, etc.) and 2) signal processing (channel MSE, symbol MSE, BER, etc.). An excellent recent survey of this area which contains an extensive reference list is presented in [TSD04].

Conventionally, the pilot symbols are transmitted time-multiplexed with the data, see [HH03] for a detailed analysis of such a Multiple-Input Multiple-Output (MIMO) system. However, other results suggest that it might be beneficial to superimpose the pilots to the data, a technique called Superimposed Pilots (SIP). The idea of superimposing known sequences to data is closely related to digital watermarking techniques [HK99], and the connection between watermarking and communications with side-information

has been made in [CMM99]. Superimposing pilots to data was already suggested in [MF87] and has been used to solve various synchronization issues in, e.g., [HF90] and [TFHE99]. The use of SIP for channel estimation was introduced in [FB95] and has received more recent attention in, e.g., [HT99, Maz00, ZVM03, ZFB03, TL03, OLLM04, GMAHS05]. The advantage of SIP, compared to conventional time-multiplexed training, is that data is transmitted in all time slots. That is, no slots are purely dedicated to known pilots, which has been argued to lead to higher spectral efficiency. The drawback of SIP is a degradation in the quality of the channel estimate, which is due to the presence of unknown data during channel estimation. During detection, a poor channel estimate will render a *Signal-to-Noise Ratio (SNR)* penalty which in turn leads to a lower reliable information transmission rate.

Clearly, there is a trade-off between achieving a high-quality channel estimate and the information throughput. On the one hand, to achieve a high-quality channel estimate, a larger portion of the available time/power needs to be allocated for training, which leaves little time/power for information transmission. On the other hand, if too little time/power is spent on training, the channel estimate will be poor, which also deteriorates the information throughput due to a *mismatched decoder* [MKLS94,LN98,MÓ0,LS02]. Hence, a performance measure that captures this effect is needed when comparing the two schemes. One such measure is the ergodic *channel capacity*, which denotes the maximum information rate we can achieve with an arbitrarily low probability of error. For discrete time memoryless channels we know that the capacity is given by the maximum *Mutual Information (MI)* between the transmitted and received signals. Hence, in this work we will maximize the MI of these training-based MIMO systems, since it better captures the essence of a communication system (high data rate with arbitrarily low probability of error), which makes it a good *figure-of-merit* of the system performance. When we use the word *capacity*, we mean the approximate mathematical expressions for the maximum MI of the system that we are working with, hence it should not be interpreted as Shannon's channel capacity. In the derivations, only the first order effects are taken into account when the data sequences are chosen, i.e., we will select the distribution of the input symbols that maximizes the MI when the channel is assumed to be known. Thus, we will not consider that the distribution of the data also effects the channel estimate, and instead only take into account how the data power influences the channel estimate.

The performance of SIP compared to conventional time-multiplexed pilots for channel tracking using Kalman filters has been studied in [DTS04], where (for both schemes) a fixed percentage of the available transmit power was allocated for pilot and data symbols. The results showed that SIP out-

performed, in terms of channel minimum mean square error and bit error rate, the conventional pilot for fast fading channels and/or low SNR. In order to make a less *ad hoc* and more fair comparison between the schemes, we first find how the available resources (time and power, see Figure 7.1) should optimally be allocated for the transmission of pilots and data symbols. For each scheme, the parameters are tuned to optimal operation, i.e., such that they maximize the derived expression for the capacity, and the resulting capacities are then compared.

The work presented in Chapter 7 is based on [HH03], where a tight lower bound on the capacity for conventional time-multiplexed training-based MIMO systems is established. Similar lower bounds have also been used to relate channel estimation errors to capacity to find optimal values of training parameters for various systems in, e.g., [ATV02, SM03, MGO03, VHHK04, OG04, MGO05]. Here we extend the models in [HH03] to also incorporate a scheme based on a general superimposed pilot model, of which the conventional pilot is a special case, and make comparisons of the performances of the two schemes. To simplify the derivations, we introduce an abstract projection-based problem viewpoint using vector spaces. By using projections, we find the optimal number of training symbols and that the conventional pilot scheme is suboptimal w.r.t. the SIP-based scheme. In Chapter 8, the work is extended to also allow for variable coding rates within the coherence block, using symbol-by-symbol detection of the individual symbols in the coherence block. This extension eliminates the SIP scheme's drawback of attaining poor channel estimates. Finally, in Chapter 9, we apply the theories to a frequency-selective Single-Input Single-Output (SISO) channel.

Throughout this work we will refer to four different schemes, namely: *Superimposed Pilots (SIP)*, *Conventional (time-multiplexed) Pilots (CP)*, *Decision-Directed Superimposed Pilots (DD-SIP)*, e.g., SIP with channel re-estimation, and *Decision-Directed Conventional (time-multiplexed) Pilots (DD-CP)*.

6.2 Information Theory

Information theory spans over many fields such as, e.g., probability theory, statistics, physics and communication theory, only to mention a few. The general focus of this part of the thesis is on communication theory, and especially on deriving and optimizing a lower-bound on the so-called *Mutual Information (MI)*. This section gives a very short introduction to the different concepts used in this part of the thesis.

When introducing the fundamental concepts of *entropy*, *mutual infor-*

mation, *capacity*, etc., it is common to start with discrete random variables and extend the theory to also cover continuous random variables. Since this part of the thesis only covers the continuous case, we leave out the discrete case. For excellent textbooks on information theory, the reader is referred to, e.g., [Gal68, CT91].

6.2.1 Entropy

A good way of interpreting entropy is to think of it as a measure of *uncertainty*, and it is related to the average amount of information needed to describe a random variable. High entropy implies high uncertainty and vice versa.

Definition 1 (DIFFERENTIAL ENTROPY) *The differential entropy of a continuous random variable X is defined by*

$$h(X) = -\int_{x\in\mathcal{X}} f_X(x)\log_2 f_X(x)\,dx, \tag{6.1}$$

where $f_X(x)$ is the Probability Density Function (PDF), $\mathcal{X}$ denotes the support set $\{x : f_X(x) > 0\}$, and $\log_2(\cdot)$ is the base-2 logarithm. Hence, the entropy is measured in binary units (bits).

Unlike the entropy of discrete random variables, the differential entropy can be negative. Given a certain variance, it is maximized over all possible distributions by the Gaussian PDF [CT91].

Definition 2 (CONDITIONAL ENTROPY) *If the continuous random variable pair (X, Y) have a joint PDF $f(x, y)$, then the conditional entropy $h(X|Y)$ is defined as*

$$h(X|Y) = -\int f(x,y)\log_2 f(x|y)\,dx\,dy = h(X,Y) - h(Y), \tag{6.2}$$

where

$$h(X,Y) = -\int f(x,y)\log_2 f(x,y)\,dx\,dy \tag{6.3}$$

is the differential entropy of the random variable pair (X, Y).

The conditional entropy satisfies $h(X|Y) \leq h(X)$ with equality *iff* X and Y are independent. That is, by observing Y, one can not increase the uncertainty of X.

6.2.2 Mutual Information

The Mutual Information (MI) between two random variables is the information one variable contains about the other.

Definition 3 (MUTUAL INFORMATION) *The mutual information $I(X;Y)$ between two random variables with joint density function $f(x,y)$ is defined as*

$$I(X;Y) = \int f(x,y) \log_2 \frac{f(x,y)}{f(x)f(y)}\, dx\, dy = I(Y;X). \tag{6.4}$$

The mutual information can also be expressed using entropies

$$I(X;Y) = h(X) - h(X|Y), \tag{6.5}$$

which leads to the interpretation that the mutual information $I(X;Y)$ is the reduction in entropy (uncertainty) of X after having observed Y (or vice versa). Clearly, if X and Y are independent, then $h(X|Y) = h(X)$ and $I(X;Y) = 0$. The mutual information satisfies $I(X;Y) \geq 0$ with equality *iff* X and Y are independent. To put it into a communications context, one can think of X as being the transmitted signal, and Y the received (and observed) signal. Then, the MI between the signals X and Y represents the information conveyed by the transmission.

Figure 6.1 is adopted from [CT91], and it displays the relationship between the different entropies and the mutual information.

6.2.3 Capacity

The *channel capacity* is in itself only a definition, but it becomes of fundamental importance since it can be proven that it serves as the maximum rate with which we can transmit information over a channel, and at the same time have arbitrarily small probability of error. The above is stated by the *channel coding theorem*, where the theorem and its proof can be found in, e.g., [CT91]. The channel capacity of a discrete time channel is commonly measured in information bits per channel use. For continuous time band-limited channels, the capacity is measured in bits/sec/Hz. In the following, we will only consider a discrete time channel model and, consequently, the capacity is measured in bits per channel use.

Definition 4 (CHANNEL CAPACITY) *The channel capacity C of a discrete time memoryless channel is given by the maximum of the mutual information*

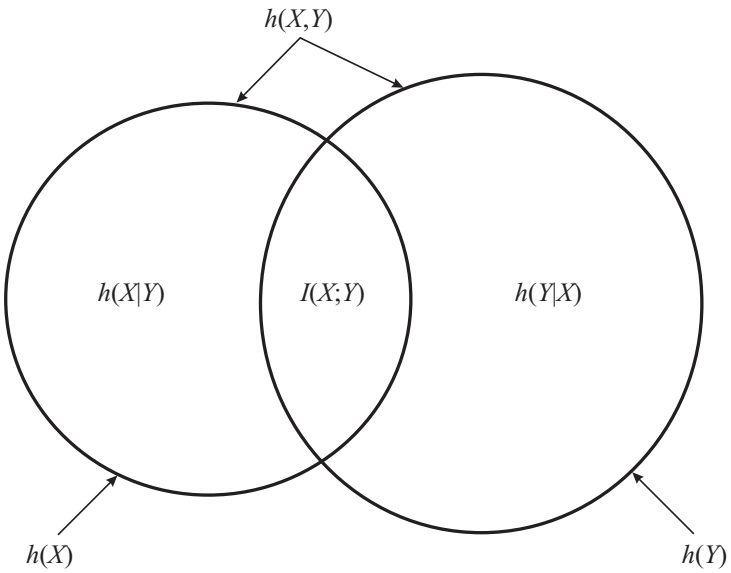

Figure 6.1: Venn diagram that displays the relationship between entropy and mutual information.

between the channel input and output

$$C = \max_{\substack{f_X(x) \\ \mathrm{E}[X^2] \leq P}} I(X;Y). \tag{6.6}$$

The maximization is over all possible input distributions $f_X(x)$*, with the average transmit power constraint* $\mathrm{E}[X^2] \leq P$*.*

One can think of constraints other than the average transmit power, such as the peak power constraint (or equivalently the maximum amplitude constraint) in [SBD95], although, it is beyond the scope of this thesis.

MIMO Channel Capacity

The use of *Multiple-Input Multiple Output (MIMO)* antenna systems enables wireless communication with high data rates. Without any increase in bandwidth or power consumption, pioneering work in [Fos96] and [Tel99] show a linear (in the number of antennas) increase in capacity by using MIMO systems over single-antenna systems for frequency-flat *Rayleigh fading channels* [Pro01].

Consider a discrete time single user frequency-flat fading *Additive White Gaussian Noise (AWGN)* channel, [Pro01], with multiple transmit and receive antennas, such as the noise-free MIMO link depicted in Figure 6.2. The

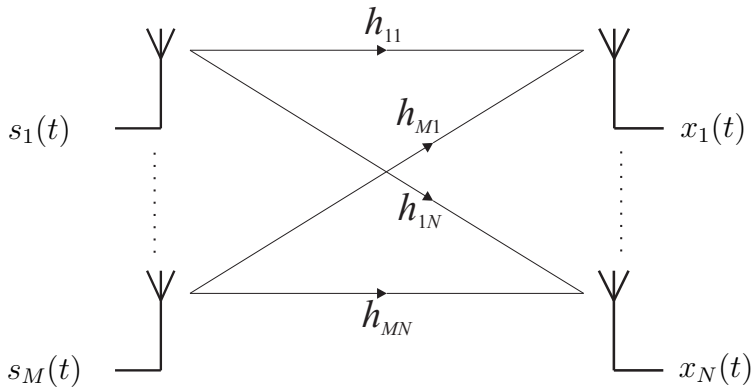

Figure 6.2: Multiple-Input Multiple-Output system with M transmit and N receive antennas.

input and output relation for such a narrowband MIMO link can be modeled as

$$\mathbf{x} = \mathbf{sH} + \mathbf{v}, \tag{6.7}$$

where $\mathbf{x} = [x_1(t), \ldots, x_N(t)]$ is the received signal (row) vector at time t, $\mathbf{H}$ the $(M \times N)$ channel matrix, $\mathbf{s} = [s_1(t), \ldots, s_M(t)]$ the transmitted signal (row) vector at time t, and $\mathbf{v}$ is the zero-mean circularly symmetric complex Gaussian noise (row) vector with covariance matrix $\mathrm{E}[\mathbf{v}^H\mathbf{v}] = \mathbf{I}_N$. M is the number of transmit antennas and N is the number of receive antennas. It is further assumed that the transmitted signal vector satisfies the average power constraint $\mathrm{E}[\mathbf{ss}^H] = \mathrm{ETr}\{\mathbf{s}^H\mathbf{s}\} \leq P$, where $\mathrm{ETr}\{\cdot\}$ denotes statistical expectation of the trace of a matrix. The $(i,j)^{\text{th}}$ entry of the channel matrix $\mathbf{H}$ is denoted by h_{ij} and represents the complex channel gain between the i^{th} transmit and j^{th} receive antenna. We model the magnitude $|h_{ij}|$ as *Rayleigh distributed* and the phase $\phi_{ij} = \angle h_{ij}$ as *uniformly distributed*. This is often used to model rich scattering environments in the absence of *Line-Of-Sight (LOS)*. The MIMO channel matrix is written as

$$\mathbf{H} = \begin{bmatrix} h_{11} & \cdots & h_{1N} \\ \vdots & \ddots & \vdots \\ h_{M1} & \cdots & h_{MN} \end{bmatrix}, \tag{6.8}$$

where

$$\begin{aligned} h_{ij} &= \alpha_{ij} + j\beta_{ij} && (6.9)\\ &= \sqrt{\alpha_{ij}^2 + \beta_{ij}^2} \cdot e^{j\phi_{ij}} && (6.10)\\ &= |h_{ij}| \cdot e^{j\phi_{ij}}, && (6.11) \end{aligned}$$

and α_{ij}, β_{ij} are i.i.d. (also from entry to entry), zero-mean, variance equal to 1/2, normal distributed random variables. Thus, the complex valued entries $\{h_{ij}\}$ have an independent, circularly symmetric, complex normal distribution with zero mean and unit variance, i.e., $h_{ij} \sim \mathcal{CN}(0,1)$ and i.i.d.

In [Fos96, FG98, Tel99], the capacity is reported for the case when $\mathbf{H}$ models the frequency-flat Rayleigh fading channel. It is assumed that the channel realizations are *perfectly known* at the receiver and that the transmitter has no channel state information. Further, the channel is modeled as memoryless, i.e., a new independent channel realization $\mathbf{H}$ is drawn for each use of the channel. The results from [Tel99] are summarized in the following theorem

Theorem 5 (MIMO CHANNEL CAPACITY) *Suppose* $\mathbf{H} \in \mathbb{C}^{M\times N}$ *and* $\mathbf{v} \in \mathbb{C}^{1\times N}$ *are circularly symmetric complex Gaussian with independent, zero-mean, and unit variance entries. The mutual information between the channel input,* $\mathbf{s}$*, and what is observed and known at the output,* $(\mathbf{x}, \mathbf{H})$*, is for the model* $\mathbf{x} = \mathbf{sH} + \mathbf{v}$ *given by*

$$\begin{aligned} I\big(\mathbf{s};(\mathbf{x},\mathbf{H})\big) &= I\big(\mathbf{s};\mathbf{H}\big) + I\big(\mathbf{s};\mathbf{x}|\mathbf{H}\big) \\ &= I\big(\mathbf{s};\mathbf{x}|\mathbf{H}\big). \end{aligned} \tag{6.12}$$

The ergodic channel capacity is given by the maximum of the mutual information (averaged over all channel realizations), and evaluates to

$$C = \mathrm{E}_{\mathbf{H}}\left[\log_2 \det\left(\mathbf{I}_M + \frac{P}{M}\mathbf{H}\mathbf{H}^H\right)\right] \quad \textit{bits/channel use.} \tag{6.13}$$

It is attained when $\mathbf{s}$ *is a circularly symmetric complex Gaussian vector with zero-mean and covariance matrix* $\mathrm{E}[\mathbf{s}^H\mathbf{s}] = (P/M)\mathbf{I}_M$*.*

Proof: The proof is found in [Tel99]. □

Since the determinant of a square matrix can be written as the product of its eigenvalues, the capacity given by (6.13) can be re-written as [Tel99]

$$C = \mathrm{E}_{\lambda}\left[\sum_{i=1}^{m} \log_2\left(1 + \frac{P}{M}\lambda_i\right)\right], \tag{6.14}$$

where $m = \min(M, N)$, and λ_i is the i^{th} eigenvalue of the non-negative definite matrix

$$\mathbf{W} = \begin{cases} \mathbf{H}^H\mathbf{H} & N < M \\ \mathbf{H}\mathbf{H}^H & N \geq M, \end{cases}$$

and the distribution of $\mathbf{W}$ is called the complex Wishart distribution [TC94]. The reparameterized capacity is, thus, given by taking the expected value over the unordered eigenvalues

$$\begin{aligned} C &= \sum_{i=1}^{m} \mathrm{E}_{\lambda}\left[\log_2\left(1+\frac{P}{M}\lambda_i\right)\right] = m\mathrm{E}_{\lambda_1}\left[\log_2\left(1+\frac{P}{M}\lambda_1\right)\right] \\ &= m\int_0^{\infty} \log_2\left(1+\frac{P}{M}\lambda_1\right) p(\lambda_1)d\lambda_1, \end{aligned} \tag{6.15}$$

where the eigenvalue λ_1 has a known density function $p(\lambda_1)$, which involves Laguerre polynomials, and is given in [Tel99]. Hence, we can compute the MIMO capacity by evaluating the integral in (6.15).

The ergodic capacity in (6.13), or equivalently in (6.15), is valid when the channel is perfectly known to the receiver, and is commonly referred to as the ergodic *coherent channel capacity*. Hence, to approach the Shannon limit, channel coding is performed over multiple transmitted blocks of signal vectors, i.e., the code stretches over multiple independently fading channel realizations [Tel99]. Obviously, due to the random nature of the wireless channel, it is not realistic to have perfect channel knowledge, and the coherent channel capacity may, therefore, only serve as a upper bound on the achievable performance. Instead of having full knowledge of the actual realization of the random channel, it is more realistic that the receiver only has some information about the statistical distribution of the channel. Therefore, the *non-coherent channel capacity*, i.e., the capacity when the channel is unknown to both the transmitter and the receiver, better represents the achievable performance of a MIMO system, and it is reported in [MH99, HM00, ZT02]. For a further introduction to MIMO systems and their performances, we refer to, e.g., [GJJV03] and [PGNB04].

In the next two chapters, we will study the MIMO capacity (or actually a lower bound of it) for a system where the channel realization is unknown and where the receiver gains its channel knowledge by forming a training-based channel estimate. The channel estimate is then used as the true channel in the decoding process. Training-based schemes are usually suboptimal compared to schemes that do not require an explicit channel estimate. But, on the other hand, they offer low-complexity receivers. When applicable, we will compare our results to the non-coherent capacity bound reported in [ZT02].

Chapter 7

Performance of Training-Aided MIMO Systems

In this chapter, we compare the performance of two different training-based schemes for MIMO channel estimation. The compared schemes are the conventional time-multiplexed pilot scheme and the superimposed pilot scheme. Their performance is evaluated by deriving, optimizing, and comparing a lower bound on their respective capacity. The material in this chapter has been previously published in the conference papers [CB03, BC04b], and has been submitted as a journal article in [CB05a].

7.1 Training-Aided MIMO Channel Estimation

When transmitting a block of T signal vectors over a MIMO channel with M transmit and N receive antennas, the relation between the input and output matrices of a narrowband link can be described by the discrete time baseband model

$$\mathbf{X} = \sqrt{\frac{\sigma^2}{M}}\mathbf{S}\mathbf{H} + \mathbf{N}, \tag{7.1}$$

where $\mathbf{X} \in \mathbb{C}^{T\times N}$ is the received signal matrix, $\mathbf{H} \in \mathbb{C}^{M\times N}$ is the complex channel matrix, $\mathbf{S} \in \mathbb{C}^{T\times M}$ is the transmitted signal matrix, $\mathbf{N} \in \mathbb{C}^{T\times N}$ is the noise matrix, and σ^2 denotes the average transmit power.

The channel matrix $\mathbf{H}$ is modeled as a stochastic matrix with independent, circularly symmetric, $\mathcal{CN}(0,1)$ entries (path gains). The channel is constant for a discrete time interval T, after which it changes to a new independent realization. Hence, the channel is *memoryless* on the block level. The time, T, over which the channel is constant is referred to as the *channel*

coherence time. The validity of this model from a practical point of view can of course be discussed but the model is commonly used in the literature, and can be seen as a coarse discrete approximation of a time-varying flat fading continuous channel, and is often referred to as a *block-wise Rayleigh fading channel* model [BPS98]. It is reasonable for, e.g., *Time-Division Multiple-Access (TDMA)*, *frequency-hopping*, or *block-interleaved* systems. This type of channel is of full-rank (w.p.1) and models rich scattering environments in the absence of line-of-sight. Each entry in the signal matrix $\mathbf{S}$ may consist of both a known and an unknown random symbol. The known symbols are used for estimating the channel and the random symbols represent the transmitted information. The entries of the signal matrix are normalized to have unit mean-square. The additive noise matrix $\mathbf{N}$ is modeled as having i.i.d. circularly symmetric complex normal distributed entries with zero mean and unit variance, and is independent of both the data and the channel. Thus, the average total transmit power σ^2 becomes the expected SNR at each receive antenna.

7.1.1 Superimposed Pilot

In the general SIP scheme, the transmission of a block of T symbols is divided into two modes. The first mode is the *SIP mode*, in which the pilot symbols are superimposed to low-power data symbols. The length of the SIP block is T_t symbols. The second mode is the pure data mode, in which only a block of T_d information symbols is transmitted. Since the channel is assumed to be constant over the coherence interval and memoryless from block to block, there is no loss in generality by placing the SIP block at the beginning of each block. The SIP scheme is illustrated in Figure 7.1. Note that the time-multiplexed *Conventional Pilot (CP)* and the *Overlay Pilot (OP)*, see [JHJ+01]), schemes are special cases, i.e., the two extremes of the generalized SIP scheme. All parameter settings are summarized in Table 7.1. This choice of SIP setting gives a useful framework for comparing the different pilot schemes. In this work we will only look at the optimal choice of training length (given that we are free to adjust the power between the modes). Hence, we will not consider schemes with constant average power such as the overlay pilot scheme.

SIP Mode

During the SIP mode, the training symbols that are used for channel estimation are transmitted in a block of length T_t symbols. The SIP part of the

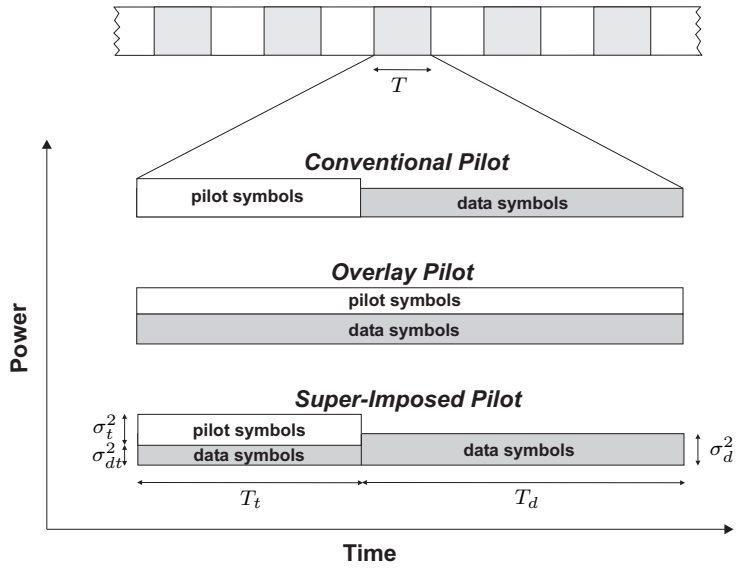

Figure 7.1: Symbol block with conventional pilot insertion, overlay pilot, and superimposed pilot. The channel coherence time is $T = T_t + T_d$, and the total block energy is $(\sigma_t^2 + \sigma_{dt}^2)T_t + \sigma_d^2 T_d = \sigma^2 T$.

Scheme	Variables	Constraints
SIP	$\sigma_t^2, \sigma_{dt}^2, \sigma_d^2, T_t, T_d$	
CP	$\sigma_t^2, \sigma_d^2, T_t, T_d$	$\sigma_{dt}^2 = 0$
OP	$\sigma_t^2, \sigma_{dt}^2$	$\sigma_d^2 = 0,\ T_t = T$

Table 7.1: Parameter settings for the different training schemes.

received signal (7.1) can be written as

$$\mathbf{X}_t = \left(\sqrt{\frac{\sigma_t^2}{M}} \mathbf{S}_t + \sqrt{\frac{\sigma_{dt}^2}{M}} \mathbf{S}_{dt} \right) \mathbf{H} + \mathbf{N}_t, \tag{7.2}$$

where $\mathbf{X}_t \in \mathbb{C}^{T_t \times N}$ is the received matrix, $\mathbf{S}_t \in \mathbb{C}^{T_t \times M}$ and $\mathbf{S}_{dt} \in \mathbb{C}^{T_t \times M}$ denote the transmitted complex-valued known pilot symbol and random data symbol matrices, respectively. Further, $\mathbf{N}_t \in \mathbb{C}^{T_t \times N}$ is the noise matrix, σ_t^2 and σ_{dt}^2 are the average transmit powers allocated for training and data symbols in the SIP block, respectively.

We also define the training "covariance" matrix

$$\mathbf{R}_{\mathbf{S}_t} \;=\; \mathbf{S}_t^H \mathbf{S}_t, \tag{7.3}$$

and the data covariance matrix

$$\mathbf{R}_{\mathbf{S}_{dt}} = \mathrm{E}\left[\mathbf{S}_{dt}^H \mathbf{S}_{dt}\right], \tag{7.4}$$

which are normalized to

$$\mathrm{Tr}\{\mathbf{R}_{\mathbf{S}_t}\} = MT_t \tag{7.5}$$
$$\mathrm{Tr}\{\mathbf{R}_{\mathbf{S}_{dt}}\} = MT_t. \tag{7.6}$$

Note that $\mathbf{S}_t$ is considered deterministic and $\mathbf{S}_{dt}$ stochastic. Since we introduced power constraints on the signal covariance matrices, the transmitted power is accounted for in the parameters σ_t^2 and σ_{dt}^2. The special case $\sigma_{dt}^2 = 0$ corresponds to the CP-scheme, i.e., there is no superposition of training and data symbols.

Data Mode

After transmission of the SIP block, a data block consisting of $T_d = T - T_t$ data symbols is transmitted. Hence, the received signal in the data mode is given by

$$\mathbf{X}_d = \sqrt{\frac{\sigma_d^2}{M}}\mathbf{S}_d\mathbf{H} + \mathbf{N}_d, \tag{7.7}$$

where $\mathbf{S}_d \in \mathbb{C}^{T_d \times M}$ is the random data matrix and $\mathbf{N}_d \in \mathbb{C}^{T_d \times N}$ represents the noise matrix.

The covariance matrix of the data is defined as

$$\mathbf{R}_{\mathbf{S}_d} = \mathrm{E}\left[\mathbf{S}_d^H \mathbf{S}_d\right], \tag{7.8}$$

and is normalized to

$$\mathrm{Tr}\{\mathbf{R}_{\mathbf{S}_d}\} = MT_d. \tag{7.9}$$

Time and Energy Constraints

The total block length of T symbols is split into two sub-blocks; the SIP block and the data block. The length of the SIP block is T_t, the length of the data block is T_d, and the total transmitted energy is $\sigma^2 T$, where σ^2 is the mean power spent on the transmitted total block. This energy is shared between the SIP block and the data block. Thus, we have the following constraints

$$T_t + T_d = T \tag{7.10}$$
$$(\sigma_t^2 + \sigma_{dt}^2)T_t + \sigma_d^2 T_d = \sigma^2 T. \tag{7.11}$$

The relation between these parameters are also depicted in Figure 7.1.

7.1.2 Equivalent Projection-Based Model

To gain further insights into this data model, in this section we will adopt a more abstract viewpoint, where the intuitive physical aspects such as antennas and time slots are removed, and instead the signals are viewed as vectors in a linear vector space.

Consider again the MIMO system with M transmit and N receive antennas, transmitting over a frequency-flat block-fading channel where each channel coefficient is modeled as an i.i.d., circularly symmetric, complex Gaussian variable with unit variance. Since, the coherence length, T, of the channel determines the dimensionality of the space, we will be working in $\mathbb{C}^T$.

The received discrete baseband signal $\mathbf{X}$ can be written as

$$\mathbf{X} = \mathbf{S}_{\text{tot}}\mathbf{H} + \mathbf{N} \tag{7.12}$$

where $\mathbf{S}_{\text{tot}} \in \mathbb{C}^{T\times M}$ denotes the matrix of complex transmitted signals, and $\mathbf{H} \in \mathbb{C}^{M\times N}$ denotes the channel matrix. The spatially and temporally white additive noise $\mathbf{N} \in \mathbb{C}^{T\times N}$ is assumed to be complex Gaussian distributed with zero mean and unit variance. Now, since we are looking at a training-based system, the transmitted signal can be decomposed into a, to the receiver, known and unknown part. This is expressed as

$$\mathbf{S}_{\text{tot}} = \sqrt{\frac{\sigma_t^2}{M}}\mathbf{S}_t + \sqrt{\frac{\sigma_{d'}^2}{M}}\mathbf{P}\mathbf{S}_{\text{data}} \tag{7.13}$$

where

$$\mathbf{P} = \alpha\mathbf{P}_{\mathbf{S}_t} + (1-\alpha)\mathbf{P}_{\mathbf{S}_t}^{\perp}. \tag{7.14}$$

Here

$$\mathbf{P}_{\mathbf{S}_t} = \mathbf{S}_t\left(\mathbf{S}_t^H\mathbf{S}_t\right)^{-1}\mathbf{S}_t^H \tag{7.15}$$

is the projection matrix onto the subspace occupied by the training signal, i.e., spanned by the columns of $\mathbf{S}_t \in \mathbb{C}^{T\times M}$ (which we will call the *training subspace*), and $\mathbf{P}_{\mathbf{S}_t}^{\perp}$ is the projection matrix onto the orthogonal complement of the column space of $\mathbf{S}_t$, i.e., $\mathbf{P}_{\mathbf{S}_t}^{\perp} = \mathbf{I}_T - \mathbf{P}_{\mathbf{S}_t}$. This subspace will be referred to as the *data subspace*. Note that we have assumed that $\mathbf{S}_t$ is of full column rank, which is a requirement for channel identifiability. All the information symbols are here contained in the data matrix $\mathbf{S}_{\text{data}} \in \mathbb{C}^{T\times M}$. In this model the parameter α ($0 \le \alpha \le 1$) adjusts how much power is allocated to data in the training subspace versus data in the data subspace, i.e., the relation between σ_{dt}^2 and σ_d^2, and $\alpha = 0$ is the special case where no data is present in the training subspace.

Using this model of the transmitted signal and denoting $\sigma_{dt}^2 = \alpha^2\sigma_{d'}^2$ and $\sigma_d^2 = (1-\alpha)^2\sigma_{d'}^2$, (7.12) becomes

$$\mathbf{X} = \sqrt{\frac{\sigma_t^2}{M}}\mathbf{S}_t\mathbf{H} + \sqrt{\frac{\sigma_{dt}^2}{M}}\mathbf{P}_{\mathbf{S}_t}\mathbf{S}_{\text{data}}\mathbf{H} + \sqrt{\frac{\sigma_d^2}{M}}\mathbf{P}_{\mathbf{S}_t}^{\perp}\mathbf{S}_{\text{data}}\mathbf{H} + \mathbf{N}. \tag{7.16}$$

If we consider the singular value decomposition (SVD) of the training signal $\mathbf{S}_t = \mathbf{U}\bar{\mathbf{\Sigma}}\mathbf{V}^H$, where $\mathbf{U}$ and $\mathbf{V}$ are $T \times T$ and $M \times M$ unitary matrices, respectively, $\bar{\mathbf{\Sigma}}$ is a $T \times M$ matrix with the M non-zero singular values $\sigma_i,\ i = 1, \ldots, M$, on its main diagonal, we can write the projection matrices as

$$\mathbf{P}_{\mathbf{S}_t} = \mathbf{U}\begin{bmatrix}\mathbf{I}_M & \mathbf{0} \\ \mathbf{0} & \mathbf{0}_{T-M}\end{bmatrix}\mathbf{U}^H \tag{7.17}$$

$$\mathbf{P}_{\mathbf{S}_t}^{\perp} = \mathbf{U}\begin{bmatrix}\mathbf{0}_M & \mathbf{0} \\ \mathbf{0} & \mathbf{I}_{T-M}\end{bmatrix}\mathbf{U}^H. \tag{7.18}$$

The *Mutual Information (MI)* between the transmitted and received signal remains unchanged when we introduce the reversible coordinate change

$$\begin{aligned}\mathbf{X}_1 = \mathbf{U}^H\mathbf{X} &= \sqrt{\frac{\sigma_t^2}{M}}\mathbf{U}^H\mathbf{U}\bar{\mathbf{\Sigma}}\mathbf{V}^H\mathbf{H} + \sqrt{\frac{\sigma_{dt}^2}{M}}\mathbf{U}^H\mathbf{U}\begin{bmatrix}\mathbf{I}_M & \mathbf{0} \\ \mathbf{0} & \mathbf{0}_{T-M}\end{bmatrix}\mathbf{U}^H\mathbf{S}_{\text{data}}\mathbf{H} \\ &\quad + \sqrt{\frac{\sigma_d^2}{M}}\mathbf{U}^H\mathbf{U}\begin{bmatrix}\mathbf{0}_M & \mathbf{0} \\ \mathbf{0} & \mathbf{I}_{T-M}\end{bmatrix}\mathbf{U}^H\mathbf{S}_{\text{data}}\mathbf{H} + \mathbf{U}^H\mathbf{N} \\ &= \sqrt{\frac{\sigma_t^2}{M}}\bar{\mathbf{\Sigma}}\bar{\mathbf{H}} + \sqrt{\frac{\sigma_{dt}^2}{M}}\begin{bmatrix}\mathbf{I}_M & \mathbf{0} \\ \mathbf{0} & \mathbf{0}_{T-M}\end{bmatrix}\bar{\mathbf{S}}_{\text{data}}\bar{\mathbf{H}} \\ &\quad + \sqrt{\frac{\sigma_d^2}{M}}\begin{bmatrix}\mathbf{0}_M & \mathbf{0} \\ \mathbf{0} & \mathbf{I}_{T-M}\end{bmatrix}\bar{\mathbf{S}}_{\text{data}}\bar{\mathbf{H}} + \bar{\mathbf{N}},\end{aligned} \tag{7.19}$$

where $\bar{\mathbf{H}} = \mathbf{V}^H\mathbf{H}$, $\bar{\mathbf{S}}_{\text{data}} = \mathbf{U}^H\mathbf{S}_{\text{data}}\mathbf{V}$, and $\bar{\mathbf{N}} = \mathbf{U}^H\mathbf{N}$. Now, since $\mathbf{H}$ is complex Gaussian distributed with i.i.d. entries, and hence rotationally invariant, $\bar{\mathbf{H}}$ has the same distribution as $\mathbf{H}$. Similarly, since it is later argued that the data and noise are i.i.d. and complex Gaussian random matrices, we also realize that the signal matrix $\bar{\mathbf{S}}_{\text{data}}$ and the noise matrix $\bar{\mathbf{N}}$ have the same distributions (i.i.d. and complex Gaussian) as $\mathbf{S}_{\text{data}}$ and $\mathbf{N}$, respectively. By using this model we see that the model discussed previously is the special case when the timeslots are chosen as the coordinate base, but here we are not restricted to time multiplexing of the symbols and can choose any orthogonal scheme that we like.

Now we can switch back to our original notation, and consider $\mathbf{S}_{dt} \in \mathbb{C}^{M\times M}$ that occupies the entire training subspace, and $\mathbf{S}_d \in \mathbb{C}^{T_d\times M}$, where

$T_d = T - M$, that occupies the data subspace. Then we can write

$$\mathbf{X}_t = \sqrt{\frac{\sigma_t^2}{M}}\mathbf{\Sigma}\mathbf{H} + \sqrt{\frac{\sigma_{dt}^2}{M}}\mathbf{S}_{dt}\mathbf{H} + \mathbf{N}_t \tag{7.20}$$

$$\mathbf{X}_d = \sqrt{\frac{\sigma_d^2}{M}}\mathbf{S}_d\mathbf{H} + \mathbf{N}_d, \tag{7.21}$$

where $\mathbf{\Sigma}$ is the $M \times M$ matrix containing the non-zero rows of $\bar{\mathbf{\Sigma}}$, i.e., $\bar{\mathbf{\Sigma}} = \begin{bmatrix} \mathbf{\Sigma} \\ \mathbf{0}_{(T-M)\times M} \end{bmatrix}$ and $\mathbf{N} = \begin{bmatrix} \mathbf{N}_t \\ \mathbf{N}_d \end{bmatrix}$.

The signals are normalized according to

$$\mathrm{Tr}\{\mathbf{S}_t\mathbf{S}_t^H\} = \mathrm{Tr}\{\mathbf{\Sigma}^2\} = MT_t \tag{7.22}$$

$$\mathrm{ETr}\{\mathbf{S}_{dt}\mathbf{S}_{dt}^H\} = \mathrm{ETr}\{\bar{\mathbf{S}}_{dt}\bar{\mathbf{S}}_{dt}^H\} = M^2 \tag{7.23}$$

$$\mathrm{ETr}\{\mathbf{S}_d\mathbf{S}_d^H\} = \mathrm{ETr}\{\bar{\mathbf{S}}_d\bar{\mathbf{S}}_d^H\} = MT_d \tag{7.24}$$

$$\mathrm{ETr}\{\mathbf{N}\mathbf{N}^H\} = \mathrm{ETr}\{\bar{\mathbf{N}}\bar{\mathbf{N}}^H\} = NT \tag{7.25}$$

$$\sigma_t^2 T_t + \sigma_{dt}^2 M + \sigma_d^2 T_d = \sigma^2 T, \tag{7.26}$$

where $M \leq T_t \leq T$ and σ^2 denotes the expected SNR at each receive antenna. Thus, the different power levels is accounted for in the variables σ_t^2, σ_{dt}^2 and σ_d^2.

The results of this section are summarized in the following theorems.

Theorem 6 *Consider the data model given by (7.12) and (7.13), and let the channel matrix* $\mathbf{H} \in \mathbb{C}^{M\times N}$*, data matrix* $\mathbf{S}_{\mathrm{data}} \in \mathbb{C}^{T\times M}$*, and the noise matrix* $\mathbf{N} \in \mathbb{C}^{T\times N}$ *be composed of i.i.d. complex Gaussian random variables. Let the deterministic training matrix, normalized according to (7.22), be given by*

$$\mathbf{S}_t = \begin{bmatrix} \bar{\mathbf{S}}_t \\ \mathbf{0}_{(T-T_t)\times M} \end{bmatrix} \in \mathbb{C}^{T\times M}, \tag{7.27}$$

where $\bar{\mathbf{S}}_t \in \mathbb{C}^{T_t\times M}$ *and has full column rank* M*. Then, in the MI sense, it holds that for* any T_t *such that* $M \leq T_t \leq T$ *there exists an equivalent data model where the training matrix is a real-valued and diagonal* $M \times M$ *matrix.*

Proof: The theorem follows directly from inserting the zero-padded training matrix (7.27) into the derivations of the diagonalized model (7.20). □

The above theorem states that there is no loss or gain in MI between the transmitted and received signal by varying the number of training vectors T_t given that $M \leq T_t \leq T$.

Theorem 7 *Given $\alpha = 0$ and the same conditions as in Theorem 6, the projection-based signaling scheme (7.16) will always have better performance (meaning larger MI) than CP for $M < T_t \leq T$. They have identical performance for $T_t = M$, since the two schemes then are equivalent in the MI sense.*

Proof: Consider the zero-padded training matrix (7.27) and let $\alpha = 0$ in (7.14), i.e.,

$$\mathbf{P} = \mathbf{P}_{\mathbf{S}_t}^{\perp} = \mathbf{I}_T - \mathbf{P}_{\mathbf{S}_t} = \mathbf{U} \begin{bmatrix} \mathbf{0}_M & \mathbf{0} \\ \mathbf{0} & \mathbf{I}_{T-M} \end{bmatrix} \mathbf{U}^H. \tag{7.28}$$

On the other hand, the equivalent projection matrix for the CP-scheme would be the following

$$\mathbf{P}_{\mathrm{CP}} = \mathbf{U} \begin{bmatrix} \mathbf{0}_{T_t} & \mathbf{0} \\ \mathbf{0} & \mathbf{I}_{T-T_t} \end{bmatrix} \mathbf{U}^H, \tag{7.29}$$

where $M \leq T_t \leq T$. This matrix imposes the additional constraint on the CP-scheme that no data can be transmitted along the same dimensions (time slots) as the training dimensions. Both systems will have the identical training data given by (7.20), rendering identical channel estimates, and the difference lies in that the projection-based system will receive the data signal

$$\mathbf{X}_d = \sqrt{\frac{\sigma_d^2}{M}} \begin{bmatrix} \mathbf{0}_M & \mathbf{0} \\ \mathbf{0} & \mathbf{I}_{T-M} \end{bmatrix} \mathbf{S}_{\mathrm{data}} \mathbf{H} + \mathbf{N}_d, \tag{7.30}$$

while the CP-based system will receive the data signal

$$\mathbf{X}_{d,\mathrm{CP}} = \sqrt{\frac{\sigma_d^2}{M}} \begin{bmatrix} \mathbf{0}_{T_t} & \mathbf{0} \\ \mathbf{0} & \mathbf{I}_{T-T_t} \end{bmatrix} \mathbf{S}_{\mathrm{data}} \mathbf{H} + \mathbf{N}_d. \tag{7.31}$$

The proof is concluded by noticing that the CP-based system, with the same channel and power, transmits $T_t - M$ data symbols less than the projection-based system, and if $T_t = M$ the systems have identical performance. □

Corollary 1 *It is optimal for CP to choose $T_t = M$.*

Proof: The corollary is a direct result of Theorems 6 and 7. □

So what have we then gained by these little exercises? To answer this question we first consider a conventional time-multiplexed pilot (CP) scheme, such as the one analyzed in [HH03]. In such a scheme the pilot symbols are transmitted exclusively in the time slots allocated for training. This means that the subspace spanned by the pilot signals (which always is restricted to have dimension M) will lie in a T_t dimensional subspace of $\mathbb{C}^T$. So if $T_t > M$, we will have $T_t - M$ dimensions that are "free", but can not be used for data,

since the data is constrained to be in the $T - T_t$ dimensions that are given by the training free time slots. Considering the projection-based approach discussed above we see that all the free dimensions can be utilized for data even if we want to transmit pilots in more than M time slots. On the one hand, we can conclude that no performance is lost or gained by transmitting $T_t = M$ (or any other number $M \leq T_t \leq T$) pilot symbols as long as we can adjust the power accordingly, since additional training power is the only thing that is gained by increasing the number of time slots allocated for additional training symbols. On the other hand, if there are limitations on the power allocations, such as for a system with a constant average power limitation, it might be necessary to consider $T_t > M$ in order to get a sufficiently good channel estimate. These kind of systems, such as the previously mentioned overlay pilot scheme, are not considered in this work, and from now on only $T_t = M$ will be considered.

7.1.3 Channel Estimation

A natural choice of channel estimator is the *Minimum Mean Square Error (MMSE)* estimator, since it renders the lowest channel estimation error. This estimator also has the desired property that the estimate becomes uncorrelated with the estimation error. Unfortunately, the problem with this estimator is that the analysis becomes too complicated for any analytical expressions for the problem at hand. Hence, we will limit ourselves to the class of linear estimators, whereof the popular and widely used *Linear Minimum Mean Square Error (LMMSE)* estimator is used to estimate the MIMO channel. It is used since the channel is considered random and, besides having a closed-form solution, along with the MMSE estimate it also has the desirable property that the resulting estimate is uncorrelated with the estimation error. The orthogonality property becomes very useful in the forthcoming derivations of the optimal training matrix. To form the LMMSE estimator, the data in (7.20) is treated as noise. Thus, the fact that the noise contains a part that is colored by the channel is neglected and it makes the estimator suboptimal.

As previously stated, the data in (7.20) is incorporated into the noise and the resulting total noise is uncorrelated with the channel matrix. The LMMSE estimate of the channel given by [Kay93]

$$\hat{\mathbf{H}} = \mathbf{R}_{\mathbf{H}\mathbf{X}_t}\mathbf{R}_{\mathbf{X}_t}^{-1}\mathbf{X}_t = \underbrace{\sqrt{\frac{M}{\sigma_t^2}}\left(\frac{M(\sigma_{dt}^2+1)}{\sigma_t^2}\mathbf{I}_M + \mathbf{\Sigma}^2\right)^{-1}\mathbf{\Sigma}}_{\triangleq \mathbf{D}}\,\mathbf{X}_t \tag{7.32}$$

where

$$\mathbf{R}_{\mathbf{H}\mathbf{X}_t} = \mathrm{E}\left[\mathbf{H}\mathbf{X}_t^H\right] = N\sqrt{\frac{\sigma_t^2}{M}}\mathbf{\Sigma} \tag{7.33}$$

$$\mathbf{R}_{\mathbf{X}_t} = \mathrm{E}\left[\mathbf{X}_t\mathbf{X}_t^H\right] = \frac{N\sigma_t^2}{M}\mathbf{\Sigma}^2 + (\sigma_{dt}^2+1)N\mathbf{I}_M \tag{7.34}$$

The diagonal matrix $\mathbf{D}$ is introduced here for notational convenience since this matrix will appear frequently in the forthcoming derivations, and $\mathbf{D}$ is given by

$$\mathbf{D} = \sqrt{\frac{\sigma_t^2}{M}}\,\mathrm{diag}\bigg(\frac{\sigma_1}{\sigma_t^2\sigma_1^2/M+\sigma_{dt}^2+1}, \frac{\sigma_2}{\sigma_t^2\sigma_2^2/M+\sigma_{dt}^2+1}, \cdots \\ \cdots, \frac{\sigma_M}{\sigma_t^2\sigma_M^2/M+\sigma_{dt}^2+1}\bigg). \tag{7.35}$$

To arrive at the second equality in (7.32), we have assumed that $\mathbf{S}_{dt}$ has zero mean and is uncorrelated with $\mathbf{H}$, and that $\mathrm{E}[\mathbf{S}_{dt}\mathbf{S}_{dt}^H] = M\mathbf{I}_M$. It is later argued that choosing the data to be spatio-temporally uncorrelated maximizes the mutual information between the transmitted and the received signal matrices, which is also a reasonable signaling choice since the channel is unknown in the transmitter.

After removing the known pilot symbols and using the channel estimate as if it was the true channel, the following signal model is used in the SIP mode

$$\mathbf{X}_t' = \mathbf{X}_t - \sqrt{\frac{\sigma_t^2}{M}}\mathbf{\Sigma}\hat{\mathbf{H}} = \sqrt{\frac{\sigma_{dt}^2}{M}}\mathbf{S}_{dt}\hat{\mathbf{H}} + \underbrace{\sqrt{\frac{\sigma_t^2}{M}}\mathbf{\Sigma}\tilde{\mathbf{H}} + \sqrt{\frac{\sigma_{dt}^2}{M}}\mathbf{S}_{dt}\tilde{\mathbf{H}} + \mathbf{N}_t}_{\triangleq\mathbf{N}_t'}, \tag{7.36}$$

where $\tilde{\mathbf{H}}$ is the channel estimation error, i.e., $\tilde{\mathbf{H}} = \mathbf{H} - \hat{\mathbf{H}}$, and is zero-mean and uncorrelated with the LMMSE channel estimate $\hat{\mathbf{H}}$. The average noise power is given by the following theorem

Theorem 8 *Let $\mathbf{n}_t'$ be the vectorized version of the noise matrix $\mathbf{N}_t'$ defined in (7.36), i.e., $\mathbf{n}_t' = \mathrm{vec}(\mathbf{N}_t')$. Then, the elements of the noise matrix are uncorrelated with an average noise variance $\sigma_{\mathbf{N}_t'}^2$ given by*

$$\begin{aligned}\sigma_{\mathbf{N}_t'}^2 &\triangleq \frac{1}{NM}\mathrm{E}\left[\mathbf{n}_t'^H\mathbf{n}_t'\right] \\ &= \frac{2\sigma_t^2\sigma_{dt}^2}{M^3}\mathrm{Tr}\{\mathbf{\Sigma}\mathbf{D}\}^2 - \frac{1}{M}\sqrt{\frac{\sigma_t^2}{M}}\left(1+\frac{(2+M)\sigma_{dt}^2}{M}\right)\mathrm{Tr}\{\mathbf{\Sigma}\mathbf{D}\} \\ &\quad + (\sigma_{dt}^2+1) + \frac{\sigma_t^2\sigma_{dt}^2}{M^2}\mathrm{Tr}\{\mathbf{\Sigma}^2\mathbf{D}^2\} + \frac{1}{M}\left(\sigma_{dt}^2+\frac{(1+M^2)\sigma_{dt}^4}{M^2}\right)\mathrm{Tr}\{\mathbf{D}^2\}.\end{aligned} \tag{7.37}$$

Proof: See Appendix 7.A. □

The SIP scheme ignores the fact that the total noise in (7.20), besides data, also contains channel information, when it forms the LMMSE channel estimate. Hence, in our case the MMSE estimate is not linear, and therefore the LMMSE estimate is not the MMSE estimate. Nonetheless, this is a conscious choice of estimator made by the SIP-scheme and the data is simply incorporated in the noise term, essentially rendering a low-complexity channel estimator at the expense of a lower SNR.

For the CP case analyzed in [HH03], the LMMSE estimator is also the MMSE estimator which makes its effective noise (the equivalent to our $\mathbf{N}'_t$) uncorrelated with the data. This, together with a Gaussian assumption is the worst case noise in the sense that it minimizes the capacity [HH03]. Here, the LMMSE estimator is not the MMSE estimator and, hence, the effective noise $\mathbf{N}'_t$ becomes correlated with the data. This means that if we replace our noise matrix $\mathbf{N}'_t$ with another noise matrix that is uncorrelated with the data and has the same variance, it gives only an approximate result, although, numerical evaluations indicate that the capacity is quite insensitive to doing so. In fact, the actual SNR in the data $\mathbf{X}'_t$ differs for different realizations of the channel matrix estimate, but we approximate the capacity by instead using the average noise power $\sigma^2_{\mathbf{N}'_t}$. To allow some informality, one might even be able to apply Jensen's inequality [CT91] to argue that using the average noise power will only give an even lower bound on the capacity due to the convexity (w.r.t. the noise) of the capacity formula, [Tel99] and [HH03]. Nonetheless, we replace the noise $\mathbf{N}'_t$ with a Gaussian noise matrix that has the same variance $\sigma^2_{\mathbf{N}'_t}$ and the property of being uncorrelated (conditioned on $\mathbf{X}_t$ and $\mathbf{\Sigma}$) with the data. This choice of noise matrix is not necessarily the worst case noise but serves a good approximation of the actual noise.

Using the channel estimate as if it was the true channel, we have the following signal model in the data mode

$$\mathbf{X}_d = \sqrt{\frac{\sigma_d^2}{M}}\mathbf{S}_d\hat{\mathbf{H}} + \underbrace{\sqrt{\frac{\sigma_d^2}{M}}\mathbf{S}_d\tilde{\mathbf{H}} + \mathbf{N}_d}_{\triangleq \mathbf{N}'_d}, \tag{7.38}$$

where the noise matrix $\mathbf{N}'_d$ has uncorrelated elements with average variance

$$\begin{aligned}
\sigma^2_{\mathbf{N}'_d} &\triangleq \frac{1}{NT_d}\mathrm{ETr}\left\{\mathbf{N}'^H_d\mathbf{N}'_d\right\} \\
&= \frac{1}{NT_d}\mathrm{ETr}\left\{\left(\sqrt{\tfrac{\sigma^2_d}{M}}\mathbf{S}_d\tilde{\mathbf{H}}+\mathbf{N}_d\right)^H\left(\sqrt{\tfrac{\sigma^2_d}{M}}\mathbf{S}_d\tilde{\mathbf{H}}+\mathbf{N}_d\right)\right\} \\
&= \frac{1}{NT_d}\mathrm{ETr}\left\{\tfrac{\sigma^2_d}{M}\mathbf{S}_d\tilde{\mathbf{H}}\tilde{\mathbf{H}}^H\mathbf{S}_d^H+\mathbf{N}_d^H\mathbf{N}_d\right\} \\
&= \sigma^2_d\sigma^2_{\tilde{\mathbf{H}}}+1, \qquad (7.39)
\end{aligned}$$

where $\sigma^2_{\tilde{\mathbf{H}}} \triangleq \frac{1}{MN}\mathrm{ETr}\{\tilde{\mathbf{H}}\tilde{\mathbf{H}}^H\}$ is defined as the variance of the channel estimation error. Again, it is assumed that the data is white, i.e., $\mathrm{E}[\mathbf{S}_d^H\mathbf{S}_d] = T_d\mathbf{I}_M$. As for the SIP part, the noise $\mathbf{N}'_d$ is replaced by a Gaussian noise matrix with the same variance $\sigma^2_{\mathbf{N}'_d}$ and uncorrelated (conditioned on $\mathbf{X}_t$ and $\mathbf{S}_t$) with $\mathbf{S}_d$. We want to point out that there is a fundamental difference between the models given by (7.20) and (7.21), and their counterparts (7.36) and (7.38). In (7.20) and (7.21) the channel is unknown, while in (7.36) and (7.38) the channel is known. In the next section we will find expressions for the capacity for the known channel case.

7.1.4 Capacity Bounds and Optimization

Mutual Information

Let $\hat{\mathbf{H}} = f(\mathbf{X}_t, \mathbf{S}_t)$ be the channel estimate, formed by treating the data $\mathbf{S}_{dt}$ as noise. Using the data processing inequality and the chain-rule [CT91], the mutual information (MI) between what is known and observed in the receiver and the unknown transmitted signals can be lower bounded and written as

$$\begin{aligned}
I_{\mathrm{tot}} &= I\big((\mathbf{X}_t, \mathbf{X}_d, \mathbf{S}_t); (\mathbf{S}_{dt}, \mathbf{S}_d)\big) && (7.40)\\
&\geq I\big((\underbrace{f(\mathbf{X}_t, \mathbf{S}_t)}_{=\hat{\mathbf{H}}}, \mathbf{X}_t, \mathbf{X}_d); (\mathbf{S}_{dt}, \mathbf{S}_d)\big) && (7.41)\\
&= \underbrace{I\big((\hat{\mathbf{H}}, \mathbf{X}_t, \mathbf{X}_d); \mathbf{S}_{dt} \,|\, \mathbf{S}_d\big)}_{\triangleq I_t} + \underbrace{I\big((\hat{\mathbf{H}}, \mathbf{X}_t, \mathbf{X}_d); \mathbf{S}_d\big)}_{\triangleq I_d}. && (7.42)
\end{aligned}$$

We continue with lower-bounding I_t by using the chain-rule and the non-negativeness property of the MI

$$\begin{aligned} I_t &= \underbrace{I\big(\mathbf{X}_d; \mathbf{S}_{dt} \,|\, (\mathbf{S}_d, \hat{\mathbf{H}}, \mathbf{X}_t)\big)}_{\geq 0} + I\big((\hat{\mathbf{H}}, \mathbf{X}_t); \mathbf{S}_{dt} \,|\, \mathbf{S}_d\big) && (7.43)\\ &\geq I\big((\hat{\mathbf{H}}, \mathbf{X}_t); \mathbf{S}_{dt} \,|\, \mathbf{S}_d\big) && (7.44)\\ &= I\big((\hat{\mathbf{H}}, \mathbf{X}_t); \mathbf{S}_{dt}\big) && (7.45)\\ &= I\big(\mathbf{X}_t; \mathbf{S}_{dt} \,|\, \hat{\mathbf{H}}\big) + \underbrace{I\big(\hat{\mathbf{H}}; \mathbf{S}_{dt}\big)}_{\geq 0} && (7.46)\\ &\geq I\big(\mathbf{X}_t; \mathbf{S}_{dt} \,|\, \hat{\mathbf{H}}\big), && (7.47) \end{aligned}$$

where the equality (7.45) follows from the fact that $\mathbf{S}_d$ is independent of $\hat{\mathbf{H}}$, $\mathbf{X}_t$ and $\mathbf{S}_{dt}$.

Finally, we also lower-bound I_d by using the chain-rule and the data processing inequality, as

$$\begin{aligned} I_d &= I\big((\mathbf{X}_t, \mathbf{X}_d); \mathbf{S}_d \,|\, \hat{\mathbf{H}}\big) + \underbrace{I\big(\hat{\mathbf{H}}; \mathbf{S}_d\big)}_{=0} && (7.48)\\ &\geq I\big(\mathbf{X}_d; \mathbf{S}_d \,|\, \hat{\mathbf{H}}\big). && (7.49) \end{aligned}$$

The idea of using a training-based system is to use the channel estimate as if it was the true channel (certainty equivalence principle). Hence, we use the lower-bounds of the MI which are only conditioned on the channel estimate, and, finally, the SIP-based system capacity is given by the maximum, with respect to the training matrix and the distributions of $\mathbf{S}_{dt}$ and $\mathbf{S}_d$, of the MI lower bound

$$\begin{aligned} C_{\text{SIP}} &= \max \frac{1}{T} \Big\{ I(\mathbf{X}_t; \mathbf{S}_{dt} \,|\, \hat{\mathbf{H}}) + I(\mathbf{X}_d; \mathbf{S}_d \,|\, \hat{\mathbf{H}}) \Big\} && (7.50)\\ &\quad f(\mathbf{S}_{dt}), \text{ s.t. } \mathrm{ETr}\{\mathbf{S}_{dt}\mathbf{S}_{dt}^H\} = M^2,\\ &\quad f(\mathbf{S}_d), \text{ s.t. } \mathrm{ETr}\{\mathbf{S}_d\mathbf{S}_d^H\} = MT_d. && (7.51) \end{aligned}$$

Bounds on the Capacity

The worst case noise and optimal signal distribution in a MI sense is stated in the following theorem.

Theorem 9 *From [HH03]. Consider the following multiple-antenna channel with M transmit and N receive antennas*

$$\mathbf{x} = \sqrt{\frac{\sigma^2}{M}}\mathbf{s}\mathbf{H} + \mathbf{n} \tag{7.52}$$

where $\mathbf{x} \in \mathbb{C}^{1\times N}$ *is the received signal vector,* $\mathbf{H} \in \mathbb{C}^{M\times N}$ *is the* known *channel matrix,* $\mathbf{s} \in \mathbb{C}^{1\times M}$ *is the transmitted signal vector, and* $\mathbf{n} \in \mathbb{C}^{1\times N}$ *is the additive noise. Let the signal and noise satisfy the following power constraints*

$$\mathrm{E}[\mathbf{s}\mathbf{s}^H] = M \quad \text{and} \quad \mathrm{E}[\mathbf{n}\mathbf{n}^H] = N \tag{7.53}$$

and be uncorrelated

$$\mathrm{E}[\mathbf{s}^H\mathbf{n}] = \mathbf{0}_{M\times N}. \tag{7.54}$$

Further, let $\mathbf{R}_\mathbf{s} = \mathrm{E}[\mathbf{s}^H\mathbf{s}]$ *and* $\mathbf{R}_\mathbf{n} = \mathrm{E}[\mathbf{n}^H\mathbf{n}]$ *denote the respective correlation matrices. Then the worst case noise (in the sense that it minimizes the MI between* $\mathbf{x}$ *and* $\mathbf{s}$*) has a zero mean complex Gaussian distribution, i.e.,* $\mathbf{n} \sim \mathcal{CN}(\mathbf{0}, \mathbf{R}_{\mathbf{n},\mathrm{opt}})$*, where* $\mathbf{R}_{\mathbf{n},\mathrm{opt}}$ *is the minimizing noise covariance matrix. When the distribution on the channel matrix is right rotationally invariant, i.e., the PDF* $f(\mathbf{H}\mathbf{\Theta}_2) = f(\mathbf{H})$ *for all unitary matrices* $\mathbf{\Theta}_2$*, then*

$$\mathbf{R}_{\mathbf{n},\mathrm{opt}} = \mathbf{I}_N. \tag{7.55}$$

The MI maximizing signal is also zero-mean and complex Gaussian distributed, i.e., $\mathbf{s} \sim \mathcal{CN}(\mathbf{0}, \mathbf{R}_{\mathbf{s},\mathrm{opt}})$*, where* $\mathbf{R}_{\mathbf{s},\mathrm{opt}}$ *is the maximizing signal covariance matrix. When the distribution of* $\mathbf{H}$ *is left rotationally invariant, i.e.,* $f(\mathbf{\Theta}_1\mathbf{H}) = f(\mathbf{H})$*, then*

$$\mathbf{R}_{\mathbf{s},\mathrm{opt}} = \mathbf{I}_M. \tag{7.56}$$

Hence, a zero-mean uncorrelated complex Gaussian signal maximizes the lower bound (which is given by a zero-mean uncorrelated complex Gaussian noise vector) on the MI between the input and output.

Proof: See [HH03]. □

This signaling choice is also shown to be optimal in [Tel99]. If the distribution of the channel matrix (in our case $\hat{\mathbf{H}}$) can be shown to be both left and right rotationally invariant, we can apply Theorem 9.

The following theorem shows that the channel estimate $\hat{\mathbf{H}}$ in (7.32) is rotationally invariant.

Theorem 10 *Assume that* $\mathbf{S}_{dt}$ *is rotationally invariant and consider the channel estimate* $\hat{\mathbf{H}}$ *given in (7.32). If the training matrix* $\mathbf{\Sigma}$ *is chosen as a multiple of the identity matrix, i.e.,* $\mathbf{\Sigma} = \sqrt{T_t}\mathbf{I}_M$*, the PDF of* $\hat{\mathbf{H}}$ *is both left and right rotationally invariant.*

Proof: See Appendix 7.B. □

Hence, $\mathbf{\Sigma}$ and $\mathbf{S}_{dt}$ can be chosen such that $\hat{\mathbf{H}}$ becomes rotationally invariant. In other words, we choose such a signaling scheme, and in that case we also know that it is optimal to let $\mathbf{R}_{\mathbf{S}_{dt}}$ and $\mathbf{R}_{\mathbf{S}_d}$ be multiples of the identity matrix. It is also later shown that this choice of training matrix also maximizes the effective SNR in the data mode.

To summarize, we can argue that the noise, with a given power constraint, that yields the lowest MI is uncorrelated with the transmitted signal, has a zero-mean circularly symmetric complex Gaussian distribution, and is spatio-temporally white. This worst case noise will, thus, render a lower-bound on the MI. On the other hand, the distribution of the transmitted signal that maximizes the MI in an additive Gaussian noise channel is also Gaussian distributed with zero mean and no space or time correlation.

The lower-bound on the capacity will then be composed of two terms; one for the SIP mode and one for the data mode. Hence, the capacity expression for the SIP-scheme is given by

$$C_{\text{SIP}} \geq \frac{M}{T}\mathrm{E}\left[\log_2 \det\left(\mathbf{I}_M + \frac{\rho_t}{M}\bar{\mathbf{H}}\bar{\mathbf{H}}^H\right)\right] + \frac{T_d}{T}\mathrm{E}\left[\log_2 \det\left(\mathbf{I}_M + \frac{\rho_d}{M}\bar{\mathbf{H}}\bar{\mathbf{H}}^H\right)\right] \quad \text{bits/channel use} \tag{7.57}$$

where the elements of the normalized channel estimate $\bar{\mathbf{H}} \triangleq \frac{\hat{\mathbf{H}}}{\sigma_{\hat{\mathbf{H}}}}$ will be uncorrelated with zero mean and unit variance, and have a distribution that is approximately Gaussian. The normalization constant $\sigma_{\hat{\mathbf{H}}}$ is given by $\sigma^2_{\hat{\mathbf{H}}} \triangleq \frac{1}{MN}\mathrm{ETr}\{\hat{\mathbf{H}}\hat{\mathbf{H}}^H\}$ and the effective SNRs are given by

$$\rho_t = \frac{\sigma^2_{dt}\sigma^2_{\hat{\mathbf{H}}}}{\sigma^2_{\mathbf{N}'_t}} \tag{7.58}$$

$$\rho_d = \frac{\sigma^2_d\sigma^2_{\hat{\mathbf{H}}}}{\sigma^2_{\mathbf{N}'_d}} = \frac{\sigma^2_d\sigma^2_{\hat{\mathbf{H}}}}{\sigma^2_d\sigma^2_{\tilde{\mathbf{H}}} + 1}. \tag{7.59}$$

To find the capacity, (7.57) has to be optimized with respect to the following parameters: $\mathbf{\Sigma}, \sigma^2_t, \sigma^2_{dt}, \sigma^2_d$ and M.

Optimization over $\mathbf{\Sigma}$

First, the criterion function (7.57) is to be concentrated with respect to the training matrix, $\mathbf{\Sigma}$. If the same $\mathbf{\Sigma}$ maximizes both ρ_t and ρ_d, that $\mathbf{\Sigma}$ will clearly maximize the capacity. Using the orthogonality of the LMMSE estimate, we can write $\sigma^2_{\hat{\mathbf{H}}} = 1 - \sigma^2_{\tilde{\mathbf{H}}}$, where $\sigma^2_{\tilde{\mathbf{H}}}$ is the variance of the channel estimation error.

To find the variance of the channel estimation error, let $\mathbf{h} = \text{vec}(\mathbf{H})$, $\hat{\mathbf{h}} = \text{vec}(\hat{\mathbf{H}})$, $\mathbf{x}_t = \text{vec}(\mathbf{X}_t)$ and $\mathbf{n}_t = \text{vec}(\mathbf{N}_t)$. Then, $\hat{\mathbf{h}} = \mathbf{R}_{\mathbf{hx}_t}\mathbf{R}_{\mathbf{x}_t}^{-1}\mathbf{x}_t$ is the LMMSE estimate of $\mathbf{h}$, which is only the vectorized version of (7.32)

$$\begin{aligned}\mathbf{x}_t &= \text{vec}\left(\sqrt{\frac{\sigma_t^2}{M}}\mathbf{\Sigma}\mathbf{H} + \sqrt{\frac{\sigma_{dt}^2}{M}}\mathbf{S}_{dt}\mathbf{H} + \mathbf{N}_t\right)\\ &= \sqrt{\frac{\sigma_t^2}{M}}(\mathbf{I}_N \otimes \mathbf{\Sigma})\mathbf{h} + \sqrt{\frac{\sigma_{dt}^2}{M}}(\mathbf{I}_N \otimes \mathbf{S}_{dt})\mathbf{h} + \mathbf{n}_t,\end{aligned}$$

where we have used that $\text{vec}(\mathbf{ABC}) = (\mathbf{C}^T \otimes \mathbf{A})\,\text{vec}(\mathbf{B})$ [Lüt96], and

$$\begin{aligned}\mathbf{R}_{\mathbf{x}_t} &= \text{E}[\mathbf{x}_t\mathbf{x}_t^H] = \frac{\sigma_t^2}{M}(\mathbf{I}_N \otimes \mathbf{\Sigma}^2) + \sigma_{dt}^2\mathbf{I}_N \otimes \mathbf{I}_M + \mathbf{I}_N \otimes \mathbf{I}_M\\ &= \mathbf{I}_N \otimes \left(\frac{\sigma_t^2}{M}\mathbf{\Sigma}^2 + (\sigma_{dt}^2+1)\mathbf{I}_M\right),\end{aligned} \tag{7.60}$$

$$\begin{aligned}\mathbf{R}_{\mathbf{hx}_t} &= \text{E}[\mathbf{h}\mathbf{x}_t^H] = \text{E}\left[\mathbf{h}\left(\sqrt{\frac{\sigma_t^2}{M}}(\mathbf{I}_N \otimes \mathbf{\Sigma})\mathbf{h} + \sqrt{\frac{\sigma_{dt}^2}{M}}(\mathbf{I}_N \otimes \mathbf{S}_{dt})\mathbf{h} + \mathbf{n}\right)^H\right]\\ &= \sqrt{\frac{\sigma_t^2}{M}}\mathbf{I}_N \otimes \mathbf{\Sigma}.\end{aligned} \tag{7.61}$$

Finally, the channel estimate can be identified as

$$\hat{\mathbf{h}} = \mathbf{R}_{\mathbf{hx}_t}\mathbf{R}_{\mathbf{x}_t}^{-1}\mathbf{x}_t = (\mathbf{I}_N \otimes \mathbf{D})\,\mathbf{x}_t. \tag{7.62}$$

Since $\tilde{\mathbf{h}} = (\mathbf{h} - \hat{\mathbf{h}}) \perp \hat{\mathbf{h}}$, the error covariance matrix is given by

$$\begin{aligned}\mathbf{R}_{\tilde{\mathbf{h}}} &= \text{E}[\tilde{\mathbf{h}}\tilde{\mathbf{h}}^H] = \text{E}[(\mathbf{h}-\hat{\mathbf{h}})(\mathbf{h}-\hat{\mathbf{h}})^H] = \text{E}[\mathbf{h}\mathbf{h}^H] - \text{E}[\mathbf{h}\hat{\mathbf{h}}^H]\\ &= \mathbf{I}_N \otimes \mathbf{I}_M - \text{E}[\mathbf{h}\mathbf{x}_t^H]\,(\mathbf{I}_N \otimes \mathbf{D}) = \mathbf{I}_N \otimes \left(\mathbf{I}_M - \sqrt{\frac{\sigma_t^2}{M}}\mathbf{\Sigma}\mathbf{D}\right)\\ &= \mathbf{I}_N \otimes (\sigma_{dt}^2+1)\,\text{diag}\Bigg(\frac{1}{\sigma_t^2\sigma_1^2/M + \sigma_{dt}^2 + 1}, \frac{1}{\sigma_t^2\sigma_2^2/M + \sigma_{dt}^2 + 1}, \cdots\\ &\qquad \cdots, \frac{1}{\sigma_t^2\sigma_M^2/M + \sigma_{dt}^2 + 1}\Bigg)\\ &= \mathbf{I}_N \otimes \sqrt{\frac{M}{\sigma_t^2}}(\sigma_{dt}^2+1)\mathbf{\Sigma}^{-1}\mathbf{D}.\end{aligned} \tag{7.63}$$

Hence, $\sigma^2_{\tilde{\mathbf{H}}}$ is given by

$$\begin{aligned}\sigma^2_{\tilde{\mathbf{H}}} &\triangleq \frac{1}{MN}\mathrm{E}\mathrm{Tr}\{\tilde{\mathbf{H}}\tilde{\mathbf{H}}^H\} = \frac{1}{MN}\mathrm{Tr}\{\mathbf{R}_{\tilde{\mathbf{h}}}\} \\ &= \frac{1}{M}(\sigma^2_{dt}+1)\sum_{i=1}^{M}\frac{1}{\sigma^2_t\sigma^2_i/M+\sigma^2_{dt}+1} = \frac{1}{M}\sum_{i=1}^{M}\frac{1}{\beta\sigma^2_i+1}, \quad (7.64)\end{aligned}$$

where $\beta = \frac{\sigma^2_t}{M(\sigma^2_{dt}+1)}$.

We want to choose the training matrix such that it maximizes the effective SNRs ρ_t and ρ_d in (7.58) and (7.59). Since it is difficult to analytically evaluate the effective SNR during the SIP mode, we will resort to only maximize the SNR during the data mode. Nonetheless, it seems natural that the same choice of training matrix, which turns out to be a unitary matrix, also should maximize the SNR during the SIP mode since the channel, data, and noise all are white.

To show that minimizing the channel estimation error also maximizes the effective SNR we use that $\sigma^2_{\hat{\mathbf{H}}} = 1 - \sigma^2_{\tilde{\mathbf{H}}}$, and start by rewriting (7.59) as

$$\rho_d = \frac{\sigma^2_d(1-\sigma^2_{\tilde{\mathbf{H}}})}{\sigma^2_d\sigma^2_{\tilde{\mathbf{H}}}+1} = \frac{\sigma^2_d+1}{\sigma^2_d\sigma^2_{\tilde{\mathbf{H}}}+1} - 1. \quad (7.65)$$

From (7.65), we conclude that the effective SNR, ρ_d, is maximized by minimizing the variance of the channel estimation error $\sigma^2_{\tilde{\mathbf{H}}}$, which is done next.

We need to choose $\boldsymbol{\Sigma}$ such that $\sigma^2_{\tilde{\mathbf{H}}}$ is minimized. The problem can be stated as

$$\min_{\substack{\boldsymbol{\Sigma} \\ \mathrm{Tr}\{\boldsymbol{\Sigma}^2\}=MT_t}} \sigma^2_{\tilde{\mathbf{H}}} \quad \Longleftrightarrow \quad \min_{\substack{\sigma^2_1,\ldots,\sigma^2_M \\ \sum_i \sigma^2_i = MT_t}} \sum_{i=1}^{M}\frac{1}{1+\beta\sigma^2_i}, \quad (7.66)$$

where $\beta > 0$ is a real-valued constant. This is a standard convex optimization problem and may be solved by using, e.g., Lagrange multipliers. The Lagrangian is given by

$$L(\sigma^2_1,\ldots,\sigma^2_M,\mu) = \sum_{i=1}^{M}\frac{1}{1+\beta\sigma^2_i} + \mu\left(\sum_i \sigma^2_i - MT_t\right). \quad (7.67)$$

Differentiating with respect to σ^2_i and setting the derivative to zero yields

$$\frac{\partial L}{\partial \sigma^2_i} = \frac{-\beta}{(1+\beta\lambda_i)^2} + \mu = 0 \quad \Longrightarrow \quad \mu = \frac{\beta}{(1+\beta\sigma^2_i)^2}. \quad (7.68)$$

When solving for σ^2_i, we see that all σ^2_i's equal the same constant. Since $\partial^2 L/\partial{\sigma^2_i}^2 > 0$, the solution $\sigma^2_1 = \cdots = \sigma^2_M = T_t$ follows from the constraints,

and yields $\mathbf{\Sigma} = \sqrt{T_t}\mathbf{I}_M$. This choice of training matrix does not only maximize the effective SNR, it also makes $\hat{\mathbf{H}}$ left rotationally invariant, which also is in agreement with the choice made in [HH03].

By inserting this training matrix into (7.64), the variance evaluates to

$$\sigma^2_{\tilde{\mathbf{H}}} = \frac{M(\sigma^2_{dt}+1)}{M(\sigma^2_{dt}+1)+\sigma^2_t T_t}. \tag{7.69}$$

Hence by employing the result of Theorem 8 and Equation (7.39) together with $\sigma^2_{\hat{\mathbf{H}}} = 1 - \sigma^2_{\tilde{\mathbf{H}}}$, the effective SNRs in (7.58) and (7.59) evaluate to

$$\rho_t = \frac{\sigma^2_t\sigma^2_{dt}MT_t(\sigma^2_t T_t + \sigma^2_{dt}M + M)}{\sigma^4_t\sigma^2_{dt}MT^2_t + (\sigma^2_{dt}+1)^3M^3 + (\sigma^2_{dt}+1)\sigma^2_t T_t M^2 + \sigma^2_t\sigma^4_{dt}T_t} \tag{7.70}$$

$$\rho_d = \frac{\sigma^2_d\sigma^2_t T_t}{(\sigma^2_d+1)(\sigma^2_{dt}+1)M + \sigma^2_t T_t} \tag{7.71}$$

Optimization over $\sigma^2_t, \sigma^2_{dt}, \sigma^2_d, M$

With ρ_t and ρ_d given by (7.70) and (7.71); numerical optimization of (7.57), subject to the time (7.10) and energy (7.11) constraints, is used to find the optimal values of the remaining parameters.

It might seem counter-intuitive to optimize over the number of transmit antennas, since when the channel is known, the capacity is known to be an increasing function of the number of transmit antennas [Tel99]. The reason why there will be an optimum is that the more transmit antennas we use, the more time we have to spend on transmission of non-information carrying training symbols. To build an estimate of the channel matrix, we need at least as many training measurements as we have channel parameters (there are MN complex elements in $\mathbf{H}$). One received vector measurement yields N complex measurements and, therefore, we need to transmit at least M training symbols. Since we have previously shown that there is no gain in increasing T_t beyond M (given that the training power can be adjusted accordingly), we let the number of training vectors equal the smallest possible, i.e., $T_t = M$, in all of the upcoming examples.

7.2 Numerical Examples

To illustrate the theories described in this chapter, we evaluate the capacity expression for a number of different cases. Only channels with relatively short coherence time, T, have been studied, since the SIP scheme degenerates to a CP scheme for large T. Unless otherwise stated, an average SNR of 10 dB

is considered throughout the examples, i.e., $\sigma^2 = 10$. This particular choice of SNR has little effect on the results.

7.2.1 Optimization over all Parameters

In this example we optimize over all the parameters without imposing any additional restrictions such as fixed number of transmit antennas.

Figure 7.2 shows the attained capacity versus SNR when $N = 20$ and $T = 10$, which is a typical case when it is advantageous to use SIP. The capacity of the SIP and CP-schemes increases logaritmically in the high-SNR region. The slope of the curves indicates that both schemes are able to use all the available degrees of freedom [ZT02].

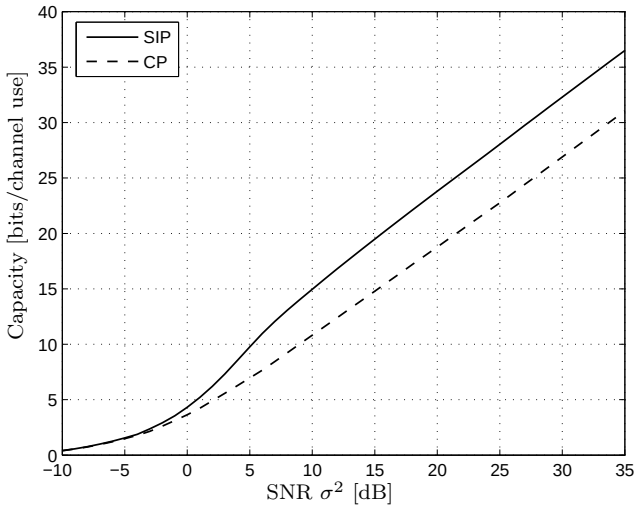

Figure 7.2: Capacity vs. SNR σ^2 when $N = 20$, $T = 10$.

The capacity versus the number of transmit antennas is shown in Figure 7.3. We see that the choice of number of transmit antennas has great impact on the capacity, since the more transmit antennas we have, the more time has to be dedicated to transmission of training symbols. Since the CP scheme can not transmit information symbols during training, its performance becomes more sensitive w.r.t. the number of antennas.

It is not specifically shown here, but we have also seen in examples that the optimal number of transmit antennas sometimes is larger for the SIP-based system than for the CP-based one. When one additional transmit antenna is introduced, the system needs to transmit one additional training

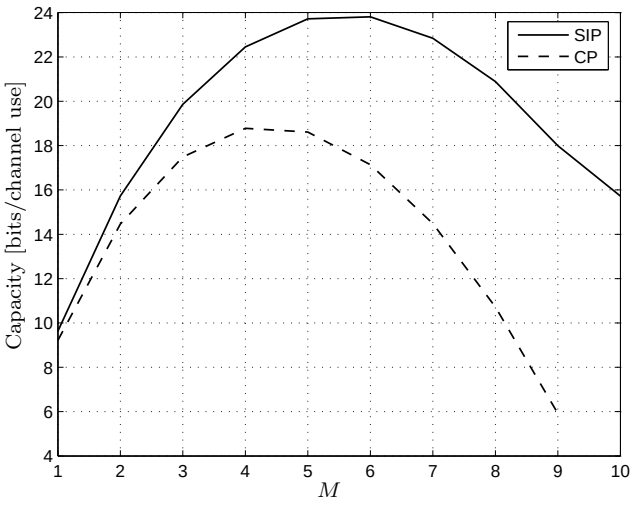

Figure 7.3: Capacity vs. transmit antennas M when $N = 20$, $T = 10$, and SNR $\sigma^2 = 20$ dB.

symbol. The conventional training scheme suffers more than the SIP scheme from this extra training symbol, since it can not transmit any data during training. At low SNR it is optimal to use fewer transmit antennas, i.e., the available transmit power is distributed only over a few antennas, which renders a higher SNR for those particular sub-channels, in accordance with the waterfilling principle for parallel channels [CT91]. We also notice that for high SNR, the optimal number of transmit antennas seems to equal half the coherence time, i.e., $M_{\text{opt}} = T/2$ for high SNR, which is in agreement with the CP-scheme analyzed in [HH03]

In order to compare the performance of the CP-based scheme to that of SIP, the performance gain $C_{\text{CP}}/C_{\text{SIP}}$ is shown in Figure 7.4. It is found that the CP-based scheme will (almost) reach the SIP-based capacity as the coherence time increases or the number of receive antennas decreases. This is because the pure training interval penalty becomes smaller for the CP-scheme as the coherence length is increased and the SNR penalty becomes larger for the SIP scheme as the number of receive antennas is decreased.

7.2.2 Fixed Number of Antennas

In this example we study a scenario where the numbers of transmit and receive antennas are fixed. This way, the system is forced to use all the available transmit antennas even if it might be suboptimal in some cases.

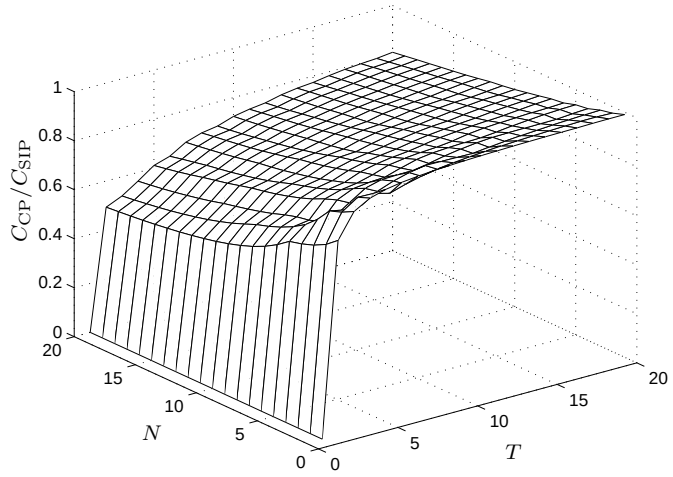

Figure 7.4: Capacity ratio between CP and SIP training, $C_{\mathrm{CP}}/C_{\mathrm{SIP}}$, vs. channel coherence time T and number of receivers N, SNR $\sigma^2 = 10$ dB.

The case $M = N = 6$ is displayed in Figure 7.5. Again, the CP scheme suffers from short coherence times, which leaves it with little time for data transmission. This loss is eliminated for large coherence times where the difference in performance gets small (the curves will merge for large T).

Figure 7.6 displays the optimal power allocation for the two schemes versus the coherence time. It is noticed that the power σ_{dt}^2 allocated for data in the SIP block decays quite quickly to almost zero. Further, we also find that the power σ_t^2 allocated for training symbols increases with the coherence time, which states that it is better to build a good channel estimate as the coherence time increases.

7.A Proof of Theorem 8: The Effective Noise Covariance Matrix

In this appendix we will calculate the effective noise variance that is used in Section 7.1.3. Hence, the aim is to calculate

$$\mathbf{R}_{\mathbf{n}_t'} = \mathrm{E}\left[\mathbf{n}_t' \mathbf{n}_t'^H\right] \tag{7.A.1}$$

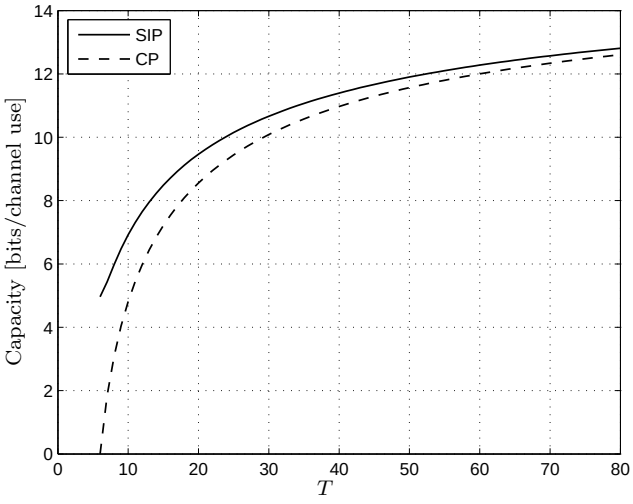

Figure 7.5: Capacity vs. coherence time T when $M = N = 6$, SNR $\sigma^2 = 10$ dB.

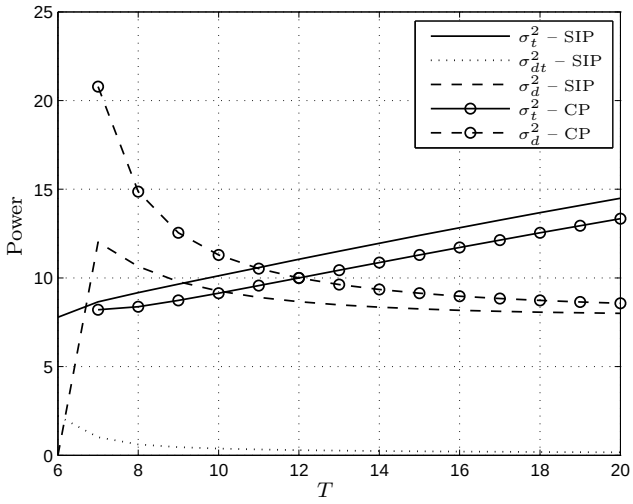

Figure 7.6: Optimal power allocation vs. coherence time T when $M = N = 6$, SNR $\sigma^2 = 10$ dB.

where $\mathbf{n}_t' = \text{vec}(\mathbf{N}_t')$ is defined in (7.36). By also introducing the vectorized versions of the channel error $\tilde{\mathbf{h}} = \text{vec}(\tilde{\mathbf{H}})$ and the background noise $\mathbf{n}_t = \text{vec}(\mathbf{N}_t)$, we get

$$\begin{aligned}\mathbf{n}'_t &= \sqrt{\frac{\sigma_t^2}{M}}\,\mathrm{vec}(\boldsymbol{\Sigma}\tilde{\mathbf{H}}) + \sqrt{\frac{\sigma_d^2}{M}}\,\mathrm{vec}(\mathbf{S}_{dt}\tilde{\mathbf{H}}) + \mathrm{vec}(\mathbf{N}_t) \\ &= \sqrt{\frac{\sigma_t^2}{M}}(\mathbf{I}_N \otimes \boldsymbol{\Sigma})\tilde{\mathbf{h}} + \sqrt{\frac{\sigma_{dt}^2}{M}}(\mathbf{I}_N \otimes \mathbf{S}_{dt})\tilde{\mathbf{h}} + \mathbf{n}_t \end{aligned} \tag{7.A.2}$$

The covariance matrix can therefore be decomposed as

$$\mathbf{R}_{\mathbf{n}'_t} = \mathbf{R}_1 + \mathbf{R}_2 + \mathbf{R}_3 + \mathbf{R}_4 + \mathbf{R}_4^H + \mathbf{R}_5 + \mathbf{R}_5^H + \mathbf{R}_6 + \mathbf{R}_6^H \tag{7.A.3}$$

where

$$\begin{aligned}\mathbf{R}_1 &= \mathrm{E}\left[\frac{\sigma_t^2}{M}(\mathbf{I}_N \otimes \boldsymbol{\Sigma})\tilde{\mathbf{h}}\tilde{\mathbf{h}}^H(\mathbf{I}_N \otimes \boldsymbol{\Sigma}^H)\right] \\ \mathbf{R}_2 &= \mathrm{E}\left[\frac{\sigma_{dt}^2}{M}(\mathbf{I}_N \otimes \mathbf{S}_{dt})\tilde{\mathbf{h}}\tilde{\mathbf{h}}^H(\mathbf{I}_N \otimes \mathbf{S}_{dt}^H)\right] \\ \mathbf{R}_3 &= \mathrm{E}\left[\mathbf{n}_t\mathbf{n}_t^H\right] \\ \mathbf{R}_4 &= \mathrm{E}\left[\frac{\sqrt{\sigma_t^2\sigma_{dt}^2}}{M}(\mathbf{I}_N \otimes \boldsymbol{\Sigma})\tilde{\mathbf{h}}\tilde{\mathbf{h}}^H(\mathbf{I}_N \otimes \mathbf{S}_{dt}^H)\right] \\ \mathbf{R}_5 &= \mathrm{E}\left[\sqrt{\frac{\sigma_t^2}{M}}(\mathbf{I}_N \otimes \boldsymbol{\Sigma})\tilde{\mathbf{h}}\mathbf{n}_t^H\right] \\ \mathbf{R}_6 &= \mathrm{E}\left[\sqrt{\frac{\sigma_{dt}^2}{M}}(\mathbf{I}_N \otimes \mathbf{S}_{dt})\tilde{\mathbf{h}}\mathbf{n}_t^H\right]\end{aligned}$$

The calculation of all these terms is tedious but straightforward. The only term that does not end up as the expectation over one, two or three Gaussian variables is $\mathbf{R}_2$, where the following lemma becomes useful.

Lemma 3 *Let* $\mathbf{S}$ *be an* $M \times M$ *matrix with i.i.d. Gaussian distributed elements with zero mean and unit variance, and* $\mathbf{D}$ *be a deterministic diagonal matrix. Then it holds that*

$$\mathrm{E}\left[\mathbf{SDSS}^H\mathbf{DS}^H\right] = M\mathrm{Tr}\{\mathbf{D}^2\}\mathbf{I}_M + \mathbf{D}^2 \tag{7.A.4}$$

Proof: This is an extension to [JS88]. □

The different terms are now evaluated as

$$\mathbf{R}_1 = \sqrt{\frac{\sigma_t^2}{M}}(\sigma_{dt}^2+1)(\mathbf{I}_N \otimes \boldsymbol{\Sigma}\mathbf{D})$$

$$\mathbf{R}_2 = \mathbf{I}_N \otimes \left\{ \frac{\sigma_{dt}^2}{M} \left(M - 2\sqrt{\frac{\sigma_t^2}{M}}\mathrm{Tr}\{\boldsymbol{\Sigma}\mathbf{D}\} \right.\right.$$
$$\left.\left. + \frac{\sigma_t^2}{M}\mathrm{Tr}\{\boldsymbol{\Sigma}^2\mathbf{D}^2\} + (1+\sigma_{dt}^2)\mathrm{Tr}\{\mathbf{D}^2\} \right) \mathbf{I}_M + \frac{\sigma_{dt}^2}{M}\mathbf{D}^2 \right\}$$

$$\mathbf{R}_3 = \mathbf{I}_{MN}$$

$$\mathbf{R}_4 = \sqrt{\frac{\sigma_t^2}{M}\frac{\sigma_{dt}^2}{M}} \left(\mathbf{I}_N \otimes \left\{ \sqrt{\frac{\sigma_t^2}{M}}\mathrm{Tr}\{\boldsymbol{\Sigma}\mathbf{D}\} - M \right\} \boldsymbol{\Sigma}\mathbf{D} \right)$$

$$\mathbf{R}_5 = -\sqrt{\frac{\sigma_t^2}{M}}(\mathbf{I}_N \otimes \boldsymbol{\Sigma}\mathbf{D})$$

$$\mathbf{R}_6 = \mathbf{0}_{MN}$$

Hence,

$$\mathbf{R}_{\mathbf{n}_t'} = \mathbf{I}_N \otimes \left\{ \left[\frac{2\sigma_t^2\sigma_{dt}^2}{M^2}\mathrm{Tr}\{\boldsymbol{\Sigma}\mathbf{D}\} - \sqrt{\frac{\sigma_t^2}{M}}(\sigma_{dt}^2+1) \right] \boldsymbol{\Sigma}\mathbf{D} \right.$$
$$+ \left[(\sigma_{dt}^2+1) + \frac{\sigma_t^2\sigma_{dt}^2}{M^2}\mathrm{Tr}\{\boldsymbol{\Sigma}^2\mathbf{D}^2\} + \frac{(1+\sigma_{dt}^2)\sigma_{dt}^2}{M}\mathrm{Tr}\{\mathbf{D}^2\} \right. \qquad (7.A.5)$$
$$\left.\left. -2\sqrt{\frac{\sigma_t^2}{M}\frac{\sigma_{dt}^2}{M}}\mathrm{Tr}\{\boldsymbol{\Sigma}\mathbf{D}\} \right] \mathbf{I}_M + \frac{\sigma_{dt}^4}{M^2}\mathbf{D}^2 \right\}.$$

The proof follows first by noticing that $\mathbf{R}_{\mathbf{n}_t'}$ is diagonal, and, finally, by taking the trace-operator. □

7.B Proof of Theorem 10: Rotational Invariance of $\hat{\mathbf{H}}$

To this end, the LMMSE estimate (7.32) is given by

$$\hat{\mathbf{H}} = \sqrt{\frac{M}{\sigma_t^2}} \left(\frac{M(\sigma_{dt}^2+1)}{\sigma_t^2}\mathbf{I}_M + \boldsymbol{\Sigma}^2 \right)^{-1} \boldsymbol{\Sigma}\mathbf{X}_t,$$

where $\boldsymbol{\Sigma}$ is the diagonal training matrix, and $\mathbf{X}$ is the received data given by (7.20)

$$\mathbf{X}_t = \left(\sqrt{\frac{\sigma_t^2}{M}}\boldsymbol{\Sigma} + \sqrt{\frac{\sigma_{dt}^2}{M}}\mathbf{S}_{dt} \right) \mathbf{H} + \mathbf{N}_t.$$

The right rotational invariance follows directly from the fact that $\mathbf{X}_t$ is right rotationally invariant. That $\mathbf{X}_t$ is right rotationally invariant follows easily, since both $\mathbf{H}$ and $\mathbf{N}_t$ are Gaussian distributed with i.i.d. elements, i.e., they are rotationally invariant. To show this, let the rotated version of $\mathbf{X}_t$ be $\mathbf{X}_t\boldsymbol{\Theta}_1 = \left(\sqrt{\frac{\sigma_t^2}{M}}\boldsymbol{\Sigma} + \sqrt{\frac{\sigma_{dt}^2}{M}}\mathbf{S}_{dt}\right)\mathbf{H}\boldsymbol{\Theta}_1 + \mathbf{N}_t\boldsymbol{\Theta}_1$. The right rotational invariance follows now from the fact that both $\mathbf{H}$ and $\mathbf{N}_t$ are rotationally invariant, i.e., $f(\mathbf{H}\boldsymbol{\Theta}_1) = f(\mathbf{H})$ and $f(\mathbf{N}_t\boldsymbol{\Theta}_1) = f(\mathbf{N}_t)$. The right rotational invariance implies that the worst case noise is spatio-temporally white noise [HH03].

Next, we prove that if the training matrix $\boldsymbol{\Sigma}$ is chosen as a multiple of the identity matrix, i.e., $\boldsymbol{\Sigma} = \sqrt{T_t}\mathbf{I}_M$, the channel estimate will also be left rotationally invariant. This result shall not come as a surprise, since by choosing the training matrix as the identity matrix we will allocate the same amount of power to each transmit antenna and, hence, all the channel parameters are estimated at the same SNR. Further, by using orthogonal training sequences we will not get any cross interferences, and since everything else is white, it is natural that the estimate becomes invariant.

Again starting from (7.32) but now also taking the assumption on the training matrix into account (7.32), becomes

$$\hat{\mathbf{H}} = \frac{\sqrt{T_t M\sigma_t^2}}{M(\sigma_{dt}^2+1)+\sigma_t^2 T_t}\mathbf{X}_t$$

And again we can conclude that $\hat{\mathbf{H}}$ is rotationally invariant (this time from the left) if $\mathbf{X}_t$ is left rotationally invariant. That $\mathbf{X}_t$ has this property can be seen if we insert $\boldsymbol{\Sigma} = \sqrt{T_t}\mathbf{I}_M$ into (7.20)

$$\mathbf{X}_t = \left(\sqrt{\frac{T_t\sigma_t^2}{M}}\mathbf{I}_M + \sqrt{\frac{\sigma_{dt}^2}{M}}\mathbf{S}_{dt}\right)\mathbf{H} + \mathbf{N}_t,$$

and look at the rotated version of $\mathbf{X}_t$

$$\begin{aligned}\boldsymbol{\Theta}_2\mathbf{X}_t &= \left(\sqrt{\frac{T_t\sigma_t^2}{M}}\boldsymbol{\Theta}_2 + \sqrt{\frac{\sigma_{dt}^2}{M}}\boldsymbol{\Theta}_2\mathbf{S}_{dt}\right)\mathbf{H} + \boldsymbol{\Theta}_2\mathbf{N}_t \\ &= \left(\sqrt{\frac{T_t\sigma_t^2}{M}} + \sqrt{\frac{\sigma_{dt}^2}{M}}\boldsymbol{\Theta}_2\mathbf{S}_{dt}\boldsymbol{\Theta}_2^H\right)\boldsymbol{\Theta}_2\mathbf{H} + \boldsymbol{\Theta}_2\mathbf{N}_t, \qquad (7.B.1)\end{aligned}$$

and by realizing that $\boldsymbol{\Theta}_2\mathbf{S}_{dt}\boldsymbol{\Theta}_2^H$ has the same distribution as $\mathbf{S}_{dt}$, $\boldsymbol{\Theta}_2\mathbf{H}$ has the same as $\mathbf{H}$ and, finally, that $\boldsymbol{\Theta}_2\mathbf{N}_t$ has the same distribution as $\mathbf{N}_t$, the proof is concluded. □

Chapter 8

Performance of Decision-Directed MIMO Systems

The work presented in this chapter is an extension to the training schemes of the previous chapter, which allows channel re-estimation when additional information in the form of detected symbols is made available. Detected data symbols are used as additional training symbols, which significantly improves the channel estimate. An improved channel estimate leads to an improvement in the receiver SNR, and, thus, a higher coding rate may successfully be applied. The material in this chapter has been published in the conference paper [BC04a], and has been submitted as a journal article in [CB05b].

8.1 Introduction

In Chapter 7, it was found that Superimposed Pilots (SIP) offer promising performance for communication over very fast fading MIMO channels and for systems equipped with many receive antennas. In other scenarios, such as slower fading and fewer receive antennas, the SIP scheme's low-quality channel estimate punished the information throughput and there was little or no gain over a conventional time-multiplexed pilot scheme. In this chapter, we extend the schemes in Chapter 7 to allow channel re-estimation when additional information in the form of detected symbols is made available. Detected data symbols are used as additional training symbols, which significantly improves the channel estimate. An improved channel estimate leads to an improvement in the receiver SNR, and, thus, a higher coding rate may successfully be applied. These variable coding rate schemes show good per-

formance. In particular, the *Decision-Directed SIP (DD-SIP)* scheme shows a performance close to the fundamental capacity of the *noncoherent* MIMO channel [MH99,HM00,ZT02], thanks to the improved channel estimates. The term *decision directed* is adopted here because of the similarity to decision directed adaptive equalizer schemes, e.g., [Qur85], where detected symbols are used in lieu of training symbols for updating the equalizer. The main objective of this work is, thus, to investigate how much the capacity will increase by allowing re-estimation of the channel when more information, i.e., detected symbols, is available. Since the SIP scheme transmits interfering low-power data superimposed to the training sequence, the SIP scheme's channel estimate is in general poor. By re-estimating the channel using detected data, the drawback of the SIP-scheme's poor channel estimate is eliminated, and the interfering low-power data instead becomes useful training power. While the SIP scheme shows a larger performance increase, the conventional time-multiplexed training scheme also shows a small performance increase by allowing channel re-estimation.

8.2 Decision-Directed MIMO Channel Modeling and Estimation

We extend the work in Chapter 7 to allow a variable coding rate within the coherence block and, hence, individual detection of the symbols on the different positions in the block as illustrated in Figure 8.1.

8.2.1 Decision-Directed MIMO Model

We will employ the same channel model that is used in Chapter 7. To recapture, the MIMO channel with M transmit and N receive antennas is modeled as a frequency-flat block-wise Rayleigh fading channel, i.e., the channel matrix $\mathbf{H} \in \mathbb{C}^{M\times N}$ contains i.i.d. $\mathcal{CN}(0,1)$ entries. The realization remains fixed for a coherence time of T symbols, after which it changes to a new independent realization. The signaling also contains a SIP block and a data block. The SIP mode is handled exactly in the same way as was done in Chapter 7, regarding both the signaling and the initial channel estimation part.

SIP mode

Assume that $T_t = M$ superimposed training symbols are collected in the diagonal matrix $\mathbf{\Sigma}$, and transmitted over the channel. The received signal

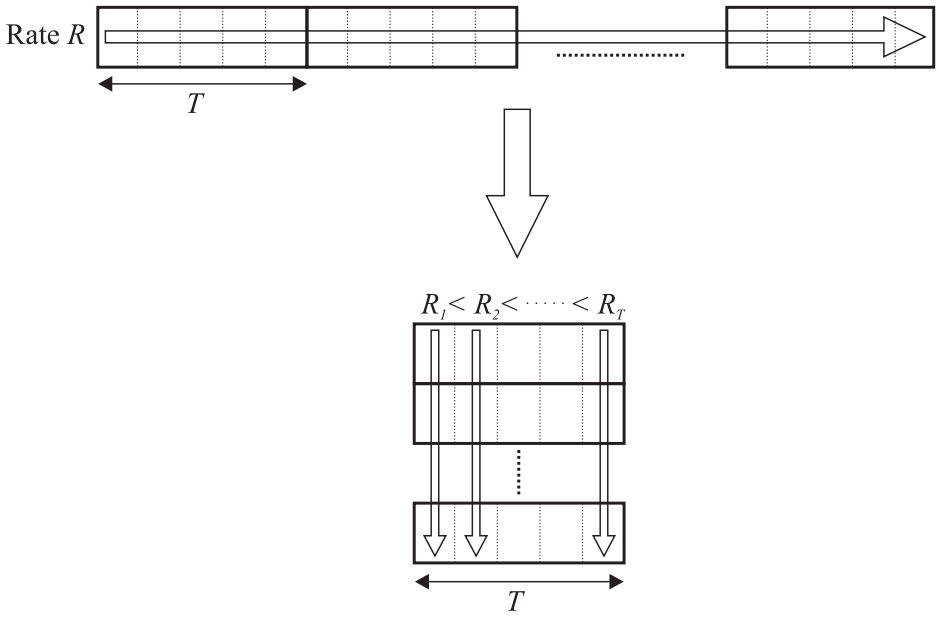

Figure 8.1: Illustration of the variable coding rate scheme. Instead of one rate over all the time slots and blocks (top), a code with one rate is used in the first time slot of each block, a code with another rate in the next, and so on (bottom).

can then be written as

$$\mathbf{X}_t = \sqrt{\frac{\sigma_t^2}{M}}\mathbf{\Sigma}\mathbf{H} + \sqrt{\frac{\sigma_{dt}^2}{M}}\mathbf{S}_{dt}\mathbf{H} + \mathbf{N}_t, \tag{8.1}$$

where $\mathbf{X}_t \in \mathbb{C}^{M\times N}$ is the received matrix, and $\mathbf{S}_{dt} \in \mathbb{C}^{M\times M}$ denotes the transmitted random data matrix. Further, $\mathbf{N}_t \in \mathbb{C}^{M\times N}$ is the additive Gaussian noise matrix, whereas σ_t^2 and σ_{dt}^2 are the average transmit powers allocated for training and data symbols in the SIP block.

The SIP block is used to acquire the initial LMMSE estimate of the channel. The channel is considered random. Thus, we use the LMMSE estimate, since it provides an estimate in closed-form that has the desired property of being uncorrelated with the estimation error. See Section 7.1 for a more detailed treatment of the SIP mode and initial channel estimation.

In Chapter 7, the initial, and quite poor, channel estimate acquired from the SIP block was used for detection of all data symbols. The main contribution in this chapter is a strategy for channel re-estimation using detected symbols. As the channel estimates gradually are improved, a higher coding rate can successfully be applied. The channel re-estimation technique is applied to the data mode and is described next.

Data mode

During the data mode the $T_d \times M$ data matrix $\mathbf{S}_d$ is transmitted. Thus, the received $T_d \times N$ signal matrix becomes

$$\mathbf{X}_d = \mathbf{\Lambda}\mathbf{S}_d\mathbf{H} + \mathbf{N}_d \tag{8.2}$$

$$\mathbf{\Lambda} = \text{ diag}\left(\sqrt{\frac{\sigma_{M+1}^2}{M}}, \cdots, \sqrt{\frac{\sigma_T^2}{M}}\right), \tag{8.3}$$

where $\mathbf{\Lambda}$ is the diagonal matrix containing the data amplitudes, $\text{Tr}\{\mathbf{R}_{\mathbf{S}_d}\} = \text{ETr}\{\mathbf{S}_d^H\mathbf{S}_d\} = MT_d$, and $\mathbf{N}_d$ is the $T_d \times N$ noise matrix with independent $\mathcal{CN}(0,1)$ entries.

Normalizations and Constraints

We normalize the transmitted signals so that we can adjust for the different power levels in the variables σ_t^2, σ_{dt}^2 and σ_d^2. Thus,

$$\text{Tr}\{\mathbf{\Sigma}^2\} = M^2 \tag{8.4}$$

$$\text{ETr}\{\mathbf{S}_{dt}\mathbf{S}_{dt}^H\} = M^2 \tag{8.5}$$

$$\text{ETr}\{\mathbf{N}_t\mathbf{N}_t^H\} = NM \tag{8.6}$$

$$\text{ETr}\{\mathbf{S}_d\mathbf{S}_d^H\} = MT_d \tag{8.7}$$

$$\text{ETr}\{\mathbf{N}_d\mathbf{N}_d^H\} = NT_d \tag{8.8}$$

$$(\sigma_t^2 + \sigma_{dt}^2)M + \sum_{i=M+1}^{T} \sigma_i^2 = \sigma^2 T, \tag{8.9}$$

where σ^2 denotes the average power spent on the whole transmitted block, and $T_d = T - M$.

8.2.2 Decision-Directed Channel Estimation

By allowing the channel to be re-estimated after each time slot, a new estimate is formed by using all detected symbols as additional pilot symbols, which improves the estimation accuracy. In this scheme the LMMSE channel estimate can, by introducing the following notation

$$\mathbf{S} = \begin{bmatrix} \sqrt{\frac{\sigma_t^2}{M}}\mathbf{S}_t + \sqrt{\frac{\sigma_{dt}^2}{M}}\mathbf{S}_{dt} \\ \mathbf{\Lambda}\mathbf{S}_d \end{bmatrix}$$

$$\mathbf{X} = \begin{bmatrix} \mathbf{X}_t \\ \mathbf{X}_d \end{bmatrix} = \mathbf{S}\mathbf{H} + \mathbf{N}, \tag{8.10}$$

after each re-estimation, be written as

$$\begin{aligned}\hat{\mathbf{H}}_i &= \mathbf{R}_{\mathbf{HX}(1:i-1)}\mathbf{R}^{-1}_{\mathbf{X}(1:i-1)}\mathbf{X}(1:i-1) \\ &= N\mathbf{S}(1:i-1)^H\mathbf{R}^{-1}_{\mathbf{X}(1:i-1)}\mathbf{X}(1:i-1), \quad i=M+1,\ldots,T, \end{aligned} \tag{8.11}$$

where $\mathbf{A}(N_1 : N_2)$ means the matrix consisting of the rows N_1 to N_2 of the matrix $\mathbf{A}$, $\mathbf{R}_{\mathbf{HX}(1:i-1)} = \mathrm{E}[\mathbf{H}\mathbf{X}^H(1:i-1)]$, and $\mathbf{R}_{\mathbf{X}(1:i-1)} = \mathrm{E}[\mathbf{X}(1:i-1)\mathbf{X}^H(1:i-1)]$. Note that the LMMSE estimate also is the MMSE estimate, since the data model is now a standard Bayesian linear model [Kay93].

Again, by using the channel estimate as the true channel, we have the following signal model for the received row vector at time i during the data-mode

$$\mathbf{X}(i) = \mathbf{S}(i)\hat{\mathbf{H}}_i + \underbrace{\mathbf{S}(i)\tilde{\mathbf{H}}_i + \mathbf{N}(i)}_{\triangleq \mathbf{n}'_i}, \quad i=M+1,\ldots,T, \tag{8.12}$$

where $\mathbf{A}(i)$ (or equivalently $\mathbf{a}_i$) denotes the i^{th} row vector of the matrix $\mathbf{A}$, and the resulting noise variance becomes

$$\sigma^2_{\mathbf{n}'_i} \triangleq \frac{1}{N}\mathrm{E}\left[\mathbf{n}'_i\mathbf{n}'^H_i\right] = \sigma^2_i\sigma^2_{\tilde{\mathbf{H}}_i} + 1, \quad i=M+1,\ldots,T. \tag{8.13}$$

Here, it is worth noting that the equivalent noise level in the channel will be different for each time instant due to the re-estimation of the channel. As the channel estimates improve when more side-information (in the form of detected symbols) is made available, the smaller the noise variance becomes. Thus, higher rate codes that still have arbitrarily low probability of error can be used. Further, the resulting noise $\mathbf{n}'_i$ will be uncorrelated (conditioned on $\mathbf{X}(1:i-1)$ and $\mathbf{S}(1:i-1)$) with the signal $\mathbf{s}_i$ for $i=M+1,\ldots,T$, since

$$\begin{aligned}&\mathrm{E}[\mathbf{s}_i^H\mathbf{n}'_i \,|\, \mathbf{X}(1:i-1), \mathbf{S}(1:i-1)] \\ &\qquad = \mathrm{E}[\mathbf{s}_i^H(\mathbf{s}_i\tilde{\mathbf{H}}_i + \mathbf{n}_i) \,|\, \mathbf{X}(1:i-1), \mathbf{S}(1:i-1)] \\ &\qquad = \mathrm{E}[\mathbf{s}_i^H\mathbf{s}_i\tilde{\mathbf{H}}_i \,|\, \mathbf{X}(1:i-1), \mathbf{S}(1:i-1)] \\ &\qquad\quad + \underbrace{\mathrm{E}[\mathbf{s}_i^H\mathbf{n}_i \,|\, \mathbf{X}(1:i-1), \mathbf{S}(1:i-1)]}_{=0} \\ &\qquad = \mathrm{E}[\mathbf{s}_i^H\mathbf{s}_i \,|\, \mathbf{X}(1:i-1), \mathbf{S}(1:i-1)] \\ &\qquad\quad \times \mathrm{E}[\tilde{\mathbf{H}}_i \,|\, \mathbf{X}(1:i-1), \mathbf{S}(1:i-1)] \\ &\qquad = \mathbf{0}_{M\times N},\end{aligned}$$

where the channel estimate is the MMSE estimate and, thus,

$$\mathrm{E}[\tilde{\mathbf{H}}_i \,|\, \mathbf{X}(1:i-1), \mathbf{S}(1:i-1)] = \mathbf{0}_{M\times N}.$$

It is well known that the worst case noise is achieved by replacing $\mathbf{n}'_i$ by i.i.d. zero-mean complex Gaussian noise with the same variance $\sigma^2_{\mathbf{n}'_i}$ [HH03]. Hence, the capacity is lower-bounded by assuming Gaussian noise.

Remark: Note that the LMMSE estimate in Chapter 7 was not the MMSE estimate which made the resulting noise correlated with the signal. Hence, in Chapter 7, an approximation of the bound was used, while the bound attained here is, thanks to the channel re-estimation, no longer an approximation.

8.3 Mutual Information and Capacity Bounds

To get a more intuitive picture of the idea, one can think of each row vector in the transmitted data matrix as a separate channel and then consider a number of parallel such channels. If we now want to design a decision-directed system we can use different codebooks, i.e., rates for the different channels. For the first symbols, where the channel estimate is poor we use a lower rate to ensure error free communication. After the first symbols are detected, we can use the received codeword (which we know is correct according to the channel coding theorem) as known information when estimating the channel for the next position, and so on.

In order to put this into a more stringent mathematical framework, we will rely on a decomposition of the MI. The following derivation is based on the MI chain-rule [CT91], and is identical to the one presented in [MS01]. It is included here because of its importance in the derivations and for completeness.

The total MI between the transmitted signal and the received signal is given by

$$
\begin{aligned}
I(\mathbf{X};\mathbf{S}) &= I\big(\mathbf{X};\mathbf{S}(1),\mathbf{S}(2:T)\big) && (8.14)\\
&= I\big(\mathbf{X};\mathbf{S}(1)\big) + I\big(\mathbf{X};\mathbf{S}(2:T)\,|\,\mathbf{S}(1)\big) && (8.15)\\
&= I\big(\mathbf{X};\mathbf{S}(1)\big) + I\big(\mathbf{X}(1),\mathbf{X}(2:T);\mathbf{S}(2:T)\,|\,\mathbf{S}(1)\big) && (8.16)\\
&= I\big(\mathbf{X};\mathbf{S}(1)\big) + \underbrace{I\big(\mathbf{X}(1);\mathbf{S}(2:T)\,|\,\mathbf{S}(1)\big)}_{=0} \\
&\quad + I\big(\mathbf{X}(2:T);\mathbf{S}(2:T)\,|\,\mathbf{X}(1),\mathbf{S}(1)\big), && (8.17)
\end{aligned}
$$

where $\mathbf{X}$ and $\mathbf{S}$ are the output and input matrices, respectively. The total number of symbols per block is T, and $I\big(\mathbf{X}(1);\mathbf{S}(2:T)\,|\,\mathbf{S}(1)\big) = 0$ since $\mathbf{X}(1)$ is independent of $\mathbf{S}(2:T)$ conditioned on $\mathbf{S}(1)$.

By iterating the steps (8.14)-(8.17) for $i = 2, \ldots, T$, we find the following result

$$I(\mathbf{X};\mathbf{S}) = \sum_{i=1}^{T} I\big(\mathbf{X};\mathbf{S}(i)\,|\,\mathbf{X}(1:i-1),\mathbf{S}(1:i-1)\big) \tag{8.18}$$

$$= \sum_{i=1}^{T} I\big(\mathbf{X}(i);\mathbf{S}(i)\,|\,\mathbf{X}(1:i-1),\mathbf{S}(1:i-1)\big) + \sum_{i=1}^{T-1} I\big(\mathbf{X}(i+1:T);\mathbf{S}(i)\,|\,\mathbf{X}(1:i),\mathbf{S}(1:i-1)\big), \tag{8.19}$$

where (8.19) follows from applying the chain-rule to (8.18). Hence, the total MI over the whole block is decomposed into two parts. One part which is the MI between the input and output at a specific time instant, conditioned on all the previously transmitted symbols, received data and pilot symbols. The second part is the blind MI between the present input and all future outputs conditioned on the same variables as above plus the received signal at the specific time instant.

We are only considering systems based on channel estimates from known symbols that use these estimates as if they were true. The second term in (8.19) is therefore ignored, and the first term can be lower bounded by the data processing inequality by conditioning on $\hat{\mathbf{H}}_i = f\big(\mathbf{X}(1:i-1),\mathbf{S}(1:i-1)\big)$, see Chapter 7. Thus, the channel estimate based on all previous inputs and output pairs, including the pilots, is used as the true channel.

Here, one can also notice that the MI for the *data block*, I_{DD}, in the decision-directed schemes (DD-SIP, DD-CP) can be lower bounded as

$$I_{\mathrm{DD}} = \sum_{i=M+1}^{T} I(\mathbf{x}_i;\mathbf{s}_i\,|\,\hat{\mathbf{H}}_i) \tag{8.20}$$

$$\geq T_d\, I(\mathbf{x}_i;\mathbf{s}_i\,|\,\hat{\mathbf{H}}_0) = I_{\mathrm{T}}, \quad i = M+1,\ldots,T, \tag{8.21}$$

where $\hat{\mathbf{H}}_0$ is the initial channel estimate that is based only on the pilot symbols in the SIP block, and I_{T} is the MI that is achieved by schemes that, given the same power constraints, do not employ channel re-estimation, such as the SIP and CP schemes that were described and analyzed in Chapter 7.

However in this work, we continue with the capacity lower bound for the decision-directed schemes, which is given by the maximum of the MI bounds

$$C_{\mathrm{DD}} = \max \frac{1}{T}\left\{ I(\mathbf{X}_t;\mathbf{S}_{dt}\mid\hat{\mathbf{H}}_0) + \sum_{i=M+1}^{T} I(\mathbf{x}_i;\mathbf{s}_i\mid\hat{\mathbf{H}}_i)\right\}, \tag{8.22}$$

where $I(\mathbf{X}_t; \mathbf{S}_{dt} \mid \hat{\mathbf{H}}_0)$ is the MI lower bound in the SIP block, and the second term is the MI lower bound in the data block. This bound is maximized with respect to the input signal distributions under the power constraints.

Since we only take into account how the data power influences the channel estimate, the maximum of each term in (8.22) is achieved when the distribution of the transmitted data is i.i.d. complex Gaussian. That is, both $\mathbf{R}_{\mathbf{S}_{dt}} = \mathrm{E}[\mathbf{S}_{dt}^H \mathbf{S}_{dt}]$ and $\mathbf{R}_{\mathbf{S}_d} = \mathrm{E}[\mathbf{S}_d^H \mathbf{S}_d]$ should be multiples of the identity matrix. Together with the Gaussian noise assumption, these input signals will give the following capacity lower bound

$$C_{\mathrm{DD}} \geq \frac{M}{T}\mathrm{E}\left[\log_2 \det\left(\mathbf{I}_M + \frac{\rho_t}{M}\bar{\mathbf{H}}_0\bar{\mathbf{H}}_0^H\right)\right] + \frac{1}{T}\sum_{i=M+1}^{T}\mathrm{E}\left[\log_2 \det\left(\mathbf{I}_M + \frac{\rho_i}{M}\bar{\mathbf{H}}_i\bar{\mathbf{H}}_i^H\right)\right] \quad \text{bits/channel use.} \tag{8.23}$$

The elements of the normalized channel $\bar{\mathbf{H}}_i \triangleq \frac{\hat{\mathbf{H}}_i}{\sigma_{\hat{\mathbf{H}}_i}}$ will be uncorrelated with zero mean and unit variance and have a distribution that is Gaussian (approximately for $\bar{\mathbf{H}}_0$). The normalization constant $\sigma_{\hat{\mathbf{H}}_i}$ is given by $\sigma^2_{\hat{\mathbf{H}}_i} \triangleq \frac{1}{MN}\mathrm{E}\mathrm{Tr}\{\hat{\mathbf{H}}_i\hat{\mathbf{H}}_i^H\}$ where $\hat{\mathbf{H}}_i$ is given by (8.11). The criterion function (8.23) is also to be concentrated with respect to the training sequence, $\mathbf{\Sigma}$. As was shown in Chapter 7, the optimal training sequence is to choose $\mathbf{\Sigma}$ as a multiple of the identity matrix, i.e., $\mathbf{\Sigma} = \sqrt{M}\mathbf{I}_M$, since this maximizes the effective SNR. Hence, the effective SNR, ρ_t, during the SIP mode evaluates to (see Chapter 7)

$$\rho_t = \frac{\sigma_t^2\sigma_{dt}^2 M T_t(\sigma_t^2 T_t + \sigma_{dt}^2 M + M)}{\sigma_t^4\sigma_{dt}^2 M T_t^2 + (\sigma_{dt}^2+1)^3 M^3 + (\sigma_{dt}^2+1)\sigma_t^2 T_t M^2 + \sigma_t^2\sigma_{dt}^4 T_t}, \tag{8.24}$$

and, at each time instant i, the effective SNR ρ_i in the data block can be shown to be

$$\begin{aligned}\rho_i &= \frac{\sigma_i^2\sigma^2_{\hat{\mathbf{H}}_i}}{\sigma^2_{\mathbf{n}'_i}} = \frac{\sigma_i^2\sigma^2_{\hat{\mathbf{H}}_i}}{\sigma_i^2\sigma^2_{\tilde{\mathbf{H}}_i}+1} \\ &= \frac{\sigma_i^2((\sigma_t^2+\sigma_{dt}^2)T_t + \sum_{k=M+1}^{i-1}\sigma_k^2)}{(\sigma_i^2+1)M + (\sigma_t^2+\sigma_{dt}^2)T_t + \sum_{k=M+1}^{i-1}\sigma_k^2}, \quad i = M+1,\ldots,T.\end{aligned} \tag{8.25}$$

It is worth comparing the expression (8.25) attained for the decision-directed scheme to its equivalent effective SNR attained for the non-decision-directed scheme, which was given in Chapter 7 as

$$\rho_d = \frac{\sigma_d^2\sigma_t^2 T_t}{(\sigma_d^2+1)(\sigma_{dt}^2+1)M + \sigma_t^2 T_t}. \tag{8.26}$$

Their relation is evident when one interprets the power of the detected data at time i; σ_{dt}^2, $\{\sigma_k^2\}_{k=M+1}^{i-1}$, together with the power of the training sequence σ_t^2, as pure training power, which corresponds to σ_t^2 in (8.26). Also note that σ_{dt}^2 in (8.25) is no longer interfering "noise" power, but useful training power.

To maximize the capacity, (8.23) has to be optimized with respect to the following parameters: $\sigma_t^2, \sigma_{dt}^2, \{\sigma_i^2\}_{i=M+1}^{T}$ and M, subject to the energy constraint given by (8.9). As was discussed in the previous chapter, it might seem counter-intuitive to optimize over the number of transmit antennas. Again, however, the problem is that we need to sacrifice degrees of freedom in the data-mode in order to estimate all the new channel parameters. Also, for the noncoherent channel at high SNR, it is shown in [ZT02] that the optimal number of transmit antennas is given by $M = \min\{N, T/2\}$, where N is the number of receive antennas and T is the coherence time.

The channel estimate will of course improve when more known symbols are available, which will lead to higher effective SNR for symbols later in the block. By interpreting the data block as T_d parallel channels, each with different effective SNR, the task is now to distribute the power in an optimal way. Here, one can not simply rely on the classical water-filling arguments for parallel channels, since the effective SNR will depend on how the power is distributed. This means that there will be a tradeoff, since having much power in the beginning of the block will lead to better channel estimates faster. But on the other hand, we are then using more data power when the channel quality is poor. In the other extreme, more power is allocated to the later time slots, which then have better channels, but the channel estimates will only improve slowly and hence more channels with lower SNR will be present. Extensive numerical calculations of the achievable rates have shown that when DD-SIP is used, the optimal power distribution over the data symbols is almost constant over the whole data-block, and for DD-CP only a little bit more power should be allocated for the first few symbols in the data-block. Hence, it is concluded that the DD-systems are relatively insensitive to this power distribution $\{\sigma_i^2,\, i = M+1, \ldots, T\}$, which means that there is little loss in setting $\sigma_i^2 = \sigma_d^2, \forall\, i = M+1, \ldots, T$. However, what is important is how the power is distributed between σ_t^2, σ_{dt}^2, and σ_d^2. The optimization over the remaining parameters is done numerically, and is discussed in the next section.

Using this re-estimation technique on a SIP-based system will lead to a better performance increase than using it on a CP-system, since the data term in the SIP-mode, that increases the noise level during the estimation phase, can now be utilized as additional training power in the next re-estimation of the channel. By this, the extra symbols that are transmitted during the SIP-mode will not degrade the channel estimate during the data-mode.

8.3.1 High SNR Approximation of the Noncoherent MIMO Capacity

To compare the bounds calculated above to the capacity of the noncoherent MIMO channel, we will use the following theorem.

Theorem 11 *From [ZT02]. For the multiple antenna channel with M transmit, N receive antennas ($M > N$) and coherence time $T \geq 2N$, the high SNR capacity is given by*

$$C_{M,N}(\mathrm{SNR}) = C_{N,N}(\mathrm{SNR}) + o(1) \tag{8.27}$$

where $C_{N,N}$ is the capacity for N receive and N transmit antennas, and is given by

$$\begin{aligned} C_{N,N}(\mathrm{SNR}) = N\left(1-\frac{N}{T}\right)\log_2 \mathrm{SNR} + N\left(1-\frac{N}{T}\right)\log_2\frac{T}{N\pi e} \\ + \left(1-\frac{N}{T}\right)\sum_{i=1}^{N}\mathrm{E}[\log_2\chi^2_{2i}] + \frac{1}{T}\log_2\frac{\prod_{i=T-N+1}^{T}\frac{2\pi^i}{(i-1)!}}{\prod_{i=1}^{N}\frac{2\pi^i}{(1-i)!}}, \end{aligned} \tag{8.28}$$

where χ^2_{2i} denotes a Chi-square random variable of dimension $2i$, and $o(1)$ is a term that goes to zero at high SNR. This capacity can be achieved by using N transmit antennas.

Proof: See [ZT02]. □

8.4 Numerical Examples

In this section we will, for a number of different scenarios, evaluate the capacity and find optimal values of the parameters for the systems described above. Since it has been found that the capacity is relatively insensitive to the power levels during the data-mode, we have kept these parameters constant, i.e., $\sigma_i^2 = \sigma_d^2,\ \forall\, i = M+1,\ldots,T$, to decrease the number of optimization parameters. In all scenarios, we have evaluated a system with $N = 4$ receive antennas and with different numbers of transmit antennas as well as different SNRs. The SNR is defined as the mean power over a coherence block divided by the noise power, i.e., $\mathrm{SNR} = \sigma^2$, since the noise power is normalized to unity. In all the plots we will compare the CP and SIP based systems, with and without the re-estimation steps. Figure 8.2 shows the capacity bounds versus number of transmit antennas, and it is obvious that there is an optimal number of transmit antennas. It is worth noting that the maximum capacity in this scenario is achieved for $M = 5$ transmit antennas for the

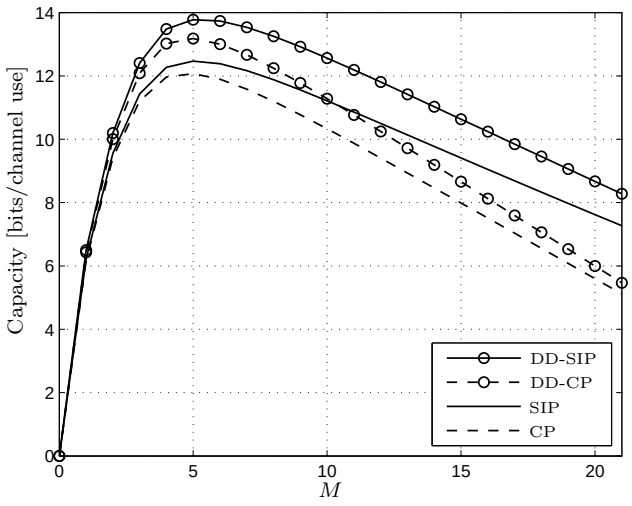

Figure 8.2: Capacity vs. number of transmit antennas M, $T = 31$, $N = 4$, SNR $\sigma^2 = 15$ dB.

analyzed schemes. Theorem 11 tells us that for the noncoherent channel, the optimal number is given by N since $T > 2N$, which in this scenario implies $M = N = 4$. In scenarios with lower SNR and/or shorter coherence length, the optimal number will decrease and for very low SNR and/or small T, it is optimal with a single transmit antenna.

Figure 8.3 compares the capacity lower bounds versus SNR, and we can conclude from the figure that all the analyzed schemes exploit all the available degrees of freedom. The latter can be thought of as the slope of the capacity curve in the high SNR region, [ZT02]. It is also found that the DD-SIP curve is close to the capacity of the noncoherent channel. One should keep in mind here, that the formula for the noncoherent capacity is a high SNR approximation. Hence, it should not be considered reliable in the low SNR regions, which is why the analyzed suboptimal schemes are above the bound at low SNR.

In Figure 8.4, the capacity bounds are plotted against the channel coherence time. It can be seen from the figure that the capacity of the conventional schemes do not fully reach their respective SIP-based equivalents when the coherence time is below 30 symbols. They will of course merge and the difference should go to zero as M/T tends to zero. In this plot the optimal number of transmit antennas is used, ranging from $M = 1$ for $T = 1$ up to $M = 5$ when $T = 30$.

Depending on the coherence length of the channel, the optimal alloca-

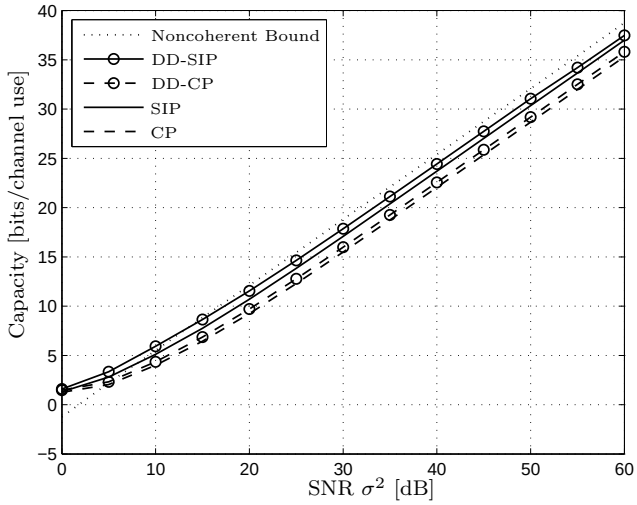

Figure 8.3: Capacity vs. SNR σ^2, $T = 8$, and $M = N = 4$. The dotted line represents the asymptotic (for high SNR) capacity bound for the noncoherent channel [ZT02].

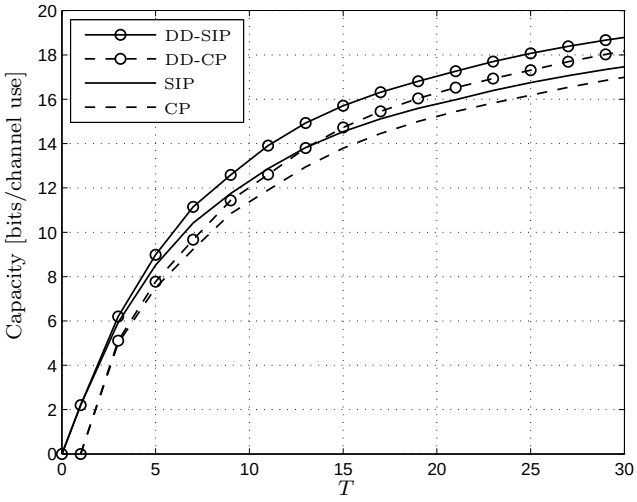

Figure 8.4: Capacity vs. coherence time T, $N = 4$, SNR $\sigma^2 = 20$ dB.

tion of the powers will vary. In Figure 8.5, the different power levels are plotted against the coherence time of the channel. It is observed that the DD-systems are relatively insensitive to the power distribution, i.e., a wide range of parameter values satisfying the constraints give almost the same

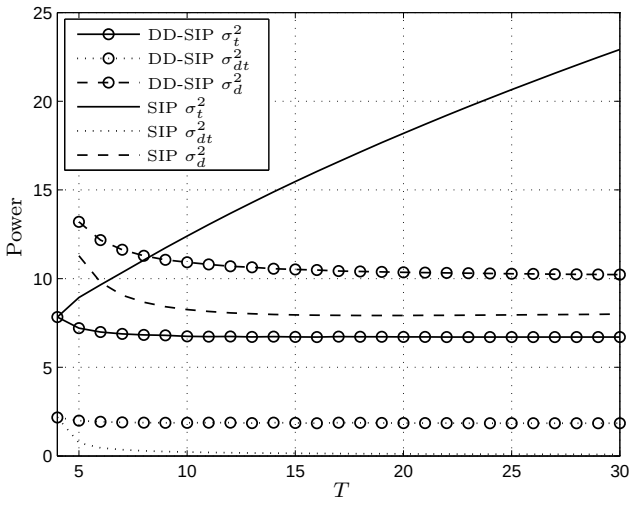

Figure 8.5: Optimal power allocation vs. coherence time T, $M = N = 4$, and SNR $\sigma^2 = 10$ dB.

capacity. In fact, the major difference between the SIP and DD-SIP schemes is that the power levels are almost constant for DD-SIP. On the contrary, especially the pilot power increases quickly with increasing block lengths for the SIP scheme. Also, the data power during the SIP-mode tends quickly to zero for the SIP scheme, which means that the optimal SIP scheme quickly degenerates to a CP scheme for increasing coherence time. This observation was also made in the previous chapter.

Chapter 9

Performance of Training-Aided SISO Systems

In this chapter, we apply the same problem formulation as in the previous two chapters to a frequency-selective block-wise fading Single-Input Single-Output (SISO) channel. The work presented in this chapter has previously been published in the conference paper [CB04].

9.1 Training Based FIR Models

In all the other chapters in the second part of the thesis we have only considered frequency flat channels. Although incorporating some of the fading aspects, this model is not always applicable for some channels especially in the case of more wideband channels. When the bandwidth of the transmitted signal becomes larger than the coherence bandwidth of the channel, the multipath propagation will lead to *Inter-Symbol Interference (ISI)* [Pro01]. Combating ISI is a very well studied problem in the communication literature. To determine the transmitted data at the receiver, the receiver needs to equalize the impact of the unknown frequency-selective channel, and to do so an estimate of the channel is often used. Discussions regarding frequency-selective fading can be found in most textbooks, see, e.g., [Pro01], and for a thorough review of the information theoretic aspects, see [BPS98].

In this chapter, we will see how the introduction of superimposed pilots will effect the capacity of this type of channel. A similar analysis was done for conventional training in [VHHK04].

9.2 Data Modeling

Several versions of the same data models are used and their structure depends on what we are trying to achieve (channel estimation or data detection). For example, the channel parameters are the unknowns during channel estimation, and the data symbols are the unknowns during data detection. We start with describing the SIP model and the channel model that we employ.

9.2.1 SIP Model

A short description of the SIP-based system is that it operates in two modes when transmitting a block consisting of T symbols. The first mode is the *training mode* which is followed by the *data mode*. The received signal during the training mode is

$$\mathbf{x}_t = \mathbf{H}_t \left(\sigma_t \mathbf{s}_t + \sigma_d \mathbf{s}_{dt}\right) + \mathbf{n}_t, \tag{9.1}$$

where $\mathbf{H}_t \in \mathbb{C}^{T_t \times T_t}$ is the convolution matrix for a channel with a *Finite Impulse Response (FIR)* of length L

$$\mathbf{H}_t = \begin{bmatrix} h_1 & & & & & \\ \vdots & h_1 & & & & \\ h_L & \vdots & \ddots & & & \\ & h_L & & h_1 & & \\ & & \ddots & \vdots & \ddots & \\ & & & h_L & \cdots & h_1 \end{bmatrix}, \tag{9.2}$$

and $\{\sigma_t^2,\ \sigma_d^2\}$ denote the power allocated for training and data symbols, respectively. Observe that in this setting, we have a constant data power over the whole block. The T_t-long normalized sequences of training and data symbols are contained in the vectors $\mathbf{s}_t \in \mathbb{C}^{T_t \times 1}$ and $\mathbf{s}_{dt} \in \mathbb{C}^{T_t \times 1}$. Finally, the additive noise $\mathbf{n}_t \in \mathbb{C}^{T_t \times 1}$ is modeled as complex white Gaussian noise.

The channel is modeled as a frequency-selective block-wise fading channel. Hence, the channel is fixed during the transmission of one block and then it attains a new independent realization for the next block, and so on. The time (block size) over which the channel is fixed is commonly referred to as the *channel coherence time*. This type of channel model is a discrete approximation of a time-varying continuous channel and occurs in, e.g., TDMA in the GSM standard or frequency-hopping systems, where the user attains a new independent channel realization for each channel use.

During the data mode, the received signal is

$$\mathbf{x}_d = \sigma_d \mathbf{H}_d \mathbf{s}_d + \sigma_t \mathbf{H}'_t \mathbf{s}_t + \sigma_d \mathbf{H}'_t \mathbf{s}_{dt} + \mathbf{n}_d \tag{9.3}$$

where σ_d^2 again denotes the data power of the normalized data vector $\mathbf{s}_d \in \mathbb{C}^{T_d \times 1}$, $\mathbf{H}_d \in \mathbb{C}^{T_d+L-1 \times T_d}$ is the convolutional channel matrix (the receiver collects data until the channel is "emptied", which also provides a guard interval between successive channel realizations)

$$\mathbf{H}_d = \begin{bmatrix} h_1 & & & & \\ \vdots & h_1 & & & \\ h_L & \vdots & \ddots & & \\ & h_L & & \ddots & \\ & & \ddots & & h_1 \\ & & & \ddots & \vdots \\ & & & & h_L \end{bmatrix}, \tag{9.4}$$

$\mathbf{H}'_t \in \mathbb{C}^{T_d+L-1 \times T_t}$ represents the tail "leaking in" from the training mode (since there is no guard interval between the training and data blocks)

$$\mathbf{H}'_t = \begin{bmatrix} h_L & h_{L-1} & \cdots & h_2 \\ & h_L & \cdots & h_3 \\ & & \ddots & \vdots \\ & & & h_L \\ & & & \\ & & & \end{bmatrix}, \tag{9.5}$$

and $\mathbf{n}_d \in \mathbb{C}^{T_d+L-1 \times 1}$ is additive complex white Gaussian noise. The transmitted signal vectors are normalized such that $\mathbf{s}_t^H \mathbf{s}_t = T_t$, $\mathrm{E}[\mathbf{s}_{dt}^H \mathbf{s}_{dt}] = T_t$ and $\mathrm{E}[\mathbf{s}_d^H \mathbf{s}_d] = T_d$.

9.2.2 Channel Estimation

With knowledge of the transmitted pilot sequence, the receiver regards the unknown data term $\sigma_d \mathbf{H}_t \mathbf{s}_{dt}$ in (9.1) as additional noise and forms the Linear Minimum Mean Square Error (LMMSE) estimate of the channel. The LMMSE channel estimate is given by [Kay93]

$$\hat{\mathbf{h}} = \sigma_t \left[\mathbf{R}_{\mathbf{h}}^{-1} + \sigma_t^2 \mathbf{S}_t^H \mathbf{R}_{\mathbf{n}'_t}^{-1} \mathbf{S}_t \right]^{-1} \mathbf{S}_t^H \mathbf{R}_{\mathbf{n}'_t}^{-1} \mathbf{x}_t, \tag{9.6}$$

where $\hat{\mathbf{h}} = [\hat{h}_1, \ldots, \hat{h}_L]^T \in \mathbb{C}^{L\times 1}$ is the vector containing the estimated channel parameters, $\mathbf{S}_t \in \mathbb{C}^{T_t \times L}$ is the convolutional training matrix, and $\mathbf{n}'_t = \sigma_d \mathbf{H}_t \mathbf{s}_{dt} + \mathbf{n}_t \in \mathbb{C}^{T_t \times 1}$ is the effective noise term during channel estimation with covariance matrix $\mathbf{R}_{\mathbf{n}'_t} = \mathrm{E}[\mathbf{n}'_t \mathbf{n}'^H_t]$. Here and in the remainder of this chapter, it is assumed that $\mathbf{h} \sim \mathcal{CN}(0, \mathbf{R}_\mathbf{h})$, where $\mathbf{R}_\mathbf{h} = \mathrm{E}[\mathbf{h}\mathbf{h}^H] = \mathbf{I}_L$, i.e., the channel taps are uncorrelated complex Gaussian random variables.

In the SIP setting, the training sequence is simply realized by an impulse that satisfies the power constraint and is transmitted in the first time slot. The channel response to the impulse is present at the output during the first $T_t = L$ (the number of channel taps) symbols. Hence, let $\mathbf{S}_t = \sqrt{T_t}\mathbf{I}_{T_t}$, where $T_t = L$, which is also the smallest value of T_t to ensure identifiability. While this choice of training sequence is the optimal choice for the conventional scheme studied in [VHHK04], the SIP scheme studied in this chapter uses an impulse as a predefined design choice [ZVM03]. In [ZVM03] the impulse was inserted periodically. But from a channel estimation point of view, a single impulse might as well be inserted in the first time slot $n = 1$. This has two major advantages: (1) The interfering noise (during channel estimation), which consists of unknown data symbols, is increasing with time in its interfering noise power. Since the channel output at the first time instant, $n = 1$, contains only one interfering data symbol, and at the second time instant, $n = 2$, it contains two interfering data symbols, and so on. It is easily verified that at time $n = L$, the output contains the maximum noise power $L\sigma_d^2\sigma_h^2 + 1$. (2) Inserting the pilot periodically requires the channel to remain static over a longer period of time.

One motivation in using an impulse which also is intuitively appealing, is that it is desired to make the training sequence as short as possible not only to leave a lot of time for information transmission, but also since it does not interfere too much with the data when the training sequence later is removed for data detection. Of course, for various practical reasons it might not always be desired to transmit an instantaneous power peak, and even if it is suboptimal in the Mutual Information (MI) sense, other training sequences might be preferable.

For a more detailed description, SIP or pilot embedding for Single-Input Single-Output (SISO) FIR channel estimation has been discussed in, e.g., [ZVM03, FB95].

9.2.3 Data Detection

The received signal can be treated as a single block of data. After the channel has been estimated and the training sequence has been removed, we will have

$$\begin{aligned}\mathbf{x}' &= \mathbf{x} - \sigma_t\hat{\mathbf{H}}\mathbf{s}_t \\ &= \sigma_d\mathbf{H}\mathbf{s} + \sigma_t\tilde{\mathbf{H}}\mathbf{s}_t + \mathbf{n} \\ &= \sigma_d\hat{\mathbf{H}}\mathbf{s} + \sigma_d\tilde{\mathbf{H}}\mathbf{s} + \sigma_t\tilde{\mathbf{H}}\mathbf{s}_t + \mathbf{n} \\ &= \sigma_d\hat{\mathbf{H}}\mathbf{s} + \mathbf{n}', \end{aligned} \tag{9.7}$$

where all the received data is stacked into a single vector, i.e., $\mathbf{x} = [\mathbf{x}_t;\, \mathbf{x}_d] \in \mathbb{C}^{T+L-1\times 1}$, $\mathbf{s} = [\mathbf{s}_{dt};\, \mathbf{s}_d] \in \mathbb{C}^{T\times 1}$, $\mathbf{n} = [\mathbf{n}_t;\, \mathbf{n}_d] \in \mathbb{C}^{T+L-1\times 1}$, $\mathbf{s}_t = [\sqrt{T_t},\, 0,\, \ldots,\, 0]^T \in \mathbb{R}^{T\times 1}$, and $\hat{\mathbf{H}} \in \mathbb{C}^{T+L-1\times T}$ is the channel matrix estimate

$$\hat{\mathbf{H}} = \begin{bmatrix} \hat{h}_1 & & & & \\ \vdots & \hat{h}_1 & & & \\ \hat{h}_L & \vdots & \ddots & & \\ & \hat{h}_L & & \ddots & \\ & & \ddots & & \hat{h}_1 \\ & & & \ddots & \vdots \\ & & & & \hat{h}_L \end{bmatrix}. \tag{9.8}$$

Further, $\tilde{\mathbf{H}} = \mathbf{H} - \hat{\mathbf{H}}$ denotes the channel estimation error, and $\mathbf{n}' = \sigma_d\tilde{\mathbf{H}}\mathbf{s} + \sigma_t\tilde{\mathbf{H}}\mathbf{s}_t + \mathbf{n}$ denotes the effective noise. As for any training-based scheme, the effective noise term will always depend on the data. In general for training-based schemes, this dependence is always neglected when the channel estimates are assumed to be correct.

9.3 Mutual Information

In order to compare the different schemes, we will maximize a parameterized version of the MI of the two systems under study. Since the systems are modeled using discrete time memoryless channels, the capacity can be found as the maximum of the MI. The results for the conventional training-based scheme can be found in [VHHK04].

We will bound the mutual information of the SIP-based system by assuming that the channel estimate is correct, i.e, starting from (9.7) we can write the MI as $I(\mathbf{x}';\mathbf{s}|\hat{\mathbf{H}})$. We note that the noise $\mathbf{n}'$ in (9.7) is approximately

Gaussian and depends on the signal due to the conditioning on the channel estimate. But to make the analysis tractable we ignore this dependence and only take the effects of the power into account, and substitute the noise with a Gaussian distributed noise term that is uncorrelated with the signal but has the same covariance as $\mathbf{n}'$. Under these assumptions it is well known that the input signal that maximizes the MI is a Gaussian distributed signal, and since the transmitter has no knowledge about the channel we will use a white process, i.e., $\mathbf{R}_{\mathbf{s}} = \mathrm{E}[\mathbf{s}\mathbf{s}^H] = \mathbf{I}_T$. The optimality regarding this choice has been discussed in, e.g., [HH03]. From this, and the arguments used in the previous chapters, the maximum of the MI can be lower-bounded as

$$I_{\max} \geq \max_{\sigma_t^2, \sigma_d^2} \mathrm{E}\left[\log_2 \det\left(\mathbf{I}_{T+L-1} + \sigma_d^2 \mathbf{R}_{\mathbf{n}'}^{-1} \hat{\mathbf{H}} \hat{\mathbf{H}}^H\right)\right], \tag{9.9}$$

where the expectation is over the distribution of $\hat{\mathbf{H}}$. The MI is indirectly parameterized by the powers σ_t^2 and σ_d^2, over which a numerical optimization is performed to find the maximum of the MI subject to the energy constraint $\sigma_t^2 T_t + \sigma_d^2 T = \sigma^2 T$ (where $T_t = L$). When comparing the SIP scheme to the conventional training-based one, one should note that in the SIP scheme the effect of the correlation between the signal and the noise is ignored. This approximation is not necessary in the derivation of the conventional training scheme since the LMMSE and MMSE will coincide and make the signal and effective noise uncorrelated.

9.4 Numerical Examples

To compare the performances, the optimal values (for each scheme) of the power parameters $\{\sigma_t^2, \sigma_d^2\}$ are found by using numerical optimization of the MI (9.9) subject to $\sigma_t^2 T_t + \sigma_d^2 T = \sigma^2 T$ (where $T_t = L$). The inverse covariance matrix of the effective noise $\mathbf{R}_{\mathbf{n}'}^{-1}$ is evaluated empirically[1]. After attaining the optimal powers, each system is operating in an optimal way, thus allowing a fair comparison of their performances.

In this example, the available transmit power is $\sigma^2 = 8$ dB, and the number of channel taps to be estimated is $L = 4$. The figures display the capacity versus coherence time, capacity versus SNR, and the optimal power allocation versus coherence time. The capacity bound is here defined as the lower bound of the maximum MI (9.9) scaled by $1/(T + L - 1)$, the total time (including the guard interval) it takes to transmit a single block over the channel.

[1]We evaluate it empirically and do not apply an analytic bound as is done for the conventional case in [VHHK04].

From Figure 9.1, one can see that when a larger part of the channel coherence time has to be spent on training (T small), it is advantageous to use the SIP scheme. This is due to that the SIP scheme allows for data transmission over the whole block, while the conventional scheme has little time left over for data transmission. We find that the conventional scheme quickly outperforms the SIP scheme for increasing coherence times, which is an effect of the SIP scheme's poor channel estimate. This result differs from the previous chapters since the SIP scheme is in this chapter not allowed to vary the data power in the training block, so the data power is kept constant over the whole block. This choice is made to decrease the number of parameters used in the numerical optimization, since the capacity lower bound is computed empirically for each parameter combination. If the data power in the training block would be allowed to vary, the curves would coincide as they did in the previous chapters.

When increasing the SNR as shown in Figure 9.2, we find that the conventional scheme attains a superior channel estimate, while the SIP scheme is self-interfering due to the unknown "noisy" data.

Figure 9.3 displays the optimal power allocation, and we see that the SIP scheme has to allocate a lot more power for training than for data. The reason why the optimal data power is low is that it is interfering during channel estimation, and this is why it has a lower information throughput compared to the conventional scheme, which can allocate more power to data without a large penalty in effective SNR.

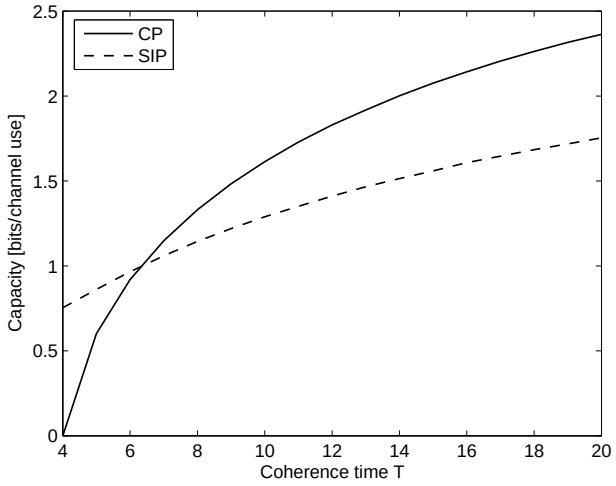

Figure 9.1: Capacity vs. channel coherence time T for $L = 4$ and $\sigma^2 = 8$ dB.

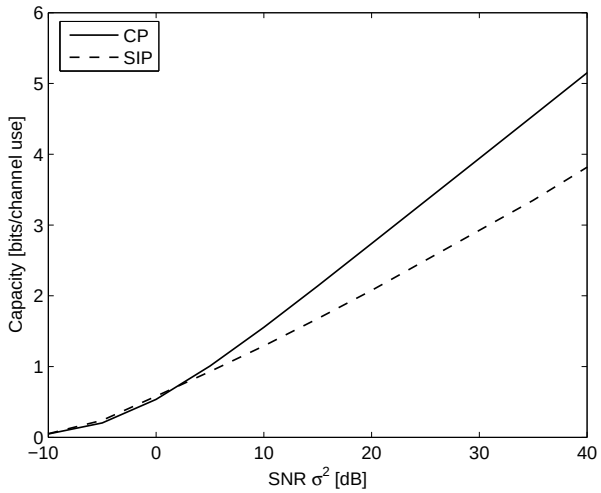

Figure 9.2: Capacity vs. SNR for $L = 4$ and $T = 8$.

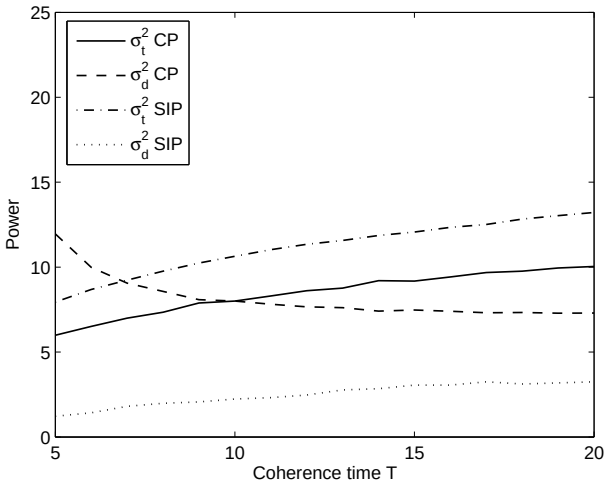

Figure 9.3: Optimal power allocation vs. channel coherence time T for $L = 4$ and $\sigma^2 = 8$ dB.

Chapter 10

Conclusions

This chapter concludes the second part of the thesis, and provides a discussion of the findings, followed by suggestions for future work.

10.1 Discussion and Conclusions

The main aim of this work was to find answers to if and when it is beneficial to use superimposed pilots (SIP) over conventional time-multiplexed pilots. We looked at the case when transmission of known pilot sequences was used to estimate a frequency-flat, block-wise Rayleigh fading MIMO channel. When using the maximum reliable information rate as a performance measure, it was found that SIP showed promising performance for fast-fading channels and for many receive antennas. In other cases, the SIP scheme's low-quality channel estimate punished the information transmission and there was little or no gain over the conventional pilot scheme (a variable rate scheme that eliminates the poor channel estimates was introduced in Chapter 8). By using an equivalent projection-based model, it was shown that increasing the number of transmitted training symbols beyond the number of transmit antennas in order to achieve better channel estimates could instead be achieved by keeping the number of training symbols intact and instead increasing the transmitted training power. The main conclusion, though, is that SIP show little gain over conventional pilots unless the channel experiences very fast fading. For such fast fading channels one might want to consider other non-coherent schemes.

In Chapter 8, we extended the schemes to allow channel re-estimation when additional information in the form of detected symbols was made available. These variable coding rate schemes showed good performance and the

decision-directed SIP scheme showed a performance close to the fundamental capacity of the noncoherent channel [ZT02], which was due to the elimination of the problem of having to rely on a poor channel estimate.

Finally, we applied the analysis to a frequency-selective channel. As one might have expected, the results showed that SIP-based systems, compared to conventional training-based systems, gained in capacity in scenarios where one needs to spend a lot of the available time on training and leave less time for transmission of information. That is, SIP is only advantageous when there are many channel parameters to estimate and little time to do it. The perception that SIP can estimate a static frequency-selective channel without any loss of information rate is misleading. In its present form and in many scenarios (e.g., long channel coherence times), SIP can not estimate the channel without a loss of information throughput, which is due to a penalty in effective SNR. The information loss can always be compensated by an increase in the transmit power, but given a power increase the conventional scheme will in most scenarios outperform the SIP scheme. The performance of the SIP scheme can also here be increased if we can mitigate the problem of gaining a poor channel estimate and exploit the advantage that we can transmit the pilot embedded in the data. This can be done in similar ways as was done in Chapter 8, but it was not studied any closer.

10.2 Future Work

The ideas that are presented in the second part of the thesis are quite general. It would, therefore, be interesting to see how the work can be extended to other data models, such as, e.g., time varying channels and Orthogonal Frequency Division Multiplexing (OFDM) channels. Prior to this, a more thorough study should be carried out to investigate the quality of the approximations that were used when deriving the MI lower bounds. The approximations were used to circumvent the problem of having a noise term that is statistically correlated with the signal, since keeping the correlation appears to be, at the least, a formidable task. This problem was, although, eliminated for the decision-directed SIP scheme in Chapter 8. Because in that case, the LMMSE estimate also was the MMSE estimate, which made the noise uncorrelated with the signal.

If it is possible, another interesting study would be to compare the results obtained by the methods described here to the ones obtained by minimizing the error rate of a communication system with a predefined coding scheme, or by studying the outage capacity. Either way, it is most importance to emphasize that when comparing different training schemes, one must to make

sure that one compares their, in some sense, optimal performance. Otherwise, one can get totally arbitrary results favoring either method when comparing their suboptimal performance.

Bibliography

[AO98] D. Astély and B. Ottersten. "The effects of local scattering on direction of arrival estimation with MUSIC and ESPRIT". In *Proc. ICASSP 98*, volume 6, pages 3333–3336, 1998.

[AO99] D. Astély and B. Ottersten. "The Effects of Local Scattering on Direction of Arrival Estimation with MUSIC". *IEEE Trans. on Signal Processing*, 47(12):3220–3234, December 1999.

[AT98] A. L. Andrew and R. C. E. Tan. "Computation of Derivatives of Repeated Eigenvalues and the Corresponding Eigenvectors of Symmetric Matrix Pencils". *SIAM Journal on Matrix Analysis and Applications*, 20(1):78–100, 1998.

[ATV02] S. Adireddy, L. Tong, and H. Viswanathan. "Optimal Placement of Training for Frequency-Selective Block-Fading Channels". *IEEE Trans. on Information Theory*, 48(8):2338–2353, August 2002.

[Bal97] C.A. Balanis. *Antenna Theory: Analysis and Design*. John Wiley and Sons, Inc., New York, second edition, 1997.

[Bar83] A.J. Barabell. "Improving the Resolution Performance of Eigenstructure Based Direction-Finding Algorithms". In *Proc. IEEE ICASSP 83*, pages 336–339, Boston, MA, 1983.

[BC04a] P. Bohlin and M. (Tapio) Coldrey. "Optimized Data Aided Training in MIMO Systems". In *Proc. IEEE VTC 2004 Spring*, volume 2, pages 679–683, Milan, Italy, May 2004.

[BC04b] P. Bohlin and M. (Tapio) Coldrey. "Performance Evaluation of MIMO Communication Systems based on Superimposed Pi-

lots". In *Proc. IEEE ICASSP 04*, volume 4, Montreal, Canada, May 2004.

[Ben99] M. Bengtsson. *"Antenna Array Signal Processing for High Rank Data Models"*. PhD thesis, Royal Institute of Technology, Stockholm, Sweden, 1999.

[BO00] M. Bengtsson and B. Ottersten. "Low-Complexity Estimators for Distributed Sources". *IEEE Trans. on Signal Processing*, 48(8):2185–2194, August 2000.

[BO01] M. Bengtsson and B. Ottersten. "A Generalization of Weighted Subspace Fitting to Full-Rank Models". *IEEE Trans. on Signal Processing*, 49(5):1002–1012, May 2001.

[BPS98] E. Biglieri, J. Proakis, and S. Shamai. "Fading Channels: Information-Theoretic and Communications Aspects". *IEEE Trans. on Information Theory*, 44(6):2619–2692, October 1998.

[BS00] O. Besson and P. Stoica. "Decoupled Estimation of DOA and Angular Spread for a Spatially Distributed Source". *IEEE Trans. on Signal Processing*, 48(7):1872–1882, July 2000.

[Cap69] J. Capon. "High Resolution Frequency Wave Number Spectrum Analysis". *In Proc. IEEE*, 57:1408–1418, 1969.

[CB03] M. (Tapio) Coldrey and P. Bohlin. "Performance Evaluation of MIMO Wireless Communication Systems Employing Pilot Training for Channel Estimation". In *Proc. PCC Workshop & Ericsson/TeliaSonera Research Days 2003*, pages 33–37, Stockholm, Sweden, November 2003.

[CB04] M. (Tapio) Coldrey and P. Bohlin. "A Capacity Comparison between Time-Multiplexed and Superimposed Pilots". In *Proc. 38th Asilomar Conference on Signals, Systems and Computers*, volume 1, pages 1049–1053, Monterey, USA, November 2004.

[CB05a] M. (Tapio) Coldrey and P. Bohlin. "Training-Based MIMO Systems: Part I–Performance Comparison". *Submitted for review to IEEE Trans. on Signal Processing. Also available as technical report no. R032/2005 at http://www.chalmers.se/s2*, November 2005.

[CB05b] M. (Tapio) Coldrey and P. Bohlin. "Training-Based MIMO Systems: Part II–Improvements using a Variable Coding Rate Scheme". *Submitted for review to IEEE Trans. on Signal Processing. Also available as technical report no. R033/2005 at http://www.chalmers.se/s2*, November 2005.

[CMM99] I.J. Cox, M.L. Miller, and A.L. McKellips. "Watermarking as Communications with Side Information". *Proceedings of the IEEE*, 87(7):1127–1141, July 1999.

[Col02a] M. (Tapio) Coldrey. "Beamforming-based Estimators for Spatially Distributed Signals". In *Proc. PCC Workshop & Radiovetenskap och Kommunikation, RVK'02*, pages 319–323, Stockholm, Sweden, June 2002.

[Col02b] M. (Tapio) Coldrey. "Direction and Spread Estimation of Spatially Distributed Signals via The Power Azimuth Spectrum". In *Proc. IEEE ICASSP 02*, volume 3, pages 3005–3008, Orlando, FL, May 2002.

[Col03] M. (Tapio) Coldrey. "On the use of beamforming for estimation of spatially distributed signals". In *Proc. IEEE ICASSP 03*, volume 5, pages 369–372, Hong Kong, China, April 2003.

[CT91] T.M. Cover and J.A. Thomas. *Elements of Information Theory*. John Wiley and Sons, Inc., New York, 1991.

[CV03] M. (Tapio) Coldrey and M. Viberg. "Analysis of Spectral-based Localization of Spatially Distributed Sources". In *Proc. SYSID 2003, 13th IFAC Symposium on System Identification*, Rotterdam, Netherlands, August 2003.

[CV06] M. (Tapio) Coldrey and M. Viberg. "Generalization and Analysis of the Conventional Beamformer for Localization of Spatially Distributed Sources". In *review for the 14th European Signal Processing Conference, EUSIPCO 2006*, Florence, Italy, September 2006.

[Da00] J.M.B. Dias and J.M.N. Leit ao. "Nonparametric Estimation of Mean Doppler and Spectral Width". *IEEE Trans. on Geoscience and Remote Sensing*, 38(1):271–282, January 2000.

[DTS04] M. Dong, L. Tong, and B.M. Sadler. "Optimal Insertion of Pilot Symbols for Transmissions Over Time-Varying Flat Fading Channels". *IEEE Trans. on Signal Processing*, 52(5):1403–1418, May 2004.

[Ert98] R.B. Ertel et al. "Overview of Spatial Channel Models for Antenna Array Communication Systems". *IEEE Personal Communications Magazine*, 5(1):10–22, February 1998.

[FB95] B. Farhang-Boroujeny. "Pilot-based channel identification: Proposal for semi-blind identification of communication channels". *Electronics Letters*, 31(13):1044–1046, June 1995.

[FG98] G.J. Foschini and M.J. Gans. "On Limits of Wireless Communications in a Fading Environment when Using Multiple Antennas". *Wireless Personal Communications*, 6:311–335, March 1998.

[Fos96] G.J. Foschini. "Layered Space-Time Architecture for Wireless Communication in a Fading Environment When Using Multi-Element Antennas". *Bell Labs Technical Journal*, pages 41–59, Autumn 1996.

[FW98] B. Friedlander and A.J. Weiss. "On the Second-Order Statistics of the Eigenvectors of Sample Covariance Matrices". *IEEE Trans. on Signal Processing*, 46(11):3136–3139, November 1998.

[Gal68] R. G. Gallager. *Information Theory and Reliable Communication*. John Wiley and Sons, Inc., New York, 1968.

[Gan02] M.J. Gans et al. "Outdoor BLAST Measurement System at 2.44 GHz: Calibration and Initial Results". *IEEE Journal on Selected Areas in Communications*, 20(3):570–583, April 2002.

[GJJV03] A. Goldsmith, S.A. Jafar, N. Jindal, and S. Vishwanath. "Capacity Limits of MIMO Channels". *IEEE Journal on Selected Areas in Communications*, 21(5):684–702, June 2003.

[GM98] J. Goldberg and H. Messer. "Inherent Limitations in the Localization of a Coherently Scattered Source". *IEEE Trans. on Signal Processing*, 46(12):3441–3444, December 1998.

[GMAHS05] M. Ghogho, D. McLernon, E. Alameda-Hernandez, and A. Swami. "Channel Estimation and Symbol Detection

for Block Transmission Using Data-Dependent Superimposed Training". *IEEE Signal Processing Letters*, 12(3):226–229, March 2005.

[God97a] L.C. Godara. "Applications of Antenna Arrays to Mobile Communications: Part I-Performance Improvement, Feasibility, and System Considerations". *Proceedings of the IEEE*, 85(7):1031–1060, July 1997.

[God97b] L.C. Godara. "Applications of Antenna Arrays to Mobile Communications: Part II-Beamforming and Direction-of-Arrival Considerations". *Proceedings of the IEEE*, 85(8):1195–1245, August 1997.

[God02] L.C. Godara. *Handbook of Antennas in Wireless Communications*. The Electrical Engineering and Applied Signal Processing Series, CRC Press, Boca Raton, FL, 2002.

[Hay96] M. H. Hayes. *Statistical Digital Signal Processing and Modeling*. John Wiley and Sons, Inc, New York, 1996.

[HF90] T.P. Holden and K. Feher. "A Spread Spectrum Based System Technique for Synchronization of Digital Mobile Communication Systems". *IEEE Trans. on Broadcasting*, 36(3):185–194, September 1990.

[HH03] B. Hassibi and B.M. Hochwald. "How Much Training is Needed in Multiple-Antenna Wireless Links?". *IEEE Trans. on Information Theory*, 49(4):951–963, April 2003.

[HJ85] R.A. Horn and C.R. Johnson. *Matrix Analysis*. Cambridge University Press, 1985.

[HK99] F. Hartung and M. Kutter. "Multimedia Watermarking Techniques". *Proceedings of the IEEE*, 87(7):1079–1107, July 1999.

[HM00] B.M. Hochwald and T.L. Marzetta. "Unitary Space-Time Modulation for Multiple-Antenna Communications in Rayleigh Flat Fading". *IEEE Trans. on Information Theory*, 46(2):543–564, March 2000.

[HSG04] A. Hassanien, S. Shahbazpanahi, and A.B. Gershman. "A Generalized Capon Estimator for Localization of Multiple Spread Sources". *IEEE Trans. on Signal Processing*, 52(1):280–283, January 2004.

[HT99] P. Hoeher and F. Tufvesson. "Channel Estimation with Superimposed Pilot Sequence". In *Proc. IEEE GLOBECOM '99*, volume 4, pages 2162–2166, 1999.

[Jän92] T-P. Jäntti. "The Influence of Extended Sources on the Theoretical Performance of the MUSIC and ESPRIT Methods: Narrow-band Sources". In *Proc. IEEE International Conference on Acoustics, Speech, and Signal Processing*, volume 2, pages 429–432, March 1992.

[JF04] Y. Jin and B. Friedlander. "Detection of Distributed Sources Using Sensor Arrays". *IEEE Trans. on Signal Processing*, 52(6):1537–1548, June 2004.

[JHJ+01] V. Jungnickel, T. Haustein, E. Jorswieck, V. Pohl, and C. von Helmot. "Performance of a MIMO System with Overlay Pilots". In *Proc. IEEE GLOBECOM'01*, volume 1, pages 594–598, November 2001.

[JS88] P.H. Janssen and P. Stoica. "On the Expectation of the Product of Four Matrix-Valued Gaussian Random Variables". *IEEE Trans. on Automatic Control*, 33(9):867–870, September 1988.

[Kay93] S. M. Kay. *Fundamentals of Statistical Signal Processing*. Prentice-Hall, Englewood Cliffs, NJ, 1993.

[KV96] H. Krim and M. Viberg. "Two Decades of Array Signal Processing Research: The Parametric Approach". *IEEE Signal Processing Magazine*, 13(4):67–94, July 1996.

[Lac71] R.T. Lacoss. "Data Adaptive Spectral Analysis Methods". *Geophysics*, 36:661–675, 1971.

[Lee73] W.C.Y. Lee. "Finding the Approximate Angular Probability Density Function of Wave Arrival by Using a Directional Antenna". *IEEE Trans. on Antennas and Propagation*, AP-21(3):328–334, May 1973.

[Lju87] L. Ljung. *System Identification: Theory for the User*. Prentice-Hall, Englewood Cliffs, NJ, 1987.

[LLZZ06] J. Li, X-Z Li, D-M Zhou, and E-Y Zhang. "A Novel Method for Estimating the Power Azimuth Spectrum of the Wireless Channel". *IEEE Antennas and Wireless Propagation Letters*, 5(1):11–14, 2006.

[LN98] A. Lapidoth and P. Narayan. "Reliable Communication Under Channel Uncertainty". *IEEE Trans. on Information Theory*, 44(6):2148–2177, October 1998.

[LS02] A. Lapidoth and S. Shamai. "Fading Channels: How Perfect Need "Perfect Side Information" Be?". *IEEE Trans. on Information Theory*, 48(5):1118–1134, May 2002.

[Lüt96] H. Lütkepohl. *Handbook of Matrices*. John Wiley & Sons, West Sussex, England, 1996.

[MÓ0] M. Médard. "The Effect upon Channel Capacity in Wireless Communications of Perfect and Imperfect Knowledge of the Channel". *IEEE Trans. on Information Theory*, 46(3):933–946, May 2000.

[Maz00] F. Mazzenga. "Channel Estimation and Equalization for M-QAM Transmission with a Hidden Pilot Sequence". *IEEE Trans. on Broadcasting*, 46(2):170–176, June 2000.

[MB99] A.A. Monakov and D.V. Blagoveshchensky. "A Method of Spectral Moment Estimation". *IEEE Trans. on Geoscience and Remote Sensing*, 37(2):805–810, March 1999.

[MB04] A. Monakov and O. Besson. "Direction Finding for an Extended Target with Possibly Non-Symmetric Spatial Spectrum". *IEEE Trans. on Signal Processing*, 52(1):283–287, January 2004.

[MF87] D. Makrakis and K. Feher. "A Novel Pilot Insertion-Extraction Method based on Spread Spectrum Techniques". In *Presented at Miami Technicon*, Miami, FL, 1987.

[MGO03] X. Ma, G.B. Giannakis, and S. Ohno. "Optimal Training for Block Transmissions Over Doubly Selective Wireless Fading Channels". *IEEE Trans. on Signal Processing*, 51(5):1351–1366, May 2003.

[MGO05] X. Ma, G.B. Giannakis, and S. Ohno. "Optimal Training for MIMO Frequency-Selective Fading Channels". *IEEE Trans. on Wireless Communications*, 4(2):453–466, March 2005.

[MH99] T.L. Marzetta and B.M. Hochwald. "Capacity of a Mobile Multiple-Antenna Communication Link in Rayleigh Flat Fading". *IEEE Trans. on Information Theory*, 45(1):139–157, January 1999.

[MKLS94] N. Merhav, G. Kaplan, A. Lapidoth, and S. Shamai. "On Information Rates for Mismatched Decoders". *IEEE Trans. on Information Theory*, 40(6):1953–1967, November 1994.

[Mon00] A.A. Monakov. "Observation of Extended Targets with Antenna Arrays". *IEEE Trans. on Aerospace and Electronic Systems*, 36(1):297–302, January 2000.

[MS01] A. Medles and D.T.M. Slock. "Semiblind Channel Estimation for MIMO Spatial Multiplexing Systems". In *Proc. IEEE* 35^{th} *Asilomar Conf. Sig., Syst., Comput.*, pages 999–1003, Pasific Grove, CA, November 2001.

[MSW96] Y. Meng, P. Stoica, and K.M. Wong. "Estimation of the Directions of Arrival of Spatially Dispersed Signals in Array Processing". *Proc. IEE Radar, Sonar and Nav.*, 143(1):1–9, Feb. 1996.

[OG04] S. Ohno and G.B. Giannakis. "Capacity Maximizing MMSE-Optimal Pilots for Wireless OFDM Over Frequency-Selective Block Rayleigh-Fading Channels". *IEEE Trans. on Information Theory*, 50(9):2138–2145, September 2004.

[OLLM04] A.G. Orozco-Lugo, M.M. Lara, and D.C. McLernon. "Channel Estimation Using Implicit Training". *IEEE Trans. on Signal Processing*, 52(1):240–254, January 2004.

[PGNB04] A.J. Paulraj, D.A. Gore, R.U. Nabar, and H. Bölcskei. "An Overview of MIMO Communications – A Key to Gigabit Wireless". *Proceedings of the IEEE*, 92(2):198–218, February 2004.

[Pis72] V.F. Pisarenko. "On the estimation of spectra by means of nonlinear functions of the covariance matrix". *Geophys. J. Roy. Astron. Soc.*, 28:511–531, 1972.

[PMF00] K.I. Pedersen, P.E. Mogensen, and B.H. Fleury. "A Stochastic Model for the Temporal and Azimuthal Dispersion Seen at the Base Station in Outdoor Propagation Environments". *IEEE Trans. on VT*, 49:437–447, March 2000.

[PP97] A.J. Paulraj and C.B. Papadias. "Space-Time Processing for Wireless Communications". *IEEE Signal Processing Magazine*, pages 49–83, November 1997.

[Pro01] J.G. Proakis. *Digital Communications*. McGraw-Hill, fourth edition, 2001.

[Qur85] S.U.H. Qureshi. "Adaptive Equalization". *Proceedings of the IEEE*, 73(9):1349–1387, September 1985.

[RGM98] R. Raich, J. Goldberg, and H. Messer. "Bearing Estimation for a Distributed Source via the Conventional Beamformer". *Proc. Stat. Signal Array Process. Workshop*, pages 5–8, Sep. 1998.

[RGM00] R. Raich, J. Goldberg, and H. Messer. "Bearing Estimation for a Distributed Source: Modeling, Inherent Accuracy Limitations and Algorithms". *IEEE Trans. on Signal Processing*, 48(2):429–441, February 2000.

[RK89] R. Roy and T. Kailath. "ESPRIT – Estimation of Signal Parameters via Rotational Invariance Techniques". *IEEE Trans. on ASSP*, ASSP-37(7):984–995, July 1989.

[SBD95] S. Shamai and I. Bar-David. "The Capacity of Average and Peak-Power-Limited Quadrature Gaussian Channels". *IEEE Trans. on Information Theory*, 41(4):1060–1071, July 1995.

[Sch79] R.O. Schmidt. "Multiple Emitter Location and Signal Parameter Estimation". In *Proc. RADC Spectrum Estimation Workshop*, pages 243–258, Rome, NY, 1979.

[SM97] P. Stoica and R. Moses. *Introduction to Spectral Analysis*. Prentice Hall, Upper Saddle River, NJ, 1997.

[SM03] D. Samardzija and N. Mandayam. "Pilot-Assisted Estimation of MIMO Fading Channel Response and Achievable Data Rates". *IEEE Trans. on Signal Processing*, 51(11):2882–2890, November 2003.

[SVB01] S. Shahbazpanahi, S. Valaee, and M.H. Bastani. "Distributed Source Localization Using ESPRIT Algorithm". *IEEE Trans. on Signal Processing*, 49(10):2169–2178, October 2001.

[SVG04] S. Shahbazpanahi, S. Valaee, and A.B. Gershman. "A Covariance Fitting Approach to Parametric Localization of Multiple Incoherently Distributed Sources". *IEEE Trans. on Signal Processing*, 52(3):592–600, March 2004.

[SW02] T. Svantesson and Jon Wallace. "Statistical Characterization of the Indoor MIMO Channel Based on LOS/NLOS Measurements". In *Proc. 36th Asilomar Conf. Sig., Syst., Comput.*, Pacific Grove, CA, November 2002.

[TC94] J.A. Tague and C.I. Caldwell. "Expectations of Useful Complex Wishart Forms". *Multidimensional Systems and Signal Processing*, 5:263–279, 1994.

[Tel99] I.E. Telatar. "Capacity of Multi-Antenna Gaussian Channels". *European Trans. on Telecom.*, 10:585–595, November 1999.

[TF93] D. Tholl and M. Fattouche. "Angle of Arrival Analysis of Indoor Radio Propagation Channel". *Proc. Int. Conf. on Univ. Pers. Comm.*, 1:79–83, Oct. 1993.

[TFHE99] F. Tufvesson, M. Faulkner, P. Hoeher, and O. Edfors. "OFDM Time and Frequency Synchronization by Spread Spectrum Pilot Technique". In *Proc. Eighth Communication Theory Mini-Conference in Conjunction with IEEE ICC '99*, pages 115–119, Vancouver, Canada, June 1999.

[TL03] J.K. Tugnait and W. Luo. "On Channel Estimation using Superimposed Training and First-order Statistics". *IEEE Communications Letters*, 7(9):413–415, September 2003.

[TO96] T. Trump and B. Ottersten. "Estimation of Nominal Direction of Arrival and Angular Spread using an Array of Sensors". *Signal Processing*, 50(1-2):57–69, Apr. 1996.

[TSD04] L. Tong, B.M. Sadler, and M. Dong. "Pilot-Assisted Wireless Transmissions". *IEEE Signal Processing Magazine*, 21(6):12–25, November 2004.

[VB88] B.D. Van Veen and K.M. Buckley. "Beamforming: A Versatile Approach to Spatial Filtering". *IEEE Signal Proc. Magazine*, pages 4–24, April 1988.

[VB96] C. Vaidyanathan and K.M. Buckley. "Performance Analysis of DOA Estimation Based on Nonlinear Functions of Covariance Matrix". *Signal Processing*, 50(1-2):5–16, Apr. 1996.

[VCK95] S. Valaee, B. Champagne, and P. Kabal. "Parametric Localization of Distributed Sources". *IEEE Trans. on Signal Processing*, 43(9):2144–2153, Sept. 1995.

[VHHK04] H. Vikalo, B. Hassibi, B. Hochwald, and T. Kailath. "On the Capacity of Frequency-Selective Channels in Training-Based Transmission Schemes". *IEEE Trans. on Signal Processing*, 52(9):2572–2583, September 2004.

[WF91] Q. Wu and D.R. Fuhrmann. "A Parametric Method for Determining the Number of Signals in Narrow-Band Direction Finding". *IEEE Trans. on Signal Processing*, 39(8):1848–1857, Aug. 1991.

[Zet97] P. Zetterberg. *"Mobile Cellular Communications with Base Station Antenna Arrays: Spectrum Efficiency, Algorithms and Propagation Models"*. PhD thesis, Royal Institute of Technology, Stockholm, Sweden, 1997.

[ZFB03] H. Zhu and B. Farhang-Boroujeny. "Pilot Embedding for Joint Channel Estimation and Data Detection in MIMO Communication Systems". *IEEE Communications Letters*, 7(1):30–32, January 2003.

[ZO95] P. Zetterberg and B. Ottersten. "The Spectrum Efficiency of a Base-Station Antenna Array System for Spatially Selective Transmission". *IEEE Trans. on VT*, 44(3):651–660, 1995.

[ZT02] L. Zheng and D.N.C. Tse. "Communication on the Grassman Manifold: A Geometric Approach to the Noncoherent Multiple-Antenna Channel". *IEEE Trans. on Information Theory*, 48(2):359–383, February 2002.

[ZVM03] G.T. Zhou, M. Viberg, and T. McKelvey. "A first-order statistical method for channel estimation". *IEEE SP Letters*, 10:57–60, March 2003.